NASA CR-174624
GARRETT 21-4804

DILUTION JET MIXING PROGRAM PHASE II REPORT

by

R. SRINIVASAN
E. COLEMAN
K. JOHNSON

Garrett Turbine Engine Company
A Division of the Garrett Corporation

June 1984

Prepared for

National Aeronautics and Space Administration
NASA-Lewis Research Center

Contract NAS3-22110

1. Report No. NASA CR-174624	2. Government Accession No.	3. Recipient's Catalog No.

4. Title and Subtitle	5. Report Date
Dilution Jet Mixing Phase II Program	June 1984
	6. Performing Organization Code

7. Author(s)	8. Performing Organization Report No.
R. Srinivasan E. Coleman K. Johnson	Garrett 21-4804
	10. Work Unit No.

9. Performing Organization Name and Address	11. Contract or Grant No.
Garrett Turbine Engine Company A Division of the Garrett Corporation Phoenix, Arizona 85010	NAS3-22110
	13. Type of Report and Period Covered

12. Sponsoring Agency Name and Address	14. Sponsoring Agency Code
National Aeronautics and Space Administration Washington, D.C. 20546	Phase II Completion

15. Supplementary Notes

Project Manager: Dr. J. D. Holdeman
NASA-Lewis Research Center
Cleveland, Ohio

16. Abstract

The main objectives of the NASA Dilution Jet Mixing Phase II were to quantify the mixing of opposed rows of jets (two-sided injection) in a confined cross-flow. Parametric tests were performed to determine the effects of the following on jet mixing characteristics:

- Orifice spacing to diameter ratio, S/D
- Duct height to diameter ratio, H_0/D
- Jet-to-mainstream momentum flux ratio, J
- Non-uniform mainstream profile upstream of the dilution orifices
- Flow area convergence.

The general conclusions derived from the Phase II efforts are:

- Jet penetrations for two-sided injections are less than that for single-sided injections (investigated in Phase I), but the jet spreading rates are faster for a given momentum ratio and orifice plate.
- Flow area convergence generally enhances mixing. The mixing characteristics with asymmetric and symmetric convergence are similar.
- For constant momentum ratio, the optimum S/H_0 with in-line injections is one-half of the optimum value for single-sided injections. For staggered injections, the optimum S/H_0 is twice the optimum value for single-sided injection.
- The correlations developed in this program predict the temperature distributions within first order accuracy. They provide a useful tool for predicting jet trajectory and temperature profiles in the dilution zone with two-sided jet injections.

17. Key Words (Suggested by Author(s))	18. Distribution Statement
Dilution-Zone Jet-Mixing Combustion	

19. Security Classif. (of this report)	20. Security Classif. (of this page)	21. No. of Pages	22. Price*
Unclassified	Unclassified		

*For sale by the National Technical Information Service, Springfield, Virginia 22161

TABLE OF CONTENTS

TABLE OF CONTENTS (CONTD)

LIST OF ILLUSTRATIONS

LIST OF ILLUSTRATIONS (CONTD)

LIST OF ILLUSTRATIONS (CONTD)

LIST OF ILLUSTRATIONS (CONTD)

LIST OF ILLUSTRATIONS (CONTD)

LIST OF ILLUSTRATIONS (CONTD)

LIST OF TABLES

This Page Intentionally Left Blank.

1.0 SUMMARY

The main objectives of the NASA Dilution Jet Mixing Phase II Program were to extend the data base on the mixing of a single-sided row of jets in a confined cross flow (Reference 5) and to quantify the mixing of opposed jets in confined cross flow. Parametric tests were performed to determine the effects of the following on dilution jet mixing characteristics:

- Orifice spacing to diameter ratio, S/D
- Duct height-to-diameter ratio, H_0/D
- Momentum flux ratio, J
- Non-uniform mainstream profile upstream of the dilution orifices
- Flow area convergence.

The general conclusions derived from the Phase II efforts are:

- Jet penetrations for two-sided injections are less than those for single-sided injections, but the jet spreading rates are faster for a given momentum flux ratio and orifice plate.
- The jet spreading rate in the transverse direction is faster with an in-line configuration than with a staggered arrangement for a given momentum flux ratio and orifice plate.
- For constant momentum flux ratio, the optimum ratio of orifice spacing to duct height, S/H_0, with in-line

injections is one-half of the optimum value for single-sided injections. For staggered injections, the optimum S/H_0 ratio is twice the optimum value for single-sided injection.

- The temperature distribution in the jet mixing regions is strongly influenced by the mainstream profile upstream of the injection point. A superposition of the mainstream profile on the correlations for uniform cross flow conditions yields good agreement with data.

- Flow area convergence generally enhances mixing. The two-sided jet mixing characteristics with asymmetric and symmetric convergence are very similar.

- The jet mixing characteristics of square orifices are similar to those of circular orifices with the same geometrical area and orifice spacing.

- The jet penetration and mixing characteristics of an equivalent slot are very similar to those for the orifice plate with S/D = 2.

- The correlations developed in this program predict the temperature distributions within engineering accuracy. They provide a useful tool for predicting thermal trajectory and temperature profiles in the dilution zone with two-sided jet injections.

2.0 INTRODUCTION

Advanced aircraft propulsion gas turbine engines for civil and military applications require increased thrust or horsepower per unit airflow. The increased power density often results in higher average combustor discharge temperature with attendant reduction of the available dilution air. Effective use must be made of the available dilution air to tailor the combustor discharge temperature distribution.

The combustor discharge temperature quality is influenced by nearly all aspects of the combustor design and in particular by the dilution zone. To tailor the combustor discharge temperature pattern, the discharge temperature distribution must be characterized in terms of the dilution zone geometric and flow parameters. Such characterization requires an improved understanding of the dilution jet mixing processes.

The present program has been undertaken to acquire a data base of dilution jet mixing characteristics to develop empirical jet mixing correlations and to validate combustor analytical design models.

The penetration and mixing characteristics of jets injected into a cross-stream have been investigated by many researchers and jet trajectories and mixing models have been developed empirically. In most of these cases the jets have been limited to single jets or one-sided rows of jets. In the gas turbine systems, a number of dilution jet orifices in single or multiple rows are used on both sides of combustor liners. The existing correlations for dilution jet mixing are not applicable to practical combustion systems. The availability of experimental data in practical combustor geometries is limited, which results in only qualitative application of the models in actual design practice.

The efforts reported in References 1 through 5 for a single-sided row of jets injected into a confined cross-flow provided the basis for Phase II of the Dilution Jet Mixing Program. The major part of this test program was directed toward studying the mixing characteristics of an opposed row of dilution jets (two-sided) injected into a confined cross flow. The nominal cross-stream test conditions in this study were: U_m = 15 meters/second (m/sec); T_m = 650°K. The dilution jet velocities (V_j) varied over a range of 25 to 110 m/sec with the jets at an ambient temperature of 300°K. The test conditions had a range of jet-to-mainstream momentum flux ratio ($J = \rho_j V_j^2/\rho_m U_m^2$) between 6 and 110.

The main objectives of the NASA Dilution Jet Mixing Phase II Program were as follows:

- Extend the Phase I data base on mixing of a single-sided row of jets in a confined cross flow to square holes and 2-D slots

- Quantify the effects of J, H_0/D, and S/D on penetration and mixing rows of jets injected from two opposite sides into a confined cross-flow. Investigate both in-line and staggered configurations

- Determine the effects of non-uniform cross-stream temperature and velocity profiles upstream of the dilution orifices on the mixing characteristics of two-sided jet injections in a duct

- Quantify the effects of cross-stream flow area convergence (accelerating cross-stream) with two-sided jet injections

- Develop empirical correlations for two-sided injections.

The Phase II experimental effort was divided into the following four test series:

- Series 5: In-line and staggered jet mixing in a constant area duct with uniform cross-stream profile

- Series 6: Two-sided jet mixing in a constant area duct with nonuniform (profiled) cross-stream upstream of the injection point.

- Series 7: Two-sided jet mixing in a symmetrically converging duct

- Series 8: This test series included:

  - Two-sided injections in an asymmetric convergent duct

  - In-line jets with unbalanced momentum flux ratios

  - Single-sided jet mixing characteristics of two-dimensional slots and a row of square holes.

The description of the experimental setup is presented in Section 3.0. Data acquisition and reduction details are presented in Section 4.0. Test results and the predictions obtained from the correlations are presented in Section 5.0. The details of the correlation are presented in Section 6.0 and conclusions and recommendations are provided in Section 7.0.

This Page Intentionally Left Blank

3.0 TEST RIG AND FACILITY DESCRIPTION

3.1 Test Rig

The jet mixing test rig schematic layout is presented in Figures 1 and 2. A partially assembled rig is in Figure 3. The mainstream airflow is ducted from the test cell main air supply through a 15.24 centimeter (cm) internal diameter pipe. A transition section connects the inlet pipe to a rectangular cross section of constant width (30.48 cm) and adjustable height.

A perforated plate with 25 holes of 1.43-cm diameter provides a relatively uniform airstream upstream of the profile generator plenum. The profile generator duct incorporates an adjustable bottom wall to match the test section inlet height, which can vary from 10.16 to 15.24 cm.

A separate air supply is used for the profile generator to provide the desired radial profile of temperature and velocity upstream of the jet-injection plane.

A third air supply feeds the dilution jet orifices on the top and bottom walls of the test section. Separate flow control valves facilitate independent control of the top and bottom jet velocities. The supply temperatures of the top and bottom jets are the same in this arrangement.

The rig walls are insulated with a 2.54-cm thick layer of Kaolite insulation to mimimize the rig heat losses.

In addition to a traversing $P_t/P_s/T$ rake, as shown in Figure 2, the rig instrumentation includes a number of wall static pressure taps and flow thermocouples.

A brief description of the profile generator, test sections, and dilution orifice plates is provided in the following paragraphs.

3.1.1 Profile Generator

A profile generator (Figure 4) provides a desired radial profile in the mainstream. This is achieved by varying independently the flow conditions of the approaching mainstream and the flow injected from the profile generator. As shown in Figure 2, a separate air supply is used to vary the temperature and velocity of the air supplied to the profile generator slot (2.54-cm high and 29.2-cm wide). The supply-air duct dumps the air into a rectangular plenum (or settling chamber) of 30.48 x 16.75 x 12.7-cm dimensions. The slot is fed uniformly through an inclined perforated plate having 50 orifices of 1.47-cm diameter (Figure 4).

Three wall static pressure taps and one thermocouple were used to control the plenum air pressure and temperature levels.

3.1.2 Test Sections

Three different test section configurations (Figure 5) were used in the present investigation. The dimensional parameters of these test sections are summarized in Table 1.

Test Section I has a constant channel height (H_0 = 10.16 cm) and slightly more than $2H_0$ length to allow radial profile measurements at X/H_0 = 0.25, 0.5, 1.0, and 2.0.

TABLE 1. DEFINITION OF TEST SECTIONS

Test Section Number	Description	Test Section Height (cm)		Jet Injection Angle (Degrees)		Test Section Convergence Rate $-\frac{dh}{dx}$
		Injection Plane	Exit Plane	Top	Bottom	
I	Constant Height	10.16	10.16	90.0	90.0	0
II	Symmetric Convergence	10.16	5.08	104.0	104.0	0.50
III	Asymmetric Convergence	10.16	5.08	116.6	90.0	0.50

Test Section II is symmetrically converging with a convergence rate (defined as -dh/dx)of 0.5; the corresponding inclination angle is 14.0 degrees for both top and bottom walls. The jet injection angle is 104 degrees. The test section injection to exit plane area ratio is 2.0. The duct height at the injection plane is 10.16 cm.

Test Section III is an asymmetric convergent duct with a convergence rate equal to that of Test Section II. The bottom wall of Test Section III is horizontal and the top wall inclination is 26.6 degrees with an attendant jet injection angle of 116.6 degrees.

All test sections have a 10.16-cm channel height at the injection plane. The inlet channel heights of the Test I Section is 10.16 cm whereas that of Sections II and III is 15.24 cm. To match these inlet heights, the profile generator section height was adjusted by means of a moveable bottom wall.

To provide a well-controlled boundary layer profile at the injection plane, a boundary-layer trip (0.41-cm high and 0.33-cm wide) was welded to the four walls of the test sections. The trip is located 15.24 cm upstream of the jet injection plane.

A number of static pressure taps are installed on the four walls of the test sections. As delineated in Figure 6 for Test Section I, a total of 32 wall taps were used to measure static pressure distribution. Four thermocouples (two thermocouples extending from the top wall and two through the bottom wall) were used for monitoring the mainstream gas temperature levels. These thermocouples were immersed 1.27 and 3.81 cm from the bottom and top walls, respectively.

3.1.3 Dilution Orifice Plate Geometry

Five circular dilution orifice configurations were used in this investigation. Table 2 gives the important dimensions of the orifice plates. Some of these orifices are illustrated in Figure 7. These plates are designated by 3-set numerals indicating aspect ratio, S/D and H_0/D. The aspect ratio is unity for circular orifices.

These orifice plates gave the following variations in the orifice sizes (D), S/D and H_0/D:

D 1.27, 1.80, and 2.54 cm

S/D 2.0, 2.83, and 4.0

H_0/D 4.0, 5.67, and 8.0

Where H_0 (test section height) = 10.16 cm

TABLE 2. DESCRIPTION OF DILUTION ORIFICE PLATES

Designation	Orifice Diameter, D (cm)	Number of Orifices	S/D	H_0/D	S/H_0
01/02/04	2.54	6	2	4	0.50
01/04/04	2.54	3	4	4	1.00
01/02/08	1.27	12	2	8	0.25
01/04/08	1.27	6	4	8	0.50
01/03/06	1.80	6	2.83	5.67	0.50

S = Orifice center-to-center spacing

H_0 = Test section height at the jet injection point

In addition to the above orifice plates, tests were also performed with two-dimensional slots and a row of square holes. These tests were limited to single-sided jet injections. The length of the slots used in these tests was 29.7 cm. The widths of the two slots investigated were 0.5144 and 1.024 cm, respectively. The orifice plate with square holes had 3 orifices with center-to-center orifice spacing of 9.0 cm. The sides of the square holes had the dimension of 2.25 cm. This orifice plate has the same orifice geometrical flow area as Plate No. 01/04/04.

3.2 Test Facilities

The test rig was installed in Combustion Test Cell C-100. Three separate nonvitiated air supplies were used to control flow conditions of the mainstream, profile generator, and dilution jets.

The mainstream air temperature was regulated from ambient to 725K. For the majority of the test cases the mainstream nominal temperature and flow rate were 644K and 0.27 kilogram/second (kg/sec), respectively. The mainstream temperature was measured by thermocouples located at the test section entrance. A standard ASME orifice section installed in a 15-cm inside diameter pipe was used for measuring the mainstream airflow rate.

A second, separately controlled air supply was used for the profile generator, which can be installed in either the top or bottom walls of the test rig. The mainstream profile was adjusted by varying the pressure drop across the profile generator and the attendant airflow rate. The airflow rate was measured by an ASME orifice in a 7.62-cm inside diameter pipe.

A third air supply was used for controlling the top and bottom dilution jet flow conditions. Additional flow control valves were installed in the top and bottom dilution jet flow lines to facilitate independent control of the jet flow rates. The dilution jet temperature was maintained at the ambient temperature and no external heater was required for the test cases. The dilution air flow rates were measured using a standard bellmouth nozzle section.

4.0 DATA ACQUISITION AND REDUCTION

4.1 Data Acquisition

The dilution jet mixing characteristics were determined by measuring temperature and pressure distributions within the test section at different axial stations. A traversing probe (Figure 8) was used for this purpose.

The probe consists of a 20-element thermocouple rake surrounded by 20 total-pressure sensors on one side and 20 static-pressure rakes on the other side. The nominal transverse spacing between the thermocouple rake and the total pressure rake is 0.508 mm. The spacing between the thermocouple and the static pressure elements is 0.508 mm.

The height of the probe between the top and the bottom elements is 9.35 cm. The first element is located 0.405 cm from the top wall of the constant-height test section (Test Section I). All the elements are equally spaced in the vertical direction, providing a nominal spacing of 0.492 cm.

The total-pressure sensor elements are made of Inconel tubes with an outside diameter of 0.16 cm and a wall thickness of 0.023 cm. The internal conical design of the tube at the inlet provides a $\pm$15 degree flow insensitivity angle. The static pressure tubes, similar to the total pressure sensors, are dead-ended with four bleeding holes of 0.03-cm diameter 90 degrees apart and 0.7 cm from the tip. The total temperature sensors are type K thermocouple wires with insulated junctions encased in 0.10-cm inside diameter tubes, supported by 0.21 cm inside diameter enveloping tubes. The insulated junction tubes exposed to the air stream are 0.76-cm long. The sensing elements have a straight length of 1.52 cm or more before the first bend to the probe core

where all tubes are inserted in a rectangular probe shield, 4.32 x 0.67 cm.

The probe is mounted on a traversing system (Figure 9) that allows travel in three directions. This system allows for a 30.48 cm traverse in the X-direction (mainstream flow direction) and 22.86 cm in the radial (Y) and transverse (Z) directions with an accuracy of ±0.015 percent. The flow field mapping in the Z direction is done over a distance equal to 1.0 or 1.5 times the hole spacing (S) for in-line or staggered configurations, respectively. The measurements in the Z direction for single-sided injections and in-line configurations with two-sided injection were made at the eleven transverse planes identified by Z/S = -0.5, -0.4, -0.3, -0.2, -0.1, 0, 0.1, 0.2, 0.3, 0.4, and 0.5, where Z/S = 0 denotes the center of the orifice. For the staggered configuration with two-sided injection, the measurements were for a total of sixteen transverse planes made at Z/S = -0.5 to 1.0 at intervals of 0.1. The measurements in the X-direction were made at the four axial planes X/H_0 = 0.25, 0.5, 1.0, and 2.0. The probe was traversed over a matrix of 11 x 4 survey locations for in-line orifice configurations and 16 x 4 for staggered configurations.

The temperature and pressure values from the test rig instrumentation were recorded on magnetic tape through a central computerized data acquisition system. An on-line data display system provided real-time information on selected raw data for monitoring the flow conditions. The raw data from the magnetic tape was later used for detail data reduction, analysis, and correlation.

4.2 Data Reduction

The rectangular grid network at which the measurements were made can be described with the aid of Figures 1 and 10. The X-axis is the axis along the length of the duct in the direction of the bulk flow. The X=0 station is located at the jet injection plane. The Y-axis (radial direction) is the direction along the jet injection direction. The Y=0 plane is located at the top jet orifice exit plane. The Z-axis is in the cross-stream direction. The Z=0 plane is the vertical X, Y plane at a jet centerline. The streamwise (X) and radial (Y) distances are nondimensionalized by H_0, the channel height at the jet injection plane. The lateral distance, Z, is nondimensionalized by S, the dilution orifice spacing.

The measured gas temperature distributions are presented in a nondimensionalized form as:

$$\theta(X, Y, Z) = \frac{T_m - T(X, Y, Z)}{T_m - \bar{T}_j}$$

where,

T_m or TMAIN = Mainstream stagnation temperature

$\bar{T}_j$ or TJET = Average jet stagnation temperature

T(X, Y, Z) = Stagnation temperature at the point (X, Y, Z) in the flow field.

θ is a measure of the temperature change due to the jet at any point (X, Y, Z) compared to the maximum possible temperature change and can vary from 0.0 to 1.0. θ is equal to zero when the

local temperature equals the mainstream temperature; and θ is 1.0 when the local temperature equals the jet temperature. When the jet and the mainstream are perfectly mixed, the local temperature reaches ideal equilibrium temperature, T_{EB}, given by

$$T_{EB} = \frac{\dot{m}_m T_m + \dot{m}_j T_j}{\dot{m}_m + \dot{m}_j}$$

The ideal equilibrium temperature difference ratio (θ_{EB} or THEB) is defined as

$$\theta_{EB} = \frac{T_m - T_{EB}}{T_m - T_j}$$

The parameter, θ_{EB}, provides a measure of the quality of the jet mixing. The arithmetic average temperature (T_{av}) at any X plane and the corresponding θ_{av} $\left(= \frac{T_m - T_{av}}{T_m - T_j}\right)$ are also presented with the reduced data to provide the information on the average value of the temperature field at that plane.

The measured θ values are presented in three-dimensional (oblique) plots at each X-station. The oblique plots provide a convenient means of presenting the jet trajectory and mixing. The measured θ values are also presented in the form of isopleths for each X-station for the purpose of detailed comparison with correlations. These plots are presented over a 2S span in the Z direction by assuming symmetry of the θ distribution with respect to the midplane between two orifices. This assumption was invoked only for the purpose of improving the clarity of visual presentation of the temperature distribution. The accuracy of this assumption depends upon the uniformity of flow distribution across the jet orifices. Preliminary tests were performed to

ensure that the jet mass flow was uniformly distributed over the entire orifice plate configuration. A comparison of the data and correlations is presented in a radial profile of θ versus Y/H_o along the jet centerplane at each of the measured X/H_o stations.

The pressure recordings from the probe rake were used to compute the velocity $V(X,Y,Z)$ at the point (X,Y,Z). An interpolation scheme was used to compute pressure (P_s) values at the point where probe thermocouples are located. From these total and static pressures, a nondimensionalized velocity, $V(X,Y,Z)/V_j$, was computed. $V(X,Y,Z)$ is obtained from

$$V(X,Y,Z) = \left\{2\left[P_t\ (X,Y,Z) - P_s\ (X,Y,Z)\right]/\rho(X,Y,Z)\right\}^{1/2}$$

The jet velocity, V_j, is calculated from

$$V_j = 4\ \dot{m}_j\ /\ \left(\rho_j\ N\pi D^2\ C_D\right)$$

where D is the orifice diameter, N is the number of orifices, ρ_j is the jet density (P_j/RT_j), and C_D is the orifice discharge coefficient.

The orifice discharge coefficients were determined by measuring the pressure drop across the orifice plate (without crossflow) for a range of mass flow rates. The discharge coefficient, C_D, was obtained from the relation

$$\frac{\Delta P}{P} = 1.99\left[\frac{\dot{w}_c}{AC_D}\right]^2$$

where, $\dot{w}_c$ is the corrected flow rate in $lbm/_{sec}$ and A is the geometric area of the orifices in square inches.

$$\text{Note: } \dot{w}_c = \dot{w}_a\ \frac{\sqrt{\beta}}{\delta},\ \beta = \frac{T(^oR)}{518.67},\ \text{and}\quad \delta = \frac{P(psi)}{14.696}$$

The velocity vector in the vicinity of the jet injection plane is predominantly in the radial direction. In such regions, the velocity values obtained from the rake probe are not expected to be accurate. For the sake of brevity, the measured velocity distributions are not presented in this report. However, tables of nondimensional velocity distribution, $V(X,Y,Z)/V_j$, in addition to total and static pressure distributions, are provided for each test case in the Comprehensive Data Report (CDR) on this program.

An important parameter relevant to the jet description is the jet momentum flux ratio, J, defined as

$$J = \rho_j V_j^2 \; / \; (\rho_m V_m^2)$$

where

ρ_j = Jet density

ρ_m = Mainstream density = $P_m/(RT_m)$

V_j or VJET = Jet velocity at the orifice Vena Contracta

V_m or VMAIN = Mainstream Velocity = $\dot{m}_m/(\rho_m A_m)$

A_m = Effective mainstream flow area.

Other flow parameters of interest are:

Mass flux ratio (blowing rate), M or BLORAT = $\rho_j V_j/\rho_m V_m$

Temperature ratio, TRATIO = T_j/T_m

Density ratio, DENRATIO = ρ_j/ρ_m

Velocity ratio = V_j/V_m

The geometric parameters of importance associated with the orifice configuration are: S/D_j and H_0/D_j, where D_j is the effective jet diameter defined by

$$D_j = D\sqrt{C_D}$$

The quantities described in this section define the geometric and flow conditions of each test and are reported along with the reduced data.

The average mainstream velocity, V_m and the average jet velocity, V_j, are mass weighted average values for the test. They represent the correct momentum flux for the mainstream and the jet respectively. For the two-sided injections, this procedure is adopted for the top and the bottom injections while reducing the test data. The results are presented in non-dimensional form for the two-sided injection as:

$$\theta = \frac{T_m - T}{T_m - \overline{T_j}} ,$$

where, $$\overline{T_j} = \left(T_{j_T} + T_{j_B}\right)/2$$

with T_{j_T} and T_{j_B} being the stagnation temperatures of the top and bottom jets, respectively.

This Page Intentionally Left Blank

5.0 EXPERIMENTAL DATA DISCUSSION

The Phase II test program was divided into four test series (Series 5 through 8). Series 1 through 4 testing was conducted during the Phase I program[5]. For each of the Phase II test series the measured data and predictions obtained from the correlations are discussed in the following paragraphs.

5.1 Series 5 Tests

The purpose of this test series was to investigate the jet penetration and the mixing characteristics of two-sided dilution jets injected into an isothermal, hot confined cross-flow in a straight duct (Test Section I) with a channel height of 10.16 cm. The jet configurations studied in this series included in-line and staggered arrangements. A total of 12 tests were performed. The orifice geometrical description and the nominal flow conditions are listed in Table 3.

Test No. 1 used two identical orifice plates (01/02/08) in an in-line configuration. The momentum flux ratio of the top jet (J_T) was 6.81, whereas that of the bottom jet (J_B) was 6.88. Figure 11 illustrates the measured distribution of non-dimensional temperature difference (θ).

The top part of Figure 11 shows the oblique plot of the θ profiles at four axial stations of X/H_0 = 0.25, 0.5, 1.0, and 2.0. The bottom part of the figure shows the measured contours for the corresponding stations.

The mixing performance for any given configuration can be estimated from the deviation of θ distribution about θ_{EB}. A small deviation from θ_{EB} characterizes nearly complete mixing of the jet and the mainstream. The θ_{EB} value for Test 1 is 0.1982,

TABLE 3. SERIES 5 TEST CONFIGURATION AND FLOW CONDITIONS WITH TEST SECTION I.

Test No.	Orifice Dia (CM)	S/D	H_0/D	Mainstream				Top Dilution Jet			Bottom Dilution Jet				Density Ratio (DENRATIO)	Equilibrium Theta (THEB)	Regions of Measurement	
				Mass Flow Rate (KG/S)	Temp (TMAIN) (°K)	Velocity (VMAIN) (M/S)	Mass Flow Rate (KG/S)	Momentum Flux Ratio J_T	Temp (T_{j_T}) (°K)	Velocity (V_{j_T}) (M/S)	Mass Flow Rate (KG/S)	Momentum Flux Ratio J_B	Temp (T_{j_B}) (°K)	Velocity (V_{j_B}) (M/S)			Axial Direction X/H_0	Transverse Direction (Z/S)
1	1.27	2 (INL)	8	0.2526	645.9	15.5	0.03109	6.81	310.4	28.1	0.03138	6.88	308.6	28.2	2.092	0.1983	0.25-2.0	-0.5 to +0.5
2	1.27	2 (INL)	8	0.2530	646.6	15.6	0.05893	24.95	306.8	53.3	0.0590	24.76	305.2	52.9	2.140	0.3179	0.25-2.0	-0.5 to +0.5
3	1.27	2 (INL)	8	0.2523	646.2	15.5	0.1204	101.8	303.9	104.3	0.1200	101.9	304.1	104.5	2.247	0.4879	0.25-2.0	-0.5 to +0.5
4	1.27	2 (STG)	8	0.2664	648.9	16.6	0.03118	6.53	325.7	30.0	0.03091	6.59	326.6	30.2	1.999	0.1890	0.25-2.0	-0.5 to 1.0
5	1.27	2 (STG)	8	0.2642	646.2	16.3	0.06199	25.17	314.5	56.7	0.06152	24.7	313.2	56.1	2.088	0.3186	0.25-2.0	-0.5 to 1.0
6	1.27	2 (STG)	8	0.2660	645.2	16.4	0.1252	99.3	313.5	110.2	0.1248	97.4	310.9	109.1	2.195	0.4845	0.25-2.0	-0.5 to 1.0
7	1.27	4 (INL)	8	0.2554	645.4	15.2	0.0159	7.85	326.3	30.2	0.01632	7.81	317.5	29.6	2.015	0.1121	0.25-2.0	-0.5 to +0.5
8	1.27	4 (INL)	8	0.2446	647.1	14.4	0.02952	27.92	322.6	54.5	0.02886	27.32	325.0	54.6	2.028	0.1896	0.25-2.0	-0.5 to +0.5
9	1.27	4 (INL)	8	0.2454	647.6	14.5	0.05932	108.3	319.8	107.7	0.05953	107.0	317.6	107.1	2.159	0.3291	0.25-2.0	-0.5 to +0.5
10	1.27	4 (STG)	8	0.2546	646.6	15.8	0.01435	5.97	329.1	27.6	0.01452	6.14	325.7	27.8	1.984	0.1019	0.25-2.0	-0.5 to 1.0
11	1.27	4 (STG)	8	0.2549	645.0	15.7	0.02974	25.68	322.2	55.8	0.02957	25.69	321.6	55.8	2.036	0.1888	0.25-1.0	-0.5 to 1.0
12	1.27	4 (STG)	8	0.2582	645.9	16.0	0.06076	103.1	317.9	109.9	0.0601	104.3	320.6	111.0	2.169	0.3187	0.25-2.0	-0.5 to 1.0

INL = Inline Jets

STG = Staggered Jets

which corresponds to Contour 4. In Figure 11, the θ_{EB} contours are deformed by the penetration of the jets. This deformation is gradually smoothed out farther downstream. The location of the jet centerline can be identified from the centroid of the largest contour value. For Test 1, at X/H_0 = 0.25, the jet centerline is inside Contour 10, which is at Y/H_0 = 0.20.

The jet spreading in the transverse (Z) direction can be inferred from the smoothness of the contour shapes. For Test No. 1, the presence of the individual jets can be seen at X/H_0 = 0.25 and the jets rapidly merge with adjacent jets beyond X/H_0 = 0.5. The mixing in the radial (Y) direction is substantially slower than that in the transverse direction.

The predicted theta distributions for Test No. 1 obtained from the correlations are illustrated in Figure 12. The details about the correlations are described in Paragraph 6.1.1. In Figure 12, the top part shows the predicted theta contours, while the bottom part illustrates the comparison between measured and predicted centerplane theta profiles. The predictions are represented by solid lines and the data by symbols. The correlations accurately predict the centerplate theta profiles in the region of interest. However, the correlations underestimate the jet mixing in the transverse direction as shown by the bottom part of Figure 11 and the top part of Figure 12.

Figure 13 shows the measured theta distributions for Test No. 2 with orifice plates 01/02/08 in an aligned configuration at J_T = 24.95 and J_B = 24.76. At this test condition, the jets penetrate to about 30 percent of the duct height at X/H_0 =0.25. At this axial station, the jets have not merged with the adjacent or the opposing jets. At X/H_0 = 0.5, the jets begin to interact with each other and approach the equilibrium theta value, θ_{EB} = 0.3179 (contour 6) at X/H_0 = 1.0. For this case, mixing in both

radial and transverse direction is rapid, and the mixing rates are faster than that seen in Test 1.

Test No. 2 uses the same orifice geometry as is used in Test No. 5 in Reference 5, at comparable momentum flux ratio. However, the test with two-sided injection (Test No. 2) has twice the jet flow rate. Comparison between the data for two-sided injections (Figure 13) and single-sided injection (Figure 20 of Reference 5) shows that the jet penetration is reduced, however, the mixing rate is faster for two-sided injections compared to the single-sided row of jets.

The predicted theta distributions for Test No. 2 are presented in Figure 14. At $X/H_0 = 0.25$, the correlations accurately predict the transverse as well as radial theta variations. Further downstream, the model slightly underestimates mixing rates in the transverse and the radial directions.

Figure 15 presents the measured theta distributions for Test No. 3 with orifice plates 01/02/08 in an aligned configuration at $J_T = 101.83$ and $J_B = 104.31$. For this test case, the jets impinge against each other near mid-channel at $X/H_0 = 0.25$. As a result of this impingement, the jets are well mixed with the neighboring jets thereby resulting in little variation in the transverse direction. The jet mixing in the radial direction continues beyond $X/H_0 = 1.0$.

The predicted theta distributions for Test No. 3 are illustrated in Figure 16. The predicted theta contours are in good agreement with the data (bottom part of Figure 15) throughout the region of interest. The jet spreading in the radial direction is slightly underpredicted.

Test 4 used orifice plates 01/02/08 in a staggered arrangement with J_T = 6.53 and J_B = 6.59. The measured theta distributions are presented in Figure 17. The jet penetration in Test 4 is approximately 20 percent of channel height at X/H_0 = 0.25. Comparing Figures 11 and 17 shows that the mixing characteristics for orifice plate 01/02/08 are similar for both the in-line and staggered arrangements. For small orifice spacings ($S/D \leq 2$), the jet interactions produce little temperature variations in the transverse (Z) direction. Therefore, the differences between characteristics for in-line and staggered configurations are minimal for orifice plate 01/02/08.

The predicted theta distributions for Test No. 4 are presented in Figure 18. The predictions for staggered injection are obtained by superimposing the correlations for one-sided injections from the top and the bottom. The description of the correlations is given in Paragraph 6.1.2. The radial profiles shown in Figure 18 are for the X-Y plane in-line with the top jet. The correlations overpredict the jet penetration and the mixing in the radial direction. The predicted jet spreading rate in the transverse direction compares well with the data.

The correlations for staggered injections show poor agreement with the data for orifice plate 01/02/08. Test No. 4 (with staggered injections) has comparable momentum flux ratio with Test No. 1 (with in-line injections). Comparisons of the theta distributions for these two tests (Figure 18 and Figure 11) show similar characteristics. Due to the similarities between the two, in-line correlations were used to obtain predictions for Test No. 4. These results are shown in Figure 19. The predicted centerplane theta profiles for this case are in good agreement with the data. Comparing Figures 17 and 19 shows that the correlations underestimate the mixing in the transverse direction.

The in-line correlations give better agreement than do the superimposed correlations.

Figure 20 shows the measured theta distributions for Test No. 5 with orifice plates 01/02/08 in staggered arrangement with J_T = 25.17 and J_B = 24.7. At X/H_0 = 0.25, the jets penetrate to about 35 percent of the local channel height. Beyond this axial station, the jet mixing continues gradually. Relatively uniform stream condition is approached at X/H_0 = 2.0. Comparing Figures 13 and 20 shows that at the comparable momentum flux ratio, the difference in the mixing characteristics between in-line and staggered configurations are negligible for closely spaced (S/D = 2) small orifices (D = 1.27 cm).

The predictions obtained from the superimposed correlations for Test No. 5 are illustrated in Figure 21. At X/H_0 = 0.25, the correlations underestimate the peak θ values but correctly predict the jet penetration. The predicted jet spreading in the transverse direction is faster than that indicated by the data. The agreement between predicted and measured radial profiles progressively improve with increasing axial distance.

The predicted theta distributions for Test No. 5 using the correlations for in-line injections are illustrated in Figure 22. An improved agreement is achieved (Figure 22), compared to the results shown in Figure 21.

Figure 23 shows the measured theta distributions for Test No. 6, (orifice plates 01/02/08) in staggered arrangement (J_T = 99.3 and J_B = 97.3). For this case, even though the jets are in staggered arrangement, the measured theta profiles are similar to that of in-line jets presented previously in Figure 15. There is little difference in the mixing characteristics between in-line and staggered configurations at the high momentum flux ratio.

This conclusion was also reached for the low and medium momentum flux ratios with orifice plate 01/02/08.

Figure 24 shows the predicted theta distributions from superimposed correlations for Test No. 6. For this case, the correlations slightly underestimate the mixing in the radial direction at $X/H_0 = 0.25$. Further downstream, the agreement between data and correlations is very good.

Figure 25 shows the theta distributions for Test No. 6 predicted by the correlations for in-line injection. The predicted and measured centerplane profiles are in good agreement throughout the region of interest. For this high momentum flux ratio (J = 99), the correlations show smaller differences between in-line and staggered configurations than those observed for the low and medium momentum ratio test cases.

Tests Nos. 1 through 6 were performed with orifice plate 01/02/08 which has S/D = 2, $H_0/D = 8$, and D = 1.28 cm. Tests Nos. 7 through 12 were performed with orifice plate 01/04/08 (S/D = 4, $H_0/D = 8$ and D = 1.28 cm). These tests included both in-line and staggered orifice configurations.

Figure 26 displays the measured theta distributions for Test No. 7 with orifice plates 01/04/08 in aligned configuration with $J_T = 7.85$ and $J_B = 7.81$. At $X/H_0 = 0.25$, the jets penetrate up to about 30 percent of local channel height. At this axial station, the jets do not interact with each other. Beyond $X/H_0 = 0.25$, the jets gradually mix with the mainstream and the adjacent jets and approach equilibrium theta value of 0.1121 at $X/H_0 = 2.0$. Comparing Figures 26 and 11 shows that with increasing S/D, the mixing rate in the transverse direction is reduced and the jet spreading rate in the radial direction is increased.

The predicted theta distributions for Test No. 7 are shown in Figure 27. The correlations slightly overestimate the jet penetration and peak theta values. The jet spreading in the radial and the transverse direction are accurately predicted by the correlations. Comparing Figures 12 and 27 reveals that the correlations also show an increased mixing rate with increasing S/D.

Figure 28 shows the measured theta distributions for Test No. 8 with orifice plates 01/04/08 in aligned configuration with J_T = 27.92 and J_B = 27.32 (medium momentum flux ratio). For this test case, the jets impinge with the opposing jets near mid-channel at X/H_0 = 0.25. At this station the adjacent jets have minimum interaction. Further downstream an increasing level of jet interaction can be seen. The jets gradually mix in the radial and the transverse direction and approach the equilibrium conditions (θ_{EB} = 0.1896). Comparing Figures 13 (S/D = 2.0) and 28 (S/D = 4.0) shows temperature uniformity in the transverse direction is achieved at X/H_0 = 0, whereas the radial temperature gradients exist even at X/H_0 = 2.0. The jet penetration and the mixing rates in the radial direction are enhanced by increasing jet spacing from 2D to 4D.

The predicted theta distributions for Test No. 8 are shown in Figure 29. The correlations slightly overestimate the jet penetration and the spreading in the radial direction. The predicted and measured jet spreading in the transverse direction are in good agreement. The overall agreement between data and correlations is good.

Figure 30 gives the measured theta distribution for Test No. 9 with orifice plates 01/04/08 in aligned configuration with J_T = 108.3 and J_B = 107.0 (high momentum flux ratio). The jets injected from the two sides of the duct impinge against each

other near mid-channel at X/H_0 = 0.25, and the variation in the transverse direction is small. The jets gradually mix with the mainstream and reach equilibrium theta value of 0.3271 at X/H_0 = 2. Comparing Figures 15 (S/D = 2.0) and 30 (S/D = 4.0) shows that, for S/D = 2.0, the theta isopleths are essentially horizontal lines, while for S/D = 4.0, the theta isopleths show larger variation in the transverse direction. This demonstrates that with increasing S/D ratio, the mixing rate in the transverse direction is decreased.

The predicted theta distributions for Test No. 9 are presented in Figure 31. The correlations for this test case slightly underestimate the jet spreading in the transverse direction. The correlations correctly estimate the mixing in the radial direction.

Figure 32 presents the measured theta distribution for Test No. 10 with orifice plates 01/04/08 in staggered configuration (J_T = 5.97 and J_B = 6.14). At X/H_0 = 0.25, the jets penetrate to about 0.25 channel height. They share little interaction with adjacent or opposing jets. The jets gradually mix with the mainstream and the adjacent jets and approach equilibrium conditions (θ_{EB} = 0.1019) at X/H_0 = 2.0. Comparing the relative performance of in-line (Figure 26) and staggered (Figure 32) two-sided injections with momentum flux ratio (J $\approx$ 7.0) shows that the asymptotic theta distribution is similiar and that at the initial stations, the contours are displaced in the transverse direction in the staggered configuration.

Figures 17 (S/D = 2.0) and Figure 32 (S/D = 4.0) show the effect of orifice spacing on mixing characteristics for staggered jets with low injection velocities. Better transverse-direction mixing is achieved with closely spaced orifices even though the jet momentum flux ratio is low (approximately 6.0).

The predicted results for Test No. 10 are presented in Figure 33. At X/H_0 = 0.25, the predicted mixing rates are faster than measured data. The predicted peaks of θ are approximately half of the measured peaks. The correlation progressively improves with increasing axial distance, i.e., X/H_0.

Figure 34 shows the measured theta distributions for Test No. 11 with orifice plates 01/04/08, in staggered configuration (J_T = 25.68 and J_B = 25.69). At X/H_0 = 0.25, the jets penetrate to about 40 percent of the channel height. The jets have significant interaction with opposing and adjacent jets. At the downstream stations, the jets rapidly mix with the mainstream and approach equilibrium conditions (θ_{EB} = 0.1888). Comparing the mixing performances of in-line (Figure 28) and staggered (Figure 34) configurations shows that for the staggered injections, the jet spreading rate in the radial direction is faster than that of the in-line arrangement. However, the jet spreading rate in the transverse direction for the in-line configuration is faster than that for the staggered injections.

The predicted theta distributions for Test No. 11 are shown in Figure 35. At X/H_0 = 0.25, the predicted radial profile shows relatively large deviations in theta values from the data. However, the predicted results correlate well with the data at the downstream stations. The correlations underestimate the jet spreading in the transverse direction. The overall agreement between data and predictions is good.

Figure 36 presents the measured theta distributions for Test No. 12 with orifice plates 01/04/08 in staggered configurations (J_T = 103.1 and J_B = 104.3). At X/H_0 = 0.25, the jets impinge on the opposite wall. The mixing rate is enhanced beyond that station. Comparing the mixing characteristics between in-line and staggered injections (Figures 30 and 36, respectively) shows sub-

stantial differences between the two arrangements for $X/H_0 < 2.0$. However, at $X/H_0 = 2.0$, both in-line and staggered injections give nearly uniform theta distributions with values corresponding to equilibrium conditions (θ_{EB}).

The predicted theta distributions for Test No. 12 are shown in Figure 37. The correlations underestimate the jet penetration and the maximum theta value. The agreement between data and correlations for this case is poor. For this test case, the jet to mainstream mass flow rate ratio is 0.47, which is too high for practical situations.

5.1.1 Test Series 5 Conclusions

Test Series 5 was performed with a constant cross-sectional area duct and uniform mainstream temperature. Two orifice plates (01/02/08 and 01/04/08) were used to study the mixing characteristics in two-sided, aligned and staggered dilution jet configurations. Model correlations have been obtained for two-sided injections and predictions were compared with test data. The following conclusions are made from these efforts:

- The jet penetration for two-sided in-line jet configurations is less than that for single-sided jet injection. However, the jet spreading rates in the radial and transverse directions are faster for two-sided injection at a given momentum flux ratio.

- The jet spreading rate in the transverse direction is faster with inline configuration than with the staggered arrangement of jets for a given orifice plate and momentum flux ratio.

- The jet mixing characteristics with in-line and staggered configurations for the orifice plate 01/02/08 (S/D = 2, H_0/D = 8), are almost identical at a given momentum flux ratio.

- The mixing characteristics for orifice plate 01/04/08 (S/D = 4, H_0/D = 8) with in-line arrangement is substantially different from the staggered arrangement. The jet spreading rate in the radial direction is slightly faster with orifice plates in staggered configuration.

- The correlations developed in this program predict the temperature distribution within engineering accuracy and provide a very useful tool for predicting the thermal trajectory and temperature profiles for opposed jet injections into a confined cross flow. The correlations predict the temperature field accurately for in-line configuration of jets. The correlations for staggered arrangements gives only qualitative agreements with data and further efforts are needed to refine the correlations.

- For in-line injections, with equal momentum flux ratios for the opposing jets, the effective channel height is half of the duct height.

- For a constant momentum flux ratio, comparison between data for single-sided and two-sided injections shows that the optimum ratio of orifice spacing to duct height with in-line injections (S/H) is 1/2 of the optimum value for single-sided injection. For staggered injections, the optimum S/H ratio is twice the optimum value for single-sided injection. The optimum

value of S/H for single-sided injection has been shown to be (Reference 14)

$$(S/D)_{opt} \simeq 2.5/\sqrt{J}.$$

5.2 Series 6 Tests

The objective of this test series was to investigate the mixing characteristics of two-sided, in-line and staggered jet injections with a confined cross-flow having non-uniform temperature and velocity distribution upstream of the jet injection plane. In this test series, the non-uniform mainstream temperature was generated by using a profile generator described in Section 3.0. A total of six tests were performed, with orifice geometries and flow conditions as listed in Table 4. The profile generator was located near the top wall of the test section and the resulting mainstream profiles are referred to as "top cold." Tests 13 through 15 were conducted with orifice plate 01/02/08 and Tests 16 through 18 were performed with orifice plate 01/04/08.

The mainstream temperature profiles generated in this test series are illustrated in Figure 38 in a non-dimensional form, θ_p:

$$\theta_p(y) = \frac{T_{max} - T_p(y)}{T_{max} - \bar{T}_j}$$

where

T_{max} = Maximum value of the profiled mainstream stagnation temperature.

TABLE 4. SERIES 6 TEST CONFIGURATION AND FLOW CONDITIONS USING PROFILED MAINSTREAM.

Test No.	Orifice Dia (CM)	$\frac{S}{D}$	$\frac{H_0}{D}$	Mainstream			Top Dilution Jet				Bottom Dilution Jet				Density Ratio (DENRATIO)	Equilibrium Theta (THEB)	Regions of Measurement	
				Mass Flow Rate (KG/S)	Temp (TMAIN) (°K)	Velocity (VMAIN) (M/S)	Mass Flow Rate (KG/S)	Momentum Flux Ratio J_T	Temp (T_{j_T}) (°K)	Velocity (V_{j_T}) (M/S)	Mass Flow Rate (KG/S)	Momentum Flux Ratio J_B	Temp (T_{j_B}) (°K)	Velocity (V_{j_B}) (M/S)			Axial Direction X/H_0	Transverse Direction (Z/S)
13	1.27	2 (INL)	8	0.3356	559.3	18.9	0.07235	24.63	309.9	69.3	0.07204	24.72	313.9	69.7	1.819	0.6402	0.25-2.0	-0.5 to +0.5
14	1.27	2 (STG)	8	0.3346	553.9	19.0	0.03633	6.02	321.7	35.5	0.03712	6.21	329.7	36.4	1.708	0.5990	"	-0.5 to 1.0
15	1.27	2 (STG)	8	0.3336	554.6	18.9	0.0716	23.77	318.5	69.6	0.07608	23.44	316.7	68.5	1.772	0.6541	"	"
16	1.27	4 (INL)	8	0.3269	549.9	18.6	0.03539	23.6	321.3	68.5	0.0361	24.16	330.7	70.0	1.718	0.6017	"	-0.5 to +0.5
17	1.27	4 (STG)	8	0.3321	548.1	18.8	0.07375	23.62	315.4	68.7	0.08172	24.08	327.7	70.2	1.738	0.6004	"	-0.5 to 1.0
18	1.27	4 (STG)	8	0.3347	551.1	18.9	0.07606	99.52	313.5	137.7	0.080405	99.27	315.6	135.2	1.906	0.6589	"	"

$T_p(y)$ = Local value of the mainstream stagnation temperature upstream of the jet injection plane.

$\overline{T}_j$ = Average jet stagnation temperature.

The nondimensionalized temperature variable, θ, represents the ratio of actual temperature change due to the dilution jets to the maximum possible temperature change for any given flow condition. The value of θ will always be bounded between 0 and 1. For Test Series 6 cases, the θ definition was modified to:

$$\theta(x,y,z) = \frac{T_{max} - T(x,y,z)}{T_{max} - \overline{T}_j}$$

The NASA/Garrett correlations for these test cases were also modified to be consistent with this theta definition. Details of these modifications are presented in Paragraph 6.1.3.

Figure 39 shows the measured theta distributions for Test No. 13, with top cold profile (J_T = 24.63, J_B = 24.72, S/D = 2 and $H_0/D \approx 8$). For this test case, the orifice plates were in an aligned configuration. The test data shows that the jets penetrate to about 30 percent of the duct height at X/H_0 = 0.25. Beyond that axial station, the jets gradually spread in the transverse and radial directions. At X/H_0 = 2, the theta distributions show little variation in the transverse direction, yet the radial profiles retain a shape similar to that of the mainstream theta profile (Figure 38). Comparing the data for the isothermal mainstream (Figure 13) and the profiled mainstream (Figure 39) with the same orifice plate and comparable momentum flux ratio shows that the jet penetration and mixing characteristics for the two cases are similar. The shape of the theta distributions with profiled mainstream suggests that accurate predictions may be obtained by superimposing the mainstream theta

profile on the correlations for isothermal mainstream temperature.

Figure 40 shows the predicted theta distributions for Test No. 13. The precicted results were obtained by superimposing the mainstream theta profile, $\theta_p(y)$, on the NASA/Garrett correlations for two-sided jet injections with uniform mainstream temperature. A detailed description of this method is described in Paragraph 6.1.3. The predicted theta profiles are in good agreement with the data in the regions close to the injection plane. Beyond $X/H_0 = 1$, the predictions show profiles very similar to the data, but the quantitative agreement between data and correlations is poor. Perhaps a suitable scaling parameter is needed to improve the agreement between data and correlations. These results demonstrate the dominance of the mainstream theta profile and the validity of the superposition scheme.

Figure 41 displays the measured theta distributions for Test No. 14 with top cold mainstream profile and orifice plates 01/02/08 in staggered configuration ($J_T = 6.02$ and $J_B = 6.21$). At $X/H_0 = 0.25$, the jets penetrate to about 20 percent of the channel height. They gradually spread in the transverse direction at the downstream stations. At $X/H_0 = 2.0$, the theta profiles have a shape very similar to the mainstream theta profile (Figure 38).

The predicted theta distributions for Test No. 14 are shown in Figure 42. The predicted theta profiles were obtained by superimposing the mainstream profile on the correlations for staggered injection with constant mainstream temperature. The correlations show the same trends as seen in the data. It is recalled, that for orifice plate 01/02/08 with uniform mainstream conditions, the mixing characteristics for staggered configuration were very similar to those for the in-line arrangement.

Therefore, an attempt was made to obtain predictions for Test No. 14 using correlations for the in-line arrangement. These results are presented in Figure 43. Comparing Figures 42 and 43 shows that an improvement over the radial profiles is obtained by using the correlation for in-line injection for orifice plate 01/02/08.

Figure 44 presents the measured theta distributions for Test No. 15 with orifice plates 01/02/08 in staggered arrangement (J_T = 23.77 and J_B = 23.44). The mixing characteristics for in-line (Figure 39) and staggered (Figure 44) injections into a profiled cross-flow have almost identical theta distributions at the same momentum flux ratio.

The predicted theta distributions for Test No. 15 are shown in Figure 45. The predicted results overestimate the mixing in the transverse direction. The predicted radial profiles are in qualitative agreement with the data. In view of the similarities of theta profiles between the in-line and staggered arrangements, predictions were also obtained from the correlations for the in-line arrangement. These results, shown in Figure 46, are in better agreement with the data than the correlations presented in Figure 45. The correlations overestimate the jet centerline theta values, but the jet half-widths are correctly predicted.

Figure 47 shows the measured theta distributions for Test No. 16 with orifice plates 01/04/08 in aligned configurations, (J_T = 23.6 and J_B = 24.16). At X/H_0 = 0.25, the jets penetrate to about 35 percent of channel height. They have little interaction with adjacent jets. At the downstream stations, the jet spreading rate is faster in the transverse direction than in the radial direction. The lateral jet spreading rate on the hot side (bottom) is faster than that in the cold side (top) of the duct. The mainstream profile has a dominant influence on the mixing characteristics. Comparing the data for S/D = 2.0 (Figure 39)

and S/D = 4.0 (Figure 47) shows that as S/D increases, the gradients in the transverse direction also increase. However, at X/H_0 = 2, the differences between the profiles for S/D = 2 and S/D = 4 are minimal.

The predicted theta distributions for Test No. 16 are shown in Figure 48. The predictions overestimate the mixing in the radial direction. The jet spreading rate in the transverse direction, however, is more accurately estimated by the correlations. The overall agreement between data and predictions is poor.

Figure 49 represents the measured theta distributions for Test No. 17 with orifice plates 01/04/08 in the staggered configuration, (J_T = 23.62 and J_B = 24.08). The momentum flux ratios for this test case are almost the same as that for in-line injections (Figure 47). Comparing Figures 49 and 47 shows that although some similarities exist between the two theta profiles, the staggered arrangement has a slower jet spreading rate in the transverse direction and a faster spreading rate in the radial direction than those for in-line injections.

The predicted theta distributions for Test No. 17 are presented in Figure 50. The predicted theta distribution overestimates the jet spreading in the transverse direction. The predicted radial profiles are in good agreement with data in regions close to the jet injection station. Poor agreement exists between the two profiles at X/H_0 = 2, even though the trends are correctly predicted.

Figure 51 portrays the measured theta distributions for Test No. 18 with orifice plates 01/04/08 in staggered configuration, (J_T = 99.52 and J_B = 99.27). At X/H_0 = 0.25, the jets impinge on the opposite wall. The jets rapidly mix with the mainstream and the adjacent jets and approach equilibrium condi-

tions at X/H_0 = 2.0. The ratio of total jet to mainstream mass flow rate for this test case is 0.47. This ratio is much higher than the practical combustor operating conditions. Because of the high mass flow ratio, the mixing process in this case is influenced by the mainstream profile to a lesser extent than at the lower momentum flux ratio test conditions.

The predicted theta distributions for Test No. 18 are presented in Figure 52. The correlations underestimate the jet penetration. Due to the high ratio of jet-to-mainstream mass flow rate, the validity of the superposition scheme used in the correlations is questionable. Consequently, the comparison between data and correlations is poor.

5.2.1 Test Series 6 Conclusions

The Test Series 6 were performed with constant cross-sectional area duct and top cold mainstream temperature distribution. Two orifice plates (01/02/08 and 01/04/08) were used to study the mixing characteristics of two-sided, aligned and staggered configurations. The NASA/Garrett correlations have been extended in the case of profiled mainstream. The following conclusions are made from these efforts:

- The mainstream profile has a dominant effect on the radial profiles downstream of the injection plane at low to moderate momentum flux ratios.

- The temperature distributions with in-line and staggered arrangements are similar for orifice plate 01/02/08 at a given momentum flux ratio.

- The jet spreading rate in the radial direction is faster for staggered injections than the in-line injec-

tions with orifice plate 01/04/08 at moderate momentum flux ratios.

- The jet spreading characteristics with profiled mainstream are very similar to those with uniform mainstream temperature.

- The correlations for in-line configurations are in agreement with data. The correlations for staggered injections show only qualitative agreement with measurements. Further work is needed to improve the correlations for staggered injections.

- The superposition procedure used for modifying the NASA/Garrett correlations is sufficiently accurate for dilution zone design purposes. The predicted results for staggered injections are in relatively poor agreement with the data, and further refinement of the correlations is needed.

5.3 Series 7 Tests

The objective of Test Series 7 was to investigate the jet penetration and mixing characteristics of two-sided dilution jets injected into a hot-isothermal cross flow in a converging duct. These tests were performed in a symmetrically converging duct (Test Section II) with 4 orifice plate geometries and two flow conditions for each geometry. The orifice plate configurations and flow conditions used in Test Series 7 are listed in Table 5. The convergent test section area ratio used in this test (Figure 5) was $A_0/A_{min} = 2$, where A_0 is the duct area at the jet injection plane and A_{min} is the minimum area of the duct. The test duct channel height was reduced from 10.16 cm (4 in.) to 5.08 cm

TABLE 5. SERIES 7 TEST CONFIGURATIONS AND FLOW CONDITIONS WITH TEST SECTION II.

Test No.	Orifice Dia (CM)	$\frac{S}{D}$	$\frac{H_0}{D}$	Mainstream			Top Dilution Jet				Bottom Dilution Jet				Density Ratio (DENRATIO)	Equilibrium Theta (THEB)	Regions of Measurement	
				Mass Flow Rate (KG/S)	Temp (TMAIN) (°K)	Velocity (VMAIN) (M/S)	Mass Flow Rate (KG/S)	Momentum Flux Ratio J_T	Temp (T_{j_T}) (°K)	Velocity (V_{j_T}) (M/S)	Mass Flow Rate (KG/S)	Momentum Flux Ratio J_B	Temp (T_{j_B}) (°K)	Velocity (V_{j_B}) (M/S)			Axial Direction X/H_0	Transverse Direction (Z/S)
19	1.27	2 (INL)	8	0.2662	644.8	16.5	0.06453	25.98	298.2	56.5	0.0638	25.56	298.2	56.3	2.193	0.3253	0.25-1.0	-0.5 to +0.5
20	1.27	2 (INL)	8	0.2669	644.6	16.4	0.1340	106.1	297.0	111.3	0.1348	105.9	295.0	111.3	2.306	0.5019	"	"
21	1.27	4 (STG)	8	0.2691	644.6	16.4	0.03155	25.92	302.9	57.1	0.03275	24.87	290.2	54.7	2.199	0.1929	"	-0.5 to 1.0
22	1.27	4 (STG)	8	0.2690	644.2	16.4	0.06504	107.9	298.5	112.8	0.06506	109.6	299.9	113.7	2.272	0.3260	"	"
23	2.54	4 (STG)	4	0.2681	644.9	16.5	0.03311	6.78	311.0	29.7	0.03367	6.91	310.4	30.0	2.082	0.1994	"	"
24	2.54	4 (STG)	4	0.2683	644.5	16.4	0.06359	25.84	304.2	56.9	0.0669	25.99	301.1	56.7	2.166	0.3272	"	"
25	2.54	2 (INL)	4	0.2675	645.1	16.4	0.06522	6.69	300.4	28.9	0.06554	6.71	298.9	28.9	2.162	0.3284	"	-0.5 to +0.5
26	2.54	2 (INL)	4	0.2684	644.7	16.4	0.1238	25.68	300.8	56.4	0.1250	25.97	298.9	56.6	2.181	0.4810	"	"

(2.0 in) over a length of 10.16 cm (4 in.), i.e., 0.5 cm per cm of length.

The jet injection angle in this case was 104 degrees. The measurements for this test series were made at X/H_0 = 0.25, 0.5, and 1.0.

The Test Series 7 were performed with uniform mainstream temperature profiles. The definition of theta needed to analyze the data is

$$\theta = \frac{T_m - T}{T_m - \overline{T}_j}$$

where

T_m = Mainstream stagnation temperature.

T = Local stagnation temperature.

$\overline{T}_j$ = Average jet stagnation temperature.

Figure 53 represents the measured theta distributions for Test No. 19 with symmetrically convergent duct, and orifice plates 01/02/08 in aligned configuration (J_T = 25.98, and J_B = 25.56). At X/H_0 = 0.25, the jets penetrate to about 35 percent of local duct height. At X/H_0 = 0.25 and 0.5, the data shows a lack of symmetry. This is due to the interpolation procedure used in generating the contour plots, in addition to possible slight misalignments of the orifice plates. Comparing the data for straight (Figure 13) and convergent ducts (Figure 53) at a comparable momentum flux ratio with the same orifice plate configuration shows that, with the flow area convergence, the mixing rate is enhanced, especially in the transverse direction.

The predicted theta distributions for convergent duct test cases were obtained by modifying the NASA/Garrett correlations. These modifications consider the effects of injection angle as well as flow area convergence by using an equivalent momentum flux ratio J_{eq}. Details of these modifications are described in paragraph 6.1.4.

The predicted theta distributions for Test No. 19 using the modified NASA/Garrett correlations are presented in Figure 54. The predicted results underestimate the jet penetration and mixing in both radial and transverse directions. The correlations overestimate the peak theta values by about 25 percent. At $X/H_0 = 1$, however, the centerplane radial profiles are predicted well. These correlations correctly predict the shapes of the theta profiles throughout the region of interest.

Figure 55 presents the measured theta distributions for Test No. 20 using the symmetrically convergent duct with orifice plates 01/02/08 in aligned configuration ($J_T = 106.1$ and $J_B = 105.9$). For this flow condition, the jets impinge against each other near the center of the duct at $X/H_0 = 0.25$. Consequently, the theta profiles are almost invariant in the transverse direction. At the downstream stations ($X/H_0 = 0.5$ and 1.0), the theta profiles have a nearly uniform value corresponding to equilibrium conditions ($\theta_{EB} = 0.5019$). Comparing the data for straight (Figure 15) and convergent ducts (Figure 55) shows that the flow area convergence enhances mixing in both radial and transverse directions.

The predicted theta distributions for Test No. 20 are shown in Figure 56. As observed in Test No. 19, the correlations underestimate the jet penetration and the mixing in the radial and transverse directions. The predicted radial theta profiles are within 20 percent of the data.

Figure 57 (Test No. 21) depicts the measured theta distributions, using symmetrically convergent duct with orifice plates 01/04/08 in staggered arrangement, (J_T = 25.92 and J_B = 24.86). At X/H_0 0.25, the jet penetration is about 40 percent of local channel height. The jets gradually spread in the radial and transverse directions and approach equilibrium theta value (θ_{EB} = 0.1929) at X/H_0 = 1.0. Comparing the data for straight (Figure 34) and convergent ducts (Figures 57) shows that convergence tends to improve the mixing in the radial direction.

The predicted theta variations for Test No. 21 are shown in Figure 58. The predicted radial profiles at X/H_0 = 0.25 are smaller in magnitude compared to the data. But the agreement between data and correlations are good at X/H_0 = 0.5 and 1.0. The predicted theta contours compare favorably with those corresponding to the measurements.

Figure 59 represents the measured theta distributions for Test No. 22 with orifice plates 01/04/08 in staggered configuration (J_T = 107.9 and J_B = 109.6). At X/H_0 = 0.25, the jets impinge on the opposite wall and the theta profiles are nearly uniform with the equilibrium theta value θ_{EB} = 0.326. The enhanced mixing due to convergence is demonstrated by comparing the data for straight (Figure 36) and convergent ducts (Figure 59).

The results obtained from the correlations for Test No. 22, shown in Figure 60, underpredicts the jet penetration and the jet mixing at X/H_0 = 0.25. Consequently, the predicted radial profile at X/H_0 = 0.25 is in poor agreement with the data. However, at the measurement stations downstream, the agreement between correlations and the data is within 25 percent.

Test No. 23 was performed with a symmetically convergent duct (Test Section II), orifice plates 01/04/04 (S/D = 4, H_0/D = 4) in staggered arrangement, having momentum flux ratios of J_T = 6.78 and J_B = 6.91 for the top and bottom dilution jets, respectively. The diameters of the dilution jets were 2.54 cm. The measured theta distributions for this test case are presented in Figure 61. At X/H_0 = 0.25, the jets penetrate to about 40 percent of local duct height with minimal interaction with other jets. At the downstream stations, the jets gradually interact with the mainstream and the adjacent jets and approach the equilibrium conditions (θ_{EB} = 0.1994).

The predicted theta distributions for this test case are shown in Figure 62. At X/H_0 = 0.25 and 0.5, the predicted peak theta values are underestimated by about 25 percent. However, the predicted jet penetration is in good agreement with data. At X/H_0 = 1.0 the jet penetration is overestimated and the correlations are in inferior agreement with the data.

Figure 63 shows the measured theta distributions for Test No. 24 (with Test Section II), orifice plates 01/04/04 in staggered configuration (J_T = 25.84 and J_B = 25.98). At X/H_0 = 0.25, the jets impinge against the opposite wall, followed by rapid mixing in the radial and transverse directions. At X/H_0 = 1.0, the theta distribution is nearly uniform with equilibrium theta value, θ_{EB} = 0.3272.

The predicted theta distributions for Test No. 24 are presented in Figure 64. The correlations underestimate the jet penetration and the mixing rates in the radial as well as the transverse direction. These characteristics were observed in cases where the jets overpenetrated to the opposite wall. Such flow conditions are not encountered often in practical combustor dilution zones.

Test No. 25 represents two-sided dilution jet injections into Test Section II with orifice plates 01/02/04 (S/D = 2, H_0/D = 4, D = 2.54 cm) in aligned configuration (J_T = 6.69 and J_B = 6.71). The measured theta distributions for this test case are shown in Figure 65. At X/H_0 = 0.25, the jets penetrate to about 30 percent of local channel height with little interaction with the opposing jets. However, the jets interact with the adjacent jets issuing from the same side of the duct. At the downstream stations, the jets gradually interact with the mainstream and approach equilibrium conditions (θ_{EB} = 0.3283).

The predicted theta distributions for Test No. 25 are shown in Figure 66. The correlations overpredict the peak theta values. Furthermore, the jet penetration and the spreading rate in the transverse direction are overestimated by the model. Further refinement of the correlations are needed to improve the quantitative predictions.

Figure 67 represents the measured theta distributions for Test No. 26 with Test Section II, orifice plates 01/02/04 in staggered configuration J_T = 25.68 and J_B = 25.97. At X/H_0 = 0.25, the jets impinge with the opposing jets at mid-channel, with the attendant enhancement in the transverse mixing rate. At the downstream stations, the jets gradually spread in the radial direction and approach the equilibrium conditions (θ_{EB} = 0.4810).

The predicted theta distributions for Test No. 26 are presented in Figure 68. At X/H_0 = 0.25, the predicted and measured radial theta profiles are in excellent agreement. However, the lateral mixing rate at that axial station is underestimated by the correlations. At X/H_0 = 0.5 and 1.0, the predicted radial jet spreading rates are slower than the data and the predicted

maximum theta values are smaller than the data. The jet spreading rates in the transverse direction are also underestimated by the correlations.

5.3.1 Test Series 7 Conclusions

The mixing characteristics of two-sided jets with isothermal cross-flow in a symmetrically convergent duct were investigated. Four orifice geometric configurations and two flow conditions for each orifice plate were considered. The following conclusions are drawn from these tests:

- Mixing is generally enhanced by flow area convergence. In convergent ducts, the jet spreading in radial and transverse directions occurs within a shorter distance from the jet injection plane than in the case of the straight duct.

- When the jets are injected upstream, the jet spreading rate in the transverse direction is enhanced. A similar effect is also seen for impinging opposed jets.

- The modified NASA/Garrett correlations with equivalent momentum flux ratio ($J_{eq}(X)$) yield qualitatively good comparison with data. This provides a very useful design tool, even though the predicted theta values are not accurate. These correlations are not applicable to situations where jets overpenetrate to the opposite wall of the duct. Further refinements in the correlations are needed to improve the quantitative predictions.

5.4 Series 8 Tests

The Series 8 tests consisted of the orifice plate configurations and flow conditions of interest based on the tests performed in Series 1 through 7. These tests included the following orifice plate geometries:

- Two-sided injection, in a straight duct with orifice plate 01/04/04 (S/D = H/D = 4) in aligned and staggered configurations

- Single-sided injection with a two-dimensional slot (slot width, w = 0.5144 and 1.024 cm)

- Single-sided injection in a straight duct with square holes having 2.25 cm sides

- Two-sided jet injections in a straight duct with orifice plate 01/02/08 in aligned configuration, having unbalanced momentum flux ratios from the top and bottom walls

- Two-sided jet injections in an asymmetrically convergent duct (Test Section III) with four orifice plate configurations and two flow conditions for each configuration

- Two-sided injections in a straight duct with orifice plates 01/02/04 in aligned configuration

- Single-sided injection in a straight duct with orifice plate 01/03/06 (S/D = 2.83, H/D = 5.67, D = 1.796 cm).

The orifice plate configurations, test section geometries, and the flow conditions for test Series 8 are listed in Table 6.

Test 27 corresponds to two-sided jet injections into a constant cross-sectional area duct, with staggered 01/04/04 orifice plates and J_T = 6.76 and J_B = 6.69. The measured theta distributions for this case are presented in Figure 69. At this station, the interaction between the opposing jets is minimal. Comparing the single-sided injection (Figure 16, Reference 5) and two-sided injection (Figure 69) shows that the jet penetrations for the two cases are comparable. However, the mixing of the jets with the cross-stream is significantly faster with two-sided injection compared to single-sided injection. Comparing the data for a straight (Figure 69) and symmetrically convergent duct (Figure 61) shows that the mixing rate in a converging duct is faster than in a constant cross-sectional area duct.

The predicted theta distributions for Test 27 are shown in Figure 70. The predicted jet penetrations are in good agreement with the data. But the magnitude of maximum theta is underestimated by the correlations. The correlations also underestimate the jet spreading rates in the radial direction. The overall agreement between the data and correlations for this test case is poor.

Test 28 was performed with two-sided jet injections into a constant cross-sectional area duct using orifice plates 01/04/04 in staggered configurations, J_T = 26.42 and J_B = 26.10. The measured theta distributions for Test 28 are shown in Figure 71. At X/H_0 = 0.25, the jets overpenetrate to the opposite wall. At the downstream stations, the jets gradually mix with the mainstream and reach equilibrium conditions (θ_{EB} = 0.3271) at X/H_0 = 2.0. Comparing the data for a straight duct (Figure 71) and a symme-

TABLE 6. SERIES 8 TEST CONFIGURATIONS AND FLOW CONDITIONS.

Test No.	Test Section	Orifice Dia (CM)	$\frac{s}{D}$	$\frac{H_0}{D}$	Mainstream			Top Dilution Jet				Bottom Dilution Jet				Density Ratio (Denratio)	Equilibrium Theta (THEB)	Regions of Measurement	
					Mass Flow Rate (KG/S)	Temp (TMAIN) (°K)	Velocity (VMAIN) (M/S)	Mass Flow Rate (KG/S)	Momentum Flux Ratio J_T	Temp (T_{J_T}) (°K)	Velocity (V_{J_T}) (M/S)	Mass Flow Rate (KG/S)	Momentum Flux Ratio J_B	Temp (T_{J_B}) (°K)	Velocity (V_{J_B}) (M/S)			Axial Direction X/H_0	Transverse Direction (Z/S)
27	I	2.54	4 (STG)	4	0.2719	646.3	16.6	0.03314	6.76	313.4	30.1	0.03455	6.70	305.0	29.5	2.0957	0.1993	0.25 - 2.0	-0.5 to 1.0
28	I	2.54	4 (STG)	4	0.2747	644.7	16.9	0.06534	26.42	307.4	59.4	0.06823	26.1	303.6	58.6	2.142	0.3271	0.25 - 2.0	-0.5 to 1.0
29	I	2.54	4 (INL)	4	0.2681	645.4	16.5	0.06407	26.86	307.5	58.6	0.06515	26.49	300.6	57.4	2.150	0.3253	0.25 - 2.0	-0.5 to +0.5
30	I	2.54	4 (INL)	4	0.2700	645.4	16.6	0.1306	106.9	306.9	114.9	0.1324	107.3	304.8	113.6	2.249	0.4936	0.25 - 2.0	-0.5 to +0.5
31a	I	0.5144	1	19.75	0.2719	646.0	16.8	0.03782	6.63	310.5	29.9	--	--	--	--	2.088	0.1213	0.25 - 2.0	0 to 4.0
31b	I	0.5144	1	19.75	0.2720	646.7	16.7	0.07358	26.13	308.6	21.33	--	--	--	--	2.134	0.2129	0.25 - 2.0	0 to 4.0
31c	I	0.5144	1	19.75	0.2747	646.3	16.8	0.1492	104.5	305.1	113.8	--	--	--	--	2.273	0.3520	0.25 - 2.0	0 to 4.0
32	I	2.25	4	4	0.2732	646.5	16.8	0.06414	26.1	311.0	59.1	--	--	--	--	2.105	0.1902	0.25 - 2.0	-0.5 to +0.5
33	I	1.27	2 (INL)	8	0.2713	645.1	16.6	0.07874	40.9	303.7	72.3	0.04695	14.7	299.1	43.2	2.163	0.3201	0.25 - 2.0	-0.5 to +0.5
34	I	1.27	2 (INL)	8	0.2703	645.3	16.6	0.09437	58.4	303.2	85.7	0.03289	6.47	300.6	28.7	2.167	0.3201	0.25 - 2.0	-0.5 to 0.5
35	III	1.27	2 (INL)	8	0.2684	645.0	16.4	0.06265	26.24	303.4	57.22	0.06279	25.93	301.0	56.7	2.163	0.3185	0.25 - 1.0	-0.5 to +0.5
36	III	1.27	2 (INL)	8	0.2698	644.5	16.4	0.1300	107.4	301.1	112.8	0.1294	107.8	301.6	113.4	2.268	0.4902	0.25 - 1.0	-0.5 to +0.5
37	III	1.27	4 (STG)	8	0.2683	645.6	16.4	0.03104	25.7	310.7	57.5	0.03115	26.1	309.0	57.7	2.109	0.1882	0.25 - 1.0	-0.5 to 1.0
38	III	1.27	4 (STG)	8	0.2680	645.6	16.4	0.06494	109.2	303.3	113.8	0.06379	110.0	303.3	113.8	2.252	0.3245	0.25 - 1.0	-0.5 to +1.0
39	III	2.54	4 (STG)	4	0.2707	645.6	16.5	0.03352	6.69	311.9	29.65	0.03390	6.74	307.5	29.5	2.090	0.1994	0.25 - 1.0	-0.5 to +1.0

TABLE 6. SERIES 8 TEST CONFIGURATIONS AND FLOW CONDITIONS (CONTD).

Test No.	Test Section	Orifice Dia (CM)	$\frac{S}{D}$	$\frac{H_0}{D}$	Mainstream			Top Dilution Jet				Bottom Dilution Jet				Density Ratio (Dencratio)	Equilibrium Theta (THEQ)	Regions of Measurement	
					Mass Flow Rate (KG/S)	Temp (TMAIN) (°K)	Velocity (VMAIN) (M/S)	Mass Flow Rate (KG/S)	Momentum Flux Ratio J_T	Temp (T_{j_T}) (°K)	Velocity (V_{j_T}) (M/S)	Mass Flow Rate (KG/S)	Momentum Flux Ratio J_B	Temp (T_{j_B}) (°K)	Velocity V_{j_B} (M/S)			Axial Direction X/H_0	Transverse Direction (Z/S)
40	III	2.54	4 (STG)	4	0.2727	645.7	16.6	0.06481	25.99	302.7	57.4	0.06635	25.05	293.6	55.4	2.199	0.3247	0.25 - 1.0	-0.5 to +0.5
41	III	2.54	2 (INL)	4	0.2723	645.6	16.5	0.06612	6.64	305.5	29.2	0.06633	6.68	304.9	29.3	2.124	0.3272	0.25 - 1.0	-0.5 to +0.5
42	III	2.54	2 (INL)	4	0.2726	644.8	16.4	0.1248	26.25	302.5	57.2	0.1243	26.34	303.0	57.4	2.161	0.4774	0.25 - 1.0	-0.5 to +0.5
43	III	2.54	2	4	0.3348	506.5	17.9	0.07832	6.26	310.2	34.9	--	--	--	--	1.648	0.5873	0.25 - 1.0	-0.5 to +0.5
44	III	2.54	2	4	0.3350	508.4	17.9	0.1526	24.31	307.9	67.9	--	--	--	--	1.698	0.6460	0.25 - 1.0	-0.5 to +0.5
45A	I	1.024	1	9.92	0.2688	644.7	16.5	0.0749	6.66	307.8	29.4	--	--	--	--	2.105	0.2179	0.25 - 1.0	-0.5 to -0.5
45B	I	1.024	1	9.92	0.2708	644.4	16.6	0.1434	25.34	308.7	57.3	--	--	--	--	2.125	0.3462	0.25 - 2.0	0.0 to 4.0
45C	I	1.024	1	9.92	0.2735	644.9	16.7	0.2545	78.33	307.5	98.9	--	--	--	--	2.223	0.4820	0.25 - 2.0	0.0 to 4.0
46	I	2.54	2 (INL)	4	0.2707	644.3	16.5	0.06667	6.70	304.8	29.4	0.06656	6.70	304.6	29.4	2.121	0.3299	0.25 - 2.0	0.0 to 4.0
47	I	2.54	2 (INL)	4	0.2710	644.3	16.6	0.1276	25.56	302.2	57.0	0.1273	25.75	303.6	57.3	2.153	0.4846	0.25 - 2.0	-0.5 to +0.5
48	I	2.54	2 (INL)	4	02710	644.1	16.5	0.2334	84.18	302.5	101.4	0.2334	83.92	302.5	101.2	2.234	0.6327	0.25 - 2.0	-0.5 to +0.5
49	I	1.80	2.83	5.67	0.2701	644.4	16.7	0.03539	6.49	309.5	29.4	--	--	--	--	2.090	0.1159	0.25 - 2.0	-0.5 to +0.5
50	I	1.80	2.83	5.67	0.2679	644.9	16.5	0.06924	25.48	299.5	56.3	--	--	--	--	2.191	0.2054	0.25 - 2.0	-0.5 to +0.5
51	I	2.54	4 (INL)	4	0.2679	644.3	16.5	0.03334	6.67	305.6	29.2	0.03421	6.58	295.8	28.6	2.152	0.2014	0.25 - 2.0	-0.5 to +0.5

trically convergent duct (Figure 63) shows that mixing is enhanced due to flow area convergence.

The predicted theta distributions for Test 28 are presented in Figure 72. The predicted jet penetration is smaller than the data at X/H_0 = 0.25 and 0.5. The predicted jet spreading rates in the radial direction is slower than the data. The overall agreement between data and correlations for this test case is poor.

Figure 73 represents the measured theta distribution for Test 29. Test 29 corresponds to two-sided in-line injections into a crossflow with a constant cross-sectional area duct using orifice plates 01/04/04 (J_T = 26.86 and J_B = 26.49). For this test condition, at X/H_0 = 0.25, the opposed jets impinge at the center of the duct, with attendant enhanced transverse mixing downstream. Comparing the data for in-line (Figure 71) and staggered (Figure 73) orifice configuration shows that the mixing rates are faster with stagered injections.

The predicted theta distributions for Test 29 are shown in Figure 74. In the region near the jet injection plane, the correlations are in good agreement with data. Beyond X/H_0 = 0.5, the predicted theta values are larger than the data. The correlations slightly overestimate the mixing in the transverse direction.

Test 30 corresponds to two-sided in-line injection with a cross-flow in a constant area duct using orifice plates 01/04/04 having J_T = 106.9 and J_B = 107.3. The measured theta distributions for Test 30 are shown in Figure 75. At X/H_0 = 0.25, the theta distributions are similar to those for Test 29 (Figure 73). However, at the downstream stations, the theta distributions for the two test cases are significantly different. The mixing in

the radial and transverse directions are substantially faster at higher momentum flux ratio.

The predicted theta distributions for Test 30 are shown in Figure 76. The predictions underestimate the jet mixing in the radial and transverse directions in the region upstream of X/H_0 = 1.0. At X/H_0 = 2.0, the predicted and measured radial theta profiles are in very good agreement. The overall agreement between the data and correlations for this test case is good.

Test 31 corresponds to one-sided injection into an isothermal cross flow in a constant area duct using a 0.5144 cm-wide two-dimensional slot. The geometrical area of this two-dimensional slot is the same as orifice plates 01/04/04 and 01/02/08. The tests were performed at three different momentum flux ratios, 6.63, 26.13, and 104.5.

In these tests the slotted jet was injected from the top wall. Measurements were made at four axial stations and five transverse locations. Figure 77 represents the measured theta distributions for Test 31(a) with J = 6.63. For this case, at X/H_0 = 0.25, the jet penetration is about 20 percent of the channel height. At the downstream stations, the jet penetration gradually decreases and at X/H_0 = 2, the jet reattaches on the injection wall. The ratio of jet to total mass flow rate for Test 31(a) is 0.1213. Comparing Figure 77 and those for orifice plate 01/04/04 at a comparable momentum flux ratio (Figure 16 of Reference 5) shows that the mixing rates are significantly reduced for the two-dimensional slot. The predictions for this case were obtained using the NASA/Aerojet correlations (Reference 5), with S/D = 1.0 and S/D = 2.0. The predicted theta distributions for Test 31(a) are shown in Figure 78, where the solid lines represent the correlations for S/D = 1.0 and the broken lines correspond to the predictions for S/D = 2.0. The symbols in Figure

78 correspond to data. For this test case, in the initial region with X/H = 1.0, the correlations with S/D = 1.0 show good agreement with the data. At X/H = 2.0, the correlations with S/D = 2.0 show excellent agreement with measured data.

The measured theta distributions for Test 31(b) with J = 26.13 are shown in Figure 79. The ratio of jet to total mass flow rate for this test is 0.213. At X/H_0 = 0.25, the jet penetration is 40 percent of the channel height. The jet penetration gradually increases to 50 percent of the duct height at X/H_0 = 1. The radial jet spreading rate towards the injection wall is much faster than that in the opposite direction. Comparing the theta distributions for slotted jet the 2-D slot (Figure 79) and those for orifice plate 01/04/04 (Figure 18 of Reference 5) at the comparable momentum flux ratio shows the substantially reduced mixing rate for the 2-D slot. The 0.5144 cm wide slot has the same geometrical area as orifice plate 01/02/08. Comparing the theta distributions for slotted jet (Figure 79) and those for orifice plate 01/02/08 (Figure 20 of Reference 5) reveals very similar characteristics. This suggests that the 2-D slot has mixing characteristics very similar to the orifice plate with S/D = 2.0, that has the same geometrical area.

The predicted theta distributions for Test No. 31(b) using the NASA/Aerojet correlations for one-sided injection with S/D = 1 and S/D = 2 are presented in Figure 80. At X/H_0 = 0.25, the predicted jet penetration is about 35 percent less than the measured value. The predicted theta profiles are in poor agreement with the data throughout the region of interest.

Figure 81 shows the measured theta distributions for Test 31(c) with J = 104.49. The ratio of jet-to-total mass flow rate for this case (equal to θ_{EB}) is 0.352. The measured jet penetration at X/H_0 = 0.25 is 50 percent of the channel height. The

slotted jet penetrates to about 65 percent of the channel height at $X/H_0 = 1.0$. Comparing the 2-D slot data (Figure 81) and those for orifice plate 01/02/08 at a comparable momentum flux ratio (Figure 22 of Reference 5) shows similar mixing characteristics, especially in the regions away from the jet injection plane ($X/H_0 > 1$).

The predicted theta distributions for Test 31(c) are presented in Figure 82. The predicted jet penetration at $X/H_0 = 0.25$ is about 20 percent smaller than the data. The predicted radial profiles show a reattachment of the jets towards the injection wall with little radial jet spreading in the opposite direction. The overall comparison between data and correlations is poor.

Test 32 corresponds to one-sided jet injection into an isothermal cross-flow in a constant area duct using square holes with 2.25 cm sides. The holes are spaced at a distance of 4 times the hole side. The geometric flow area of this orifice plate is the same as that of the 01/04/04 plate. The momentum flux ratio for Test 32 was 26.10. Figure 83 represents the measured theta distributions for Test 32. At $X/H_0 = 0.25$, the jet penetration is approximately 70 percent of the channel height, with little interaction between the adjacent jets. At $X/H_0 = 0.5$, the jets penetrate to the opposite wall, followed by rapid mixing, especially in the transverse direction. Comparing Figure 83 and the data for circular holes (Figure 18 of Reference 5) shows that the mixing characteristics for the square and circular orifices are similar. The effect of the orifice geometry are confined to the regions near the injection plane ($X/H_0 \leq 0.5$).

The predictions for this test case were obtained by using the NASA/Aerojet correlations, presented in Figure 84. The cor-

relations underestimate the jet penetrations at $X/H_0 = 0.25$ and 0.5. The difference between circular and square holes are seen in the centerplane profiles at $X/H_0 = 0.25$ and 0.5 near the injection wall (top) (see Figure 84 and Figure 19 of Reference 5). The theta profiles for circular holes have monotonic reduction in theta values near the top. The theta profiles for the square holes show the effects of hole shape at $X/H_0 = 0.25$ and 0.5. The correlations underestimate the jet spreading rates in the transverse direction. The predicted radial profiles beyond $X/H_0 = 0.5$ are in good agreement with the data.

Test 33 was performed with orifice plates 01/02/08 in aligned configuration, in a constant area duct having unbalanced momentum flux ratio of $J_T = 40.9$ and $J_B = 14.7$. The measured theta distributions for Test 33 are shown in Figure 85. At $X/H_0 = 0.25$, the measured jet penetrations for the top and bottom jets are 35 and 20 percent of the channel height, respectively. The jets show little interaction with the opposing jets. The jets gradually mix with the mainstream and reach equilibrium conditions ($\theta_{EB} = 0.3201$) at $X/H_0 = 2.0$. The momentum flux ratios for the top and bottom jets in Test 33 deviate by an equal amount about the average between the jets. (Compare with Test 2 for the average momentum flux ratio, shown in Figure 13). Comparing Figures 85 and 13 shows similarities in the theta distribution with the exception that the equivalent channel height (location of minimum theta value) for the two test cases are different. For Test 33, the equivalent channel height is 0.6 H_0 for the top jet. For the test case with balanced momentum flux ratio, the equivalent channel height is 0.5 H_0.

The predicted theta distributions for Test 33 are presented in Figure 86. At $X/H_0 = 0.25$, the predicted radial theta profile is in good agreement with the data. The predicted equivalent channel height (0.6 H_0 for the top injections) correlates well

with the data. At X/H_0 = 0.5 and 1.0, the correlations underestimate the jet spreading rate in the radial direction. The predicted theta variations in the transverse direction are larger than the measured variations. The overall agreement between data and correlations is good.

Test 34 corresponds to the same orifice configuration as Test 33. However, in Test 34 the momentum flux ratios for the top and bottom jets were 58.4 and 6.7, respectively. This test case provides a larger variation of momentum flux ratios about the average than those obtained in Test 33. The measured theta distributions for Test 34 are shown in Figure 87. At X/H_0 = 0.25, the jet penetrations for the top and the bottom injections are, respectively, 45 and 10 percent of the duct height. The interaction between the opposing jets is minimal at this station. Comparing the data for Test 33 (Figure 85) and Test 34 (Figure 87) shows similar theta distributions with the exception of the location of minimum theta values (equivalent channel height, Heq). The equivalent channel height for this case was 0.75 H_0 for the top injection.

The ratio of jet-to-mainstream mass flow rate and the nominal momentum flux ratios in Tests 33 and 34 are comparable to those in Test No. 2 (Figure 13). In Test 2, the two opposed rows of jets had equal momentum flux ratios. Comparison between Figure 13 (Test 2) and Figures 85 and 87 (Tests 33 and 34, respectively) show similar temperature distributions beyond X/H_0 = 1.0. In the regions closer to the jet injection plane, the jet penetrations for the top and the bottom injections are quite different for the three test cases. These test cases also have the same jet-to-mainstream mass flow rate as Test No. 6 of the Dilution Jet Mixing Program Phase I (Figure 22, Reference 5). In the latter, the same orifice plate was used with single-sided injection, having a momentum flux ratio of 107.8. The theta distribu-

tions for single-sided injection are substantially different from those for opposed injection with a comparable ratio of jet-to-mainstream mass flow rate.

The predicted theta distributions for Test 34 are presented in Figure 88. The predicted results underestimate the jet spreading rates in the transverse and radial directions. At X/H_0 = 0.25 and 0.5, the predicted and measured radial theta profiles are in good agreement. At X/H_0 = 0.25, the predicted and measured theta profiles show the location of mimimum theta values at about 75 percent of duct height. Beyond X/H_0 = 0.5, the predicted theta values are within 20 percent of the measured values. The overall agreement between data and correlations is good.

Tests 35 through 42 involve two-sided jet injection in an asymmetrically convergent duct (Test Section III). The orifice configuration and flow conditions for these tests are listed in Table VI. The configuration of Test Section III is shown in Figure 5. In these tests, the bottom wall of the test section was flat and the top wall inclined. The jet injection angles for the top and bottom injections were 116.6 and 90 degrees, respectively.

Test 35 was performed with orifice plate 01/02/08 in an aligned configuration having J_T = 26.24 and J_B = 25.93. The measured theta distributions for Test 35 are shown in Figure 89. At X/H_0 = 0.25, the jet penetration from the top is about 40 percent of the channel height, while the bottom jets penetrate to about 25 percent of the local duct height. The jets gradually interact with the adjacent jets and the mainstream and reach equilibrium conditions (θ_{EB} = 0.3185). Comparing the data for symmetric (Figure 53) and asymmetric ducts (Figure 89) shows that the theta distributions for the two convergent ducts are similar. This is

different from the characteristics observed for one-sided injection in Phase I of this program. The mixing characteristics for symmetric and asymmetric convergence with single sided rows of jets were different, especially with jet injection from inclined walls. The mixing characteristics for single-sided injection from flat walls were similar to those in a symmetrically convergent duct.

The predicted theta distributions for Test 35 are shown in Figure 90. The predictions were obtained from the correlations for converging cross-stream passages. Details of these correlations are given in Section 6.1.5. The predictions show deeper jet penetration from the flat wall injections (bottom jets) than from the inclined wall injections. However, the measured data do not show this trend. The predictions underestimate the jet mixing in the transverse direction. The predicted maximum theta values are larger than the data at $X/H_0 = 0.25$ and 0.5. At $X/H_0 = 1$, the data and correlations are in good agreement.

Figure 91 represents the measured theta distributions for Test 36. Test 36 was performed with orifice plates 01/02/08 in aligned configuration in Test Section III with $J_T = 107.4$ and $J_B = 107.8$. At $X/H_0 = 0.25$, the jets impinge against each other at mid channel followed by rapid mixing towards equilibium ($\theta_{EB} = 0.4902$). Comparing the data for symmetric (Figure 55) and asymmetric duct (Figure 91) cases show that the mixing characteristics for the two cases are similar. The convergent duct results also show enhanced mixing compared to the constant area duct.

The predicted theta distributions for Test 36 are shown in Figure 92. The correlations underestimate the jet penetration at $X/H_0 = 0.25$. The predicted results show deeper jet penetration for the flat wall injection. The correlations underestimate the

jet spreading rates in both radial and transverse directions. The predicted centerplane radial profiles correlate well with data at $X/H_0 = 1.0$.

Test 37 corresponds to two-sided injections (orifice plates 01/04/08) in a staggered arrangement ($J_T = 25.7$ and $J_B = 26.1$). The measured theta distributions for Test 37 are shown in Figure 93. The ratio of jet-to-total mass flow rate for this case is 0.1929. At $X/H_0 = 0.25$, the jet penetration is about 50 percent of local channel height for the bottom and top row of jets. The jets gradually mix with the mainstream and approach near equilibrium conditions ($\theta_{EB} = 0.1882$) at $X/H_0 = 1.0$.

The predicted theta distributions for Test 37 are shown in Figure 94. The predicted theta distributions show larger gradients in the transverse direction compared to the data. The predicted centerplane theta profile also shows larger radial gradients than the measured values. The predicted radial theta profile at $X/H_0 = 1$ gives good correlation with the data.

Test 38 was performed with orifice plates 01/04/08 in a staggered arrangement in the asymmetrically convergent duct, with $J_T = 109.2$ and $J_B = 110.0$. The ratio of jet-to-total mass flow rate (equal to θ_{EB}) was 0.3245. The measured theta distribution for this test case are presented in Figure 95. At $X/H_0 = 0.25$, the jets overpenetrate and impinge on the opposite wall. The theta distribution at the downstream stations rapidly reach equilibrium values. The measured theta values corresponding to the bottom jets are larger than those for the top injection at $X/H_0 = 0.25$. This is perhaps due to the improved mixing associated with the upstream injection from the top wall.

The predicted theta distributions for Test 38 are shown in Figure 96. The predicted results underestimate the jet penetra-

tion at $X/H_0 = 0.25$. However, the radial profiles at $X/H_0 = 0.5$ and 1.0 are in good agreement with the data. The predictions underestimate the mixing in the transverse direction. This trend has been observed in most of the test cases discussed so far.

Test 39 corresponds to two-sided injection with orifice plates 01/04/04 in staggered configuration in an asymmetric convergent duct. The momentum flux ratios for Test 39 are $J_T = 6.69$ and $J_B = 6.74$. The measured theta distributions for this test case are presented in Figure 97. AT $X/H_0 = 0.25$, the jet penetrations from the top and bottom injections are about 30 percent of the local channel height. At $X/H_0 = 1.0$, the theta profiles show significant deviations from equilibrium theta ($\theta_{EB} = 0.1994$). For this test case, at $X/H_0 = 0.25$ and 0.5, the measurements did not extend below $Y/H = 0.3$. The contour plotting routine extrapolates the profiles to obtain the theta distribution below $Y/H = 0.3$. This extrapolation method erroneously shows smaller jet penetration for the top injections. At the downstream stations, the jets gradually mix with the mainstream and the opposing jets. Note that the injections from the top (inclined) wall have a faster mixing rate compared to the bottom jets. The theta distributions are similar to those in a symmetrically convergent duct (Figure 61).

The predicted theta distributions for Test 39 are shown in Figure 98. The predicted theta distributions indicate smaller jet penetration for the injections from the top and underestimate the mixing rates in the transverse direction. The predicted centerplane radial profiles correlate well with the data.

Figure 99 depicts the measured theta distributions for Test 40. Test 40 corresponds to orifices plates 01/04/04 in a staggered configuration in Test Section III ($J_T = 25.99$ and $J_B = 25.05$). For this case, the jets overpenetrate to the opposite

wall at X/H_0 = 0.25. At the downstream stations, the jets rapidly mix with the mainstream and approach equilibrium conditions (θ_{EB} = 0.3247). The theta distributions are similar to those for a symmetric convergent duct (Figure 63).

The predicted theta distribution for Test 40 are presented in Figure 100. The correlations underpredict the jet penetration at X/H_0 = 0.25 and 0.5. As a result, the predicted centerplane theta profiles are in poor agreement with the data throughout the region of interest.

Tests 41 and 42 are two-sided injections with orifice plates 01/02/04 in aligned configuration using the asymmetrically convergent duct. Test 41 was performed with J_T = 6.64 and J_B = 6.68. The measured theta distributions for Test 41 are shown in Figure 101. At X/H_0 = 0.25, the jets penetrate to about 25 percent of the local channel height. The jets show little interaction with the opposing or adjacent jets. The jet spreading rate in the radial direction is faster than that in the transverse direction. Comparing the data for symmetric (Figure 65) and asymmetric convergent duct (Figure 101) shows the similarities in the mixing characteristics between the two convergent ducts.

The predicted results for Test 41 are shown in Figure 102. At X/H_0 = 0.25, the measured radial profiles shows deeper jet penetration for the top injection (0.4H) than the bottom jets (0.254). The predicted maximum theta values at X/H_0 = 0.25 are higher than the data. But the radial profiles show good qualitative agreement with the data. The agreement between the predicted and measured radial profiles improves at the downstream stations. The predicted jet spreading rates in the transverse direction are also in good agreement with data.

Figure 103 represents the measured data for Test 42. Test 42 corresponds to inline injections with orifice plates 01/02/04 in Test Section III, having J_T = 26.25 and J_B = 26.34. For this test, the jets impinge against each other near midchannel at X/H_0 = 0.25, followed by enhanced mixing at X/H_0 = 0.5 and 1.0. The theta distributions for Test 42 (shown in Figure 103) are similar to those in a symmetically convergent duct (Figure 67).

The predicted theta distributions for Test 42 are presented in Figure 104. The predicted results underestimate the radial spreading of the jets. At X/H_0 = 0.25, the data shows deeper jet penetration for the inclined wall injection. The inclined wall jets are injected into a region where the mainstream momentum is lower. Hence, the penetration of the inclined wall jets are deeper than the flat wall injections. The predicted radial profiles are only in qualitative agreement with the data for this test case.

The test cases discussed above correspond to two-sided injections into an isothermal mainstream in an asymmetrically convergent duct. The following two test cases were performed with single-sided injections into asymmetrically convergent duct with profiled mainstream. In these two test cases (Test 43 and 44) a "top hot" profile was used and the jets were injected from the flat wall with orifice plate 01/02/04. Test 43 corresponds to a momentum flux ratio of 6.26. The measured theta distributions for Test 43 are presented in Figure 105. At X/H_0 = 0.25, the peak theta value (jet centerline) is located approximately at 40 percent of the local duct height away from the flat wall. The jets gradually mix with the mainstream at the downstream stations. At X/H_0 = 1.0, the theta profiles have nearly uniform distribution in the transverse direction. The radial theta profiles at that station are strongly influenced by the mainstream theta profile.

The predicted theta distributions for Test 43 are shown in Figure 106. In obtaining the predictions, the mainstream theta profiles were superimposed on the theta distributions given by the NASA/Aerojet correlations. At X/H_0 = 0.25, the predicted jet penetration is in good agreement with the data. But, at this axial location, the data shows slightly lower values for the centerplane theta. The predicted and measured half inlets are in good agreement at this plane. At X/H_0 = 0.5 and 1.0, the predicted radial profiles do not agree exactly with the data. Most of the differences between data and correlations occur near the fan wall where the mainstream is colder. The predicted results show a slower mixing rate in the transverse direction compared to the measurements.

Test 44 corresponds to the same orifice configuration as Test 43, but the momentum flux ratio is 24.24. The measured theta distributions for Test 44 are shown in Figure 107. At X/H_0 = 0.25, the peak theta value is located at about 60 percent of the local duct height. For this test case, the jet spreading rate in the transverse direction is much faster than that in the radial direction. The dominating influence of the mainstream temperature profile is clearly seen in the oblique plots. The predicted theta distributions for Test 44 are presented in Figure 108. At X/H_0 = 0.25, the predicted jet penetration (peak theta location) agrees well with the data. The predicted centerplane theta profile is also in excellent agreement with the measurements. At X/H_0 = 0.5 and 1.0, the predicted centerplane theta profiles show slower radial mixing compared to measurements. The predicted results also show a slower mixing rate in the transverse direction compared to the measurements.

Test 45 corresponds to single-sided injection into an isothermal cross-flow in a constant area duct (Test Section I) using 1.024 cm-wide two-dimensional slot. This slot has the same geo-

metrical area as orifice plate 01/02/04. Three different momentum flux ratios were studied in this test case. Test 45(a) corresponds to the case with a momentum flux ratio of 6.66. The measured theta distributions for this test are presented in Figure 109. At X/H_0 = 0.25, the slotted jet penetrates to about 30 percent of the duct height. The jet penetration does not increase beyond 0.3 H_0 at the downstream stations. The width of the slot in Test 45 is twice the slot width used in Test 31. Comparing Tests 45(a) (Figure 109) and 31(a) (Figure 77) shows that the jet penetration with the 1.024 cm-wide slot is about 50 percent higher than that for the 0.5144 cm-wide slot. Furthermore, in Test 45(a), the ratio of jet-to-total mass flow ratio (equal to θ_{EB}) is 0.2179 while the corresponding value in Test 31(a) was 0.1213.

The 1.024 cm-wide 2-D slot has the same geometrical area as orifice plate 01/02/04. A comparison of the theta distributions for the 2-D slot (Figure 109) and those for orifice plate 01/02/04 at comparable momentum flux ratio (Figure 12 of Reference 5) shows similar mixing characteristics, especially in regions beyond X/H_0 = 1.0.

The predicted theta distributions for Test 45(a) are shown in Figure 110. The predictions were obtained from NASA/Aerojet correlations with S/D = 1 and S/D = 2. In Figure 110, the solid lines represent the correlations for S/D = 1.0 and the broken lines correspond to predictions with S/D = 2.0. The symbols in this figure correspond to the data. The predicted jet penetrations are higher than the data. The predicted peak theta values are much higher than the measured values. However, the differences between data and predictions become less with increasing downstream distance, X/H_0.

Figure 111 represents the measured theta distributions for Test 45(b) with J = 25.34. At X/H_0 = 0.25, the jet penetrates to approximately 40 percent of the duct height. The jet penetration increases to 50 percent of duct height at X/H_0 = 1. The mixing characteristics at this momentum flux ratio are similar to those at J = 6.6. The comparison of the data for 1.024 cm-wide slot (Figure 111) and that for 0.5144 cm-wide slot (Figure 79) show that the jet penetrations for the wider slot at a comparable momentum flux ratio is the same as that of 0.5144 cm-wide slot. However, the peak theta values are different, since the jet-to-total mass flow ratio in Test 45(b) is 0.3462, while the corresponding value for the narrow slot is 0.2129.

Figure 111 and Figure 14 of Reference 5 show the differences in the mixing characteristics of a 2-D slot and orifice plate 01/02/04, respectively. For both of these plates, the radial profiles are similar at X/H_0 = 2.0. But, in the regions closer to the jet injection plane, orifice plate 01/02/04 has larger gradients in the theta values in both radial and transverse directions compared to those observed for the 2-D slot.

The predicted theta distributions for Test 45(b) are shown in Figure 112. The predicted results overestimate the jet penetration by about 50 percent of the data at X/H_0 = 0.25. However, the agreement between the predicted and measured radial profiles improve in the downstream stations. At X/H_0 = 2.0, the predicted radial profile correlates well with the data.

Test 45(c) corresponds to a momentum flux ratio of 78.33 with a 1.024 cm-wide slot. The measured theta distributions for this test case are presented in Figure 113. The jet penetration at the momentum flux ratio of 78.33 increases from 45 to 60 percent of the duct height, between X/H_0 = 0.25 and 1.0. At this momentum flux ratio, the jet spreading rate in the regions away

from the injection wall is much larger than those observed at lower momentum flux ratios. The ratio of jet-to-total mass flow rate for this test case is 0.482. The comparison between the data for wide (Figure 113) and the narrow slots (Figure 81) at comparable momentum flux ratios shows very similar theta distributions for the two cases.

The predicted theta values for Test 45(c) are presented in Figure 114. The predicted jet penetrations are much higher than those given by the measurements at X/H_0 = 0.25 and 0.5. The predicted peak theta value at X/H_0 = 0.25 agrees well with the data. Beyond X/H_0 = 1.0, the predicted radial profile is in good agreement with the data. The correlations for the narrower slot give good results for low momentum flux ratios, but for the high momentum flux ratios the predictions are in better agreement with the data in the regions closer to the jet injection plane. The predicted results for the wider slot give better correlations with the data at the higher momentum flux ratios, and the predicted profiles are in better agreement with the data in regions away from the jet injection station.

Tests 46 through 48 correspond to two-sided injection with orifice plates 01/02/04 in aligned configuration. The jets from the two sides had equal momentum flux ratios and were injected into an isothermal cross-flow in a constant area duct. Test 46 represents the test case with J_T = 6.70 and J_B = 6.70. The measured theta distributions for Test 46 are shown in Figure 115. At X/H_0 = 0.25, the jets penetrate to about 30 percent of channel height. They show little interaction with the opposing jets. In this test case, the jet spreading rate in the transverse direction is much higher than that in the radial direction. At X/H_0 = 2, the theta distribution is nearly constant with the equilibrium value (θ_{EB} = 0.3299). Comparing the mixing characteristics in the constant area (Figure 115), asymmetric conver-

gent (Figure 101) and symmetrically convergent ducts (Figure 65) shows that the constant area duct has slower mixing rates than the convergent ducts, especially in the transverse direction.

The predicted theta distributions for Test 46 are shown in Figure 116. The predicted jet penetrations are much higher than the data. However, the predicted peak theta values compare favorably with the data. The jet spreading rate in the radial direction is underpredicted by the correlations. The overall agreement between the data and correlations for Test 46 is poor.

Figure 117 presents the measured theta distributions for Test 47, using orifice plates 01/02/04 in aligned configuration with J_T = 25.56 and J_B = 25.74. At X/H_0 = 0.25, the jets impinge with the opposing jets at midchannel. The transverse mixing rate at the downstream stations are enhanced. The comparison between the data in the constant area (Figure 117), asymmetric convergent (Figure 103) and symmetric convergent duct (Figure 67) demonstrates the enhanced mixing due to flow area convergence.

The predicted results for Test 47 are shown in Figure 118. The agreement between predicted and measured theta distributions for this case is very good throughout the region of interest.

Figure 119 represents the measured theta values for Test 48. Test 48 was performed with orifice plate 01/02/04 in aligned configuration (J_T = 84.18 and J_B = 83.92). At X/H_0 = 0.25, the opposing jets impinge against each other at midchannel, followed by enhanced mixing in the transverse direction. At X/H_0 = 2, the theta values are nearly constant at the equilibrium value (θ_{EB} = 0.6327).

The predicted theta distributions for Test 48 are shown in Figure 120. The predictions slightly underestimate the radial

jet spreading rates. The jet spreading in the transverse direction is correctly predicted by the correlations. The overall agreement between data and correlations for this test case is very good.

In the NASA Dilution Jet Mixing Program Phase I (Reference 5), it was observed that for single-sided jet injections, the mixing characteristics of orifice plates with the same S/H ratio were similar. This observation was based upon the data from two orifice plates (01/02/04 and 01/04/08), with S/H = 0.5. To increase the data base for S/H = 0.5, it was considered essential to study the mixing characteristics of single-sided injection in a straight duct with orifice plate 01/03/06. For this orifice plate, the orifice diameter was 1.796 cm with orifice spacing of 5.08 cm, (S/D = 2.83 and H/D = 5.67). Test 49 was performed with orifice plate 01/03/06, having J = 6.49. The measured theta distributions for Test 49 are presented in Figure 121. At X/H_0 = 0.25, the jet penetration is about 35 percent of duct height. The jets have little interaction with the adjacent jets at this station. At the downstream stations, the jet penetration increases to 40 percent of duct height with attendant spreading in radial and transverse directions. The comparison between the theta distributions for orifice plates 01/03/06 (Figure 120) and 01/02/04 (Figure 12 of Reference 5) show similar theta distributions. The similarity in the theta distributions is also seen between orifice plates 01/03/06 (Figure 120) and 01/04/08 (Figure 25 of Reference 3). Since both of these orifice plates have the same ratio of orifice spacing to duct height, S/H_0, of 0.50, then mixing characteristics are also expected to be similar (see Reference 5).

For Test 49, the predicted theta distributions were obtained from NASA/Garrett correlations. The predicted results for Test 49 are shown in Figure 122. The predicted jet penetrations and

the jet spreading rates are accurately predicted by the correlations. The predicted radial jet spreading rate correlates well with the data. The correlations slightly overestimate the peak theta values. The overall agreement between the data and correlations is good within engineering accuracy.

The measured theta distributions for Test 50 are shown in Figure 123. Test 50 was performed with orifice plate 01/03/06 at J = 25.48. The jet penetration at X/H_0 = 0.25 is about 55 percent of the channel height. The jets gradually interact with the mainstream and approach equilibrium conditions (θ_{EB} = 0.2054) at X/H_0 = 2.0. The comparison between orifice plates 01/03/06 (Figure 123), 01/02/04 (Figure 14 of Reference 5), and 01/04/08 (Figure 24 of Reference 5) show similar theta distributions. Although these three test cases have comparable momentum flux ratios for the same S/H ratio, the values of jet-to-total mass flow rates, $\dot{m}_j/\dot{m}_{Total}$ are different. Orifice plate 01/04/08 has the smallest value (0.1048) of jet-to-total mass flow rate, while the orifice plate 01/02/04 has the largest value (0.2705). Consequently, the peak theta values for the three cases are also different. The peak theta values are proportional to the ratio of jet-to-total mass flow rate.

The predicted theta distributions for Test 50 are shown in Figure 124. At X/H_0 = 0.25, the predicted radial profile is in good agreement with the data. The predicted jet penetrations at X/H_0 = 0.25 to 1.0 are less than the data. The peak theta values are overpredicted by the correlations. The overall correlation between data and predictions is good.

During the Phase II test results evaluation, another test case was selected. This test (Test 51) was performed with orifice plates 01/04/04 in an aligned configuration, using the constant cross-sectional area duct, having momentum flux ratios

J_T = 6.67 and J_B = 6.58. The measured theta distributions for this test case are shown in Figure 125. At X/H_0 = 0.25, the jet penetrations are about 35 percent of the duct height and the jets interact with the opposing jets. However, little interaction exists with adjacent jets from the same side the theta contours show similar characteristics between X/H_0 = 0.25 and 1.0. Beyond X/H_0 = 1.0, the mixing is enhanced in the transverse direction. The comparison between in-line (Figure 125) and staggered injections (Figure 69) at the low momentum flux ratio of 6.7 shows that the mixing rate for the in-line configuration is significantly slower than that for the staggered arrangement.

The predicted theta distributions for Test 51 are shown in Figure 126. At X/H_0 = 0.25, the jet penetrations are over-estimated by the correlations. The correlations predict jet impingement at X/H_0 = 0.25, while the data does not show such characteristics. However, at the downstream stations, the predicted centerplane radial theta profiles are in good agreement with the data. The jet spreading rates in the transverse direction are underestimated by the model. The overall correlation between data and predictions for Test 51 is good.

One of the important parameters in the dilution jet mixing problem is the turbulence intensity. Detailed flow field calculation of dilution jet mixing flow field requires initial conditions of turbulence intensities. In order to define the initial profiles of turbulence kinetic energy, it was deemed essential to measure the turbulence intensities of the cross flow using hot-wire probes.

Hot-wire measurements were made in the constant area duct (Test Section I) using a TSI X-wire probe (TSI Model 1050 system). The tests were conducted with the profile generator installed in the rig. The mainstream flow was set at 0.4982 kg/

sec at an average temperature of 319°K, resulting in an average mainstream velocity of 14.9 M/S. The flow through the profile generator was set to zero. The turbulence measurements were made at a station upstream of the jet injection plane ($X/H_0 = -1.625$). The measured non-dimensionalized turbulence intensities $\overline{u}^2$ and $\overline{w}^2$ are presented in Figure 127. This figure shows an increased turbulence intensity caused by the wake behind the profile generator lip. The turbulence intensity profiles show an anisotropic turbulence structure in that region. In the region corresponding to the core of the mainstream, the turbulence structure is essentially isotropic with a turbulence intensity of about 6.5 percent. Although the turbulence intensities are higher in the wake region behind the step, they are not expected to change the temperature distributions significantly in the mixing region. This was demonstrated in one of the tests in Phase I. It is also important to note that the higher values of turbulence intensities in the region behind the profile generator will be reduced significantly if the profile generator lip were removed.

5.4.1 Test Series 8 Conclusions

Confined jet mixing characteristics were studied for a number of orifice plate configurations. These tests included two-dimensional slots, square holes and other orifice plate configurations of interest that were not included in Test Series 1 through 7. The following conclusions are obtained from these tests.

- Mixing is enhanced with a staggered arrangement as compared with an aligned configuration for two-sided injections using orifice plate 01/04/04.

- The mixing characteristics of square orifices are similar to those for circular orifices of the same flow

area and orifice spacing. The effects of orifice shapes are confined to regions near the jet injection plane ($X/H_0<1$).

- The mixing characteristics with two-sided injections in an asymmetrically convergent duct are similar to those in a symmetrically convergent duct. The penetration of the jets injected from the inclined wall is slightly deeper than these for the jets issuing from the flat wall.

- For all orifice plates tested in this program, the flow area convergence enhances mixing, due to the effects of a strong favorable pressure gradient.

- The mixing characteristics for in-line orifice configurations with unbalanced momentum flux ratios are very similar to those for the same configurations with balanced momentum flux ratios, having the same ratio of jet-to-total mass flow rate. The major difference between the balanced and unbalanced configurations is the location of minimum theta (H_{eq}). The correlations accurately predict the equilvalent duct height, H_{eq}, for the test cases investigated.

- The jet penetration and mixing characteristics for two-dimensional slots are similar to those for orifice plate with S/D = 2, having the same geometrical area as the two-dimensional slot. This is especially true in the far field ($X/H_0>1$) of the mixing zone. In the regions near the injection plane, the two-dimensional slot has significantly reduced mixing rates as compared to a row of discrete circular jets with the same geo-

metrical area. The jet penetrations for 2-D slots are deeper than those for a row of discrete circular jets.

- For single-sided injection into a convergent duct with profiled mainstream, the mixing characteristics are strongly influenced by the mainstream temperature profile.

- The mixing characteristics of orifice plate 01/03/06 (S/D = 2.83, H_0/D = 5.66) are similar to those for the 01/02/04 plate (S/D = 2, H_0/D = 4) at the same momentum flux ratio.

- The correlations developed in this program for two-sided injections predict the theta distributions to first order accuracy. They provide a useful dilution zone design tool. However, improvements in their accuracy are needed for applications involving flow area convergence and staggered injections.

- For single-sided injections, the NASA/Aerojet correlations are applicable and provide a useful design tool for practical combustors.

- For two-dimensional slots, the NASA/Aerojet correlations using S/D = 1 predict the radial profiles within first-order accuracy.

6.0 JET MIXING CORRELATION DEVELOPMENT

A number of empirical and semiempirical models are available in the literature (References 6 through 14) for predicting jet interaction with cross flow. Most of these models are applicable only to a limited range of geometrical and flow parameters. Some of the models (References 8, 10, 12, 13, and 14) have been shown to give trajectory predictions that are in agreement with experimental data. These models provide insight into the entrainment and jet spreading characteristics, but rarely provide sufficient information to quantify the flow field in the coordinates of interest.

Due to the rapid advances in computational fluid dynamics, multidimensional Navier-Stokes Solutions are available (References 16 and 17) for complex flows, such as jets-in-cross-flow. These models are in the developmental stage and need further extensive validation efforts. The multidimensional models are time consuming and are not cost-effective for the designer at present.

Empirical models are available in the literature (References 2, 4, and 17) for applications to combustor dilution zones. These models are limited within the geometrical and flow parameters of the generating experiments and must be used with caution outside the range of their applicability. Among these models, the correlations developed by Holdeman, et al (Reference 2) are a useful and powerful tool for designing the dilution zone of practical combustors. The correlations obtained in Reference 2 were applicable to a single-sided row of jets injected into a confined cross flow. These correlations have been used to identify and optimize the major geometrical and flow parameters for single-sided injection of jets into a confirmed cross flow. A review of

the measured effects of momentum flux ratio, mainstream temperature profile, flow area convergence, and configurations of opposed jet injections are provided in Reference 19. For opposed rows of jets in aligned configurations with equal momentum flux ratios, the centerplane of the duct can be assumed to be the plane of symmetry. The effective duct height for this configuration becomes 0.5 H_0. By using the effective duct height, the correlations developed in Reference 2 can be used to predict the temperature distributions for opposed jet injections. In the present program, these predictions with effective duct height were found to give poor agreement with the data. By further modifying the correlations obtained in Reference 2, it is possible to improve their agreement with the data. The correlations developed in this program are derived from the NASA/Aerojet model and are described in Paragraph 6.1.

6.1 NASA/Garrett Correlations

The correlations developed in this program use the same nomenclatures as those employed by Holdeman and Walker (Reference 2) and are applicable to both in-line and staggered orifice configurations. Paragraph 6.1.1 describes the correlations applicable to in-line arrangements with isothermal mainstream conditions. Paragraph 6.1.2 describes the correlations for staggered injections. The correlations for non-uniform mainstream profiles are discussed in Paragraph 6.1.3 while converging duct correlations are given in Paragraph 6.1.4. In the correlations with two-sided injection, the subscript "T" refers to the top injections and the subscript "B" refers to the bottom injections.

6.1.1 Correlations for In-line Injections into Isothermal Cross Flow

The parameter used to describe the temperature distribution is the nondimensional temperature difference, theta (θ), defined as

$$\theta = \frac{T_m - T}{T_m - T_j} \tag{1}$$

where:

θ = Theta, nondimensional temperature difference at a point in the flow field

T_m = Mainstream stagnation temperature

T_j = jet stagnation temperature

T = stagnation temperature at a point in the flow field

Theta is a measure of the temperature suppression in the flow field. The value of theta can vary from one, when measured temperature equals the jet temperature, to zero, when the measured temperature equals the main stream temperature. The largest values of theta in any profile correspond to the coolest regions of the flow.

If complete mixing of the jet and mainstream flow occurs, the value of theta will be constant and the temperature will be everywhere equal to the ideal equilbrium temperature between jet and mainstream. Thus,

$$\theta_{EB} = \frac{T_m - T_{EB}}{T_m - Tj} \tag{2}$$

where:

θ_{EB} is the ideal equilibrium theta.

$$T_{EB} = \frac{\dot{m}_{j_T} T_{j_T} + \dot{m}_{j_B} T_{j_B} + \dot{m}_m T_m}{\dot{m}_{j_T} + \dot{m}_{j_B} + \dot{m}_m} \tag{3}$$

The mixing characteristics for in-line injections are similar to those with single-sided injections, with the duct height reduced to an equilvalent height, H_{eq}. For the top row of jets, the equivalent duct height has been obtained by Wittig (Reference 20) as

$$(H_{eq})_T = \frac{A_T\sqrt{J_T}}{A_T\sqrt{J_T} + A_B\sqrt{J_B}} \cdot H_0 \tag{4}$$

where:

H_0 = Duct height at the jet injection plane.
A_T = Effective area of the top injections.
and A_B = Effective area of the bottom injections.

$$(H_{eq})_B = H_0 - (H_{eq})_T \tag{5}$$

The theta distribution in the duct is then defined by

$$\theta_T = \theta \quad \text{for} \quad 0 \leq Y/H_0 \leq \frac{(H_{eq})_T}{(H_0)} \tag{6}$$

$$\theta_B = \theta \quad \text{for} \quad \frac{(H_{eq})_T}{H_0} \quad \frac{Y}{H_0} \quad 1.0 \tag{7}$$

The empirical model for the three-dimensional flow is expressed in nondimensionalized self-similar form as:

$$\theta = \theta^{\pm}_{min} + (\theta_c - \theta^{\pm}_{min}) \exp \left[\left(-\ln 2\right) \left(\frac{Y - Y_c}{W^{\pm}_{1/2}} \right)^2 \right] \tag{8}$$

This expression is applicable to both top and bottom injections. In this equation, θ_c, $\theta^{\pm}_{min}$, Y_c, and $W^{\pm}_{1/2}$ are scaling parameters as shown in Figure 128. θ_c is the maximum temperature difference ratio in the radial (vertical) profile, and Y_c is its location. Y_c represents the position of the jet centerline. Here, θ^{+}_{min} and θ^{-}_{min} are the minimum dimensionless temperature difference beyond and before the jet centerline, respectively.

Since the flow is confined, the entrainment characteristics of the jets are not necessarily symmetrical about the jet centerlines. Thus, the half widths $W^{+}_{1/2}$ and $W^{-}_{1/2}$ are different for top and bottom injections. But, for the temperature profile to be continous,

$$\left(\theta^{+}_{min}\right)_T = \left(\theta^{+}_{min}\right)_B. \tag{9}$$

The correlations describe the scaling parameters as functions of independent variables J, S/D, H_{eq}/D, X/H_{eq}, and Z/S. The scaling parameters are nondimensionalized by using the effective jet diameter, $D_j = D\sqrt{c_d}$.

Correlations for Predicting Centerplane Temperature Profiles:

(A) Jet Centerline Trajectory

$$\left(\frac{y_{c,o}}{D_j}\right) = a_1 \; J^{0.25} \left(\frac{S}{D_j}\right)^{0.14} \left(\frac{H_{eq}}{D_j}\right)^{0.38} \left(\frac{X}{D_j}\right)^{0.17} e^{-b} \qquad (10)$$

where,

$$b = 0.091 \left(\frac{X}{H_{eq}}\right)^2 \left(\frac{H_{eq}}{S} - \frac{\sqrt{J}}{3.5}\right)$$

$$a_1 = \text{Min} \left[0.3575 \left(1 + \frac{S}{H_{eq}}\right), \; 0.715\right]$$

Recommended value in Reference 2 was $a_1 = 0.539$.

(B) Centerline Temperature Difference Ratio:

$$\theta_{c,o} = \theta_{EB} + \left(1 - \theta_{EB}\right) \left[a_2 \, J^{-0.35} \left(\frac{X}{D_j}\right)^{-1}\right]^f \qquad (11)$$

where,

$$f = 1.15 \sqrt{\frac{S}{H_{eq}} \Big/ \left(1 + \frac{S}{H_{eq}}\right)}$$

$$a_2 = 1 + S/H_{eq}$$

Recommended value in Reference 2 was $a_2 = 1.452$.

Here, $\theta_{EB} = \left(\frac{T_m - T_{EB}}{T_m - T_j}\right)$; $T_{EB} = \left[\frac{\dot{m}_m T_m + \dot{m}_{j_T} T_{j_T} + \dot{m}_{j_B} T_{j_B}}{\dot{m}_m + \dot{m}_{j_T} + \dot{m}_{j_B}}\right]$ (12)

(C) Centerplane Half Width

$$\frac{W^{+}_{1/2}}{D_j} = 0.1623 \left(\frac{S}{D_j}\right)^{-0.25} \left(\frac{H_o}{D_j}\right)^{0.5} \left(\frac{X}{D_j}\right)^{0.5} J^{0.18} \tag{13}$$

$$\frac{W^{-}_{1/2}}{D_j} = 0.20 \left(\frac{S}{D_j}\right)^{0.27} \left(\frac{H_o}{D_j}\right)^{0.5} \left(\frac{X}{D_j}\right)^{0.12} J^{0.15} \tag{14}$$

(D) Minimum Centerplane Temperature Difference Ratio

$$\frac{\theta^{+}_{min}}{\theta_{c,o}} = 1 - e^{-c^{+}} \tag{15}$$

where,

$$c^{+} = a_3 J^{1.62} \left(\frac{S}{D_j}\right)^{1.5} \left(\frac{X}{D_j}\right)^{1.1} \left(\frac{H_{eq}}{D_j}\right)^{-3.67} \tag{16}$$

$$a_3 = 0.038 \quad \text{if} \quad \left(\frac{Y_{c,o}}{D_j} + \frac{W^{+}_{1/2}}{D_j}\right) \leq \frac{H_{eq}}{D_j} \tag{17}$$

$$a_3 = 0.038 \left(\frac{H_o}{H_{eq}}\right)^{3.67} \quad \text{if} \quad \left(\frac{Y_{c,o}}{D_j} + \frac{W^{+}_{1/2}}{D_j}\right) > \frac{H_{eq}}{D_j}$$

Recommended value in Reference 2 was $a_3 = 0.038$

The above modification ensures that when the jets penetrate close to H_{eq}, the Gaussian curve for the positive part of the theta profile (Figure 128) approaches a nearly flat profile. Furthermore, when the jets penetrate close to H_{eq}, the test data shows that the value of θ^{-}_{min} also approaches the value of $\theta_{c,o}$. This characteristic is modeled by the following expression:

$$\frac{\theta^-_{min}}{\theta_{c,o}} = 1 - e^{-c^-} \tag{18}$$

where,

$$C^- = C_o \qquad \text{if} \left(\frac{Y_{c,o}}{D_j} + \frac{W^+_{1/2}}{D_j} \right) \leq \frac{H_{eq}}{D_j} \tag{19}$$

$$C^- = C_o Q \qquad \text{if} \left(\frac{Y_{c,o}}{D_j} + \frac{W^+_{1/2}}{D_j} \right) > \frac{H_{eq}}{D_j}$$

$$C_o = 1.57\ J^{-0.3} \left(\frac{S}{D_j} \right)^{-1.4} \left(\frac{X}{D_j} \right)^{0.9} \tag{20}$$

$$Q = \exp \left[0.22 \left(\frac{X}{H_{eq}} \right)^2 \left(\frac{\sqrt{J}}{5} - \frac{S}{H_{eq}} \right) \right]$$

(E) Off-Centerplane Penetration

$$\frac{Y_{c,Z}}{Y_{c,o}} = 1 - \left(\frac{Z}{S/2} \right)^2 e^{-g} \tag{21}$$

where,

$$g = a_4\ J^{0.67} \left(\frac{S}{D_j} \right)^{-1} \left(\frac{X}{D_j} \right)^{0.54} \tag{22}$$

$$a_4 = 0.227$$

(F) Off-Centerplane Maximum Temperature Difference Ratio

$$\frac{\theta_{c,Z}}{\theta_{c,o}} = \left(1 - \frac{Z}{S/2} \right)^2 e^{-d} \tag{23}$$

where,

$$d = a_5 \; J^{0.53} \left(\frac{S}{D_j}\right)^{-1.53} \left(\frac{X}{D_j}\right)^{0.83} \tag{24}$$

$$a_5 = 0.452$$

Furthermore, $$\frac{\theta^{\pm}_{min,Z}}{\theta_{c,Z}} = \frac{\theta^{\pm}_{min,o}}{\theta_{c,o}} \tag{25}$$

For obtaining θ_T or θ_B in equations (16) and (17), the appropriate values of J_T or J_B and $(H_{eq})_T$ or $(H_{eq})_B$ are used in the equations (10) through (24).

6.1.2 Correlations for Staggered Injections

For staggered injections,

$$(H_{eq})_T = (H_{eq})_B = H_o \tag{26}$$

Let $$\theta_T = \frac{T_m - T_T}{T_m - \bar{T}_j}, \qquad \theta_B = \frac{T_m - T_B}{T_m - \bar{T}_j} \tag{27}$$

where T_T and T_B are the local temperature due to top or bottom injections only.

Assumption: Let T be the actual local temperature due to both top and bottom injections.

$$\theta = \frac{T_m - T}{T_m - \bar{T}_j} = \left(\frac{\frac{1}{2}\dot{m}_m + \dot{m}_{j_T}}{\dot{m}_m + \dot{m}_{j_T} + \dot{m}_{j_B}} \right) \theta_T + \left(\frac{\frac{1}{2}\dot{m}_m + \dot{m}_{j_B}}{\dot{m}_m + \dot{m}_{j_T} + \dot{m}_{j_B}} \right) \theta_B \quad (28)$$

For the top and bottom jets, T_{EB} is obtained from

$$\left(T_{EB}\right)_T = \left(\frac{\frac{1}{2}\dot{m}_m T_m + \dot{m}_{j_T} T_{j_T}}{\frac{1}{2}\dot{m}_m + \dot{m}_{j_T}} \right) \quad (29)$$

$$\left(T_{EB}\right)_B = \left(\frac{\frac{1}{2}\dot{m}_m T_m + \dot{m}_{j_B} T_{j_B}}{\frac{1}{2}\dot{m}_m + \dot{m}_{j_B}} \right) \quad (30)$$

For staggered injections, equations 10 through 24 can be used to predict the theta distributions. The equivalent channel height for staggered injection is equal to the duct height. The following modifications of the empirical constants are recommended to improve the agreement between data and correlations by assuming that the effective orifice spacing for staggered injections is S/2.

$$a_2 = 1.506 \quad (31)$$

$$a_4 = 0.454 \quad (32)$$

The correlations presented in Paragraphs 6.1.1 and 6.1.2 are applicable only for isothermal mainstream conditions. They provide a useful design tool for predicting radial profiles. The correlations for staggered injections need further refinements.

6.1.3 Correlations for Nonuniform Mainstream Temperature Profiles

The NASA/Garrett correlations described in Paragraph 6.1 were derived for a uniform flow area and uniform mainstream condition. When a nonuniform mainstream temperature profile exists, the NASA/Garrett correlations for theta, θ_{NG}, can be assumed to represent the changes in the local mainstream temperature distribution by dilution jets. In other words,

$$\theta_{NG} = (T_m(y) - T) / (T_m(y) - T_j) \qquad (33)$$

Here, θ_{NG} represents the results from equation (8).

For flows with nonuniform profiled mainstream, the ratio of actual temperature change to the maximum possible temperature change due to the jets is obtained from the following definition of nondimensionalized temperature difference ratio:

$$\theta = (T_{max} - T) / (T_{max} - T_j) \qquad (34)$$

where:

T_{max} = Maximum stagnation temperature of the undisturbed mainstream profile

T = Local stagnation temperature

T_j = Jet stagnation temperature.

Using equation (34), the profiled mainstream theta, $_m(y)$, can be defined as

$$\theta_m(y) = [T_{max} - T_m(y)] / (T_{max} - T_j) \qquad (35)$$

From equations (33), (34), and (35) it is seen that

$$\theta = \theta_m(y) + [1 - \theta_m(y)] \quad \theta_{NG} \tag{36}$$

Equation (36) is used to generate the predicted theta values for test cases in Series 2 and 4. It is important to note that the variation of the nondimensionalized temperature, θ, is conveniently scaled between 0.0 and 1.0. The nondimensional temperature distribution, θ_{NG}, is obtained from the NASA/Garrett correlations (Equation 8).

6.1.4 Correlations for Inclined Wall Injections

For inclined wall injections, the following sketch schematically represents the generalized injection configurations with wall inclinations being α_T and α_B for the top and bottom walls, respectively.

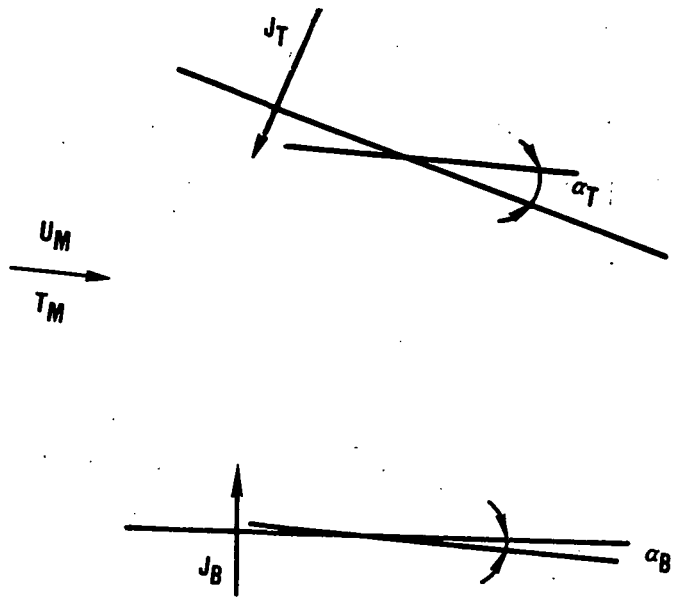

Mass injected upstream = $\dot{m}_{j_T} \sin \alpha_T + \dot{m}_{j_B} \sin \alpha_B$ (37)

Assuming this component completely mixes with the mainstream, the average mainstream temperature, T_{main}, is given by

$$T_{main} = \frac{\dot{m}_m T_m + \dot{m}_{j_T} \sin \alpha_T T_{j_T} + \dot{m}_{j_B} \sin \alpha_B T_{j_B}}{\dot{m}_m + \dot{m}_{j_T} \sin \alpha_T + \dot{m}_{j_B} \sin \alpha_B} \quad (38)$$

From the measured mainstream pressure and T_{main}, the mainstream density is computed.

Total cross flow rate = $\dot{m}_m + \dot{m}_{j_T} \sin \alpha_T + \dot{m}_{j_B} \sin \alpha_B$ (39)

From equation (39), U_m is computed.

At the injection plane, the effective momentum flux ratios for top and bottom jets are:

$$(J_T)_{eff} = \frac{\dot{m}_{j_T} V_{j_T} (\cos \alpha_T)^2 / A_{j_T}}{\rho_m U_m^2} \quad (40)$$

and

$$(J_B)_{eff} = \frac{\dot{m}_{j_B} V_{j_B} (\cos \alpha_B)^2 / A_{j_B}}{\rho_m U_m^2} \quad (41)$$

The effective momentum flux ratios are used in the correlations to predict the theta distributions.

At low Mach numbers, the average mainstream velocity increases by the relation

$$V_m(x) = U_{m_o} \frac{A_o}{A(x)} \quad (42)$$

where U_{mo} and A_o are the mainstream velocity and cross-sectional area at the jet injection plane, respectively.

Thus,

$$\rho_m(x)\ V_m^2(x) = \rho_m\ U_{m_o}^2 \left(\frac{A_o}{A(x)}\right)^2 \tag{43}$$

and the equivalent momentum flux ratio, $J_{eq}(x)$, is given by

$$J_{eq}(x) = \frac{\rho_j\ V_j^2}{\rho_m(x)\ V_m^2(x)} = \frac{\rho_j\ V_j^2}{\rho_o\ V_{m_o}^2} \left(\frac{A(x)}{A_o}\right)^2$$

or,

$$J_{eq}(x) = Jo \left(\frac{A(x)}{A_o}\right)^2 \tag{44}$$

The convergence tends to improve the mixing, especially in the transverse direction. To correctly model this effect, the constant a_5 in equation (24) should be increased by the expression,

$$a_5 = 0.452 \left(\frac{A_o}{A(x)}\right) \tag{45}$$

For convergent ducts, $J_{eq}(x)$ is used in the place of J in the NASA/Garrett correlations and equation (45) is used for a_5. This approach was found to give improved agreement with the data.

7.0 CONCLUSIONS AND RECOMMENDATIONS

Phase II of the NASA Dilution Jet Mixing Program was directed towards a better understanding of the mixing process in the dilution zone of gas turbine combustion systems. The tests performed in this program provide a data base for developing analytical models. An improved correlation based on these test data has been developed for two-sided jets injected into a confined cross-flow. The following conclusions are drawn from these tests:

- The jet penetration for two-sided injections are less than that for single-sided injections, but the jet spreading rates are faster at a given momentum ratio for the same orifice plate.

- The jet spreading rate in the transverse direction is faster with in-line configuration than with staggered arrangement for a given orifice plate.

- For the orifice plate with S/D = 2 and $H_0/D = 8$, the mixing characteristics with in-line and staggered configurations are very similar at a given momentum ratio. This is due to the small orifice spacing (S/D = 2).

- The mixing characteristics for orifices with S/D = 4 show substantial differences between in-line and staggered configurations: the jet spreading rate in the radial direction is slightly faster for staggered arrangement compared to that for in-line configuration.

- For constant momentum ratio, the comparison between data for single- and two-sided injections shows that for in-line injections, the optimum ratio of orifice spacing to duct height, S/H_0, is one-half of the opti-

mum value for single-sided injections. For staggered injections, the optimum S/H_0 ratio is twice the optimum value for single-sided injection. The optimum value of S/H_0 for single-sided injection has been shown to be (Reference 15)

$$(S/H_0)_{OPT} \cong 2.5/ J$$

- The temperature distribution in the jet mixing region with two-sided injections is strongly influenced by the mainstream temperature profile. The jet spreading rates with profiled mainstream are similar to those with uniform mainstream. This suggests that a superposition scheme may be used to predict the temperature distributions with profiled mainstream.

- Jet mixing is enhanced by flow area convergence. The jet spreading rates in the radial and transverse direction, of a convergent duct, occurs within a shorter distance from the jet injection plane than in the case of a straight duct. This is due to the acceleration caused by favorable pressure gradients.

- The jet mixing characteristics with asymmetric convergence are very similar to those in symmetrically convergent duct with the same area reduction. For the asymmetrically convergent duct with two-sided injection, the jet penetrations from the inclined wall are slightly deeper than that issuing from the flat wall.

- The mixing characteristics for in-line configurations with unbalanced momentum ratio are very similar to those with balanced momentum ratio with the same orifice plate. The major difference between the two con-

ditions lies in the value of equivalent channel height, H_{eq}.

- The jet mixing characteristics of square orifices are very similar to those of circular orifices with the same geometrical area and orifice spacing to diameter ratio, S/D.

- The jet penetration and mixing characteristics of two-dimensional slots are very similar to those for the orifice plate with S/D = 2, having the same geometrical area as the two-dimensional slot. This is especially true in the far field ($X/H_0 > 1$) of the mixing region. In the regions near the jet injection plane, the two-dimensional slot has reduced mixing rates compared to the equivalent area orifice plate with S/D = 2.

- For single-sided injection into a convergent duct with profiled mainstream, the mixing characteristics are strongly influenced by the mainstream temperature profile.

- The jet mixing characteristics for orifice plate 01/03/06 (S/D = 2.83, $H_0/D = 5.66$) are similar to those for orifice plate 01/02/04 (S/D = 2, $H_0/D = 4$) at the same momentum ratio.

- The correlations developed in this program predict the temperature distributions within first-order accuracy.

The correlations are quite accurate for in-line configurations. For staggered arrangements of jets, the correlations give qualitatively correct results, but further efforts are needed to improve their quantitative agreement with the data.

- For in-line injections, the expression suggested by Wittig (Reference 20) for equivalent channel height is in good agreement with the tests performed in this program.

- For the tests with profiled mainstream, the superposition of mainstream profile on the NASA/Garrett correlations for isothermal mainstream conditions yields results that are in agreement with the data within engineering accuracy.

- For the tests involving flow area convergence, the modified NASA/Garrett correlations with equivalent momentum ratio, J_{eq}, provide improved predictions of temperature distributions. However, this model does not correctly account for the effects of jet injection angle. Further refinements of the correlations are needed to address this deficiency.

- For single-sided injections, the NASA/Aerojet correlations predict qualitatively correct theta distributions for situations involving flow area convergence and profiled mainstream. Those correlations (using S/D = 1) accurately predict the far field ($X/H_0 > 1$) radial profiles for two-dimensional slots. The correlations using S/D = 1 give better agreement than those obtained by using S/D = 2.

The correlations developed in this program are based on the NASA/Aerojet correlations for single-sided injections. They provide a very useful and simple analytical tool for designing the dilution zone of a combustor. These correlations are applicable to a wider range of combustor configurations. However, additional work is needed to improve the accuracy of the correlations.

This Page Intentionally Left Blank

REFERENCES

1. Holdeman, J. D., R. E. Walker, and D. L. Kors, "Mixing of Multiple Dilution Jets with a Hot Primary Airstream for Gas Turbine Combustors," AIAA Paper 73-1249, Las Vegas, Nevada 1973 (also NASA TM X-71426).

2. Holdeman, J. D., and R. E. Walker, "Mixing of a Row of Jets with a Confined Cross-Flow," AIAA Journal, Vol. 15, No. 2, Feb. 1977, pp. 243-249.

3. Walker, R. E., and D. L. Kors, "Multiple Jet Study, Final Report," NASA CR-121217.

4. Walker, R. E., and R. G. Eberhardt, "Multiple Jet Study Data Correlations," NASA CR-134795, 1975.

5. Srinivasan, R., A. Berenfeld, and H. C. Mongia, "Dilution Jet Mixing Phase 1 Report," Garrett Turbine Engine Company, Phoenix, Arizona, Garrett 21-4302, Nov. 1982, (NASA CR-168031).

6. Kamotani, Y., and I. Greber, "Experiments on a Turbulent Jet in a Cross-Flow," AIAA Paper 72-149.

7. Ricou, R. P., and D. B. Spalding, "Measurements of Entrainment by Axisymmetrical Turbulent Jets," Journal of Fluid Mechanics II, 25-32 (1961).

8. Kamotani, Y., and I. Greber, "Experiments on Confined Turbulent Jets in Cross-Flow," NASA CR-2392 (1974).

9. McAllister, J. D., "A Momentum Theory for the Effect of Cross-Flow on Incompressible Turbulent Jets," Ph.D. Thesis (University of Tennessee, 1968).

10. Abramovich, G. N., The Theory of Turbulent Jets, Cambridge, Massachusetts, MIT Press, 1963.

11. Keffer, J. F., and W. D. Baines, "The Round Turbulent Jet in a Cross-Wind," J. Fluid Mech. 15, 481-496 (April 1963).

12. Stoy, R. L., and Y. Ben-Haim, "Turbulent Jets in a Confined Cross-Flow," J. Fluids Eng. 95, 551-556 (December, 1973).

13. Sucec, J., and W. W. Bowley, Prediction of the Trajectory of a Turbulent Jet Injection into Cross-Flowing Stream," J. Fluids Eng. 98, 667-673 (December, 1976).

14. Novick, A. S., J. S. Arvin, and R. E. Quinn, "Development of a Gas Turbine Combustor Dilution Zone Design Analysis," AIAA Paper 79-1194, June 1979.

15. Claus, R. W., "Analytical Calculation of a Single Jet in Crossflow and Comparison with Experiment," AIAA Paper 83-0238, January 1983 (NASA TM 83027).

16. Srinivasan, R., et al., "Aerothermal Modeling Program: Phase I Final Report," Garrett Turbine Engine Company, Phoenix, Arizona, Garrett 21-4742, Aug. 1983 (NASA CR-168243).

17. Cox, G. B., Jr., "Multiple Jet Correlations for Gas Turbine Engine Combustor Design," Journal of Engineering for Power, Vol. 98, No. 2, 1976, pp. 265-273.

18. Holdeman, J. D., "Perspectives on the Mixing of a Row of Jets with a Confined Crossflow," AIAA Paper 83-1200, June 1983 (NASA TM 83457).

19. Holdeman, J.D., R. Srinivasan, and A. Berenfeld, "Experiments in Dilution Jet Mixing," AIAA Paper 83-1201, June, 1983.

20. Wittig, S. L. K., O. M. F. Elbahar, and B. E. Noll, "Temperature Profile Development in Turbulent Mixing of Coolant Jets with a Confined Hot Cross-Flow," ASME Paper No. 83-GT-39, Mar. 1983.

LIST OF SYMBOLS

A	Test section cross-sectional area at survey plane
D	Geometric orifice diameter
D_j	Effective orifice diameter
H_o	Duct height at the jet injection plane
H	Local duct height at the survey plane
H_{EQ}	Local equivalent channel height
J	Momentum flux ratio $\rho_j V_j^2 / \rho_m V_m^2$
P_t	Stagnation pressure
P_s	Static pressure
S	Orifice spacing
T	Temperature
V	Velocity
X	x direction, parallel to duct axis
Y	y direction, parallel to orifice centerline (radial direction)
Z	z direction, normal to duct axis (transverse direction)

Greek

θ	Temperature difference ratio
ρ	Density
α	Jet injection angle

Subscripts

av	average
EB	Equilibrium value
j	Jet property

max	Maximum
m	Cross-flow property, average value
T	Top dilution jets
B	Bottom dilution jets

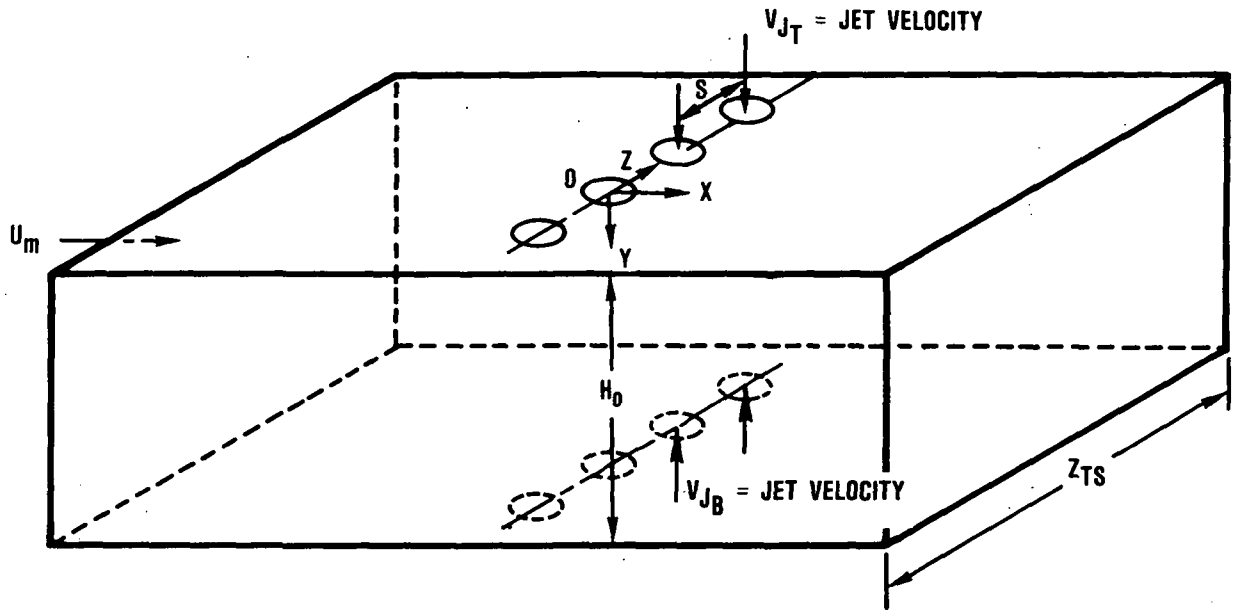

COORDINATE ORIGIN IS LOCATED AT CENTER OF ORIFICE

U_m, ρ_m, T_m	=	MAINSTREAM VELOCITY, DENSITY, AND TEMPERATURE
V_j, ρ_j, T_j	=	INITIAL JET VELOCITY, DENSITY, AND TEMPERATURE
H_0	=	TEST-SECTION HEIGHT AT INJECTION PLANE
H	=	TEST-SECTION HEIGHT AT ANY X-Y PLANE
S	=	ORIFICE SPACING ALONG Z (TRANSVERSE) DIRECTION
D	=	ORIFICE DIAMETER
D_j	=	$\sqrt{C_D}$ D
Z_{TS}	=	TEST-SECTION TRANSVERSE DIMENSION = 305mm

Figure 1. Multiple Jet Study Coordinate System and Important Nomenclature.

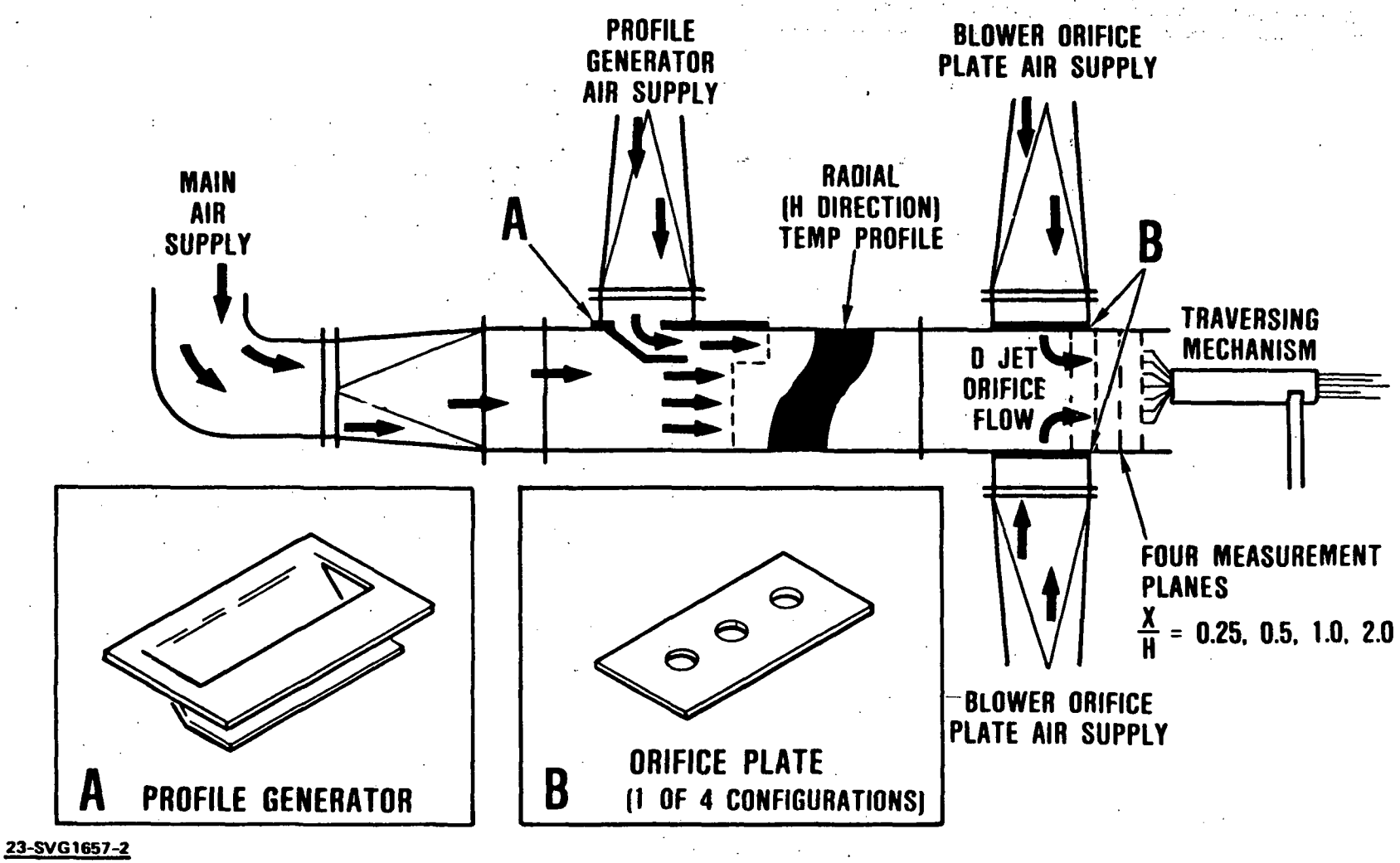

Figure 2. Dilution Jet Mixing Rig Schematic.

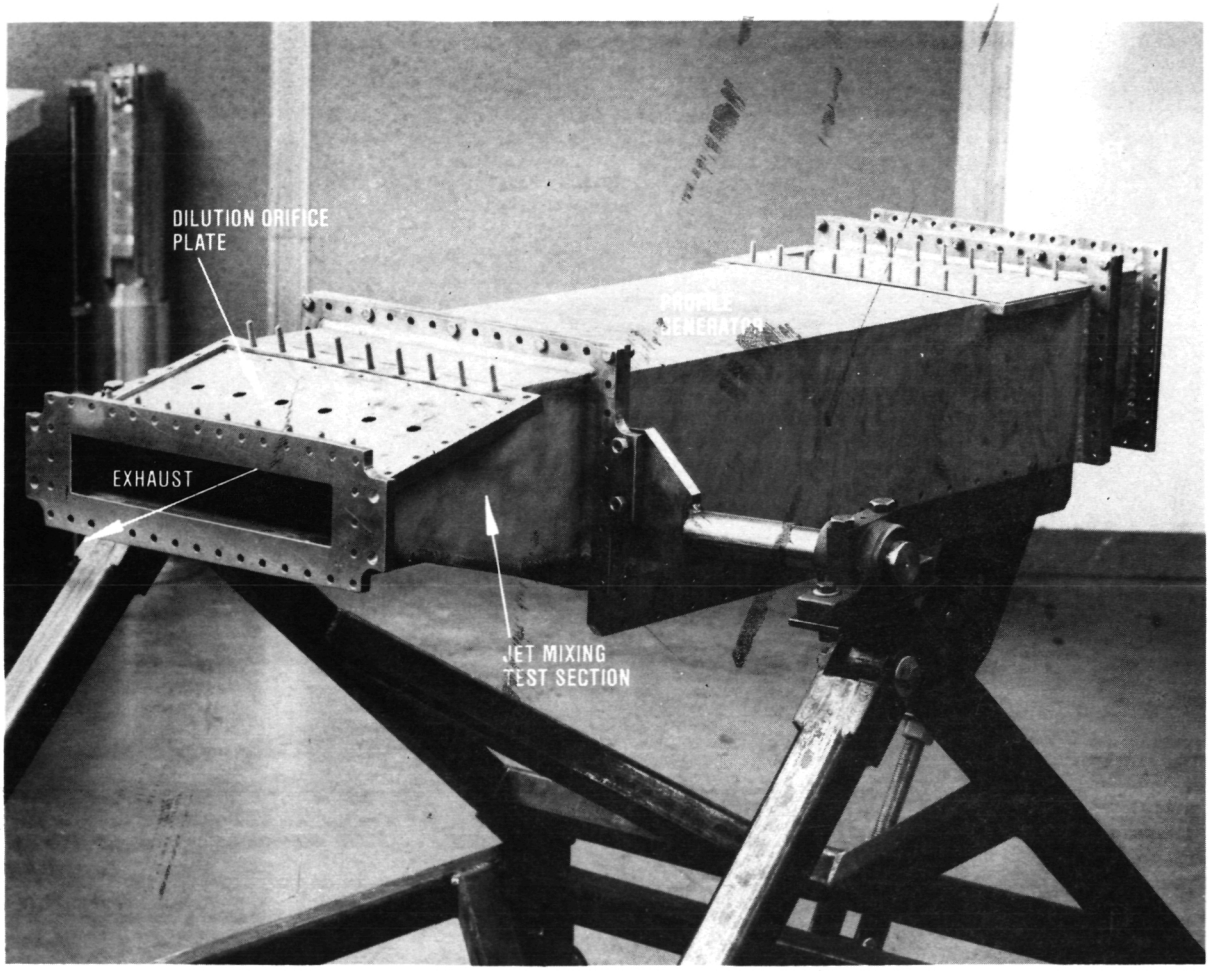

Figure 3. Partially Assembled Dilution Jet Mixing Test Rig.

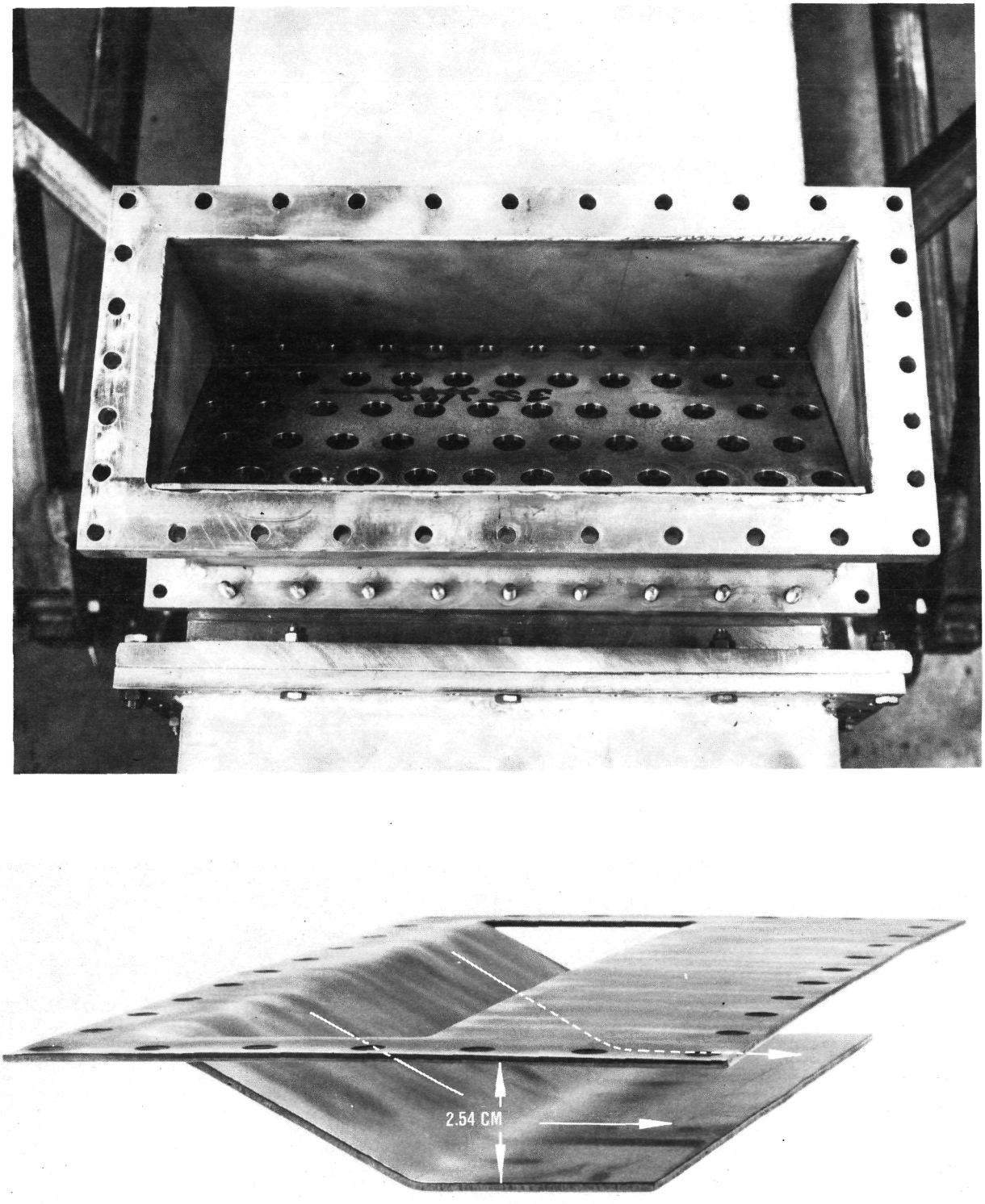

Figure 4. Profile Generator.

MP-81932

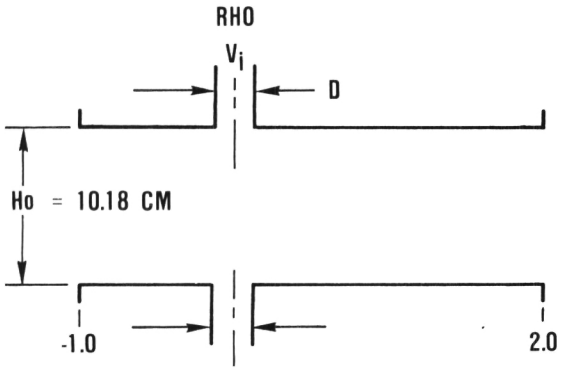

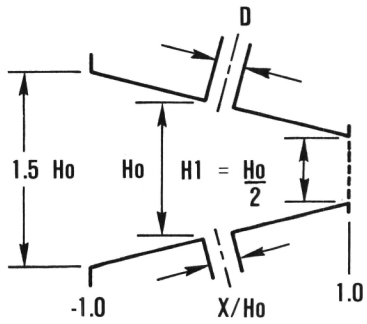

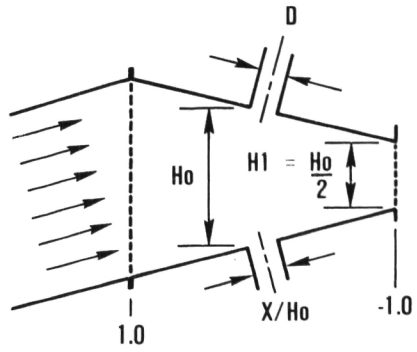

TEST SECTION I

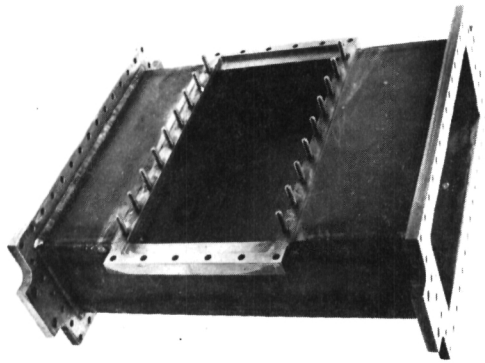

TEST SECTION II

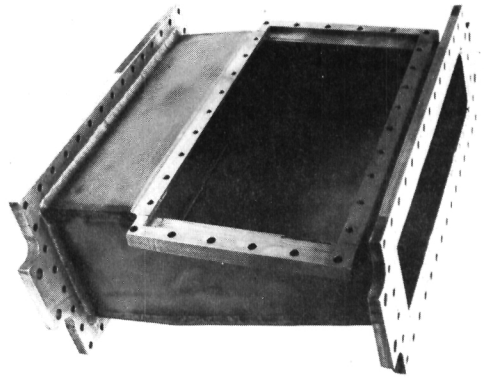

TEST SECTION III

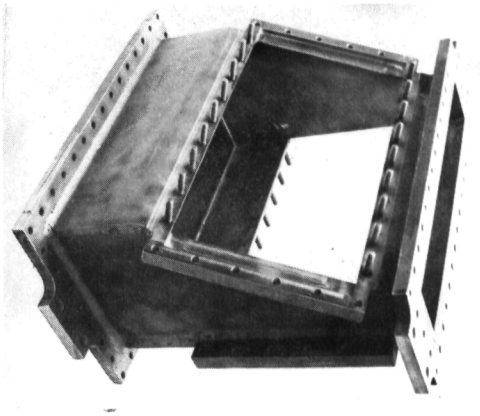

Figure 5. Jet Mixing Test Sections, H_0 = 10.16 cm.

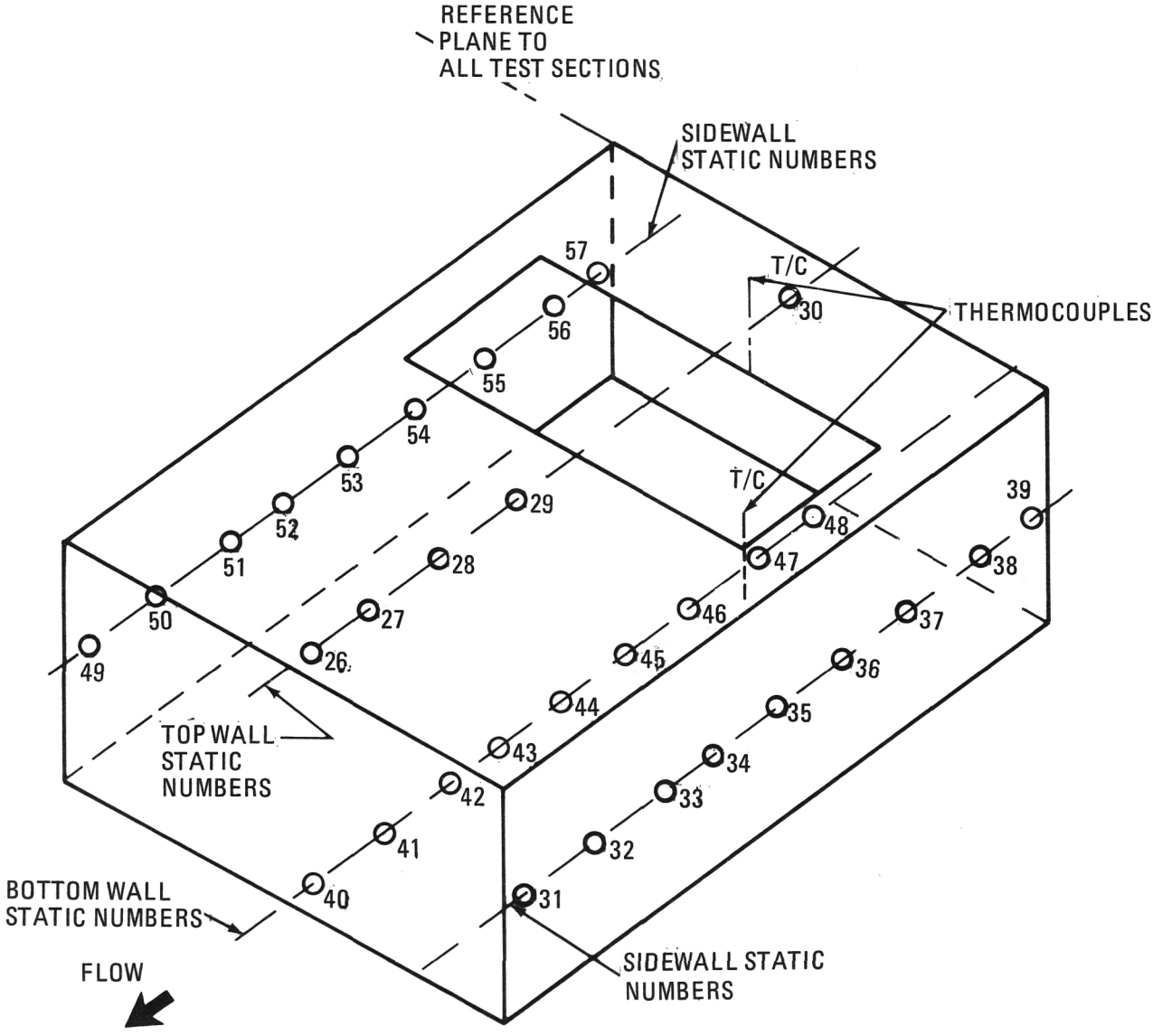

Figure 6. Wall Statics and Thermocouples for Test Section I.

[a] PLATE 01/04/04

[b] PLATE 01/02/04

[c] PLATE 01/04/08

[d] PLATE 01/02/08

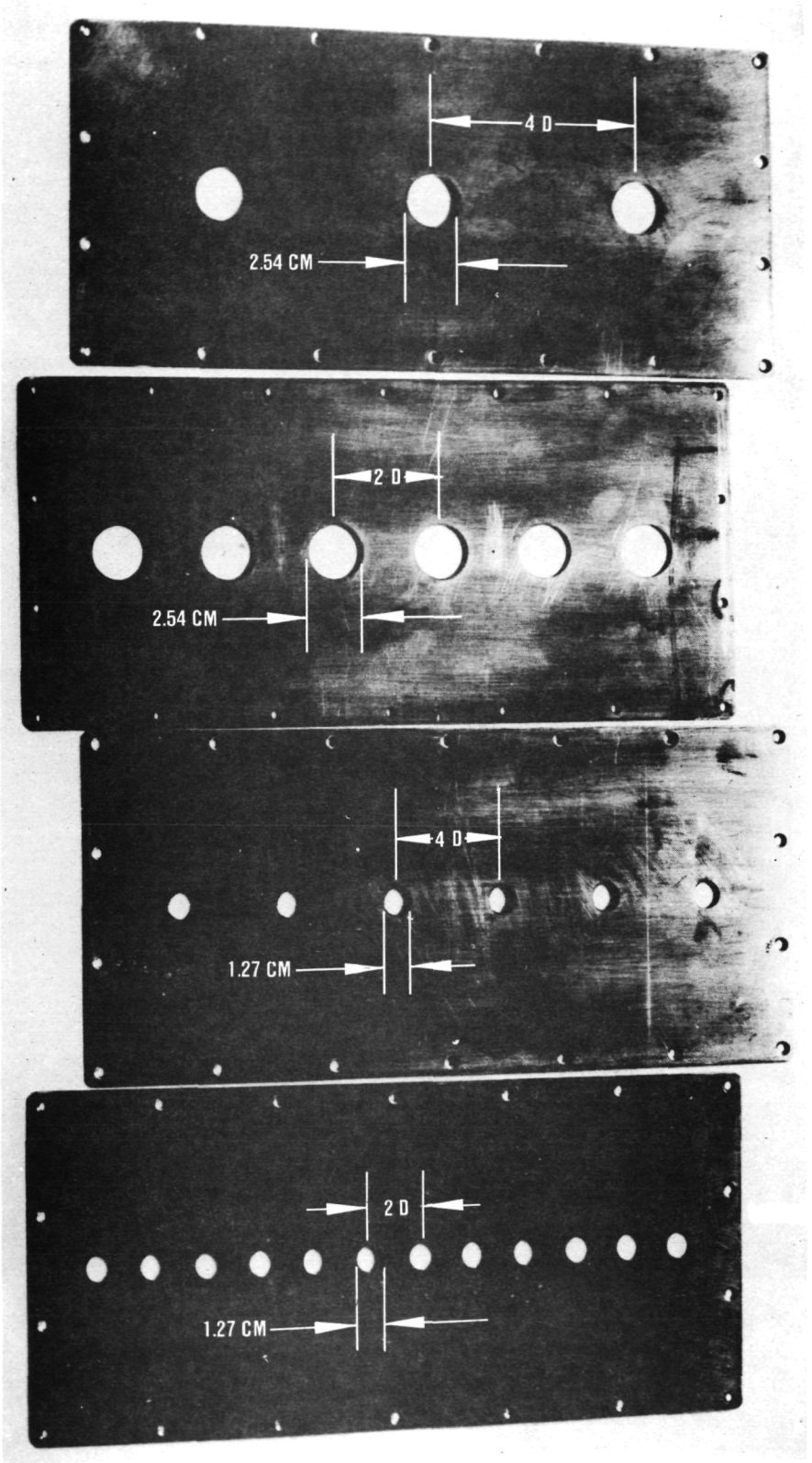

Figure 7. Dilution Orifice Plate Configurations.

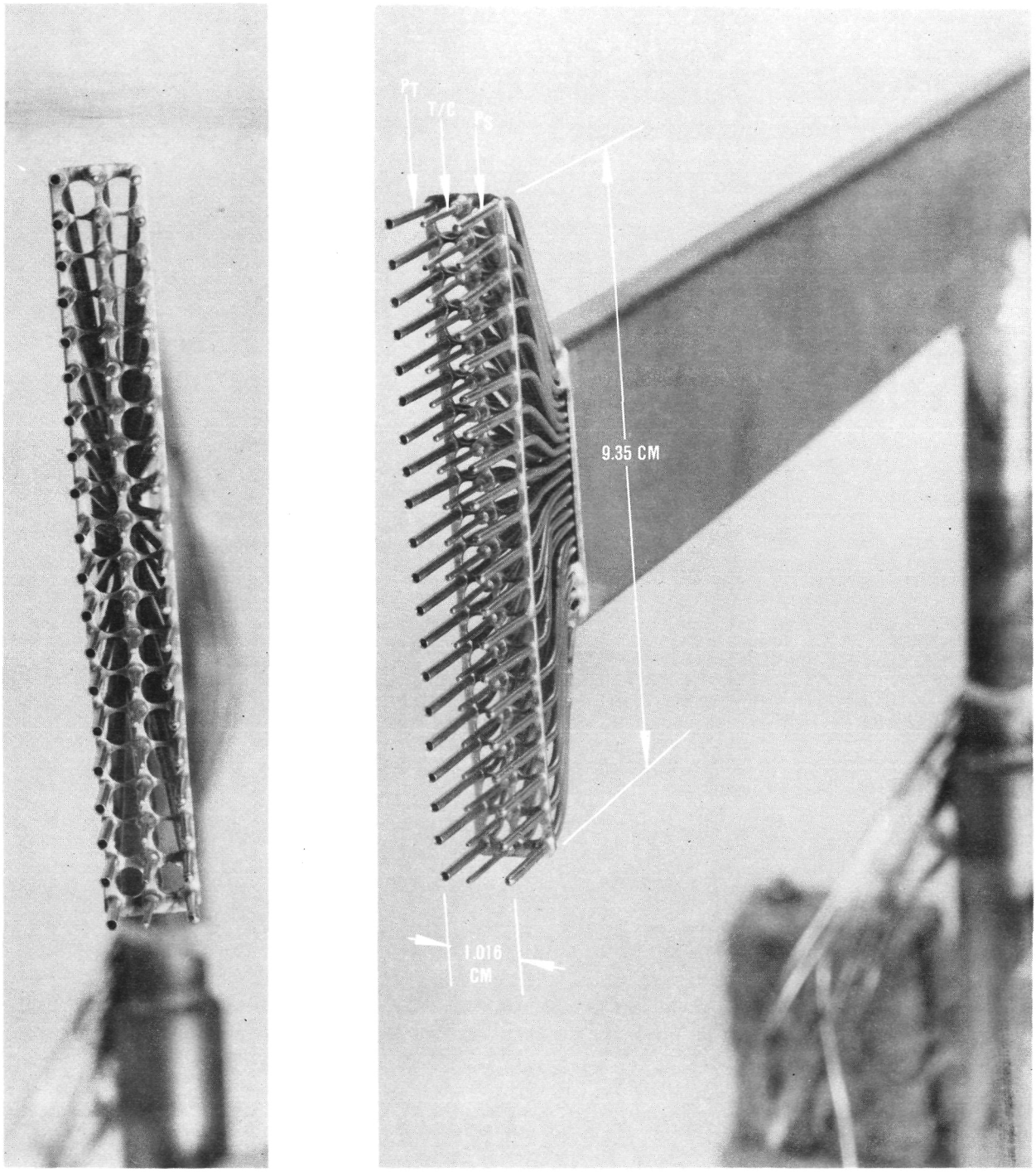

Figure 8. Total Pressure, Thermocouple, and Static Pressure Rake.

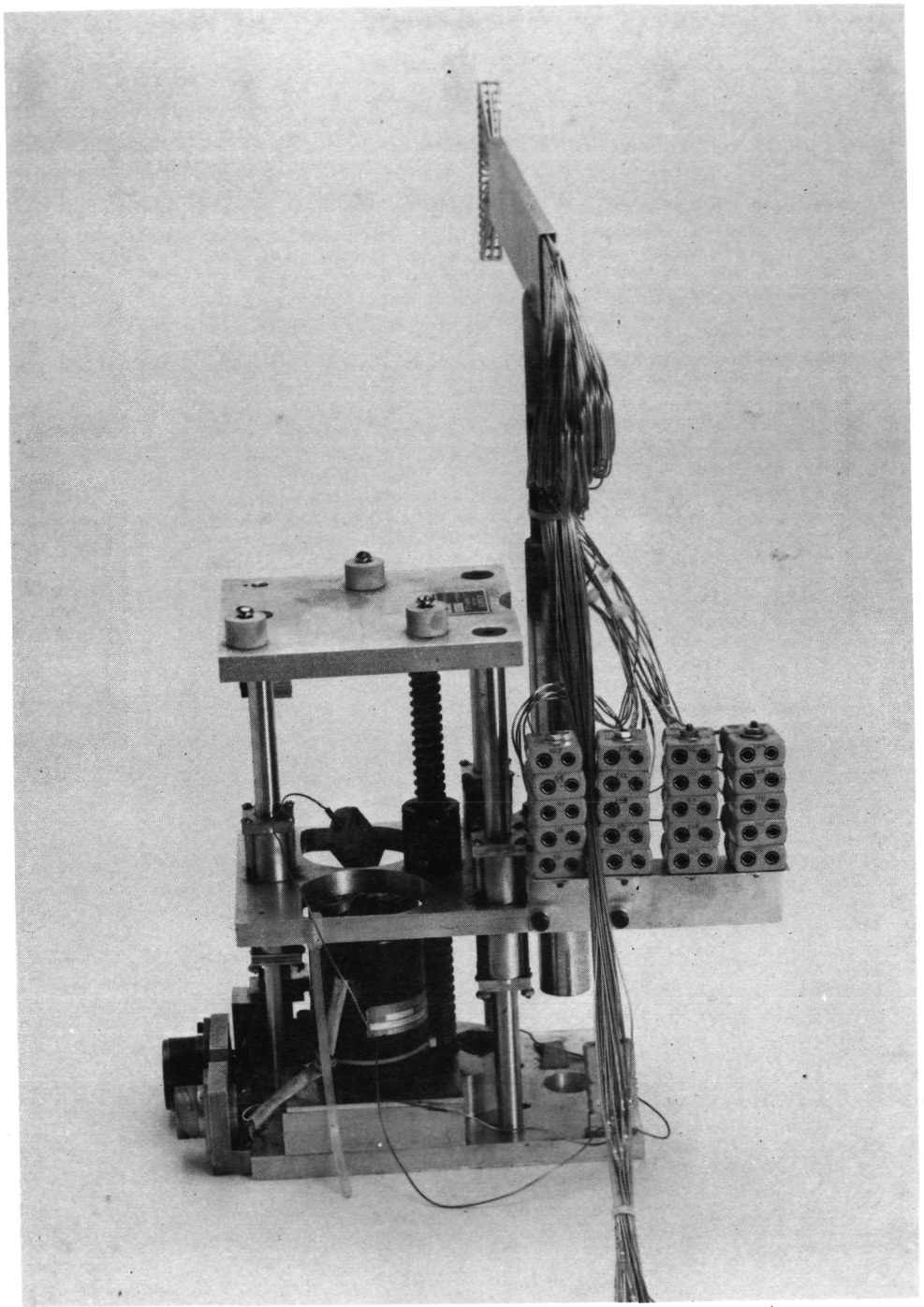

Figure 9. X-Y-Z Actuator with the Rake Mounted Thereon.

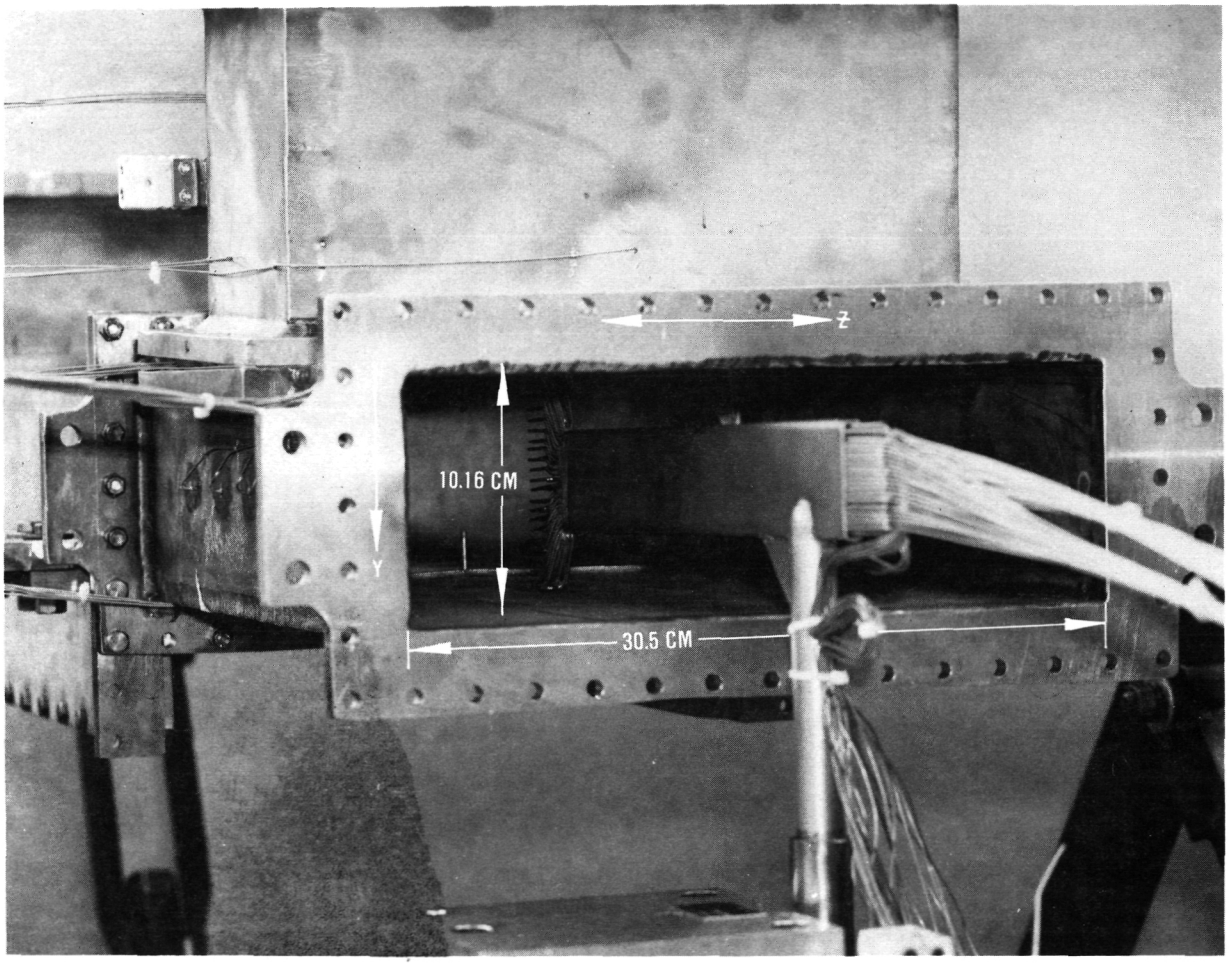

Figure 10. Jet Mixing Rig as Viewed from Rig Discharge End.

S = 0.0254 METERS S/DJ = 2.452 H0/DJ = 9.810 VMAIN = 15.5 M/SEC VJET = 28.1 M/SEC TMAIN = 645.9 K TJET = 310.4 K THEB = 0.1983 BLORAT= 3.848 DENRATIO= 2.087 TRATIO= 0.480

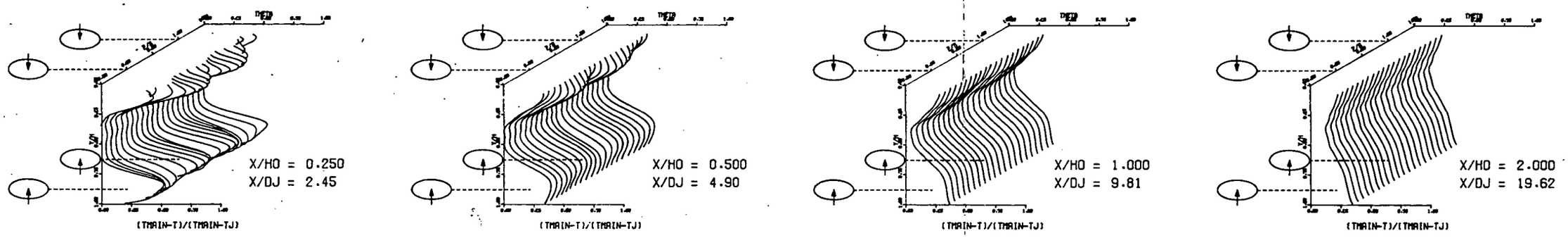

MEASURED THETA PROFILES FOR TEST NO.1, TEST SECTION I,TM=CONST (INL) , J = 6.81 , S/D = 2.00 , H/D = 8.00

CONTOUR	1	2	3	4	5	6	7	8	9	10	11
VALUE	0.0500	0.1000	0.1500	0.1982	0.2500	0.3000	0.3500	0.4000	0.4500	0.5000	0.6000

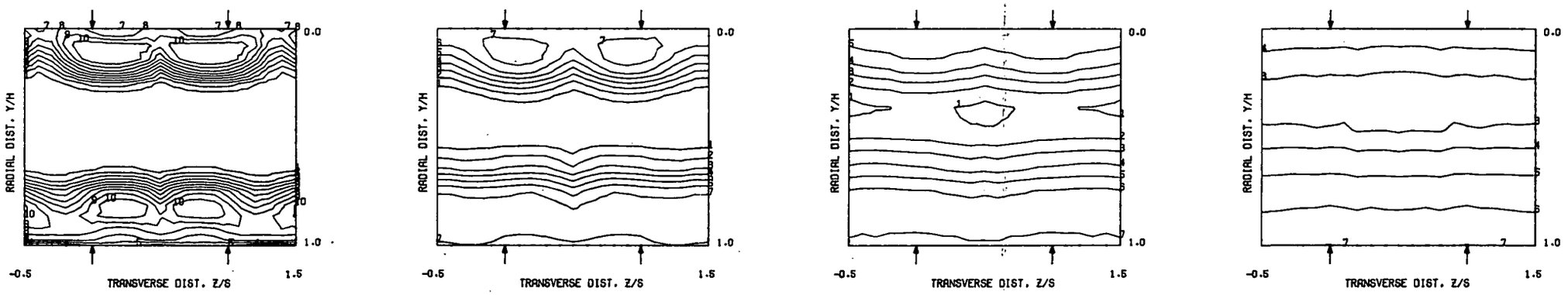

MEASURED THETA CONTOURS FOR TEST NO.1, TM=CONST (INL), J=6.81, S/D=2.0, H/D=8.0

Figure 11. Measured Theta Distributions for Test No. 1.

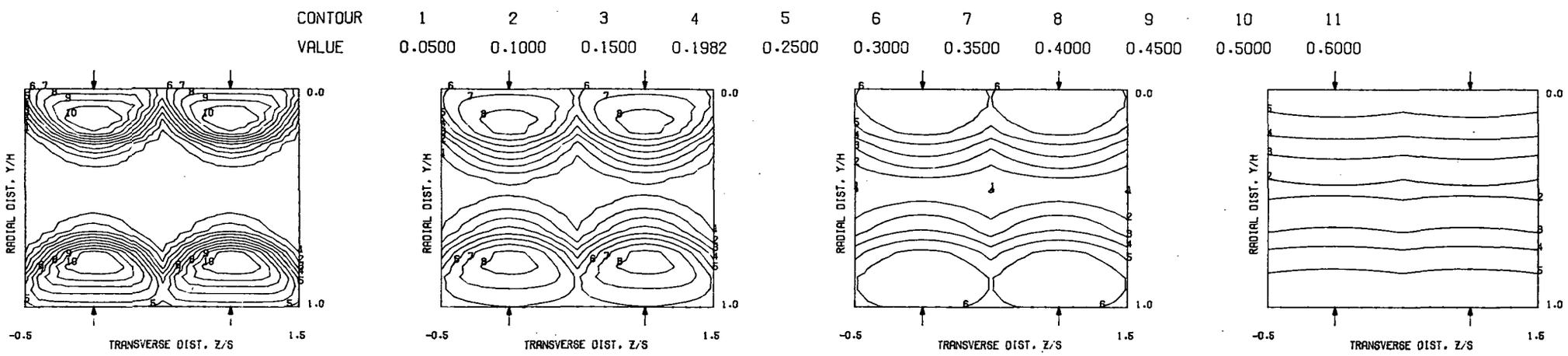

PREDICTED THETA CONTOURS FOR TEST NO. 1, TM=CONST, J=6.81, S/D=2.0, H/D=8.0

S/DJ = 2.45 HO/DJ = 4.90 VRATIO = 1.81 TRATIO = 0.480 DENRATIO=2.087 TMAIN = 645.5 K TJET = 310.4 K THEB = 0.198

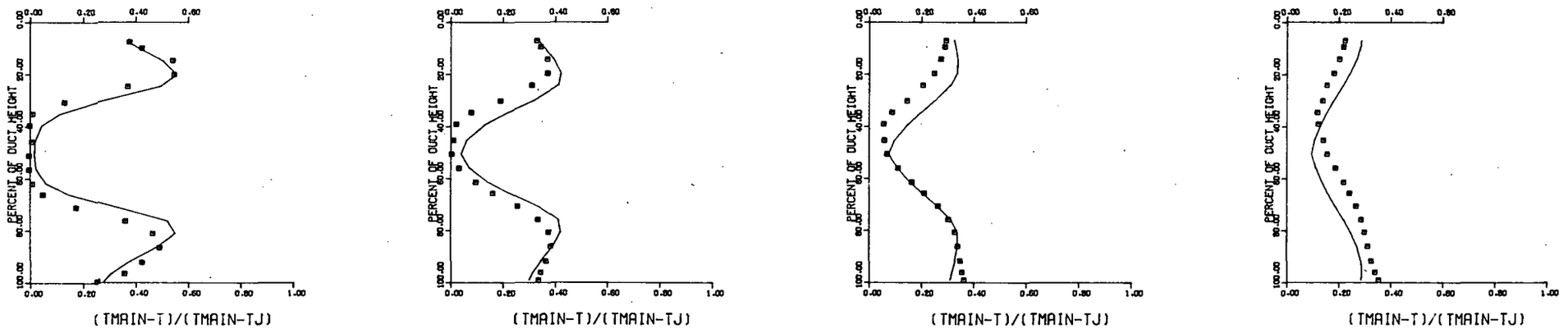

COMPARISON BETWEEN DATA AND CORRELATIONS FOR TEST NO. 1, TEST SECTION I, TM=CONST (INL), J = 6.81 , S/D =2.00 , H/D =8.00

Figure 12. Predicted Theta Distributions for Test No. 1.

S = 0.0254 METERS S/DJ = 2.480 HO/DJ = 9.921 VMAIN = 15.6 M/SEC VJET = 53.3 M/SEC TMAIN = 646.6 K TJET = 306.8 K THEB = 0.3179 BLORAT= 7.448 DENRATIO= 2.135 TRATIO= 0.474

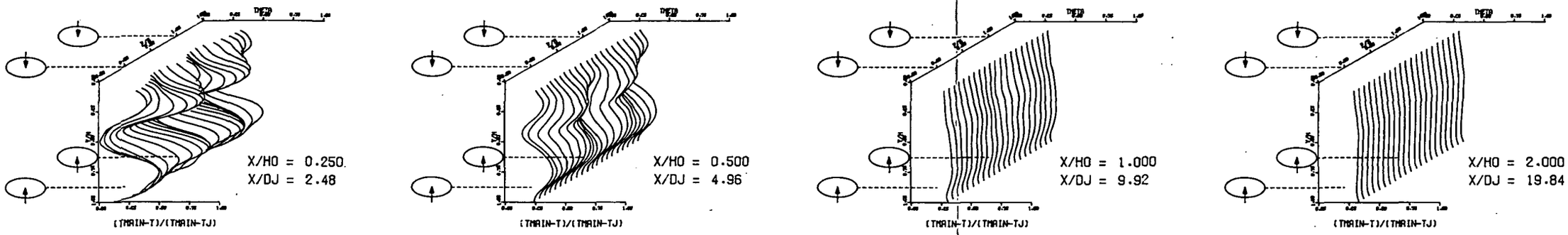

MEASURED THETA PROFILES FOR TEST NO.2, TEST SECTION I,TM=CONST (INL) , J = 24.95 , S/D = 2.00 , H/D = 8.00

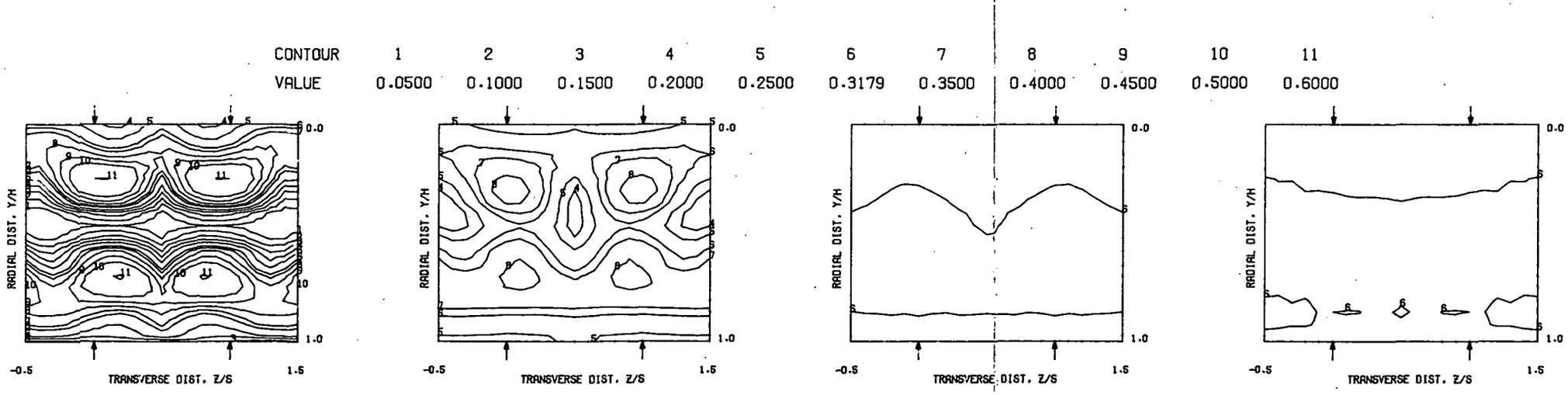

MEASURED THETA CONTOURS FOR TEST NO.2, TM=CONST (INL), J=24.96, S/D=2.0, H/D=8.0

Figure 13. Measured Theta Distributions for Test No. 2.

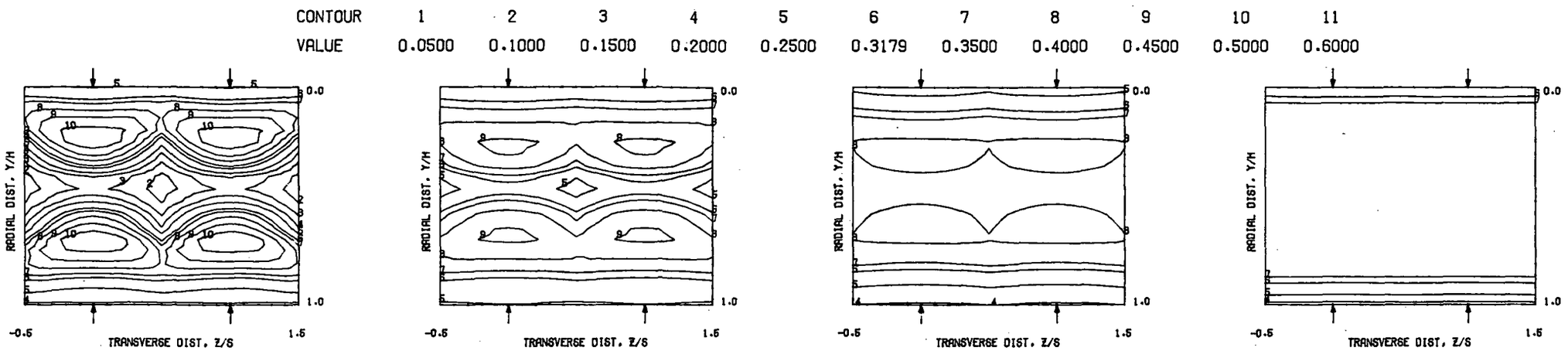

PREDICTED THETA CONTOURS FOR TEST NO. 2, TM=CONST, J=24.96, S/D=2.0, H/D=8.0

S/DJ = 2.48 HO/DJ = 4.96 VRATIO = 3.42 TRATIO = 0.474 DENRATIO=2.135 TMAIN = 646.6 K TJET = 306.8 K THEB = 0.318

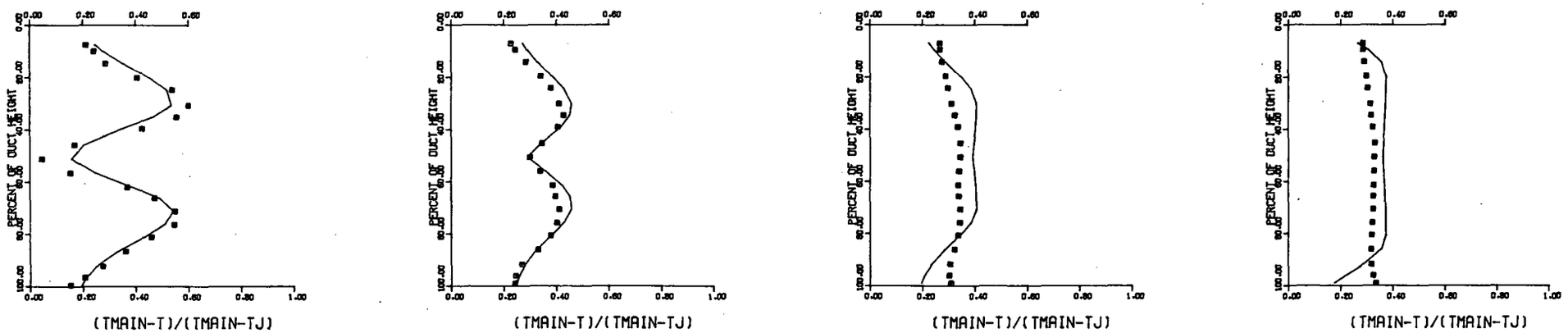

COMPARISON BETWEEN DATA AND CORRELATIONS FOR TEST NO. 2, TEST SECTION I, TM=CONST (INL), J = 24.95 , S/D =2.00 , H/D =8.00

Figure 14. Predicted Theta Distributions for Test No. 2.

S = 0.0254 METERS S/DJ = 2.496 HO/DJ = 9.983 VMAIN = 15.5 M/SEC VJET = 104.3 M/SEC TMAIN = 646.2 K TJET = 303.9 K THEB = 0.4879 BLORAT= 15.447 DENRATIO= 2.250 TRATIO=0.470

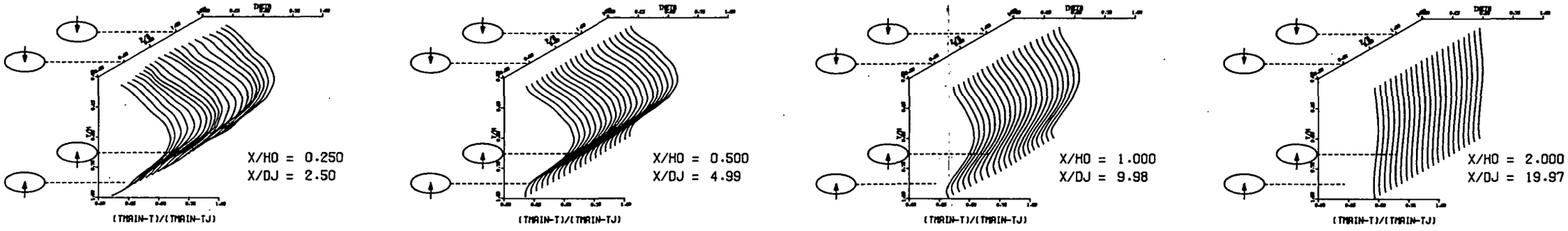

MEASURED THETA PROFILES FOR TEST NO.3, TEST SECTION I,TM=CONST (INL) , J = 101.83 , S/D = 2.00 , H/D = 8.00

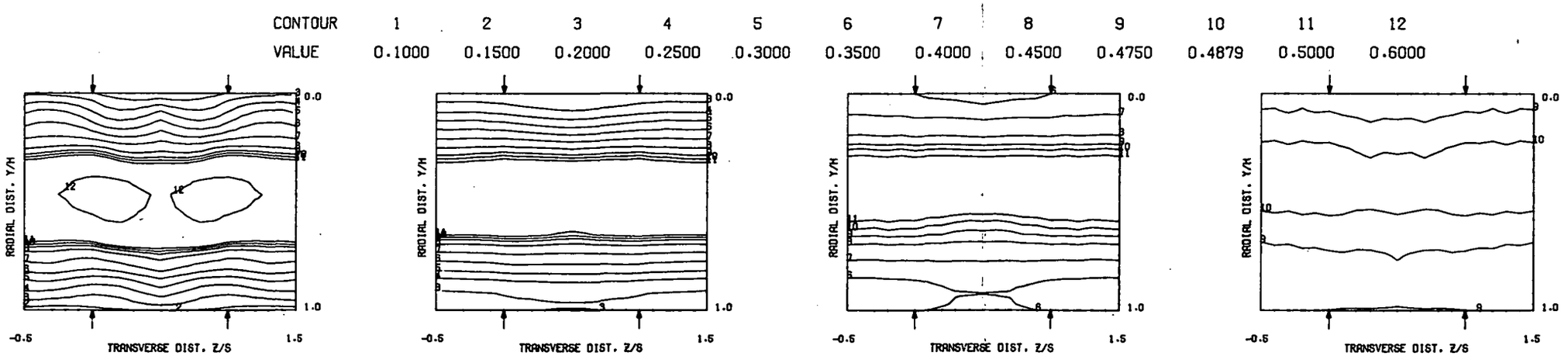

MEASURED THETA CONTOURS FOR TEST NO.3, TM=CONST (INL), J=101.8, S/D=2.0, H/D=8.0

Figure 15. Measured Theta Distributions for Test No. 3.

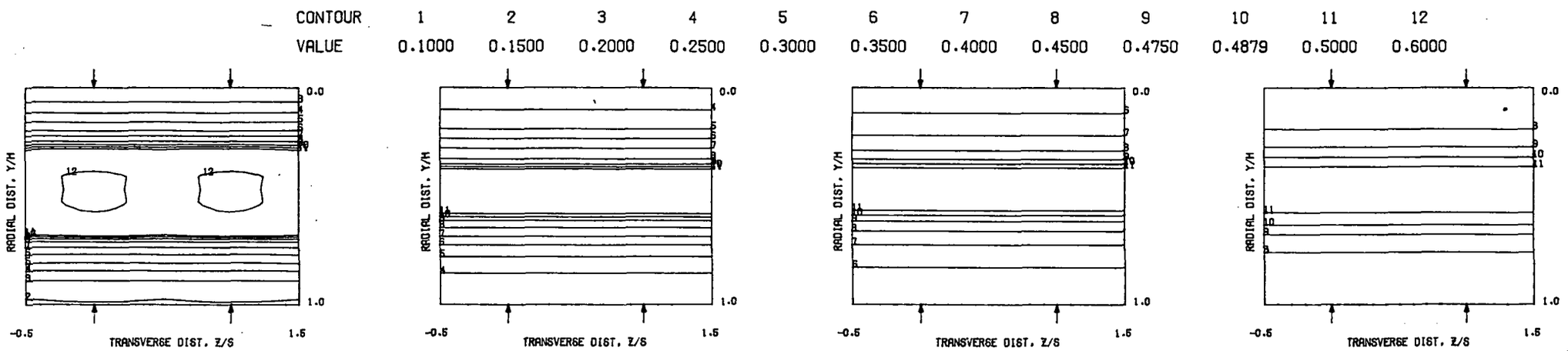

PREDICTED THETA CONTOURS FOR TEST NO. 3, TM=CONST, J=101.8, S/D=2.0, H/D=8.0

S/DJ = 2.50 HO/DJ = 4.99 VRATIO = 6.73 TRATIO = 0.470 DENRATIO=2.250 TMAIN = 646.2 K TJET = 303.9 K THEB = 0.488

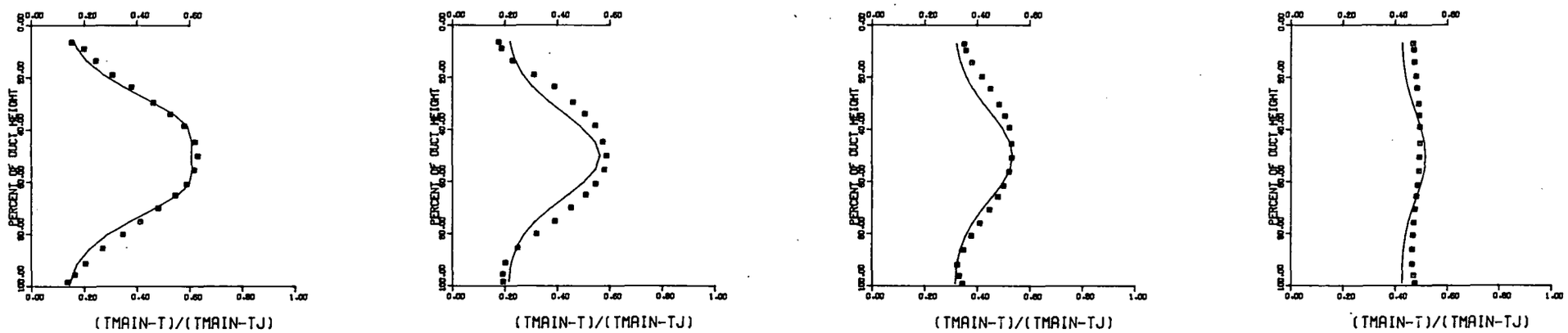

COMPARISON BETWEEN DATA AND CORRELATIONS FOR TEST NO. 3, TEST SECTION I, TM=CONST (INL), J = 101.83 , S/D =2.00 , H/D =8.00

Figure 16. Predicted Theta Distributions for Test No. 3.

S = 0.0254 METERS S/DJ = 2.461 HO/DJ = 9.844 VMAIN = 16.6 M/SEC VJET = 30.0 M/SEC TMAIN = 648.9 K TJET = 325.7 K THEB = 0.1890 BLORAT= 3.686 DENRATIO= 1.998 TRATIO= 0.502

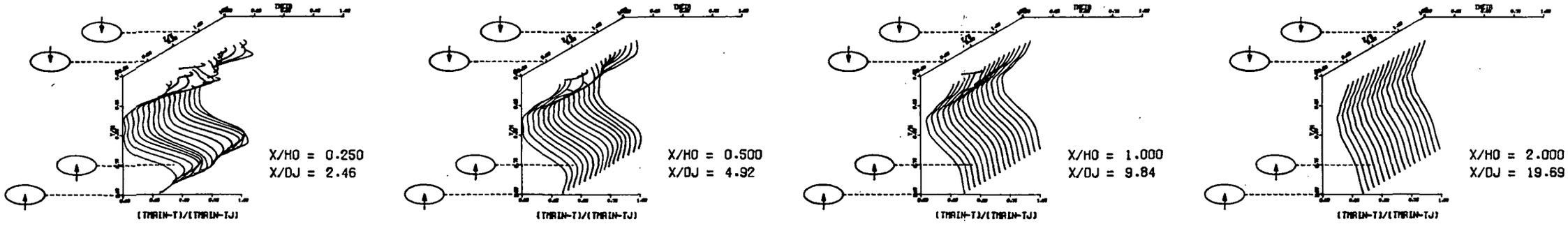

MEASURED THETA PROFILES FOR TEST NO.4, TEST SECTION I,TM=CONST (STG) , J = 6.53 , S/D = 2.00 , H/D = 8.00

CONTOUR	1	2	3	4	5	6	7	8	9	10	11
VALUE	0.0500	0.1000	0.1500	0.1890	0.2000	0.2500	0.3000	0.3500	0.4000	0.4500	0.5000

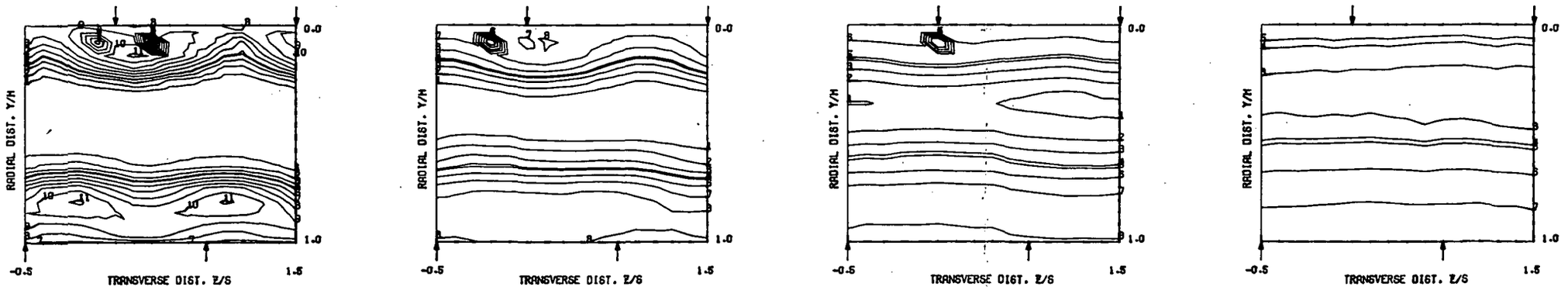

MEASURED THETA CONTOURS FOR TEST NO.4, TM=CONST (STG), J=6.53, S/D=2.0, H/D=8.

Figure 17. Measured Theta Distributions for Test No. 4.

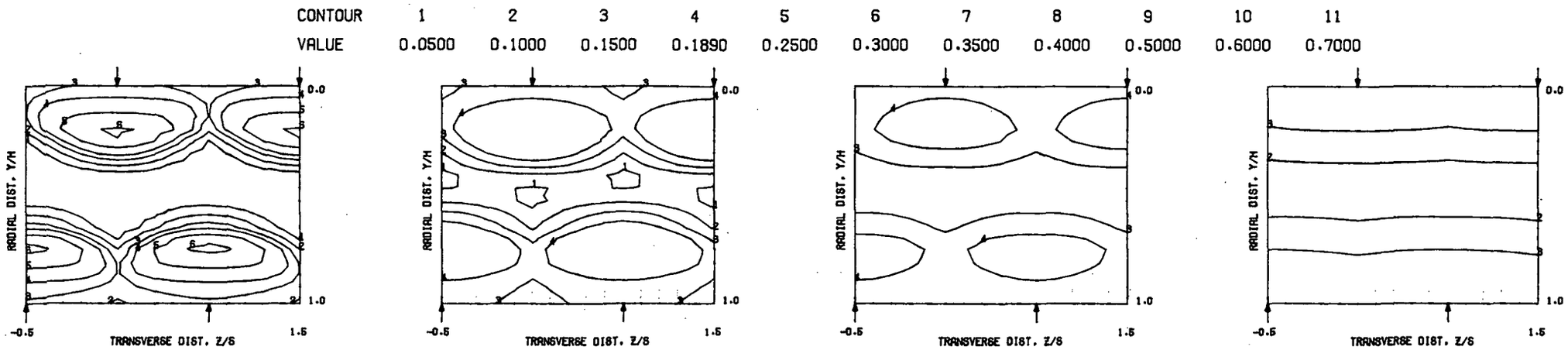

PREDICTED THETA CONTOURS FOR TEST NO 4, TM=CONST, J=6.53, S/D=2.0(STG), H/W=8.0

S/DJ = 2.46 HO/DJ = 9.84 VRATIO = 1.81 TRATIO = 0.502 DENRATIO= 1.998 TMAIN = 648.9 K TJET = 325.7 K THEB = 0.188

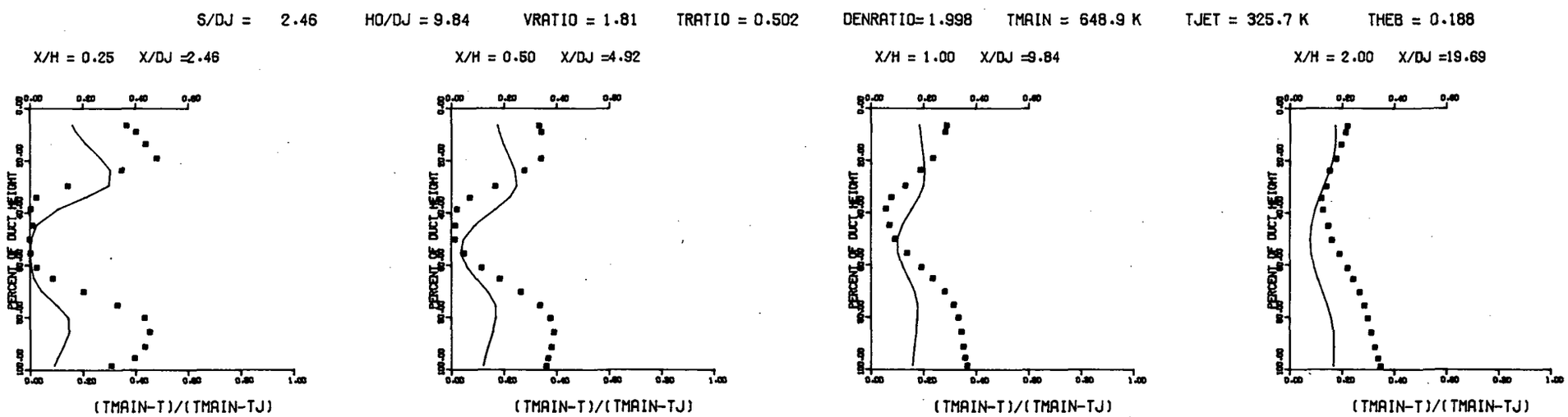

COMPARISON BETWEEN DATA AND CORRELATIONS FOR TEST NO. 4, TEST SECTION I,TM=CONST(STG), J = 6.53 , S/D =2.00 , H/D =8.00

Figure 18. Predicted Theta Distributions for Test No. 4.

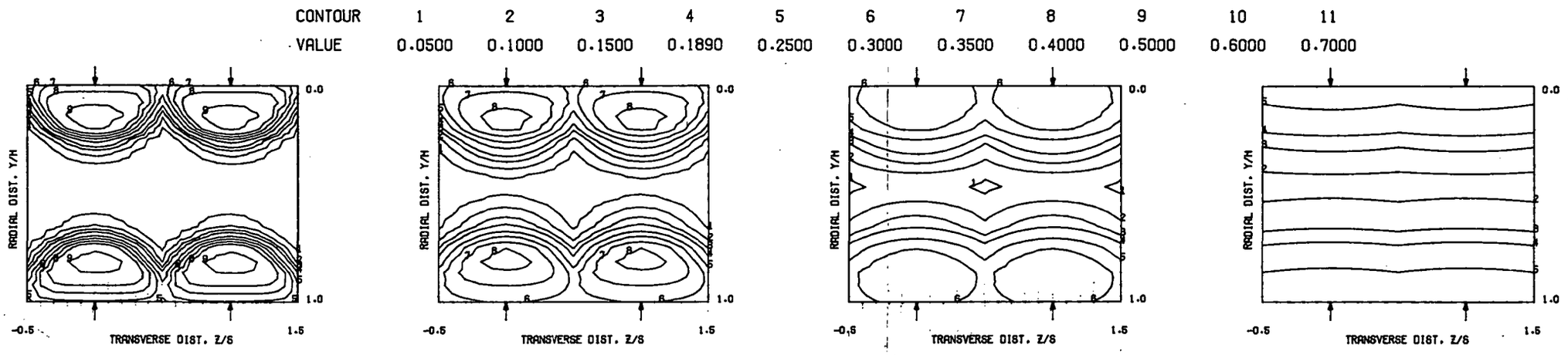

PREDICTED THETA CONTOURS FOR TEST NO 4,TM=CONST, J=6.53, S/D=2.0(STG), H/D=8.0

S/DJ = 2.46 HO/DJ = 4.93 VRATIO = 1.81 TRATIO = 0.502 DENRATIO= 1.998 TMAIN = 648.9 K TJET = 325.7 K THEB = 0.189

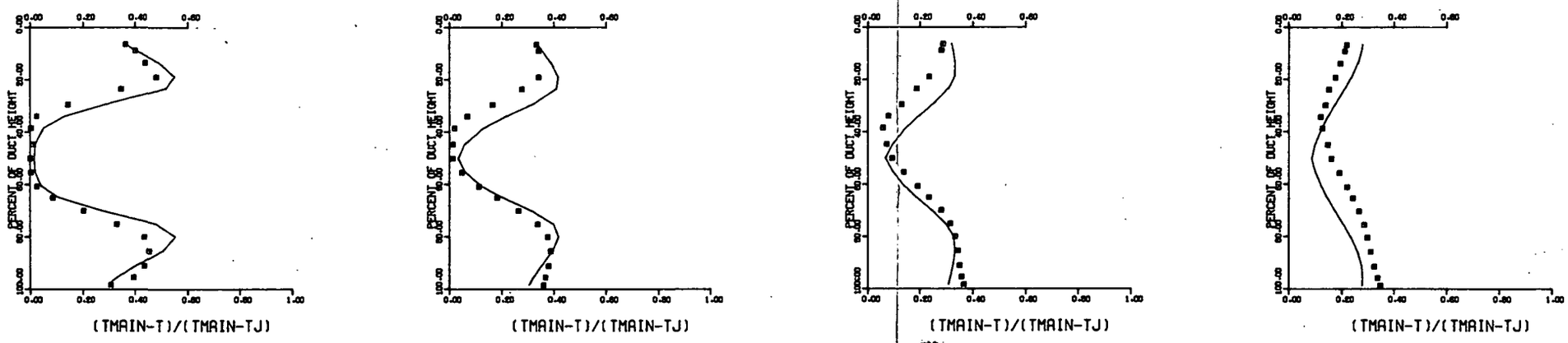

COMPARISON BETWEEN DATA AND CORRELATIONS FOR TEST NO. 4, TEST SECTION I,TM=CONST(STG), J = 6.53 , S/D =2.00 , H/D =8.00

Figure 19. Predicted Theta Distributions for Test No. 4 Using Correlations for In-Line Injections.

S = 0.0254 METERS S/DJ = 2.462 HO/DJ = 9.848 VMAIN = 16.3 M/SEC VJET = 56.7 M/SEC TMAIN = 646.2 K TJET = 314.5 K THEB = 0.3186 BLORAT= 7.393 DENRATIO= 2.086 TRATIO= 0.487

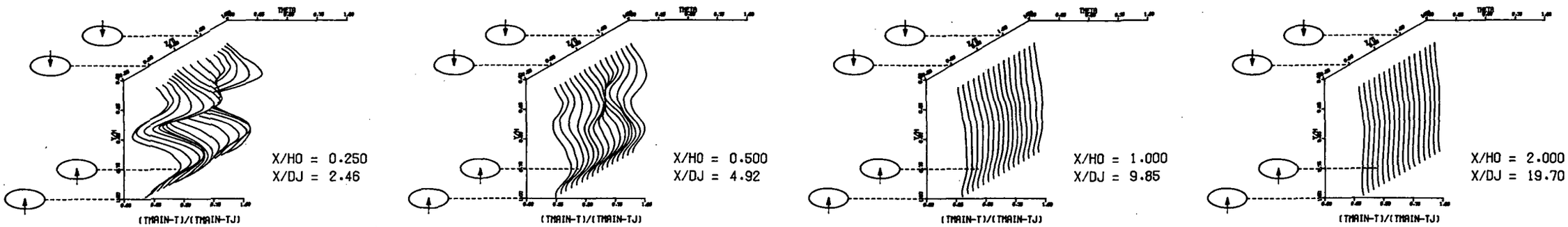

MEASURED THETA PROFILES FOR TEST NO.5, TEST SECTION I,TM=CONST (STG) , J = 25.16 , S/D = 2.00 , H/D = 8.00

CONTOUR	1	2	3	4	5	6	7	8	9	10	11
VALUE	0.0500	0.1000	0.1500	0.2000	0.2500	0.3000	0.3186	0.3500	0.4000	0.5000	0.6000

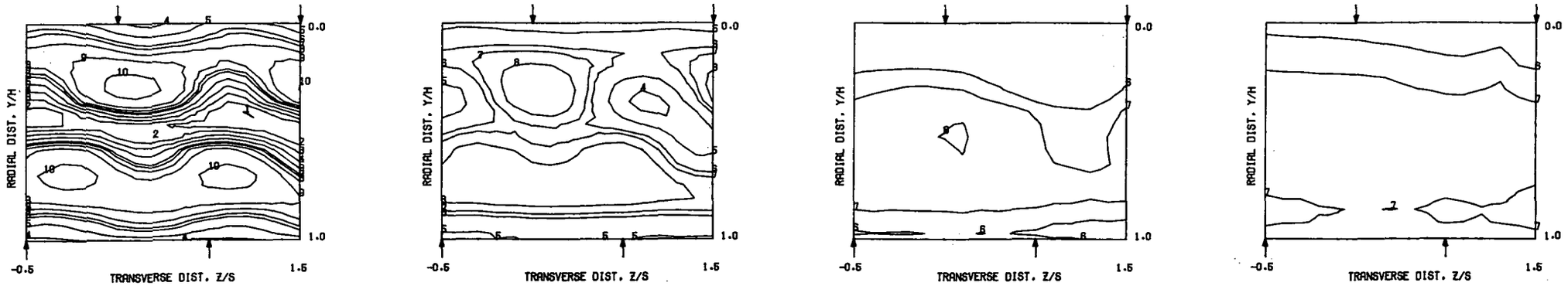

MEASURED THETA CONTOURS FOR TEST NO.5, TM=CONST (STG), J=25.17, S/D=2.0, H/D=8.0

Figure 20. Measured Theta Distributions for Test No. 5.

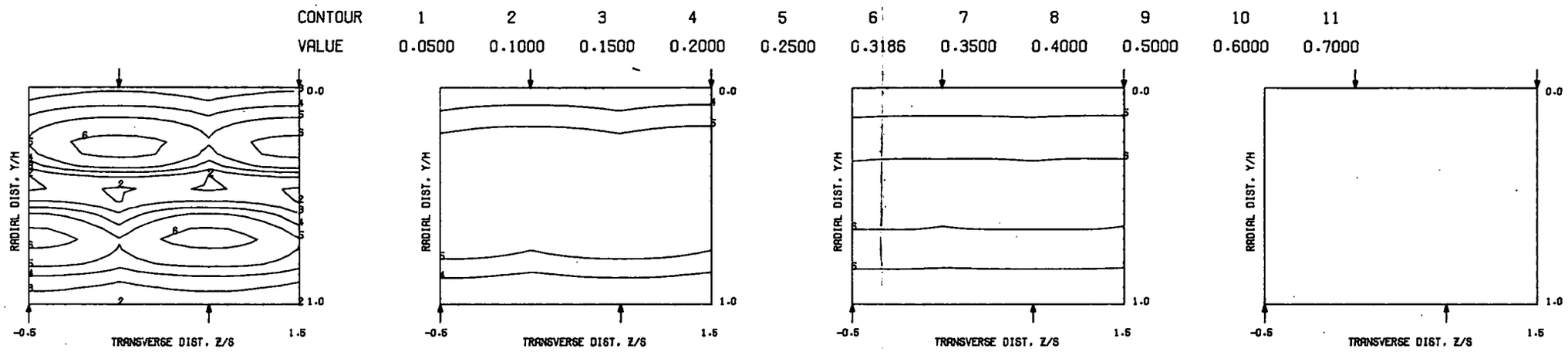

PREDICTED THETA CONTOURS FOR TEST NO 5,TM=CONST, J=27.16, S/D=2.0(STG), H/D=8.0

S/DJ = 2.46 HO/DJ = 9.85 VRATIO = 3.47 TRATIO = 0.487 DENRATIO=2.086 TMAIN = 646.2 K TJET = 314.5 K THEB = 0.318

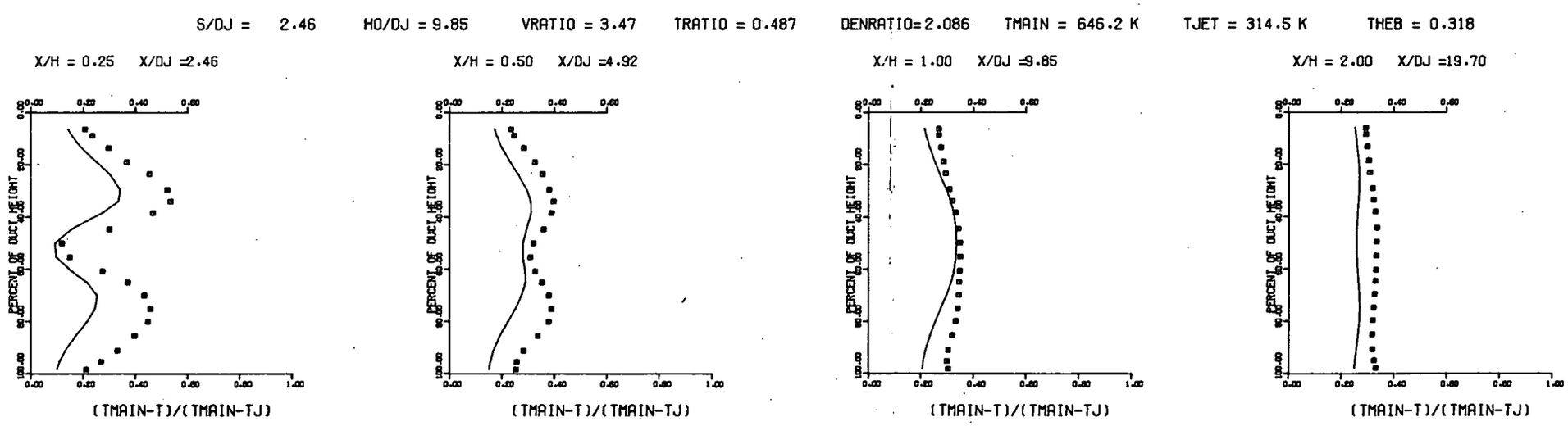

COMPARISON BETWEEN DATA AND CORRELATIONS FOR TEST NO. 5, TEST SECTION I,TM=CONST(STG), J = 25.16 , S/D =2.00 , H/D =8.00

Figure 21. Predicted Theta Distributions for Test No. 5.

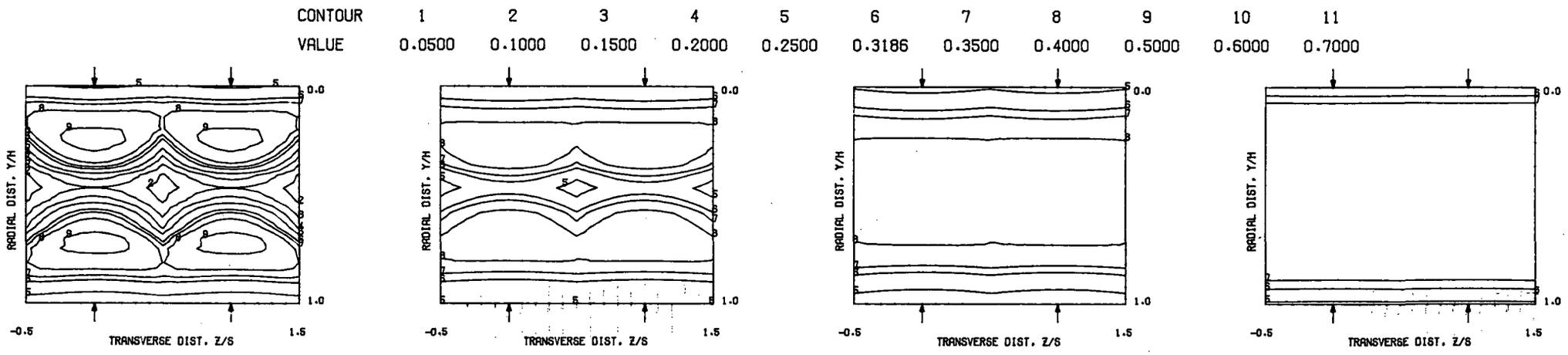

PREDICTED THETA CONTOURS FOR TEST NO 5,TM=CONST, J=25.16, S/D=2.0(STG), H/D=8.0

S/DJ = 2.46 HO/DJ = 4.90 VRATIO = 3.47 TRATIO = 0.487 DENRATIO=2.086 TMAIN = 646.2 K TJET = 314.5 K THEB = 0.319

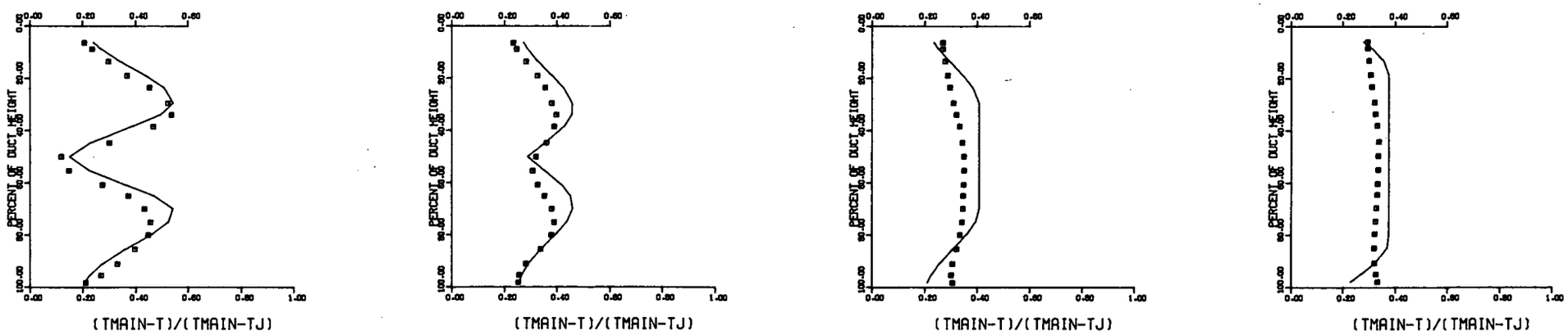

COMPARISON BETWEEN DATA AND CORRELATIONS FOR TEST NO. 5, TEST SECTION I,TM=CONST(STG), J = 25.16 , S/D =2.00 , H/D =8.00

Figure 22. Predicted Theta Distributions for Test No. 5
Using Correlations for In-line Injections.

S = 0.0254 METERS S/DJ = 2.481 HO/DJ = 9.924 VMAIN = 16.4 M/SEC VJET = 110.2 M/SEC TMAIN = 645.2 K TJET = 313.5 K THEB = 0.4845 BLORAT= 15.063 DENRATIO= 2.195 TRATIO= 0.486

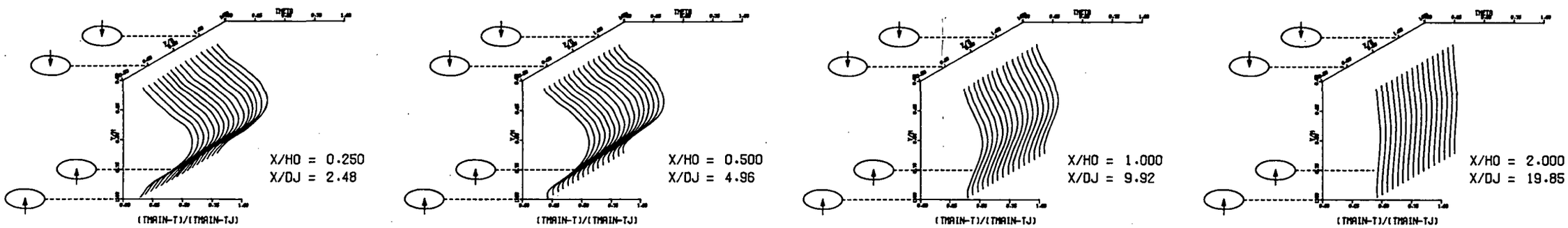

MEASURED THETA PROFILES FOR TEST NO.6, TEST SECTION I,TM=CONST (STG) , J = 99.29 , S/D = 2.00 , H/D = 8.00

CONTOUR	1	2	3	4	5	6	7	8	9	10	11
VALUE	0.0500	0.1000	0.1500	0.2000	0.2500	0.3000	0.3500	0.4000	0.4845	0.5000	0.6000

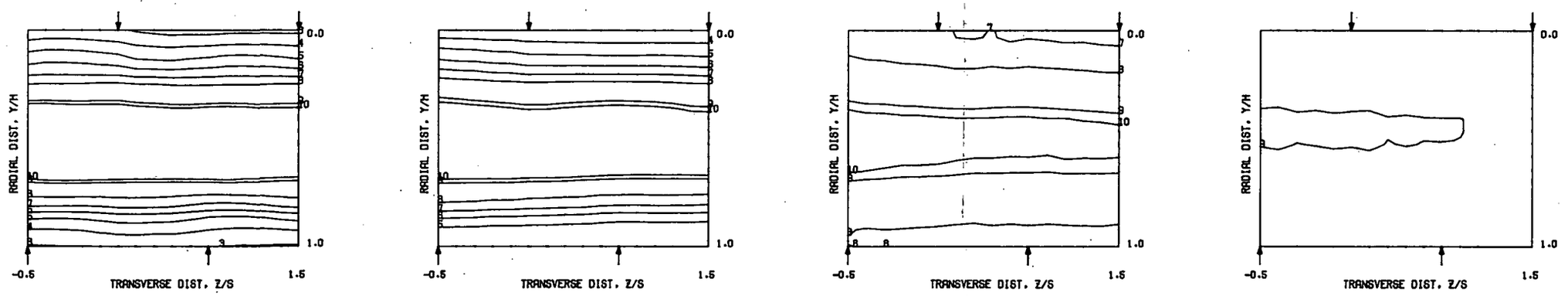

MEASURED THETA CONTOURS FOR TEST NO.6, TM=CONST (STG), J=99.29, S/D=2.0, H/D=8.

Figure 23. Measured Theta Distributions for Test No. 6.

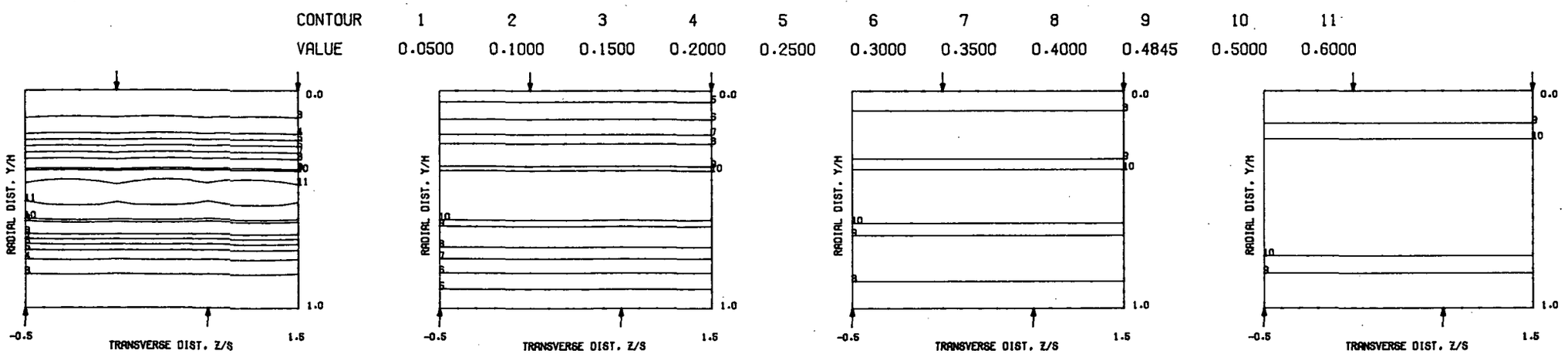

PREDICTED THETA CONTOURS FOR TEST NO 6, TM=CONST, J=99.29, S/D=2.0(STG), H/W=8.0

S/DJ = 2.48 HO/DJ = 9.92 VRATIO = 6.73 TRATIO = 0.486 DENRATIO=2.195 TMAIN = 645.2 K TJET = 313.5 K THEB = 0.486

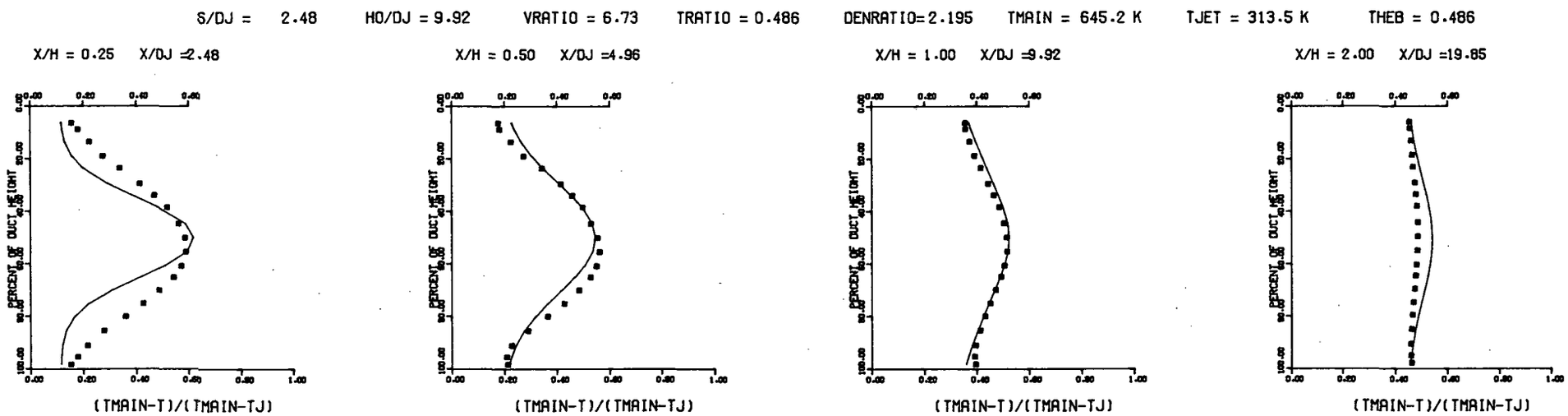

COMPARISON BETWEEN DATA AND CORRELATIONS FOR TEST NO. 6, TEST SECTION I,TM=CONST(STG), J = 99.29 , S/D =2.00 , H/D =8.00

Figure 24. Predicted Theta Distributions for Test No. 6.

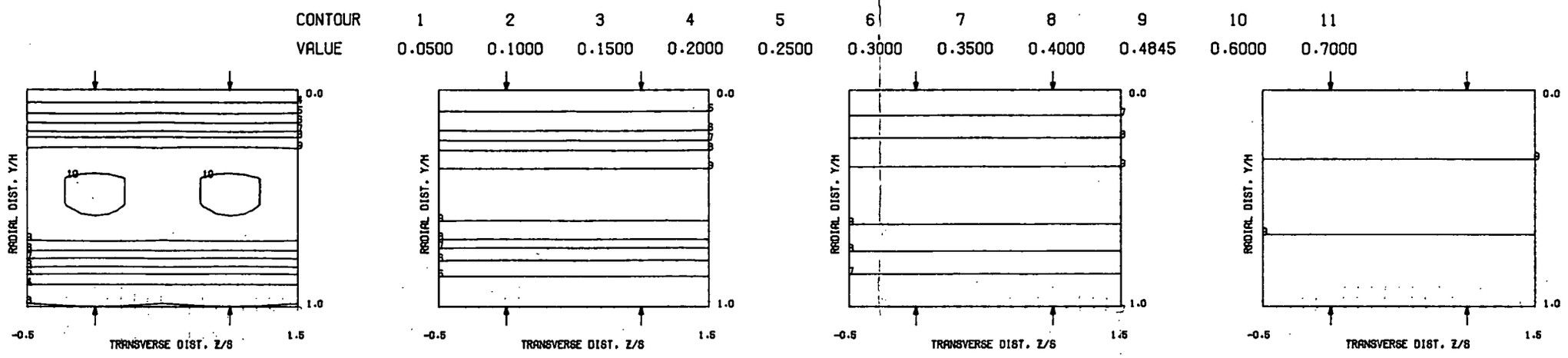

PREDICTED THETA CONTOURS FOR TEST NO 6,TM=CONST, J=99.29, S/D=2.0(STG), H/D=8.0

S/DJ = 2.48 HO/DJ = 4.94 VRATIO = 6.73 TRATIO = 0.486 DENRATIO=2.195 TMAIN = 645.2 K TJET = 313.5 K THEB = 0.485

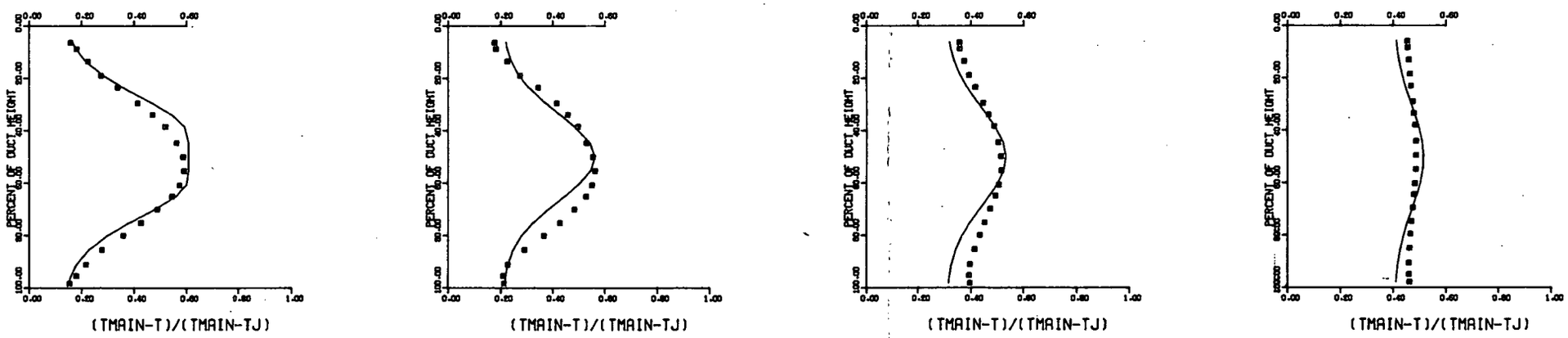

COMPARISON BETWEEN DATA AND CORRELATIONS FOR TEST NO. 6, TEST SECTION I,TM=CONST(STG), J = 99.29 , S/D =2.00 , H/D =8.00

Figure 25. Predicted Theta Distributions for Test No. 6 Using Correlations for In-line Injections.

S = 0.0508 METERS S/DJ = 4.888 HO/DJ = 9.776 VMAIN = 15.2 M/SEC VJET = 30.2 M/SEC TMAIN = 645.4 K TJET = 326.3 K THEB = 0.1120 BLORAT= 3.867 DENRATIO= 1.984 TRATIO= 0.506

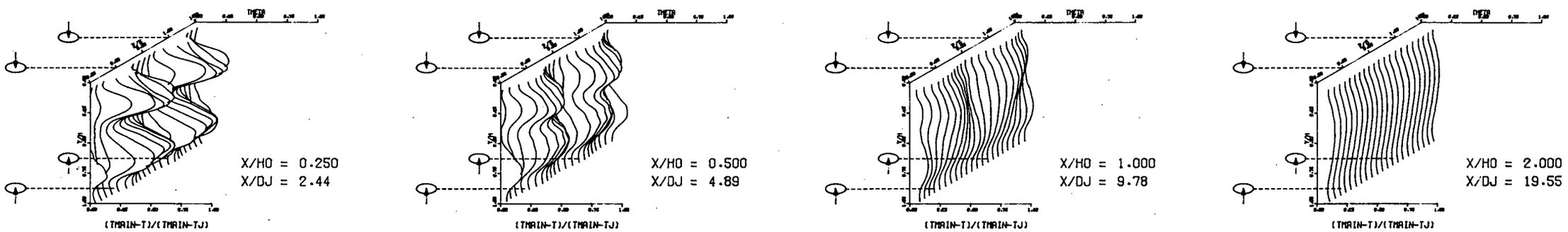

MEASURED THETA PROFILES FOR TEST NO.7, TEST SECTION I,TM=CONST (INL) , J = 7.85 , S/D = 4.00 , H/D = 8.00

CONTOUR	1	2	3	4	5	6	7	8	9	10	11
VALUE	0.0500	0.1121	0.1500	0.2000	0.2500	0.3000	0.3250	0.3500	0.4000	0.5000	0.6000

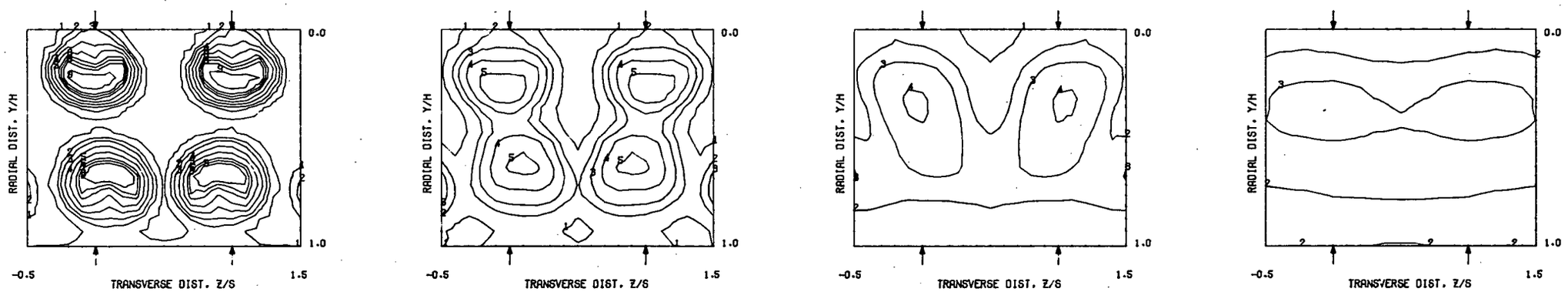

MEASURED THETA CONTOURS FOR TEST NO.7, TM=CONST (INL), J=7.85, S/D=4.0, H/D=8.

Figure 26. Measured Theta Distributions for Test No. 7.

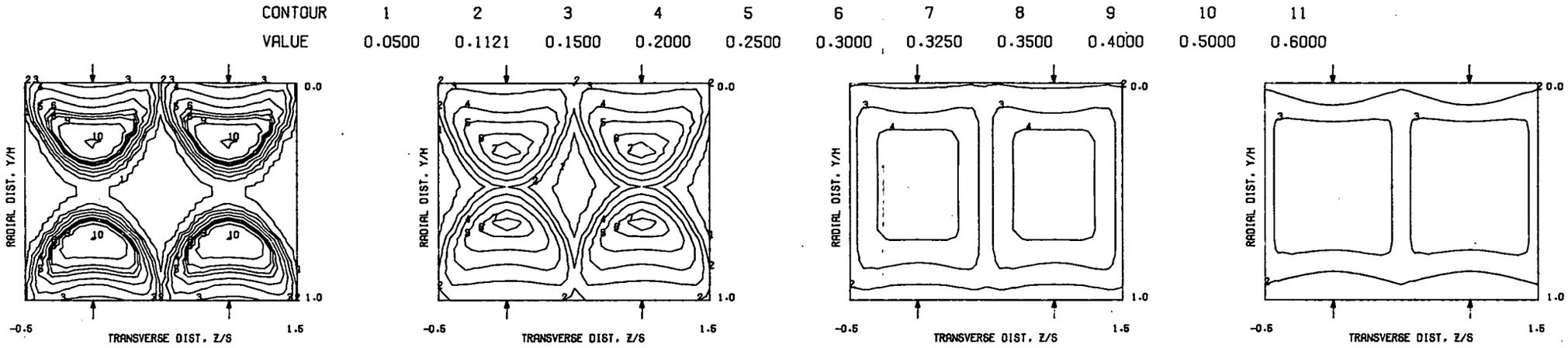

PREDICTED THETA CONTOURS FOR TEST NO 7, TM=CONST(INL),J=7.85,S/D=4.0, H/D=8.0

S/DJ = 4.89 HO/DJ = 4.89 VRATIO = 1.99 TRATIO = 0.506 DENRATIO=1.984 TMAIN = 645.4 K TJET = 326.3 K THEB = 0.112

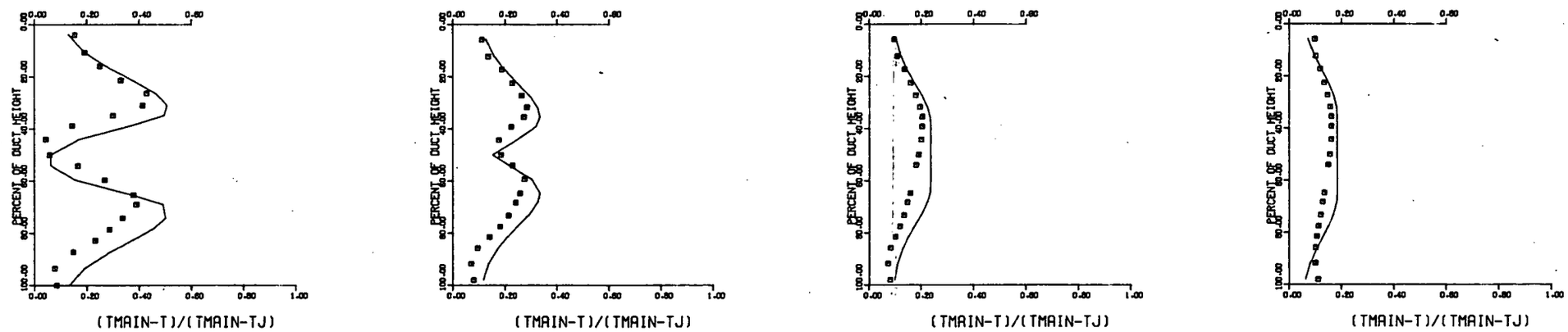

COMPARISON BETWEEN DATA AND CORRELATIONS FOR TEST NO. 7, TEST SECTION I, TM=CONST(INL), J = 7.85 , S/D =4.00 , H/D =8.00

Figure 27. Predicted Theta Distributions for Test No. 7.

S = 0.0508 METERS S/DJ = 4.961 HO/DJ = 9.921 VMAIN = 15.0 M/SEC VJET = 55.7 M/SEC TMAIN = 644.1 K TJET = 322.5 K THEB = 0.1896 BLORAT= 7.373 DENRATIO= 2.027 TRATIO= 0.501

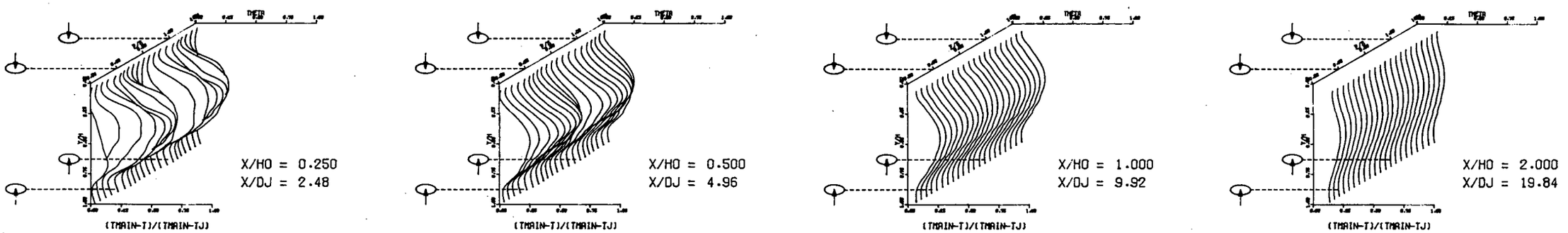

MEASURED THETA PROFILES FOR TEST NO.8, TEST SECTION I,TM=CONST (INL) , J = 27.92 , S/D = 4.00 , H/D = 8.00

CONTOUR	1	2	3	4	5	6	7	8	9	10	11
VALUE	0.0500	0.1000	0.1500	0.1896	0.2000	0.2500	0.3000	0.3500	0.4000	0.5000	0.6000

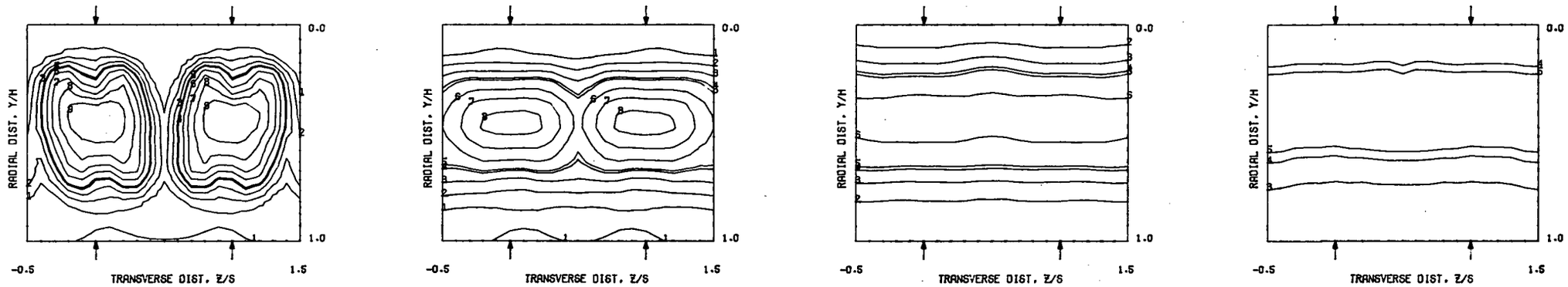

MEASURED THETA CONTOURS FOR TEST NO.8, TM=CONST (INL), J=27.92, S/D=4.0, H/D=8.

Figure 28. Measured Theta Distributions for Test No. 8.

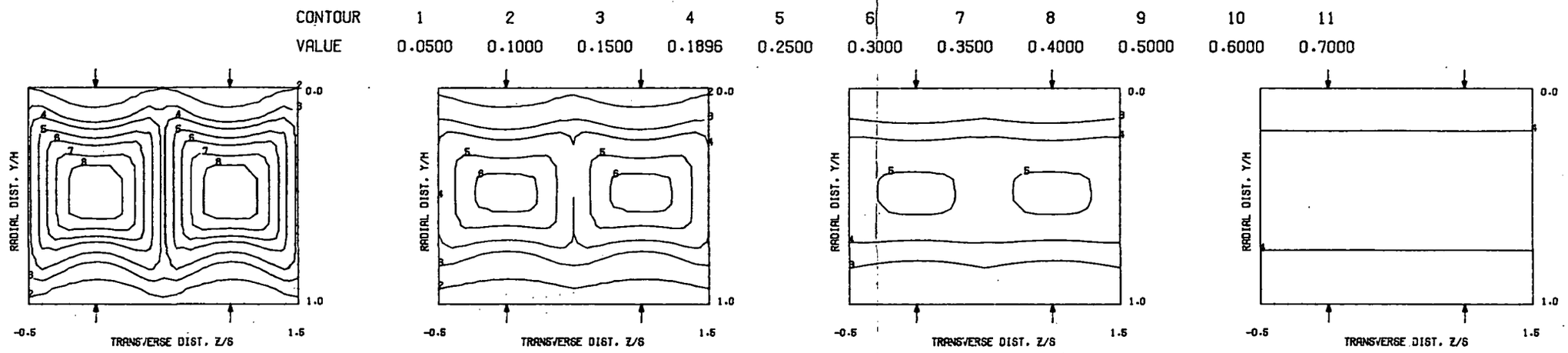

PREDICTED THETA CONTOURS FOR TEST NO 8, T.S. I, J=27.92, S/D=4.0(INL), H/D=8.0

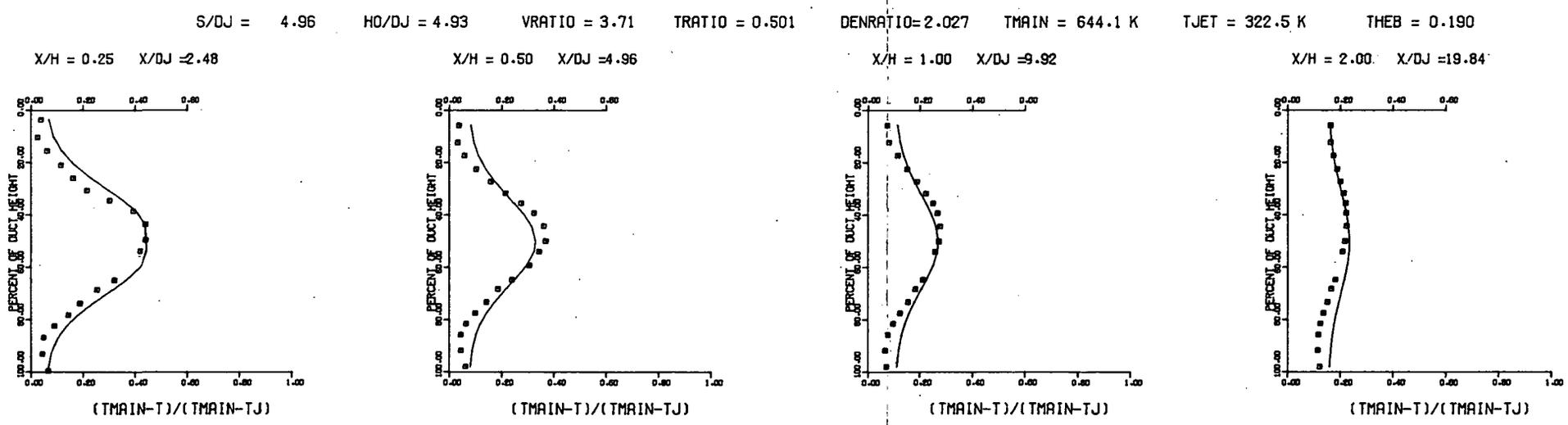

COMPARISON BETWEEN DATA AND CORRELATIONS FOR TEST NO. 8, TEST SECTION I,TM=CONST(INL), J = 27.92 , S/D =4.00 , H/D =8.00

Figure 29. Predicted Theta Distributions for Test No. 8.

S = 0.0508 METERS S/DJ = 4.961 HO/DJ = 9.921 VMAIN = 15.8 M/SEC VJET = 110.9 M/SEC TMAIN = 644.2 K TJET = 317.0 K THEB = 0.3291 BLORAT= 15.691 DENRATIO= 2.184 TRATIO= 0.492

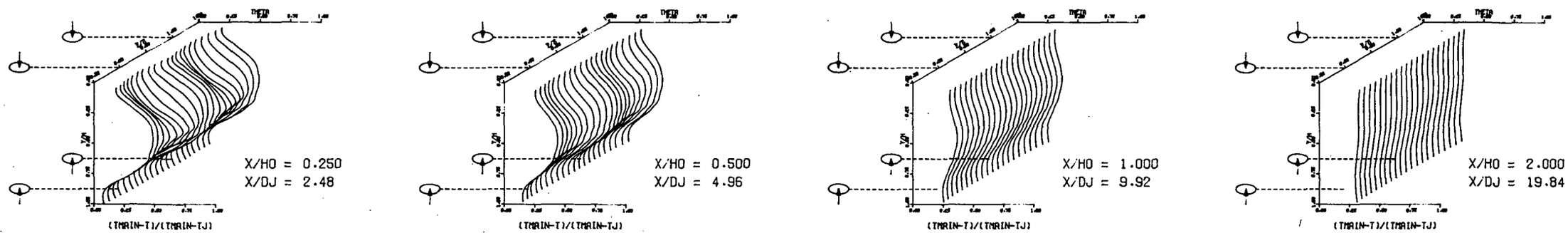

MEASURED THETA PROFILES FOR TEST NO.9, TEST SECTION I,TM=CONST (INL) , J = 108.27 , S/D = 4.00 , H/D = 8.00

CONTOUR	1	2	3	4	5	6	7	8	9	10	11
VALUE	0.0500	0.1000	0.1500	0.2000	0.2500	0.3000	0.3291	0.3500	0.4000	0.5000	0.6000

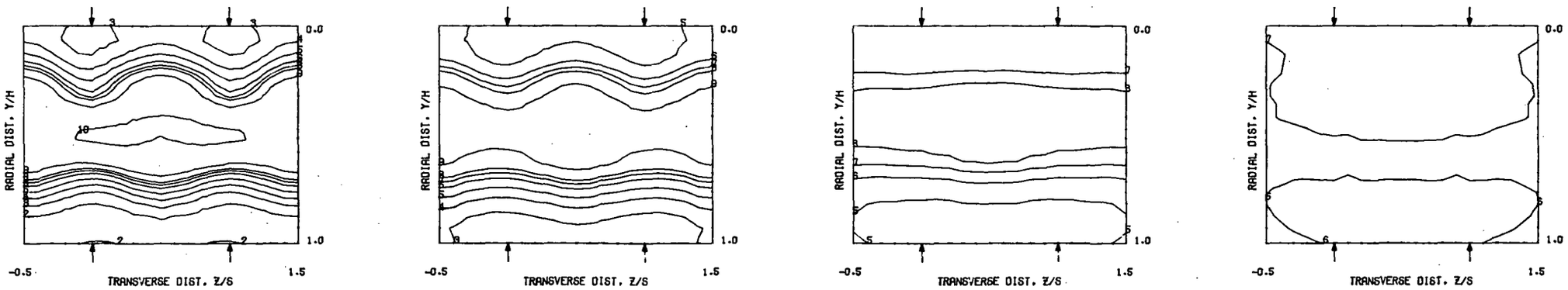

MEASURED THETA CONTOURS FOR TEST NO.9, TM=CONST (INL), J=108.3, S/D=4.0, H/D=8.

Figure 30. Measured Theta Distributions for Test No. 9.

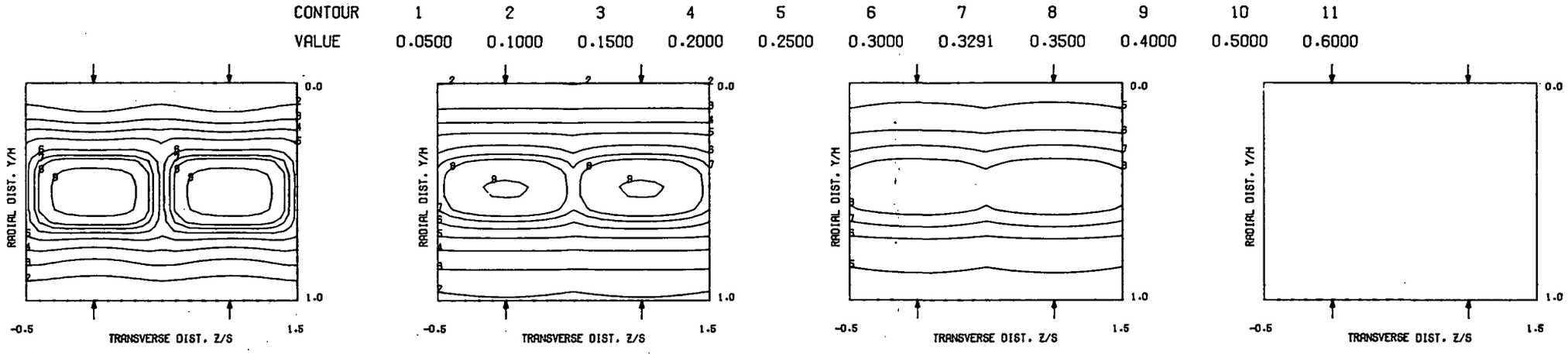

PREDICTED THETA CONTOURS FOR TEST NO. 9, TM=CONST, J=108.3, S/D=4.0, H/D=8.0

S/DJ = 4.96 HO/DJ = 4.96 VRATIO = 7.04 TRATIO = 0.492 DENRATIO=2.184 TMAIN = 644.2 K TJET = 317.0 K THEB = 0.329

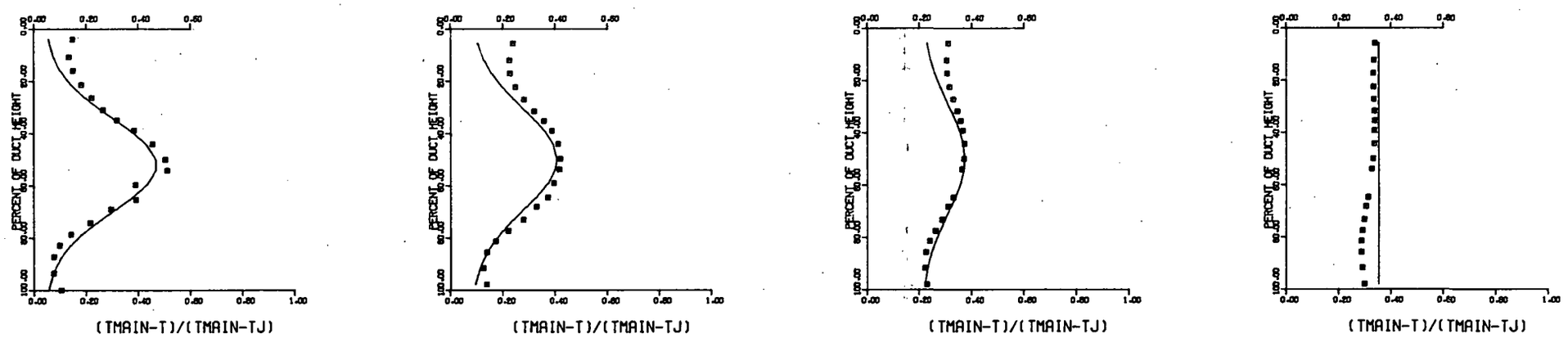

COMPARISON BETWEEN DATA AND CORRELATIONS FOR TEST NO. 9, TEST SECTION I, TM=CONST (INL), J = 108.27 , S/D =4.00 , H/D =8.00

Figure 31. Predicted Theta Distributions for Test No. 9.

S = 0.0508 METERS S/DJ = 4.888 HO/DJ = 9.776 VMAIN = 15.8 M/SEC VJET = 27.6 M/SEC TMAIN = 646.6 K TJET = 329.1 K THEB = 0.1019 BLORAT= 3.502 DENRATIO= 1.971 TRATIO= 0.509

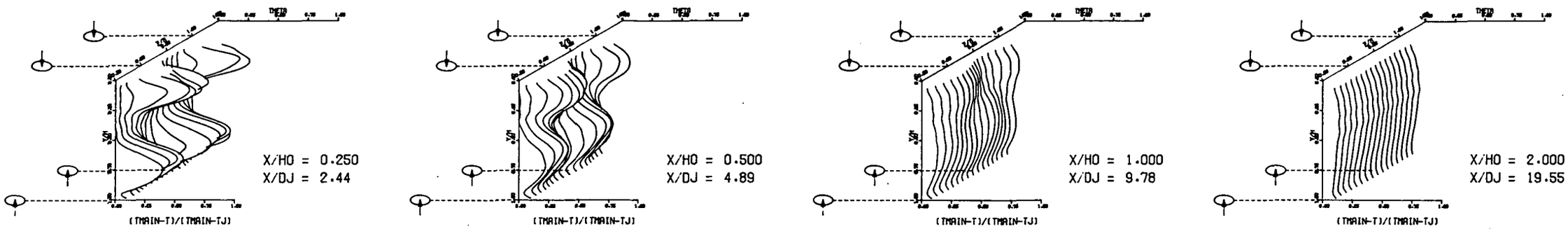

MEASURED THETA PROFILES FOR TEST NO.10, TEST SECTION I,TM=CONST (STG) , J = 5.97 , S/D = 4.00 , H/D = 8.00

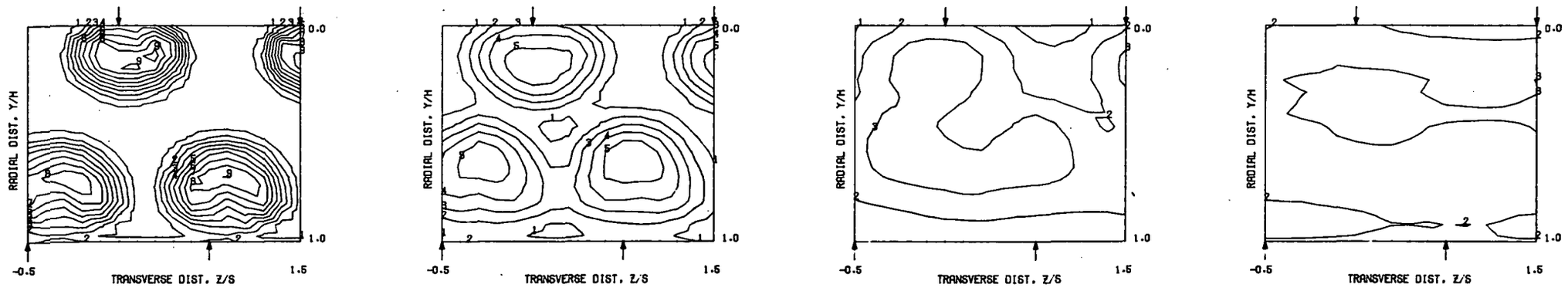

MEASURED THETA CONTOURS FOR TEST NO.10, TM=CONST (STG), J=5.97, S/D=4.0, H/D=8.0

Figure 32. Measured Theta Distributions for Test No. 10.

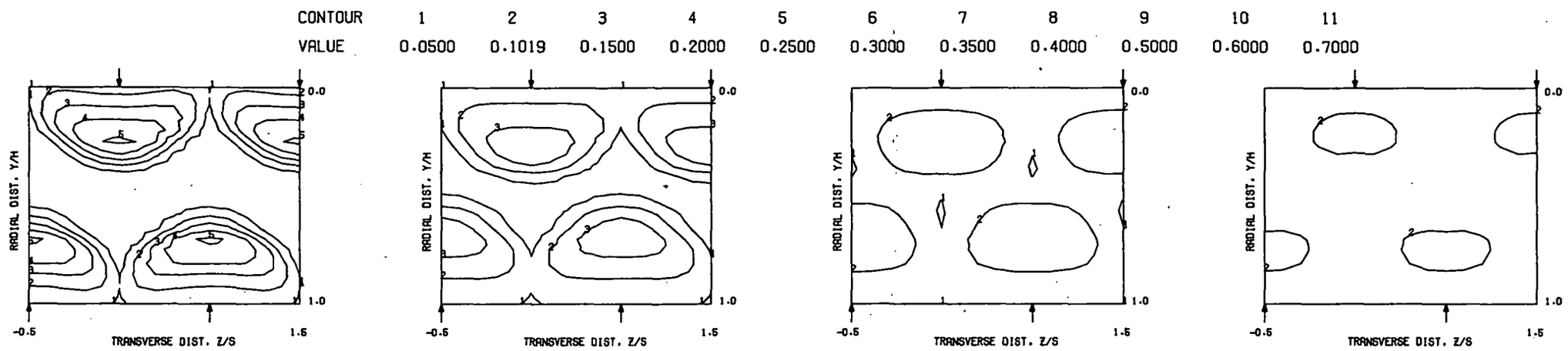

PREDICTED THETA CONTOURS FOR TEST NO 10,TM=CONST, J=5.97, S/D=4.0(STG), H/D=8.0

S/DJ = 4.89 HO/DJ = 9.78 VRATIO = 1.74 TRATIO = 0.509 DENRATIO= 1.971 TMAIN = 646.6 K TJET = 329.1 K THEB = 0.103

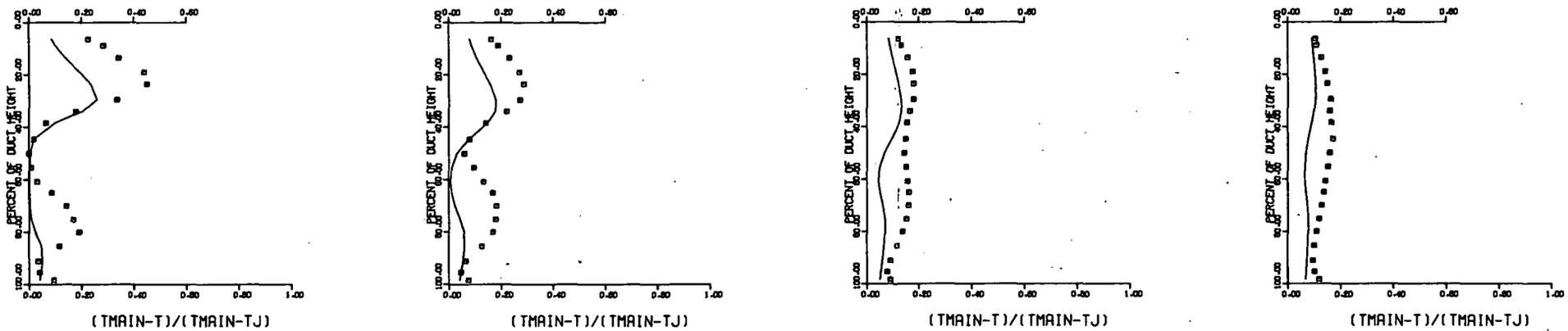

COMPARISON BETWEEN DATA AND CORRELATIONS FOR TEST NO. 10, TEST SECTION I,TM=CONST(STG), J = 5.97 , S/D =4.00 , H/D =8.00

Figure 33. Predicted Theta Distributions for Test No. 10.

S = 0.0508 METERS S/DJ = 4.925 HO/DJ = 9.851 VMAIN = 15.7 M/SEC VJET = 55.8 M/SEC TMAIN = 645.0 K TJET = 322.2 K THEB = 0.1888 BLORAT= 7.368 DENRATIO= 2.033 TRATIO= 0.500

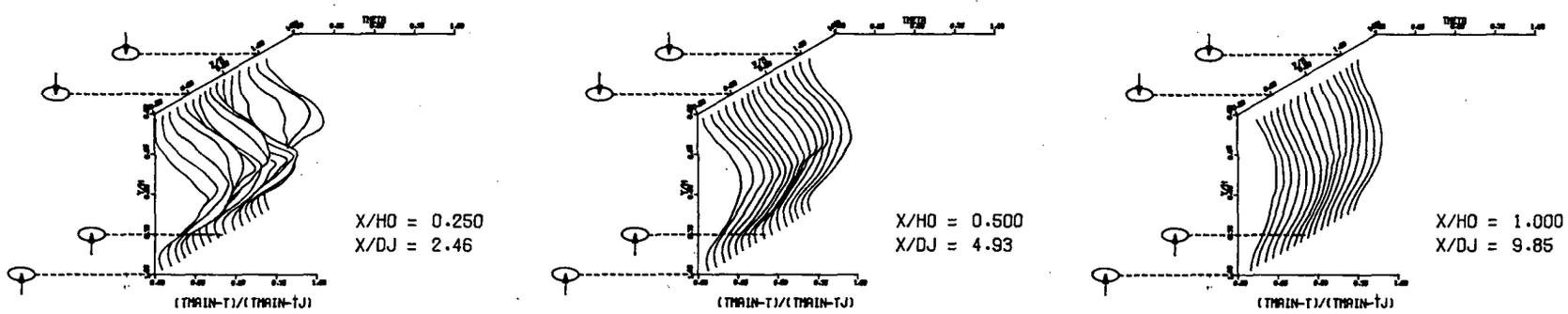

MEASURED THETA PROFILES FOR TEST NO.11, TEST SECTION I,TM=CONST (STG) , J = 25.68 , S/D = 4.00 , H/D = 8.00

CONTOUR	1	2	3	4	5	6	7	8	9	10	11
VALUE	0.0500	0.1000	0.1888	0.2000	0.2500	0.3000	0.3500	0.4000	0.5000	0.6000	0.7000

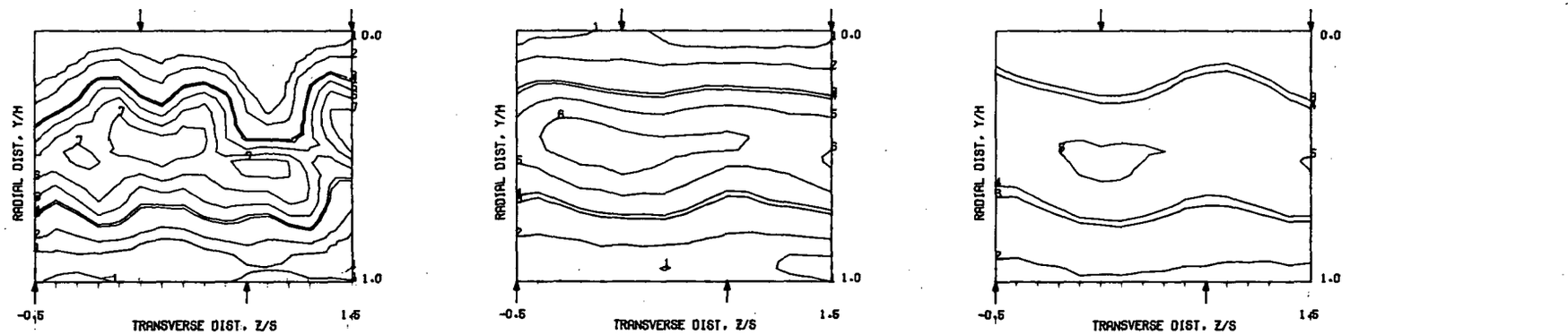

MEASURED THETA CONTOURS FOR TEST NO.11, TM=CONST (STG), J=25.68, S/D=4.0, H/D=8.

Figure 34. Measured Theta Distributions for Test No. 11.

CONTOUR	1	2	3	4	5	6	7	8	9	10	11
VALUE	0.0500	0.1000	0.1500	0.1888	0.2500	0.3000	0.3500	0.4000	0.5000	0.6000	0.7000

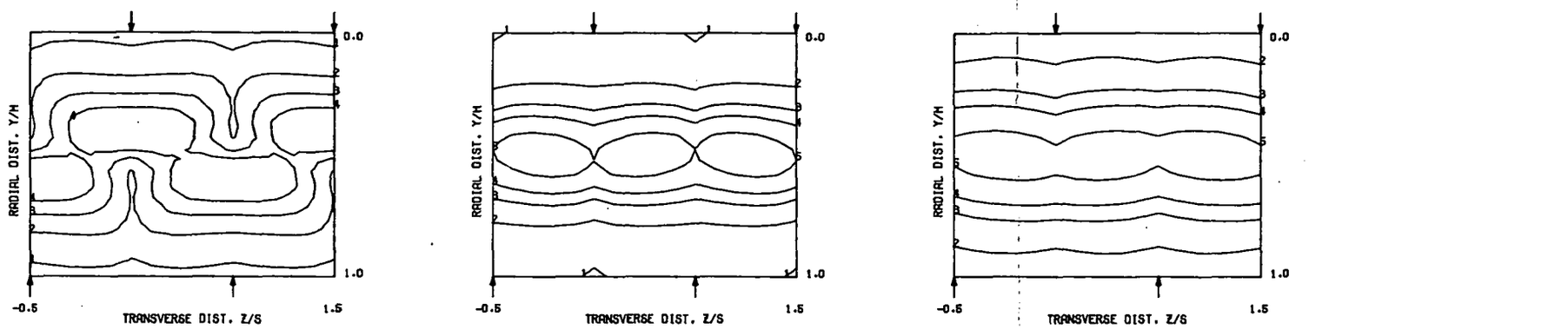

PREDICTED THETA CONTOURS FOR TEST NO 11,TM=CONST, J=25.68, S/D=4.0(STG), H/D=8.0

S/DJ = 4.93 HO/DJ = 9.85 VRATIO = 3.55 TRATIO = 0.500 DENRATIO=2.033 TMAIN = 645.0 K TJET = 322.2 K THEB = 0.189

X/H = 0.25 X/DJ =2.46 X/H = 0.50 X/DJ =4.93 X/H = 1.00 X/DJ =9.85

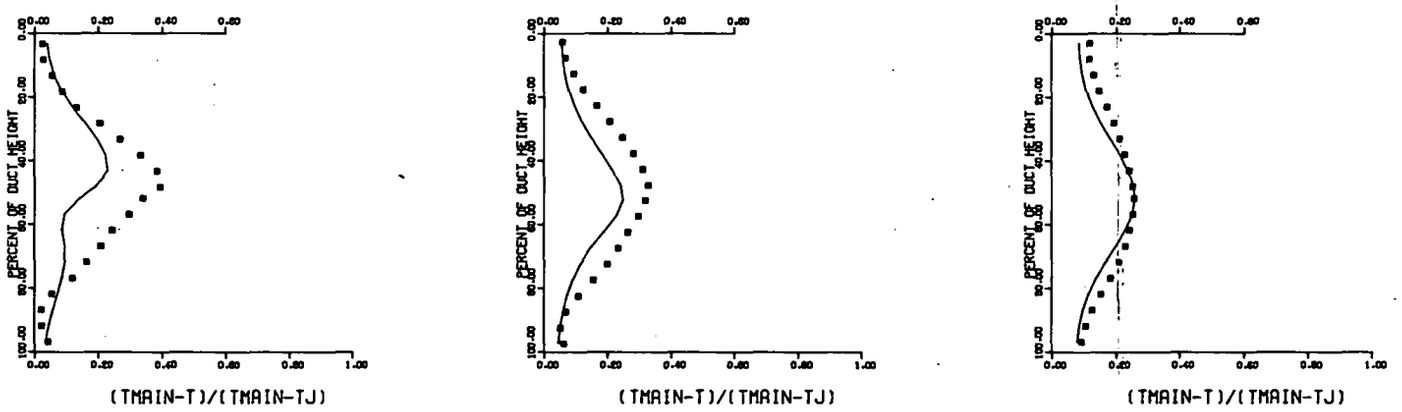

COMPARISON BETWEEN DATA AND CORRELATIONS FOR TEST NO. 11, TEST SECTION I,TM=CONST(STG), J = 25.68 , S/D =4.00 , H/D =8.00

Figure 35. Predicted Theta Distributions for Test No. 11.

S = 0.0508 METERS S/DJ = 5.000 HO/DJ = 10.000 VMAIN = 16.0 M/SEC VJET = 109.9 M/SEC TMAIN = 645.9 K TJET = 317.9 K THEB = 0.3187 BLORAT= 15.291 DENRATIO= 2.178 TRATIO= 0.492

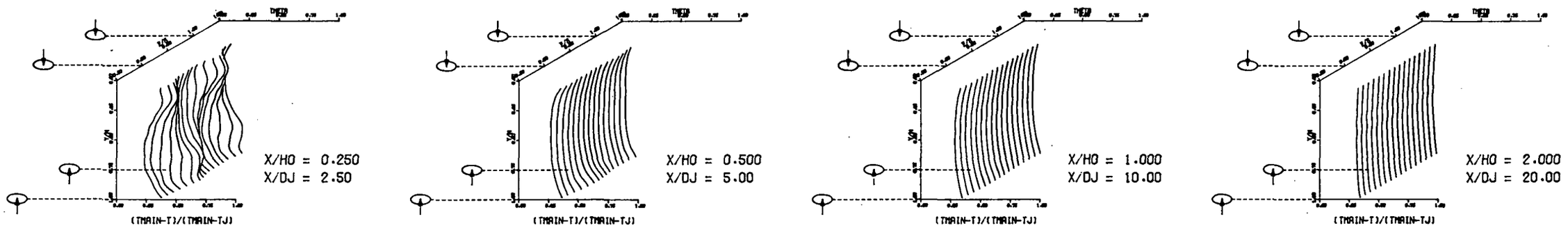

MEASURED THETA PROFILES FOR TEST NO.12, TEST SECTION I,TM=CONST (STG) , J = 103.07 , S/D = 4.00 , H/D = 8.00

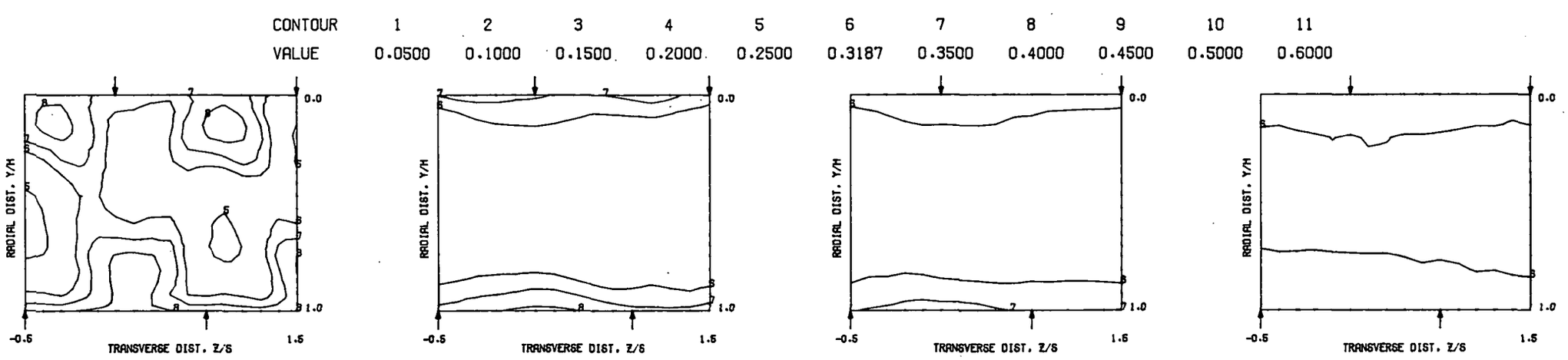

MEASURED THETA CONTOURS FOR TEST NO.12, TM=CONST (STG), J=103.1, S/D=4.0, H/D=8.

Figure 36. Measured Theta Distributions for Test No. 12.

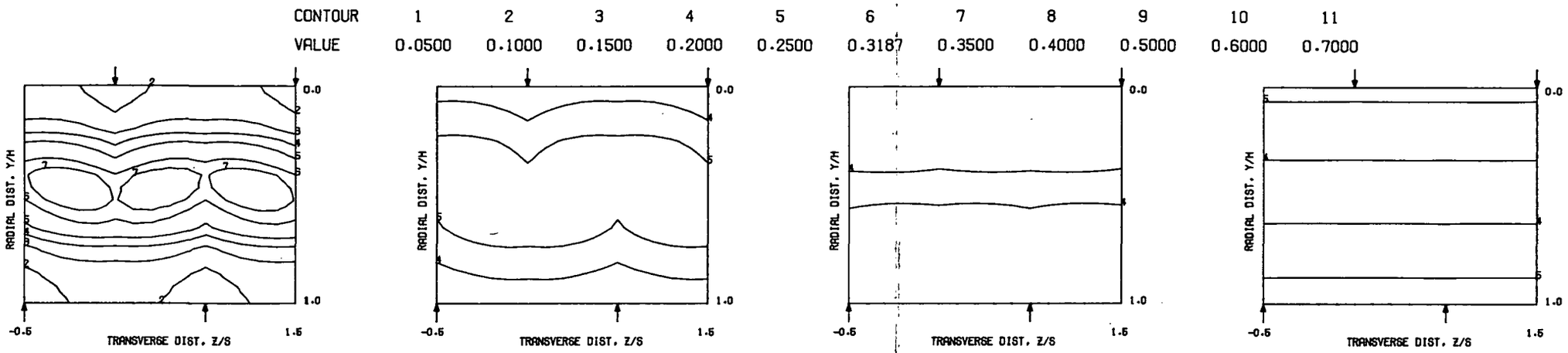

PREDICTED THETA CONTOURS FOR TEST NO 12,TM=CONST, J=103.1, S/D=4.0(STG), H/D=8.0

S/DJ = 5.00 HO/DJ = 10.00 VRATIO = 6.88 TRATIO = 0.492 DENRATIO=2.178 TMAIN = 645.9 K TJET = 317.9 K THEB = 0.316

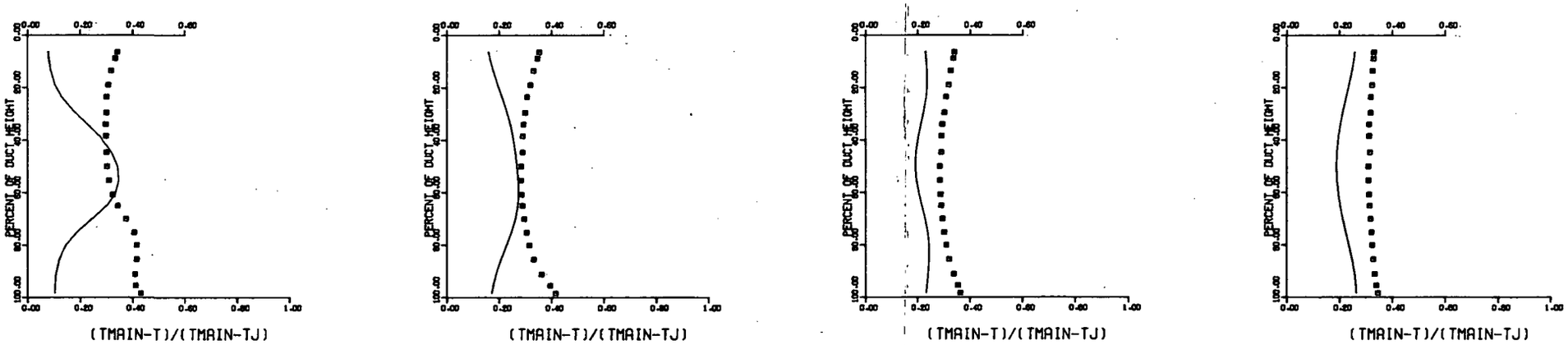

COMPARISON BETWEEN DATA AND CORRELATIONS FOR TEST NO. 12, TEST SECTION I,TM=CONST(STG), J = 103.07 , S/D =4.00 , H/D =8.00

Figure 37. Predicted Theta Distributions for Test No. 12.

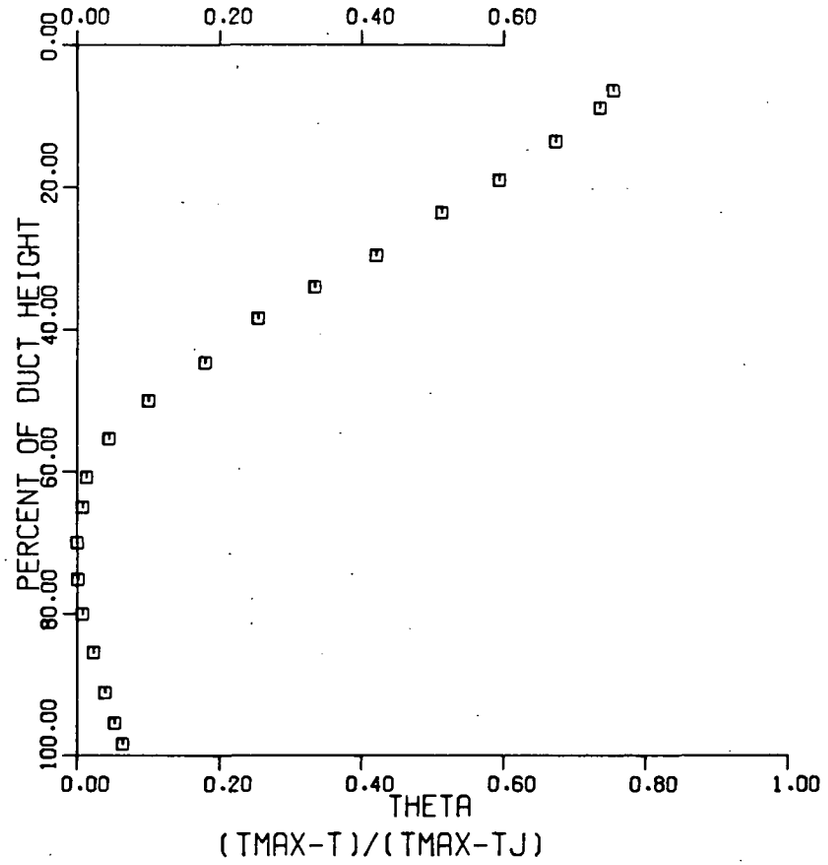

Figure 38. Profiled Mainstream Theta Distributions Used in Series 6 Tests.

S = 0.0254 METERS S/DJ = 2.540 HO/DJ = 10.159 VMAIN = 18.9 M/SEC VJET = 69.3 M/SEC TMAIN = 559.3 K TJET = 309.9 K THEB = 0.6402 BLORAT= 7.081 DENRATIO= 1.825 TRATIO= 0.554

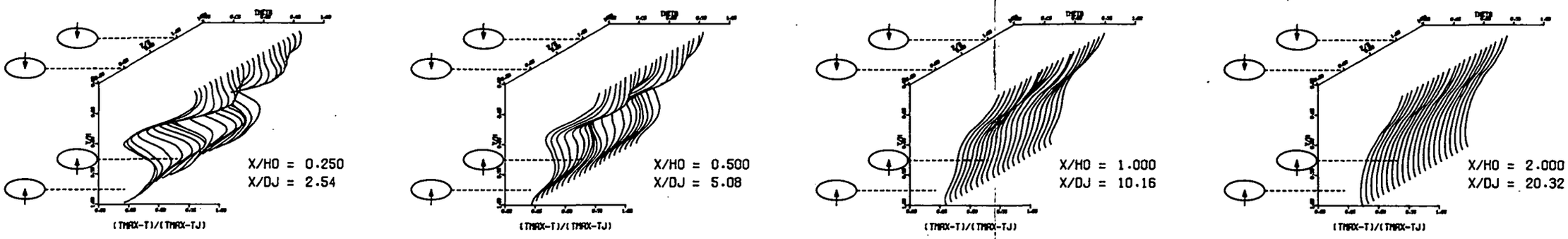

MEASURED THETA PROFILES FOR TEST NO.13, TEST SECTION I,TOP COLD (INL) , J = 24.63 , S/D = 2.00 , H/D = 8.00

CONTOUR	1	2	3	4	5	6	7	8	9	10	11
VALUE	0.1000	0.1500	0.2000	0.2500	0.3008	0.3500	0.4000	0.4500	0.5000	0.6000	0.7000

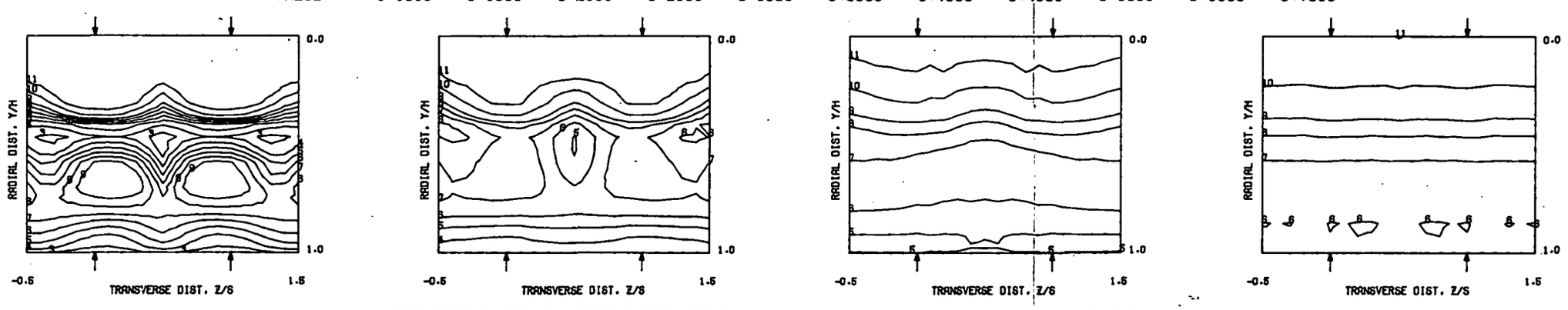

MEASURED THETA CONTOURS FOR TEST NO.13, TOP COLD (INL), J=24.63, S/D=2.0, H/D=8.

Figure 39. Measured Theta Distributions for Test No. 13.

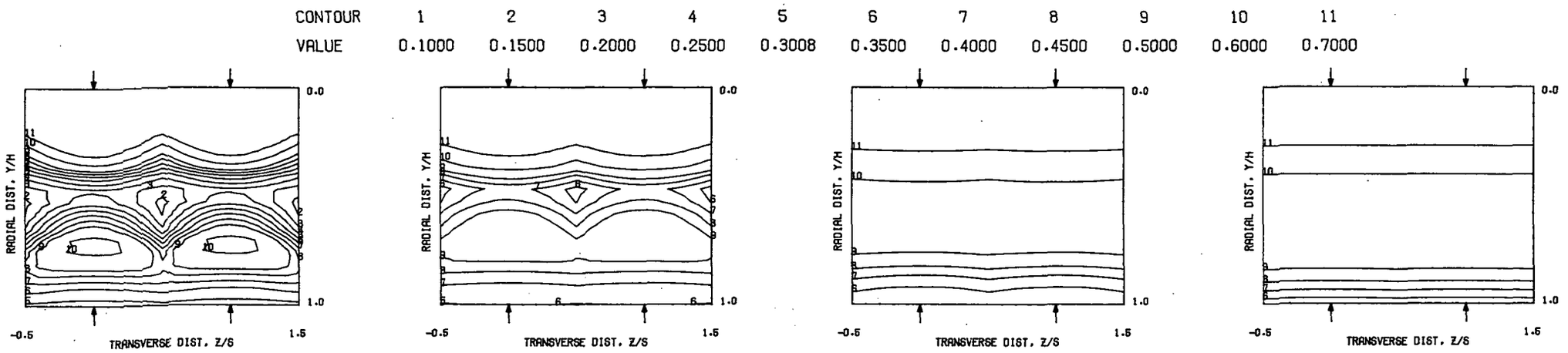

PREDICTED THETA CONTOURS FOR TEST NO 13,TOP COLD, J=24.63, S/D=2.0(INL), H/D=8.0

S/DJ = 2.54 HO/DJ = 5.08 VRATIO = 3.67 TRATIO = 0.554 DENRATIO= 1.825 TMAIN = 559.3 K TJET = 309.9 K THEB = **0.6402**

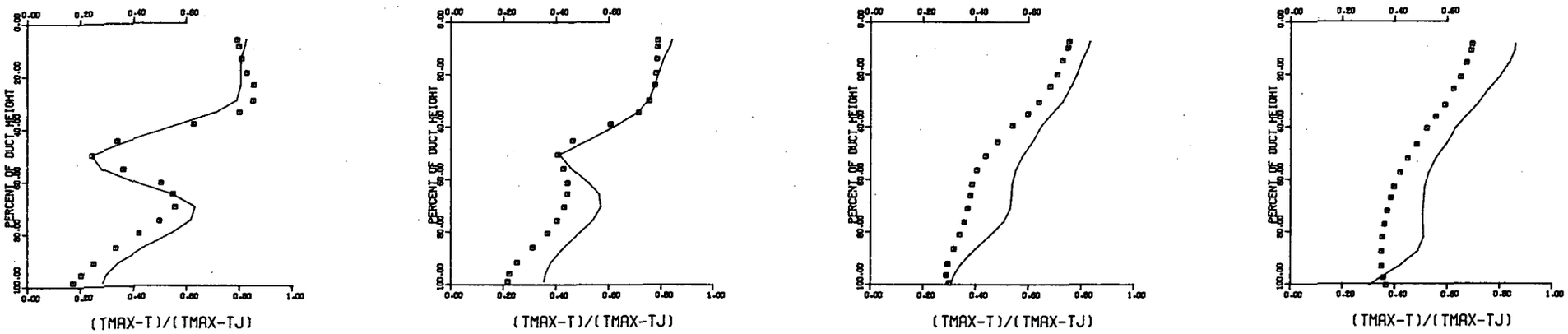

COMPARISON BETWEEN DATA AND CORRELATIONS FOR TEST NO. 13, TEST SECTION I,TOP COLD(INL). J = 24.63 , S/D =2.00 , H/D =8.00

Figure 40. Predicted Theta Distributions for Test No. 13.

S = 0.0254 METERS S/DJ = 2.500 HO/DJ = 10.000 VMAIN = 19.0 M/SEC VJET = 35.5 M/SEC TMAIN = 553.9 K TJET = 321.7 K THEB = 0.5990 BLORAT= 3.457 DENRATIO= 1.725 TRATIO= 0.581

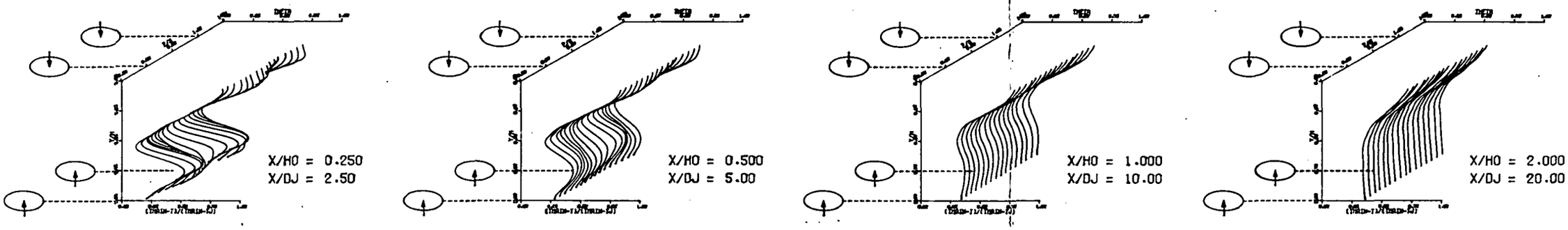

MEASURED THETA PROFILES FOR TEST NO.14. TEST SECTION I.TOP COLD (STG).. J = 6.02 . S/D = 2.00 . H/D = 8.00

CONTOUR	1	2	3	4	5	6	7	8	9	10	11
VALUE	0.0500	0.1000	0.1800	0.2000	0.2500	0.3000	0.3500	0.4000	0.5000	0.6000	0.7000

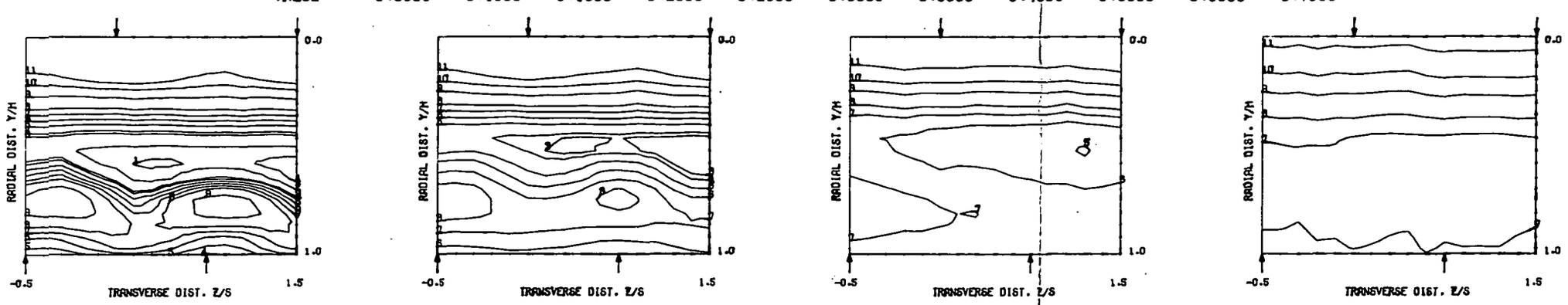

MEASURED THETA CONTOURS FOR TEST NO.14.TOP COLD (STG). J=6.02. S/D=2.0. H/D=8.0

Figure 41. Measured Theta Distributions for Test No. 14.

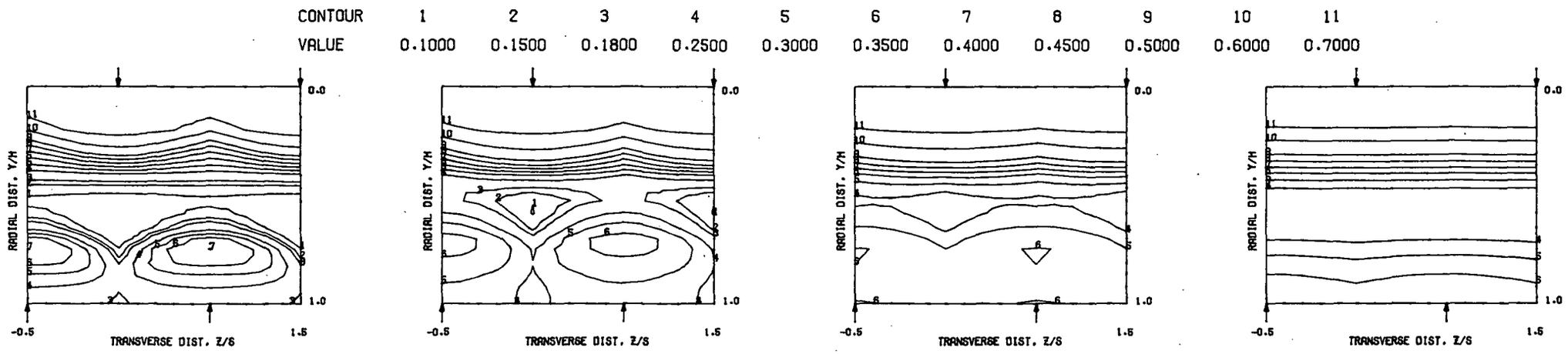

PREDICTED THETA CONTOURS FOR TEST NO 14,TOP COLD, J=6.02, S/D=2.0(STG), H/D=8.0

S/DJ = 2.46 HO/DJ = 9.85 VRATIO = 1.87 TRATIO = 0.581 DENRATIO= 1.725 TMAIN = 553.9 K TJET = 321.7 K THEB = 0.5990

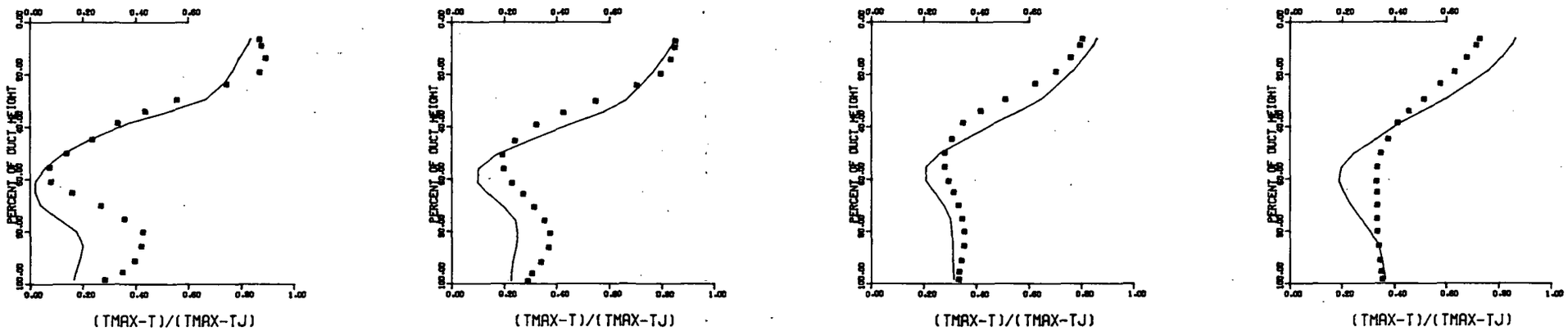

COMPARISON BETWEEN DATA AND CORRELATIONS FOR TEST NO. 14, TEST SECTION I,TOP COLD(STG), J = 6.02 , S/D =2.00 , H/D =8.00

Figure 42. Predicted Theta Distributions for Test No. 13.

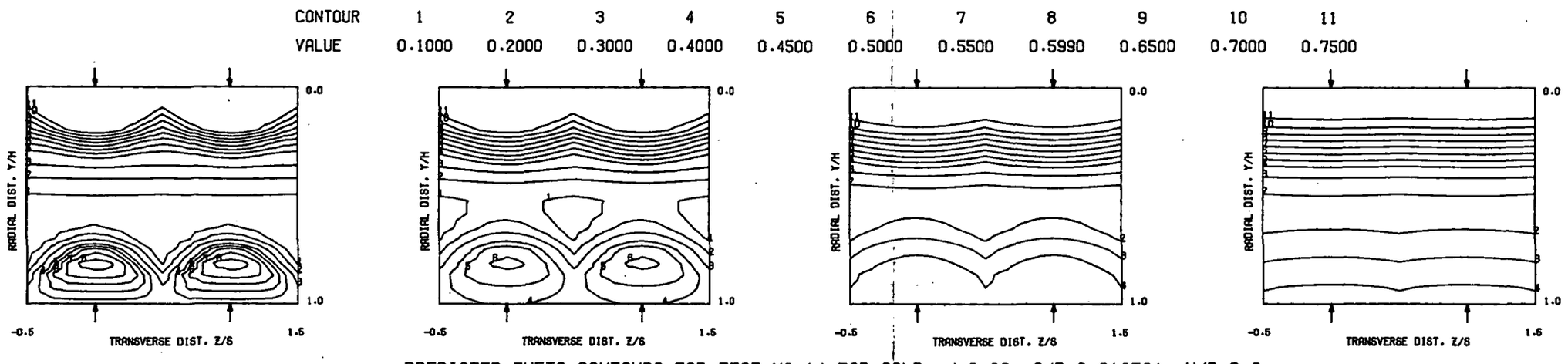

PREDICTED THETA CONTOURS FOR TEST NO 14,TOP COLD, J=6.02, S/D=2.0(STG), H/D=8.0

S/DJ = 2.46 HO/DJ = 5.04 VRATIO = 1.87 TRATIO = 0.581 DENRATIO= 1.725 TMAIN = 553.9 K TJET = 321.7 K THEB = 0.5990

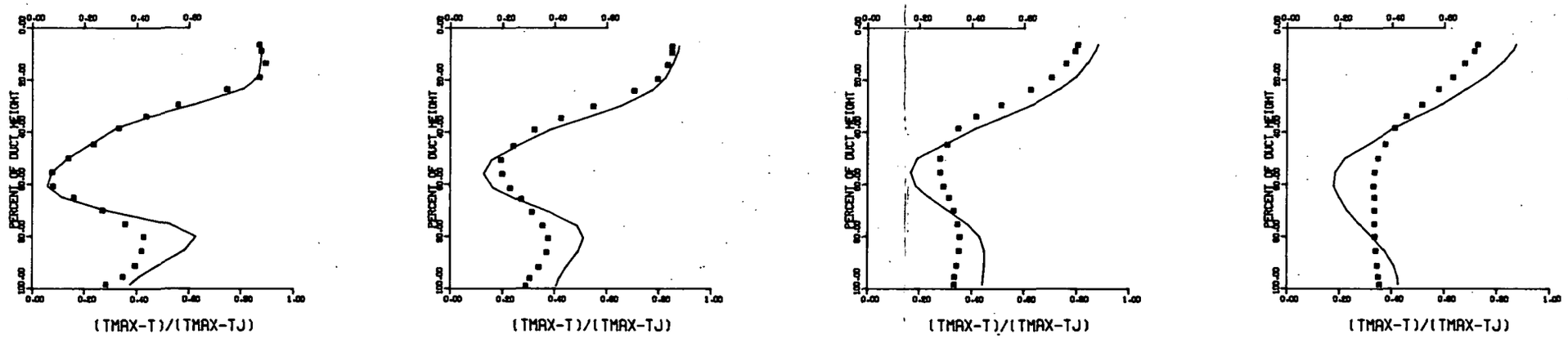

COMPARISON BETWEEN DATA AND CORRELATIONS FOR TEST NO. 14, TEST SECTION I,TOP COLD(STG), J = 6.02 , S/D =2.00 , H/D =8.00

Figure 43. Predicted Theta Distributions for Test No. 14 Using Correlations for In-line Injections.

S = 0.0254 METERS S/DJ = 2.520 HO/DJ = 10.080 VMAIN = 18.9 M/SEC VJET = 69.6 M/SEC TMAIN = 554.6 K TJET = 318.5 K THEB = **0.6541** BLORAT= 6.942 DENRATIO= 1.758 TRATIO= 0.574

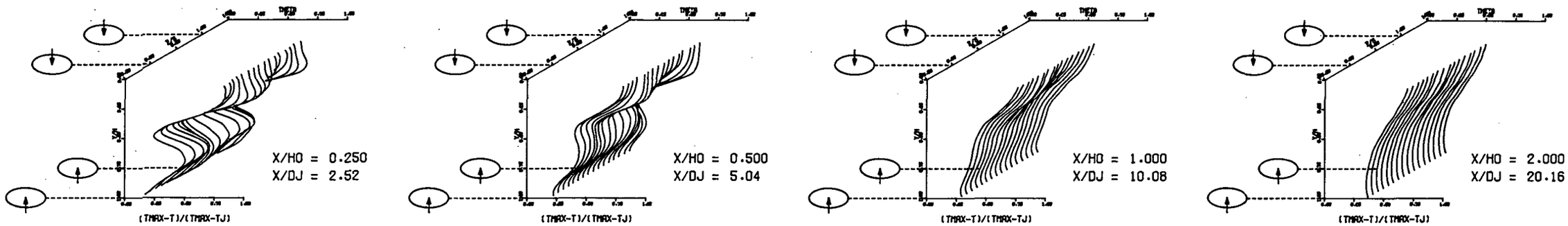

MEASURED THETA PROFILES FOR TEST NO.15, TEST SECTION I,TOP COLD (STG) , J = 23.77 , S/D = 2.00 , H/D = 8.00

CONTOUR	1	2	3	4	5	6	7	8	9	10	11
VALUE	0.1000	0.1500	0.2000	0.2500	0.3069	0.3500	0.4000	0.4500	0.5000	0.6000	0.7000

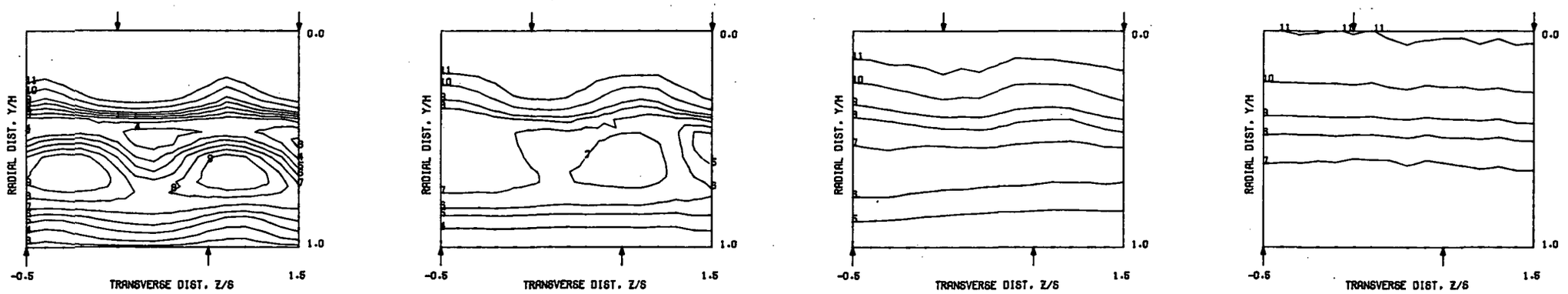

MEASURED THETA CONTOURS FOR TEST NO.15, TOP COLD (STG), J=23.77, S/D=2.0, H/D=8.

Figure 44. Measured Theta Distributions for Test No. 15.

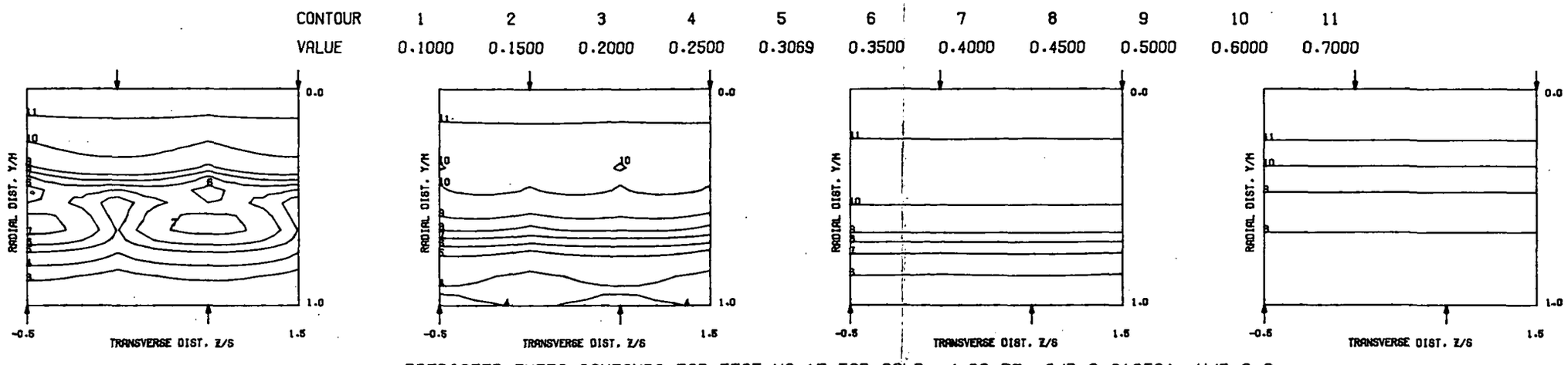

PREDICTED THETA CONTOURS FOR TEST NO 15.TOP COLD. J=23.77. S/D=2.0(STG). H/D=8.0

S/DJ = 2.52 HO/DJ = 10.08 VRATIO = 3.68 TRATIO = 0.574 DENRATIO=1.758 TMAIN = 554.6 K TJET = 318.5 K THEB = **0.6541**

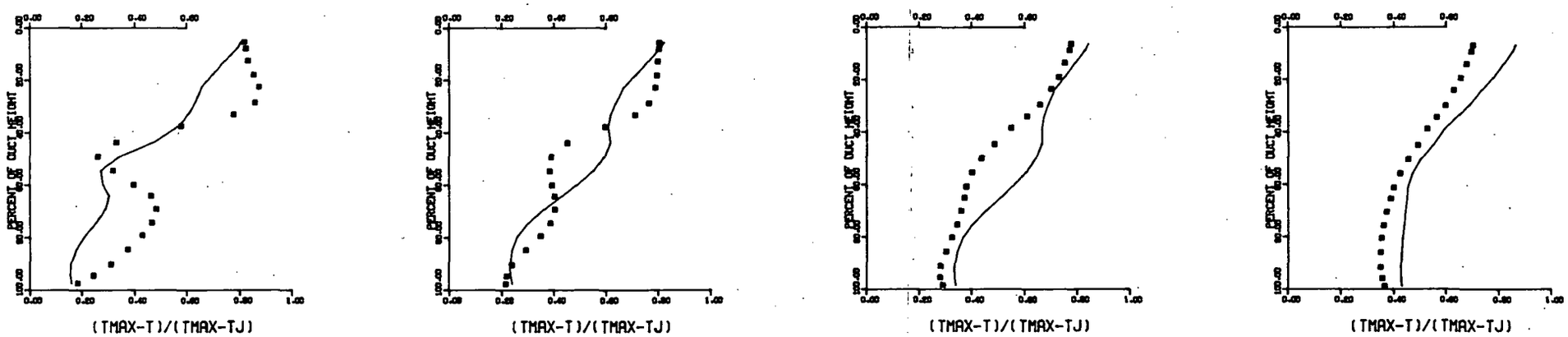

COMPARISON BETWEEN DATA AND CORRELATIONS FOR TEST NO. 15, TEST SECTION I.TOP COLD(STG). J = 23.77 , S/D =2.00 , H/D =8.00

Figure 45. Predicted Theta Distributions for Test No. 15.

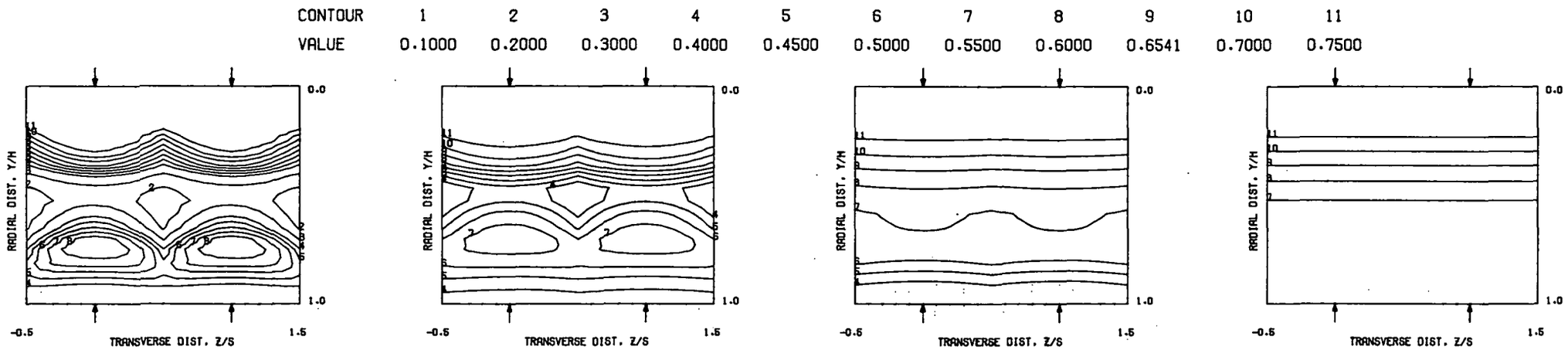

PREDICTED THETA CONTOURS FOR TEST NO 15,TOP COLD, J=23.77, S/D=2.0(STG), H/D=8.0

S/DJ = 2.52 HO/DJ = 5.02 VRATIO = 3.68 TRATIO = 0.574 DENRATIO= 1.758 TMAIN = 554.6 K TJET = 318.5 K THEB = **0.6541**

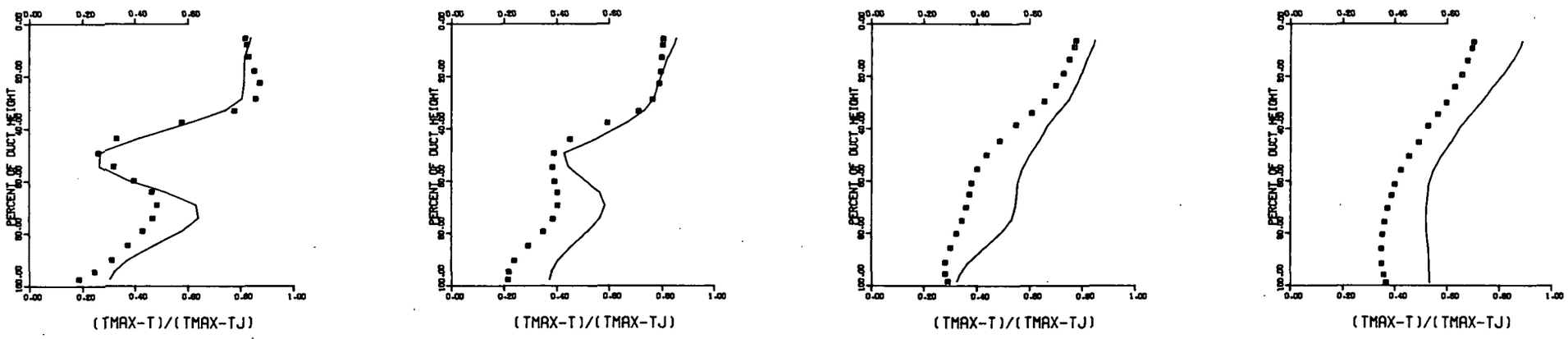

COMPARISON BETWEEN DATA AND CORRELATIONS FOR TEST NO. 15, TEST SECTION I,TOP COLD(STG), J = 23.77 , S/D =2.00 , H/D =8.00

Figure 46. Predicted Theta Distributions for Test No. 15 Using Correlations for In-line Injections.

S = 0.0508 METERS S/DJ = 5.000 HO/DJ = 10.000 VMAIN = 18.6 M/SEC VJET = 68.5 M/SEC TMAIN = 549.9 K TJET = 321.3 K THEB = 0.6017 BLORAT= 6.892 DENRATIO= 1.733 TRATIO=0.584

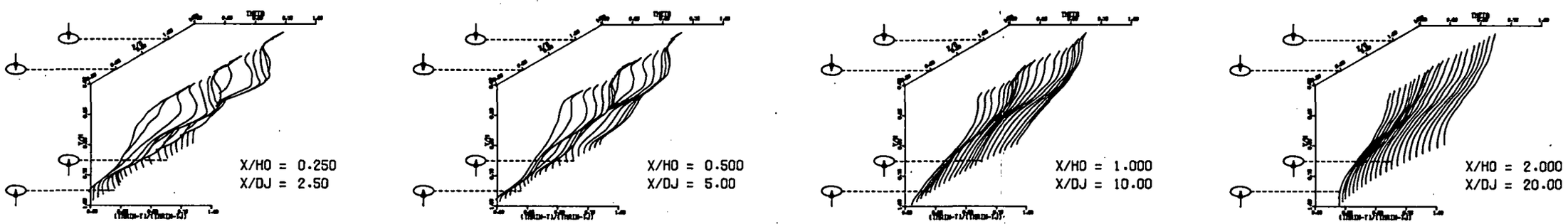

MEASURED THETA PROFILES FOR TEST NO.16, TEST SECTION I,TOP COLD (INL), J = 23.60 , S/D = 4.00 , H/D = 8.00

CONTOUR	1	2	3	4	5	6	7	8	9	10	11
VALUE	0.0500	0.1000	0.1795	0.2000	0.2500	0.3000	0.3500	0.4000	0.5000	0.6000	0.7000

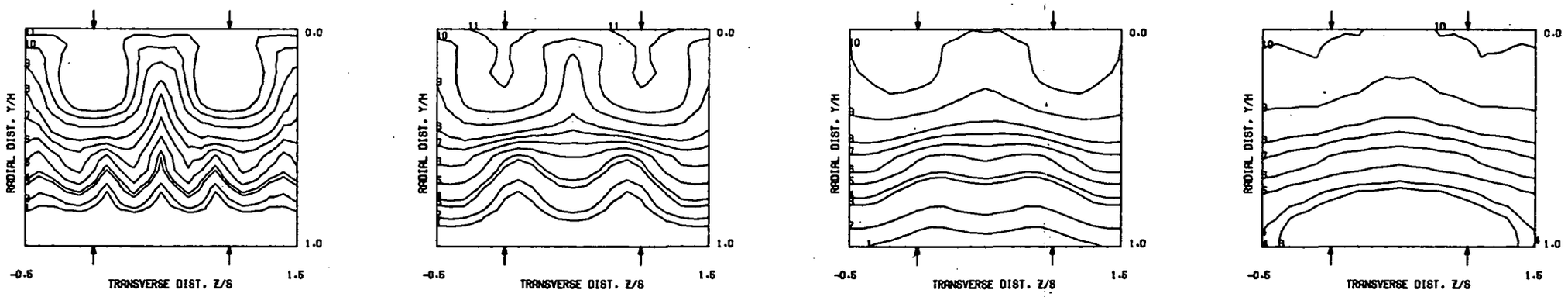

MEASURED THETA CONTOURS FOR TEST NO.16, TOP COLD (INL), J=23.6, S/D=4.0, H/D=8.0

Figure 47. Measured Theta Distributions for Test No. 16.

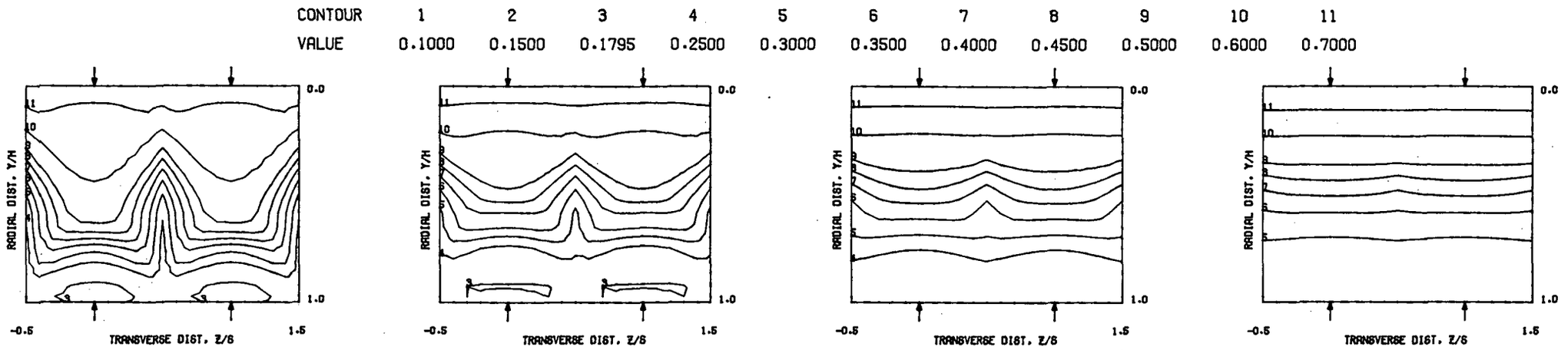

PREDICTED THETA CONTOURS FOR TEST NO 16,TOP COLD, J=23.60, S/D=4.0(INL), H/D=8.0

S/DJ = 4.94 HO/DJ = 5.03 VRATIO = 3.69 TRATIO = 0.584 DENRATIO= 1.733 TMAIN = 549.9 K TJET = 321.3 K THEB = 0.6017

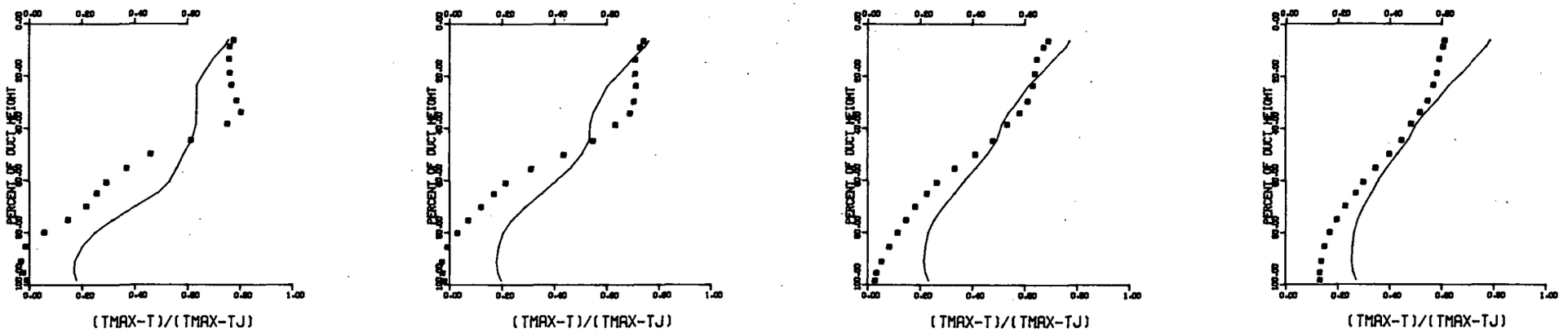

COMPARISON BETWEEN DATA AND CORRELATIONS FOR TEST NO. 16, TEST SECTION I,TOP COLD(INL). J = 23.60 , S/D =4.00 , H/D =8.00

Figure 48. Predicted Theta Distributions for Test No. 16.

S = 0.0508 METERS S/DJ = 5.017 HO/DJ = 10.033 VMAIN = 18.8 M/SEC VJET = 68.7 M/SEC TMAIN = 548.1 K TJET = 315.4 K THEB = 0.6004 BLORAT= 6.980 DENRATIO= 1.759 TRATIO=0.575

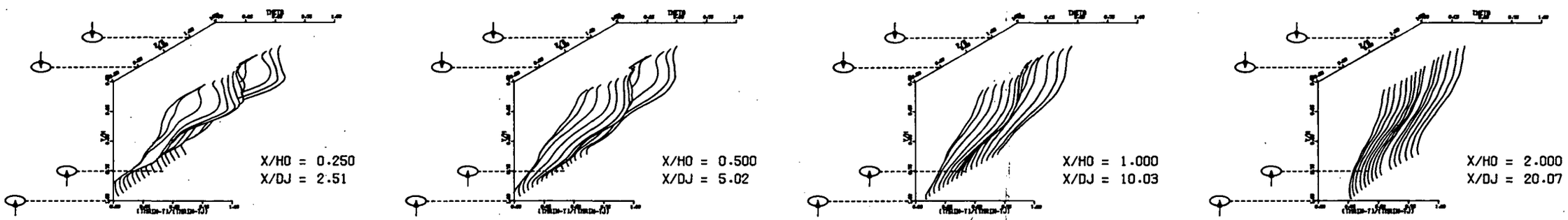

MEASURED THETA PROFILES FOR TEST NO.17, TEST SECTION I,TOP COLD (STG) , J = 23.62 , S/D = 4.00 , H/D = 8.00

CONTOUR 1 2 3 4 5 6 7 8 9 10 11
VALUE 0.0500 0.1000 0.1807 0.2000 0.2500 0.3000 0.3500 0.4000 0.5000 0.6000 0.7000

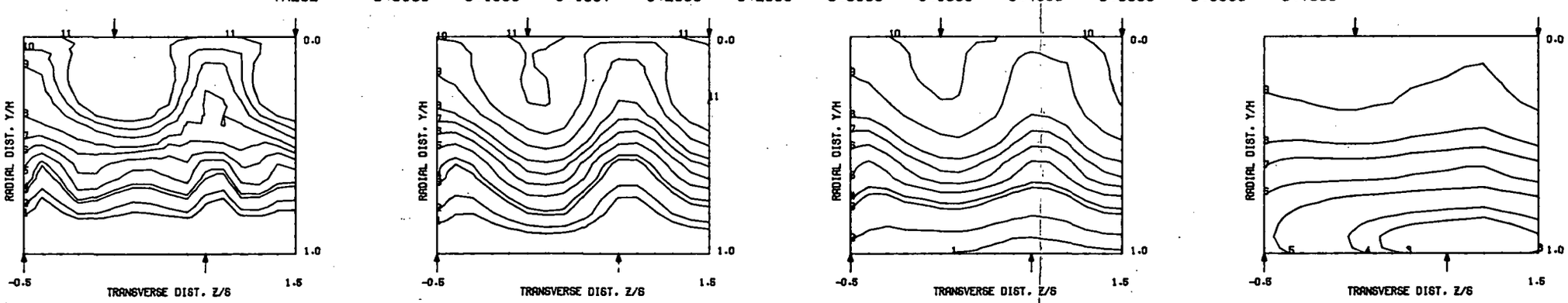

MEASURED THETA CONTOURS FOR TEST NO.17,TOP COLD (STG), J=23.6, S/D=4.0, H/D=8.0

Figure 49. Measured Theta Distributions for Test No. 17.

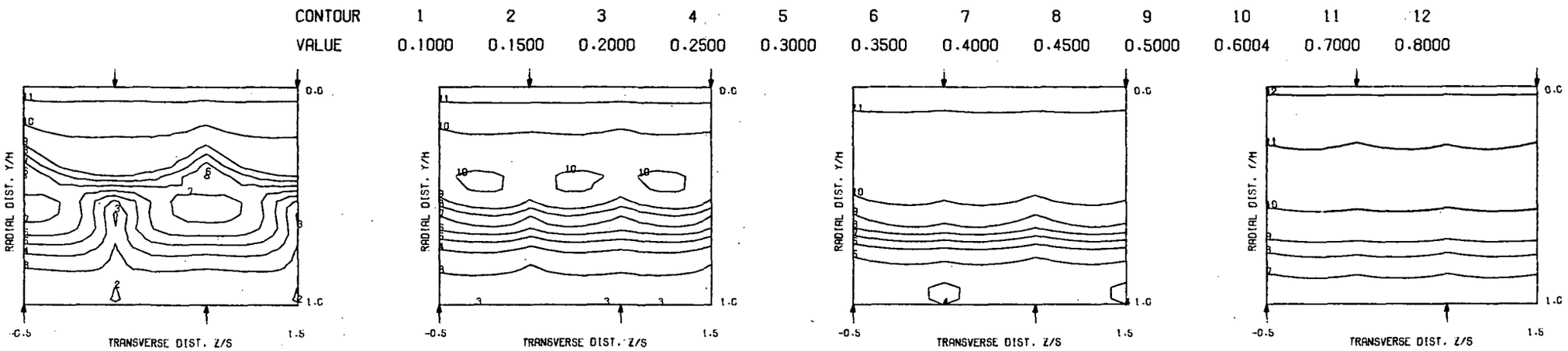

PREDICTED THETA CONTOURS FOR TEST NO 17,TOP COLD, J=23.62, S/D=4.0(STG), H/D=8.0

S/DJ = 4.89 HO/DJ = 9.78 VRATIO = 3.66 TRATIO = 0.575 DENRATIO=1.759 TMAIN = 548.1 K TJET = 315.4 K THEB = **0.6004**

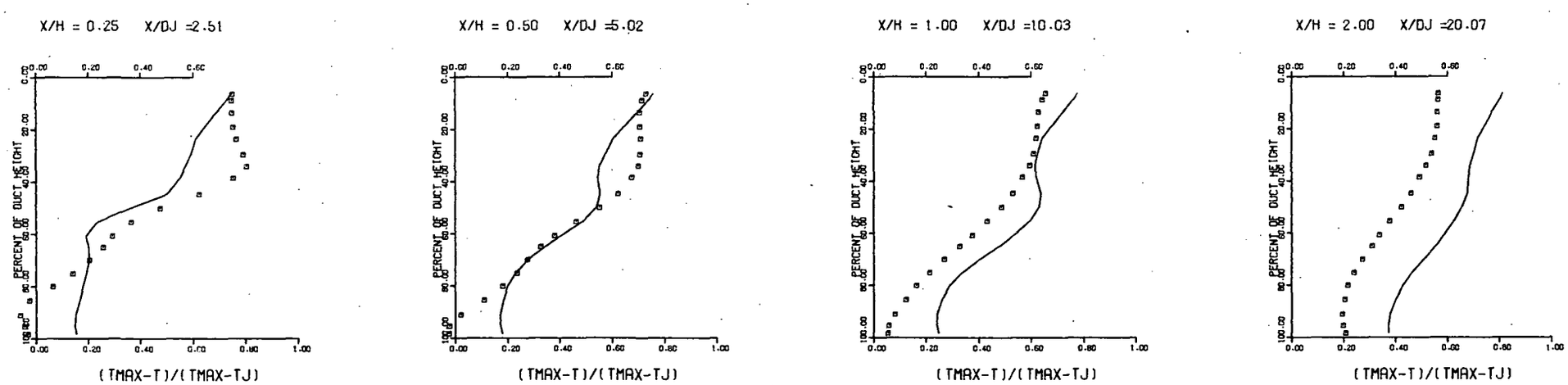

COMPARISON BETWEEN DATA AND CORRELATIONS FOR TEST NO. 17, TEST SECTION I,TOP COLD(STG), J = 23.62 , S/D =4.00 , H/D =8.00

Figure 50. Predicted Theta Distributions for Test No. 17.

S = 0.0508 METERS S/DJ = 5.040 HO/DJ = 10.080 VMAIN = 18.9 M/SEC VJET = 137.7 M/SEC TMAIN = 551.1 K TJET = 313.5 K THEB = 0.6589 BLORAT= 14.698 DENRATIO= 1.873 TRATIO=0.569

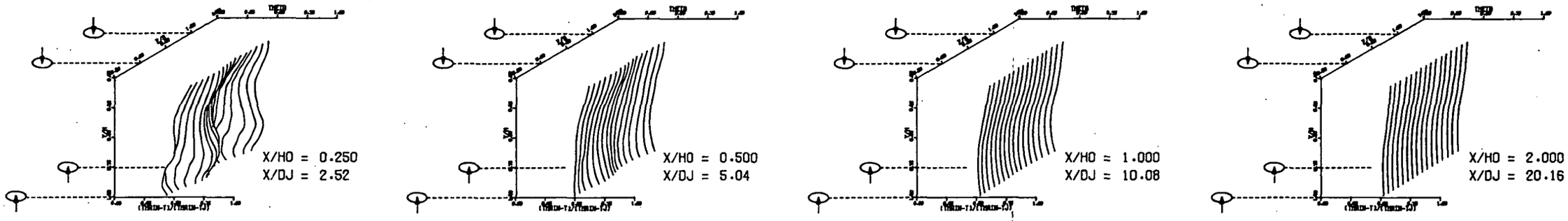

MEASURED THETA PROFILES FOR TEST NO.18, TEST SECTION I,TOP COLD (STG) , J = 99.52 , S/D = 4.00 , H/D = 8.00

CONTOUR	1	2	3	4	5	6	7	8	9	10	11
VALUE	0.3186	0.3500	0.4000	0.4500	0.4750	0.5000	0.5250	0.5500	0.5750	0.6000	0.6500

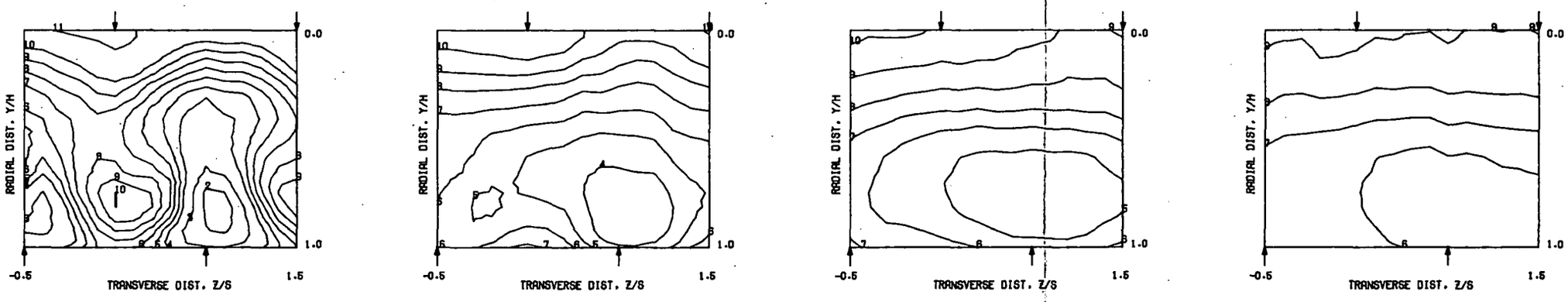

MEASURED THETA CONTOURS FOR TEST NO.18,TOP COLD (STG), J=99.5, S/D=4.0, H/D=8.0

Figure 51. Measured Theta Distributions for Test No. 18.

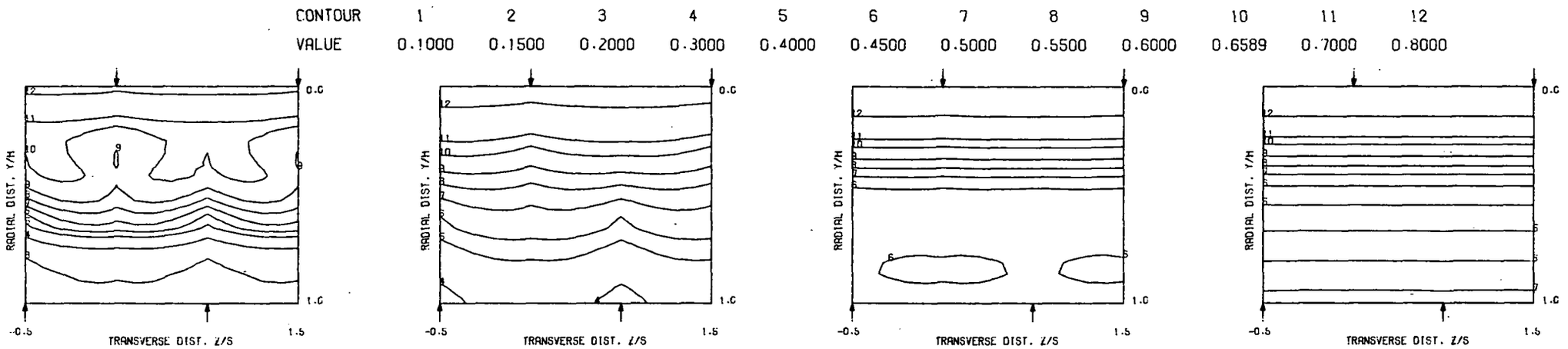

PREDICTED THETA CONTOURS FOR TEST NO 18,TOP COLD, J=99.52, S/D=4.0(STG), H/D=8.0

S/DJ = 4.94 HO/DJ = 9.88 VRATIO = 7.29 TRATIO = 0.569 DENRATIO= 1.873 TMAIN = 551.1 K TJET = 313.5 K THEB = **0.6589**

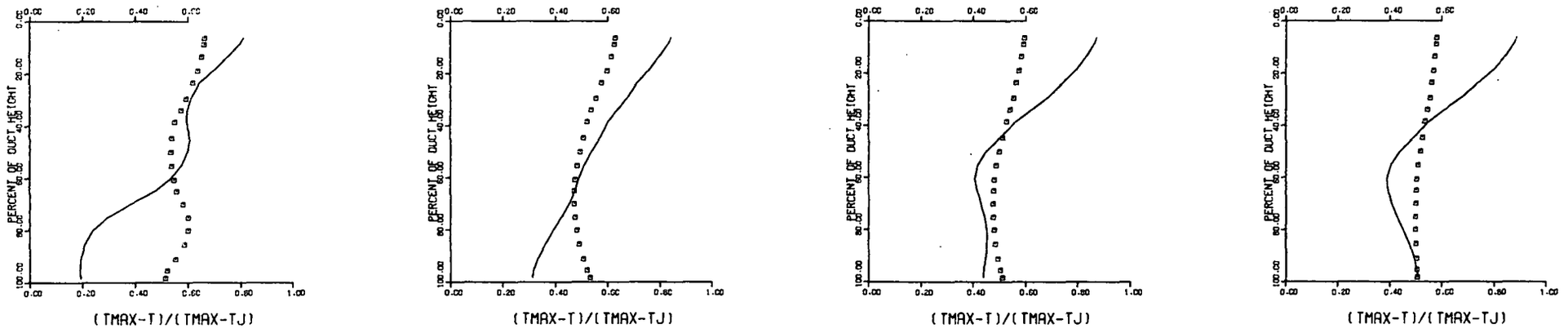

COMPARISON BETWEEN DATA AND CORRELATIONS FOR TEST NO. 18, TEST SECTION I,TOP COLD(STG), J = 99.52 , S/D =4.00 , H/D =8.00

Figure 52. Predicted Theta Distributions for Test No. 18.

S = 0.0254 METERS S/DJ = 2.475 HO/DJ = 9.899 VMAIN = 16.5 M/SEC VJET = 56.5 M/SEC TMAIN = 644.8 K TJET = 298.2 K THEB = 0.3253 BLORAT= 7.560 DENRATIO= 2.201 TRATIO=0.463

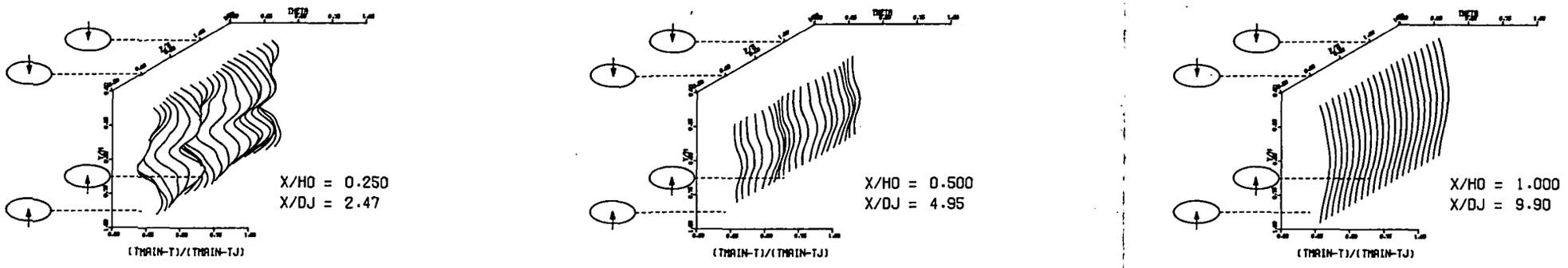

MEASURED THETA PROFILES FOR TEST NO.19, TEST SECTION II, TM=CONST(INL), J = 25.98 , S/D = 2.00 , H/D = 8.00

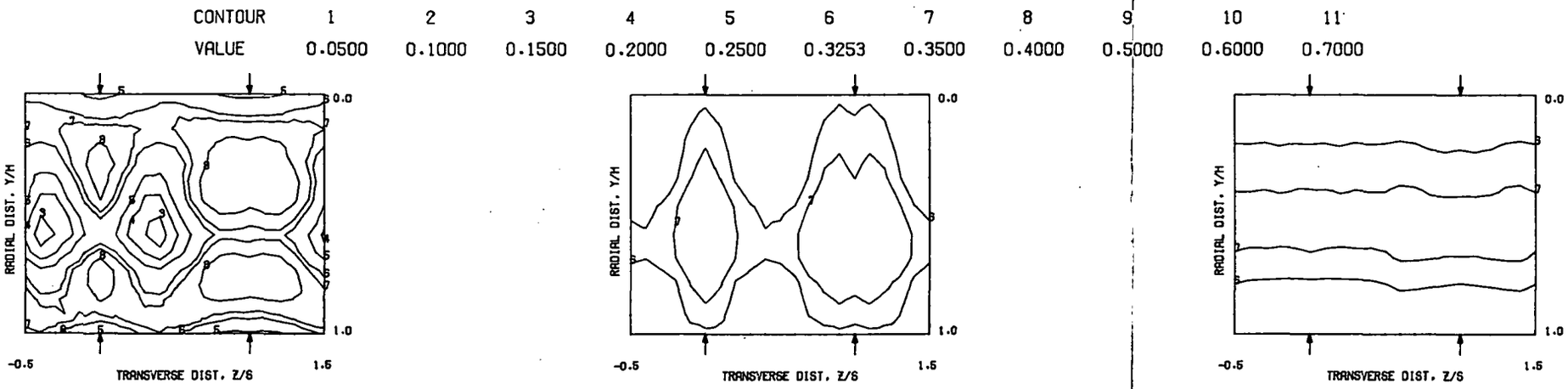

MEASURED THETA CONTOURS FOR TEST NO.19,TM=CONST (INL), J=26.00, S/D=2.0, H/D=8.0

Figure 53. Measured Theta Distributions for Test No. 19.

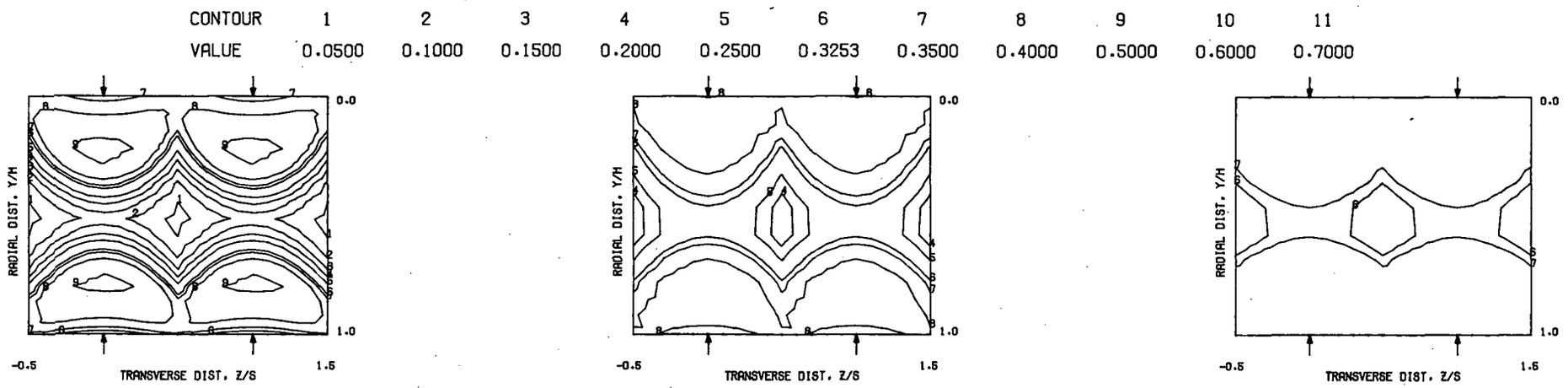

PREDICTED THETA CONTOURS FOR TEST NO 19, T.S.II, J=25.98, S/D=2.0(INL), H/D=8.0

S/DJ = 2.47 HO/DJ = 4.93 VRATIO = 3.44 TRATIO = 0.463 DENRATIO=2.201 TMAIN = 644.8 K TJET = 298.2 K THEB = 0.3253

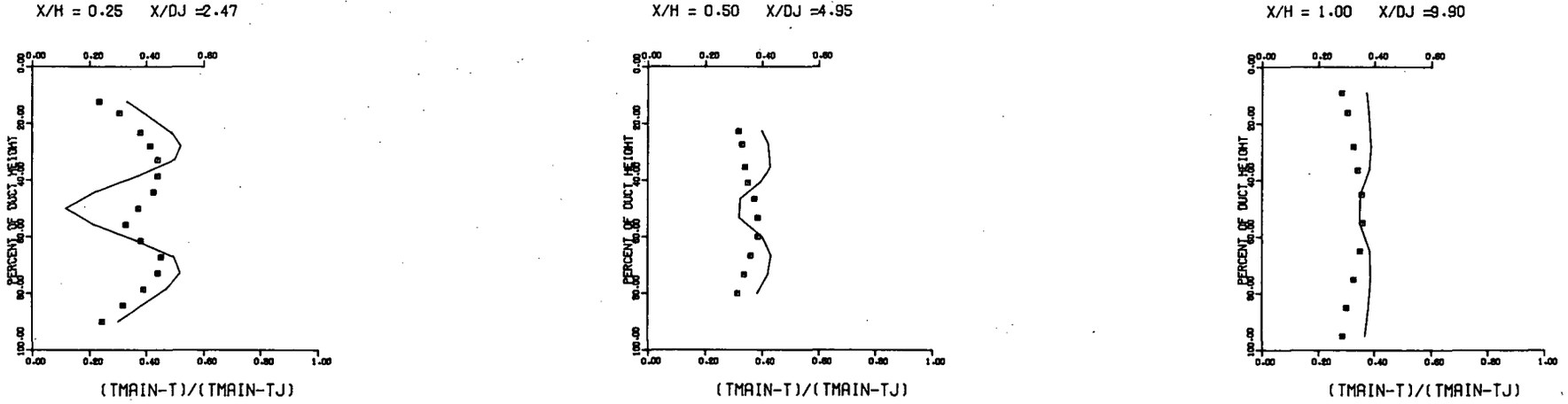

COMPARISON BETWEEN DATA AND CORRELATIONS FOR TEST NO. 19, TEST SECTION II,TM=CONST(INL), J = 25.98 , S/D =2.00 , H/D =8.00

Figure 54. Predicted Theta Distributions for Test No. 19.

S = 0.0254 METERS S/DJ = 2.475 HO/DJ = 9.899 VMAIN = 16.4 M/SEC VJET = 111.3 M/SEC TMAIN = 644.6 K TJET = 297.0 K THEB = 0.5019 BLORAT= 15.664 DENRATIO= 2.305 TRATIO= 0.461

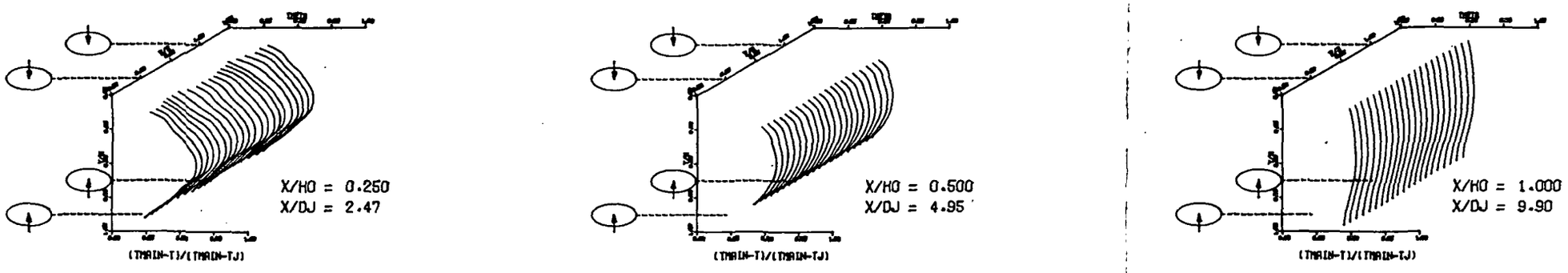

MEASURED THETA PROFILES FOR TEST NO.20, TEST SECTION II, TM=CONST(INL), J = 106.05 , S/D = 2.00 , H/D = 8.00

CONTOUR 1 2 3 4 5 6 7 8 9 10 11

VALUE 0.0500 0.1000 0.1500 0.2000 0.2500 0.3000 0.3500 0.4000 0.5019 0.6000 0.7000

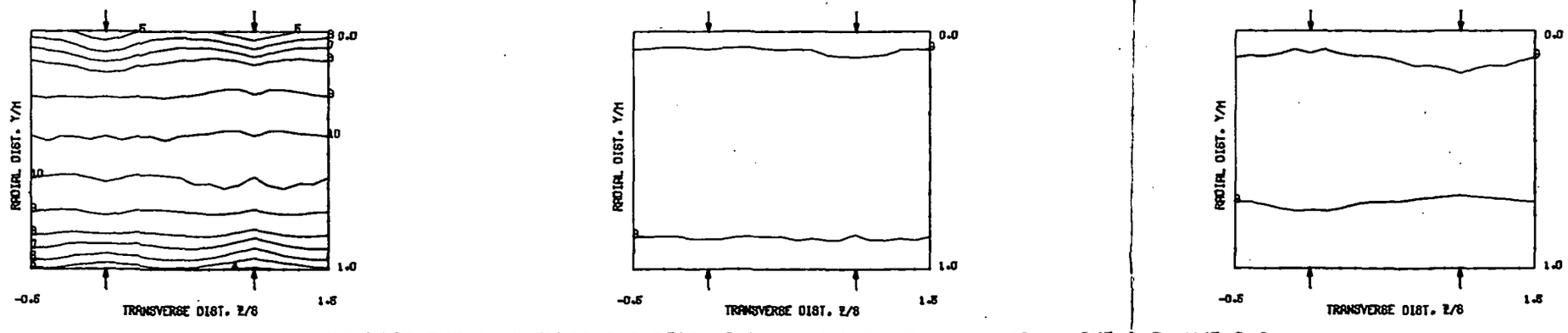

MEASURED THETA CONTOURS FOR TEST NO.20,TM=CONST (INL), J=106.1, S/D=2.0, H/D=8.0

Figure 55. Measured Theta Distributions for Test No. 20.

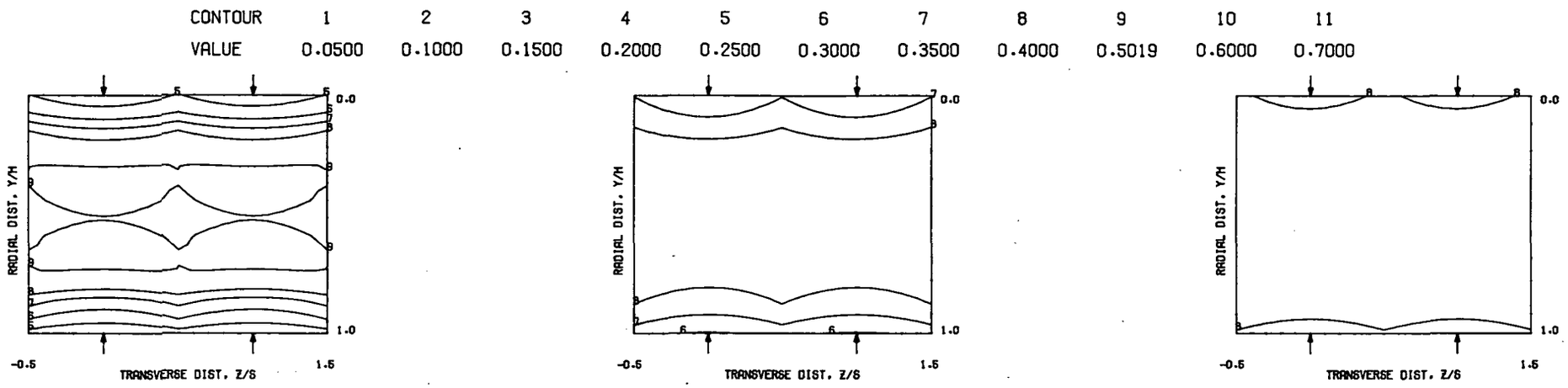

PREDICTED THETA CONTOURS FOR TEST NO 20, T.S.II, J=106.1, S/D=2.0(INL), H/D=8.0

S/DJ = 2.47 HO/DJ = 4.96 VRATIO = 6.78 TRATIO = 0.461 DENRATIO=2.305 TMAIN = 644.6 K TJET = 297.0 K THEB = 0.5019

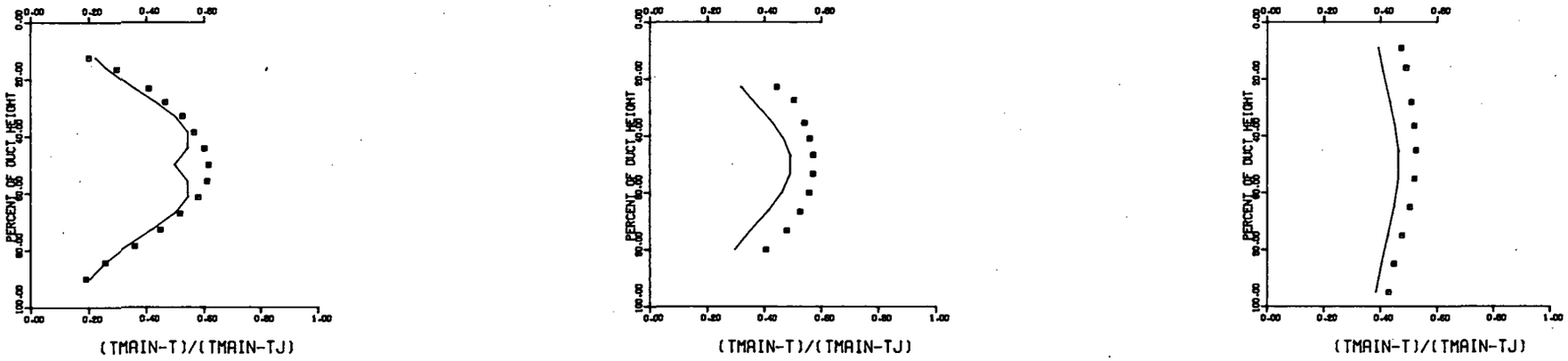

COMPARISON BETWEEN DATA AND CORRELATIONS FOR TEST NO. 20, TEST SECTION II,TM=CONST(INL), J = 106.05 , S/D =2.00 , H/D =8.00

Figure 56. Predicted Theta Distributions for Test No. 20.

S = 0.0508 METERS S/DJ = 5.000 HO/DJ = 10.000 VMAIN = 16.4 M/SEC VJET = 57.1 M/SEC TMAIN = 644.6 K TJET = 302.9 K THEB = 0.1929 BLORAT= 7.464 DENRATIO= 2.149 TRATIO= 0.470

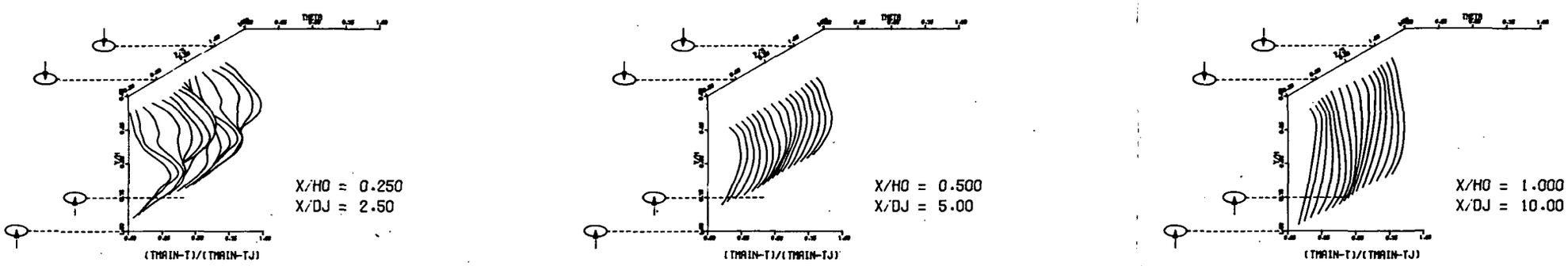

MEASURED THETA PROFILES FOR TEST NO.21, TEST SECTION II, TM=CONST(STG) , J = 25.92 , S/D = 4.00 , H/D = 8.00

CONTOUR	1	2	3	4	5	6	7	8	9	10	11
VALUE	0.0500	0.1000	0.1500	0.1929	0.2500	0.3000	0.3500	0.4000	0.5000	0.6000	0.7000

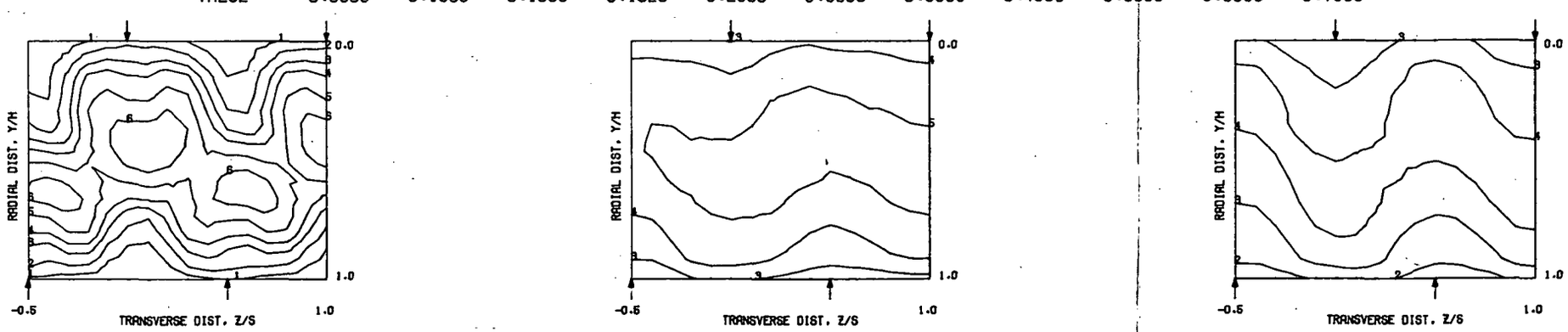

MEASURED THETA CONTOURS FOR TEST NO.21,TM=CONST (STG), J=25.9, S/D=4.0, H/D=8.0

Figure 57. Measured Theta Distributions for Test No. 21.

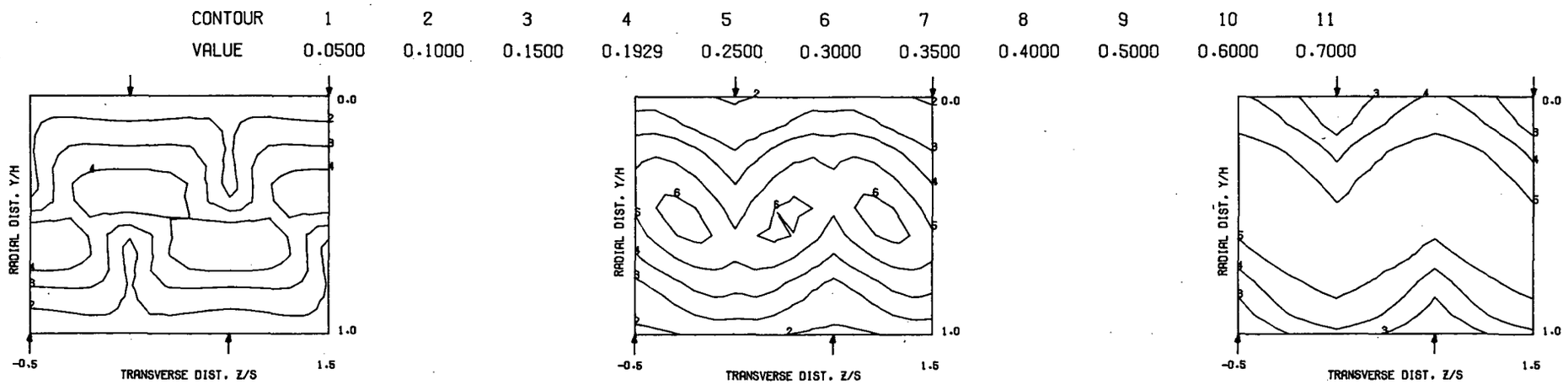

PREDICTED THETA CONTOURS FOR TEST NO 21,T.S.II, J=25.92, S/D=4.0(STG), H/D=8.0

S/DJ = 5.00 HO/DJ = 10.00 VRATIO = 3.47 TRATIO = 0.470 DENRATIO=2.149 TMAIN = 644.6 K TJET = 302.9 K THEB = 0.1929

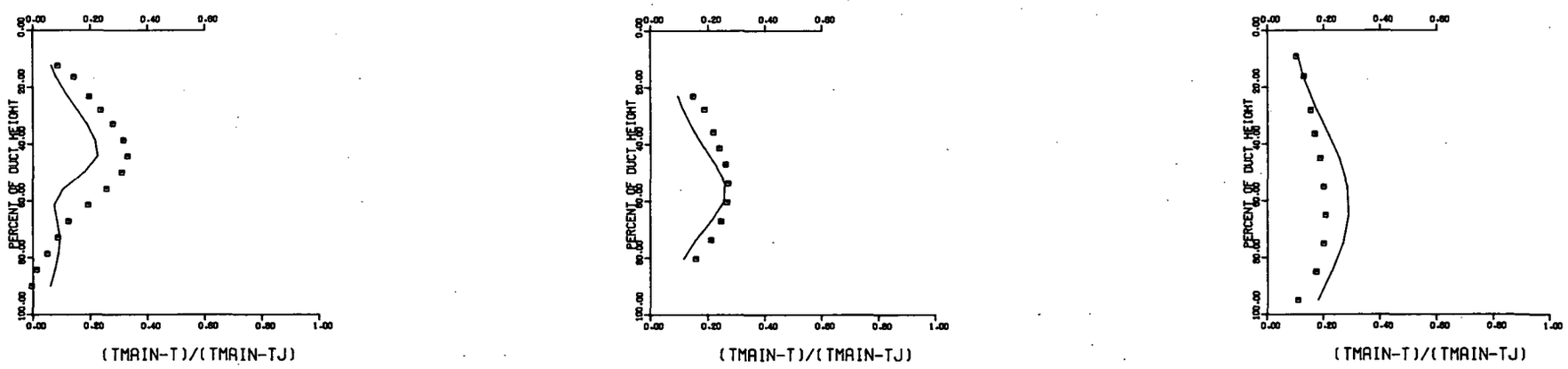

COMPARISON BETWEEN DATA AND CORRELATIONS FOR TEST NO. 21, TEST SECTION II,TM=CONST(STG), J = 25.92 , S/D =4.00 , H/D =8.00

Figure 58. Predicted Theta Distributions for Test No. 21.

S = 0.0508 METERS S/DJ = 5.040 HO/DJ = 10.080 VMAIN = 16.4 M/SEC VJET = 112.8 M/SEC TMAIN = 644.2 K TJET = 298.5 K THEB = 0.3260 BLORAT= 15.640 DENRATIO= 2.272 TRATIO=0.463

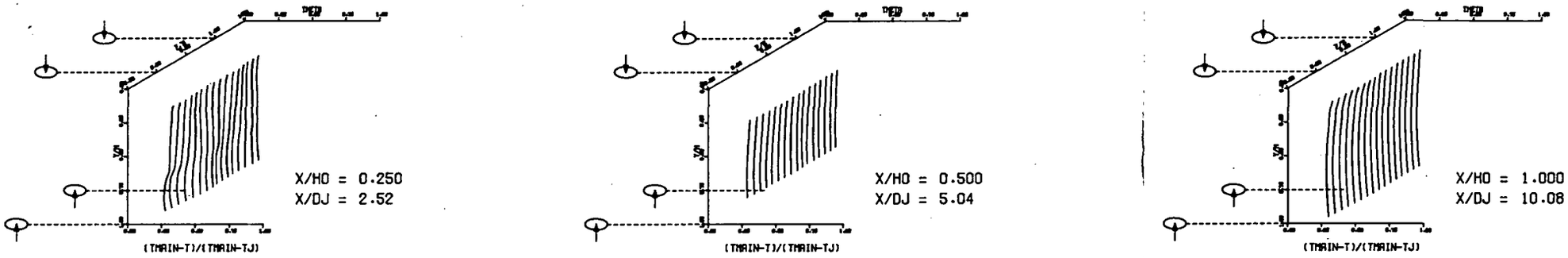

MEASURED THETA PROFILES FOR TEST NO.22, TEST SECTION II, TM=CONST(STG) , J = 107.91 , S/D = 4.00 , H/D = 8.00

CONTOUR	1	2	3	4	5	6	7	8	9	10	11
VALUE	0.0500	0.1000	0.1500	0.2000	0.2500	0.3260	0.3500	0.4000	0.5000	0.6000	0.7000

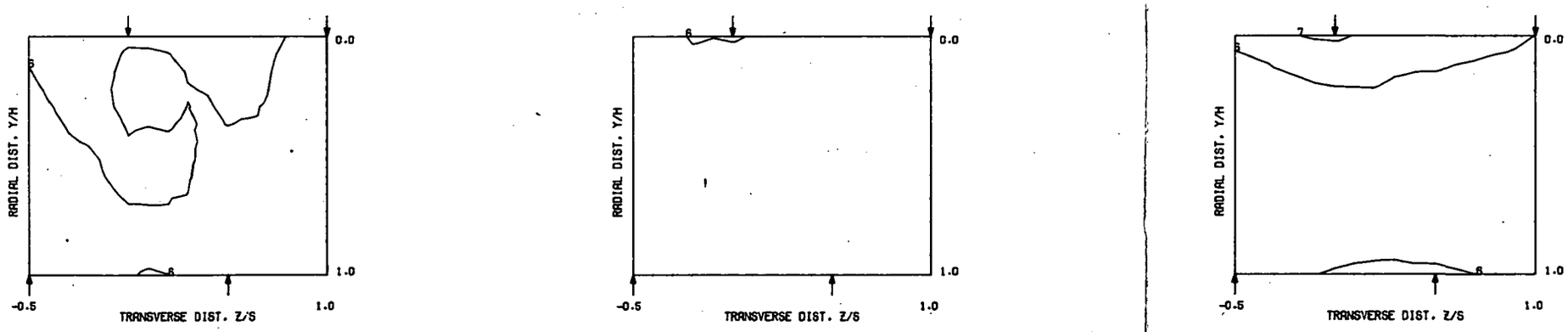

MEASURED THETA CONTOURS FOR TEST NO.22,TM=CONST (STG), J=108., S/D=4.0, H/D=8.0

Figure 59. Measured Theta Distributions for Test No. 22.

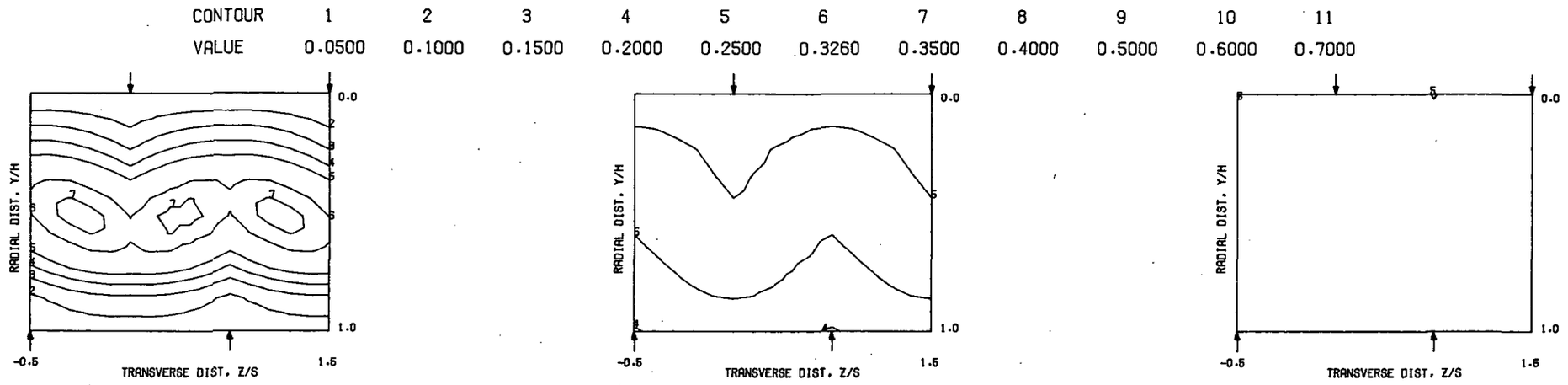

PREDICTED THETA CONTOURS FOR TEST NO 22,T.S.II, J=107.9, S/D=4.0(STG), H/D=8.0

S/DJ = 5.04 HO/DJ = 10.08 VRATIO = 6.89 TRATIO = 0.463 DENRATIO=2.272 TMAIN = 644.2 K TJET = 298.5 K THEB = 0.3260

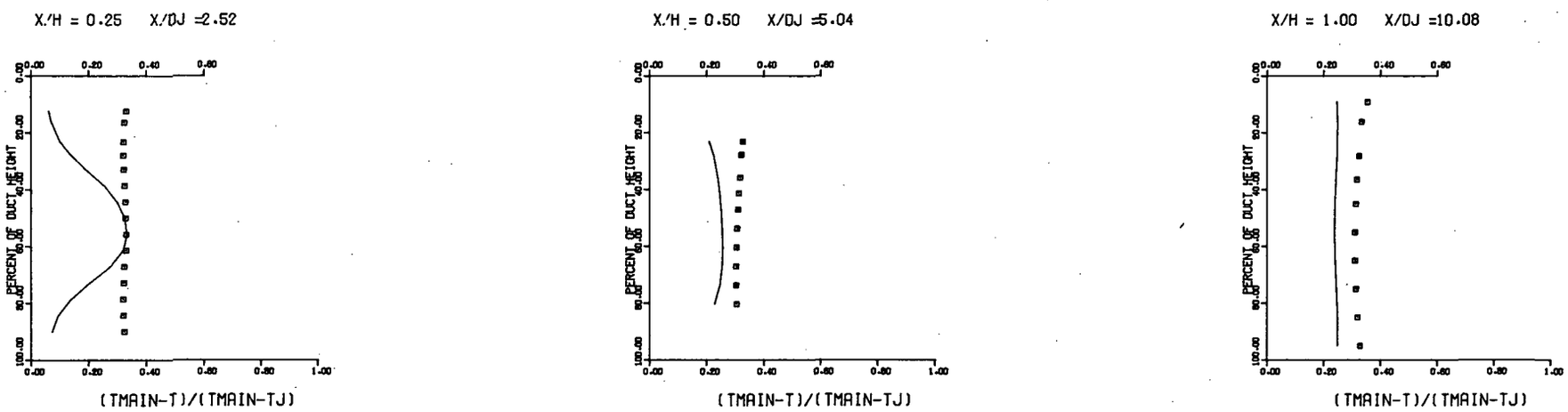

COMPARISON BETWEEN DATA AND CORRELATIONS FOR TEST NO. 22, TEST SECTION II,TM=CONST(STG), J = 107.91 , S/D =4.00 , H/D =8.00

Figure 60. Predicted Theta Distributions for Test No. 22.

S = 0.1016 METERS S/DJ = 4.886 HO/DJ = 4.886 VMAIN = 16.5 M/SEC VJET = 29.7 M/SEC TMAIN = 644.9 K TJET = 311.0 K THEB = 0.1994 BLORAT= 3.753 DENRATIO= 2.079 TRATIO= 0.482

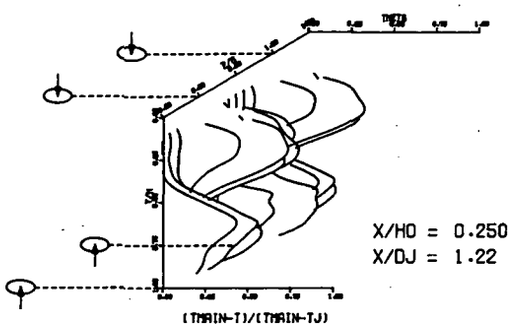

X/HO = 0.250
X/DJ = 1.22

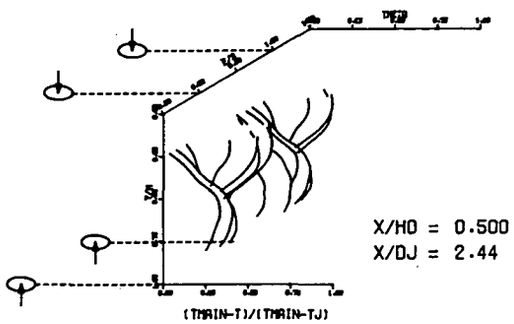

X/HO = 0.500
X/DJ = 2.44

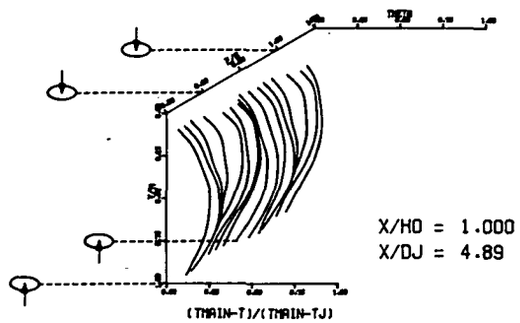

X/HO = 1.000
X/DJ = 4.89

MEASURED THETA PROFILES FOR TEST NO.23, TEST SECTION II, TM=CONST(STG) , J = 6.78 , S/D = 4.00 , H/D = 4.00

CONTOUR	1	2	3	4	5	6	7	8	9	10	11
VALUE	0.0500	0.1000	0.1500	0.1994	0.2500	0.3000	0.3500	0.4000	0.5000	0.6000	0.7000

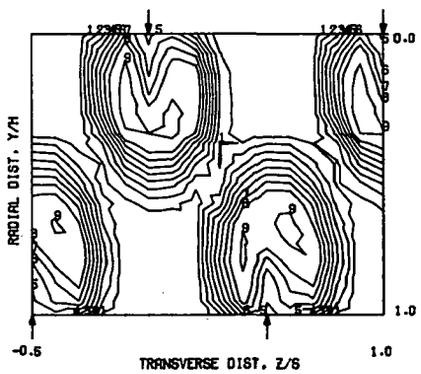

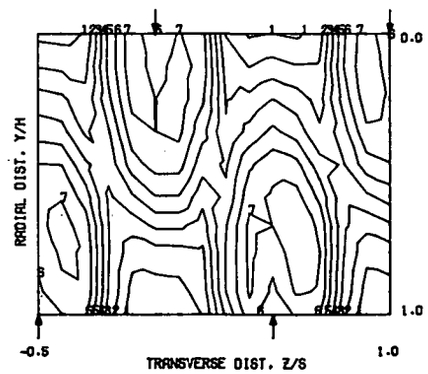

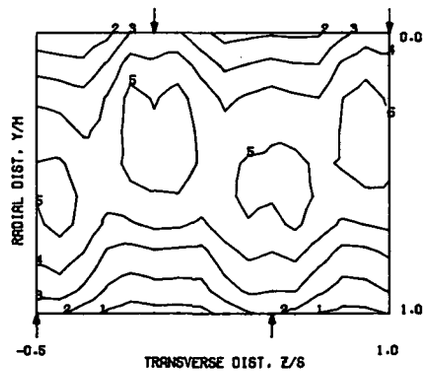

MEASURED THETA CONTOURS FOR TEST NO.23,TM=CONST (STG), J=6.78, S/D=4.0, H/D=4.0

Figure 61. Measured Theta Distributions for Test No. 23.

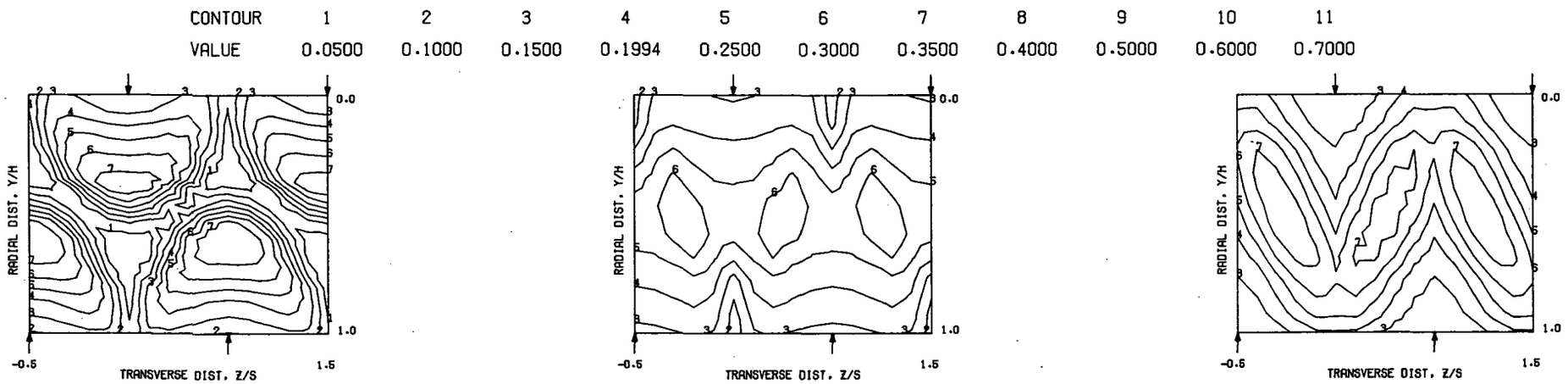

PREDICTED THETA CONTOURS FOR TEST NO 23, T.S.II, J=6.78, S/D=4.0(STG), H/D=4.0

S/DJ = 4.84 HO/DJ = 4.84 VRATIO = 1.81 TRATIO = 0.482 DENRATIO=2.079 TMAIN = 644.9 K TJET = 311.0 K **THEB = 0.1994**

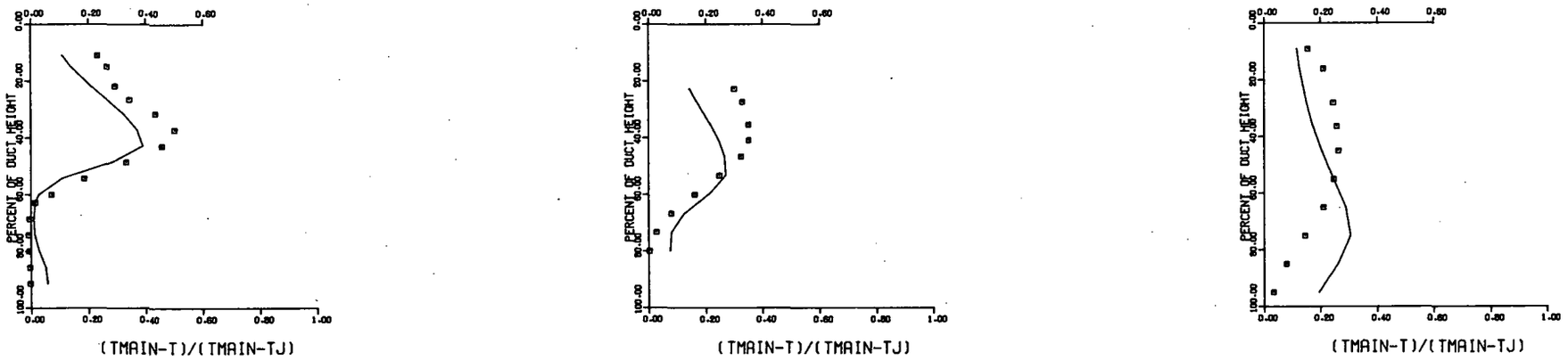

COMPARISON BETWEEN DATA AND CORRELATIONS FOR TEST NO. 23, TEST SECTION II,TM=CONST(STG), J = 6.78 , S/D =4.00 , H/D =4.00

Figure 62. Predicted Theta Distributions for Test No. 23.

S = 0.1016 METERS S/DJ = 4.969 HO/DJ = 4.969 VMAIN = 16.4 M/SEC VJET = 56.8 M/SEC TMAIN = 644.5 K TJET = 304.2 K THEB = 0.3272 BLORAT= 7.449 DENRATIO= 2.154 TRATIO=0.472

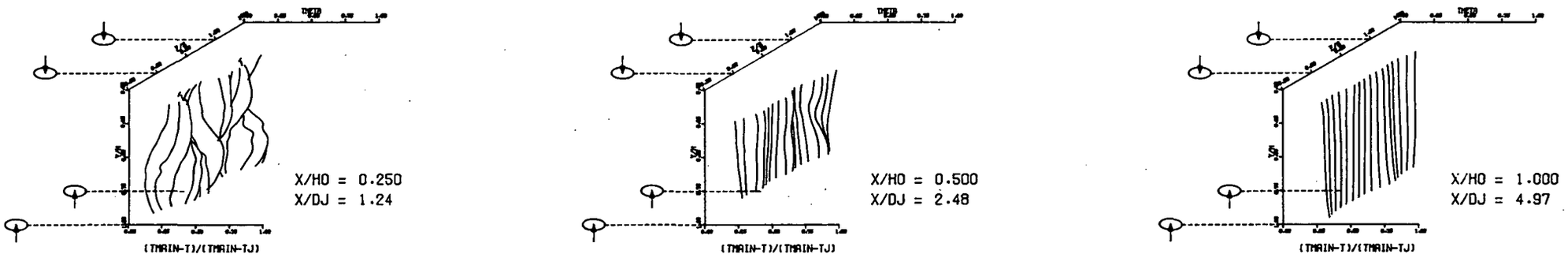

MEASURED THETA PROFILES FOR TEST NO.24, TEST SECTION II, TM=CONST(STG), J = 25.84 , S/D = 4.00 , H/D = 4.00

CONTOUR	1	2	3	4	5	6	7	8	9	10	11
VALUE	0.0500	0.1000	0.1500	0.2000	0.2500	0.3272	0.3500	0.4000	0.5000	0.6000	0.7000

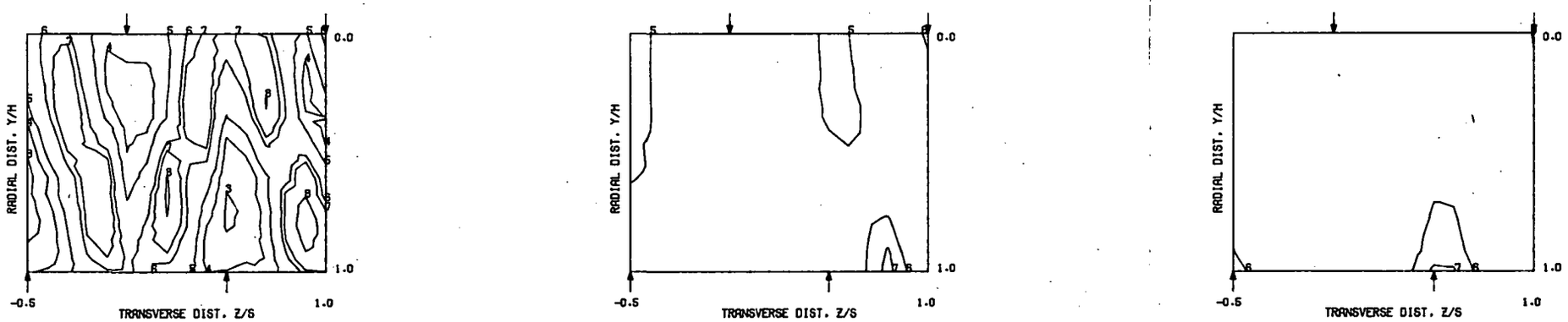

MEASURED THETA CONTOURS FOR TEST NO.24,TM=CONST (STG), J=25.84, S/D=4.0, H/D=4.0

Figure 63. Measured Theta Distributions for Test No. 24.

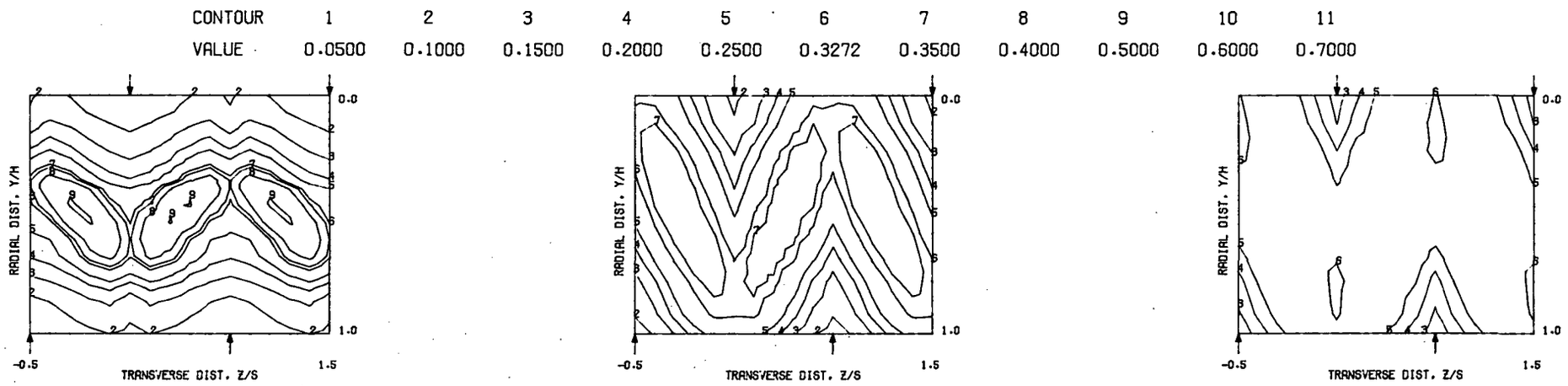

PREDICTED THETA CONTOURS FOR TEST NO 24, T.S.II, J=25.84, S/D=4.0(STG), H/D=4.0

S/DJ = 4.87 HO/DJ = 4.87 VRATIO = 3.46 TRATIO = 0.472 DENRATIO= 2.154 TMAIN = 644.5 K TJET = 304.2 K THEB = 0.3272

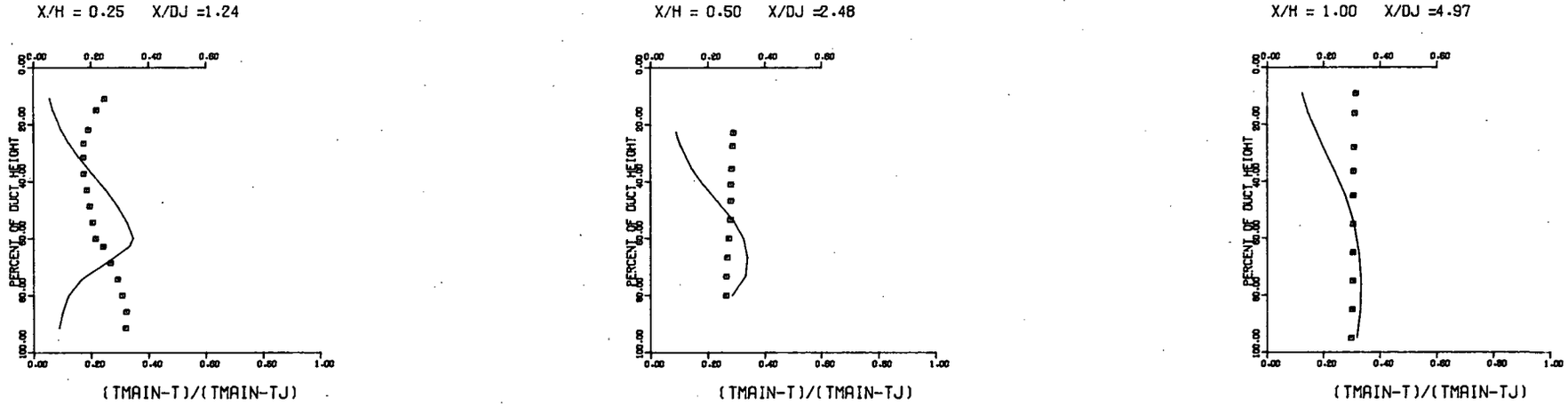

COMPARISON BETWEEN DATA AND CORRELATIONS FOR TEST NO. 24, TEST SECTION II,TM=CONST(STG), J = 25.84 , S/D =4.00 , H/D =4.00

Figure 64. Predicted Theta Distributions for Test No. 24.

S = 0.0508 METERS S/DJ = 2.471 HO/DJ = 4.942 VMAIN = 16.4 M/SEC VJET = 28.9 M/SEC TMAIN = 645.1 K TJET = 300.4 K THEB = 0.3283 BLORAT= 3.791 DENRATIO= 2.156 TRATIO= 0.466

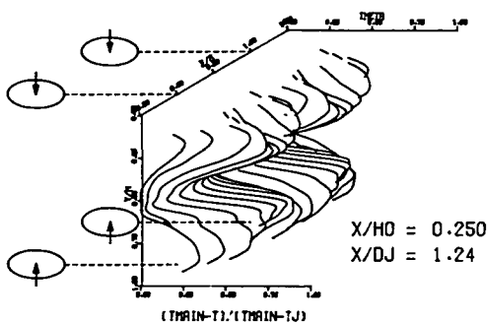

X/HO = 0.250
X/DJ = 1.24

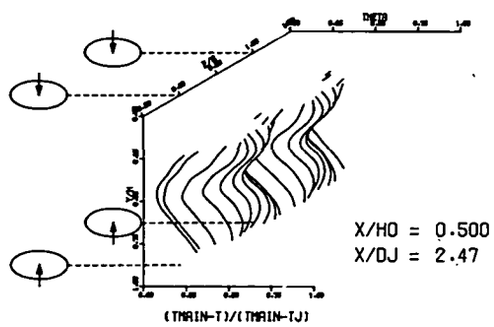

X/HO = 0.500
X/DJ = 2.47

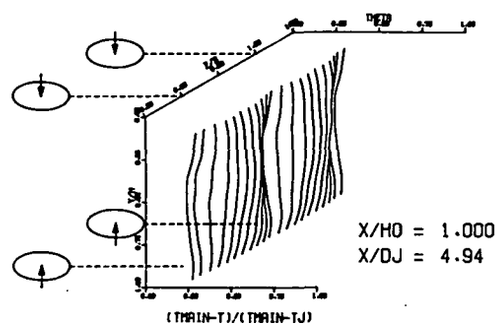

X/HO = 1.000
X/DJ = 4.94

MEASURED THETA PROFILES FOR TEST NO.25, TEST SECTION II, TM=CONST(INL), J = 6.69 , S/D = 2.00 , H/D = 4.00

CONTOUR	1	2	3	4	5	6	7	8	9	10	11
VALUE	0.0500	0.1000	0.1500	0.2000	0.2500	0.3000	0.3283	0.4000	0.5000	0.6000	0.7000

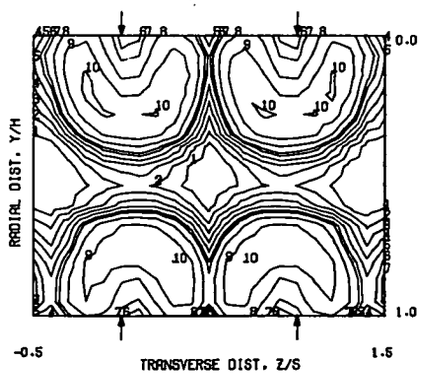

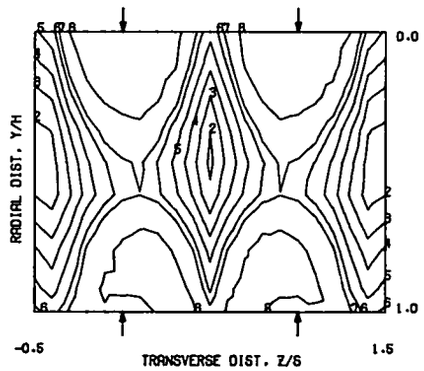

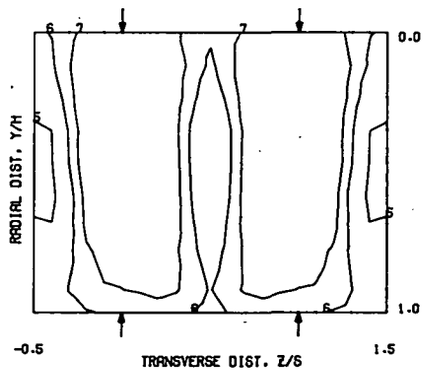

MEASURED THETA CONTOURS FOR TEST NO.25,TM=CONST (INL), J=6.69, S/D=2.0, H/D=4.0

Figure 65. Measured Theta Distributions for Test No. 25.

CONTOUR	1	2	3	4	5	6	7	8	9	10	11
VALUE	0.0500	0.1000	0.1500	0.2000	0.2500	0.3284	0.3500	0.4000	0.5000	0.6000	0.7000

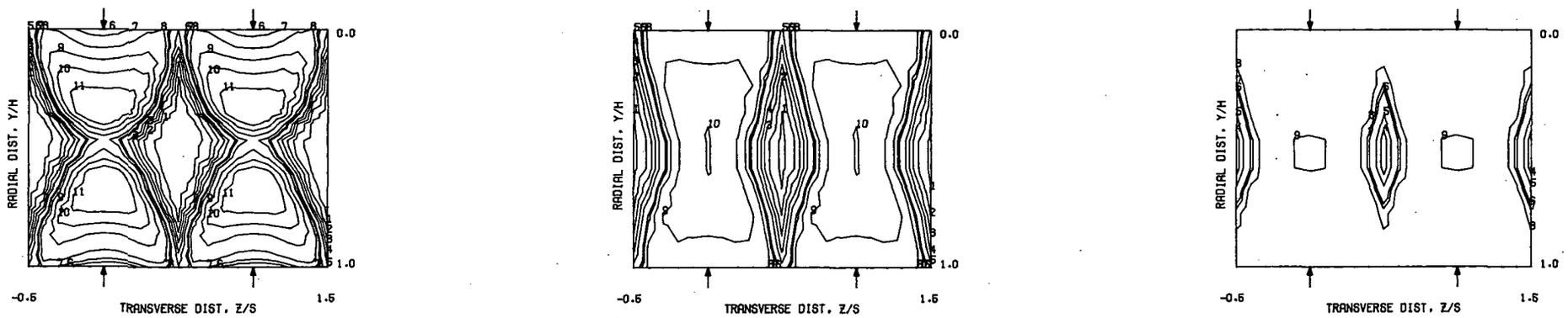

PREDICTED THETA CONTOURS FOR TEST NO 25, T.S.II, J=6.69, S/D=2.0(INL), H/D=4.0

S/DJ = 2.47 HO/DJ = 2.47 VRATIO = 1.76 TRATIO = 0.466 DENRATIO= 2.156 TMAIN = 645.1 K TJET = 300.4 K THEB = 0.3283

X/H = 0.25 X/DJ =1.24 X/H = 0.50 X/DJ =2.47 X/H = 1.00 X/DJ =4.94

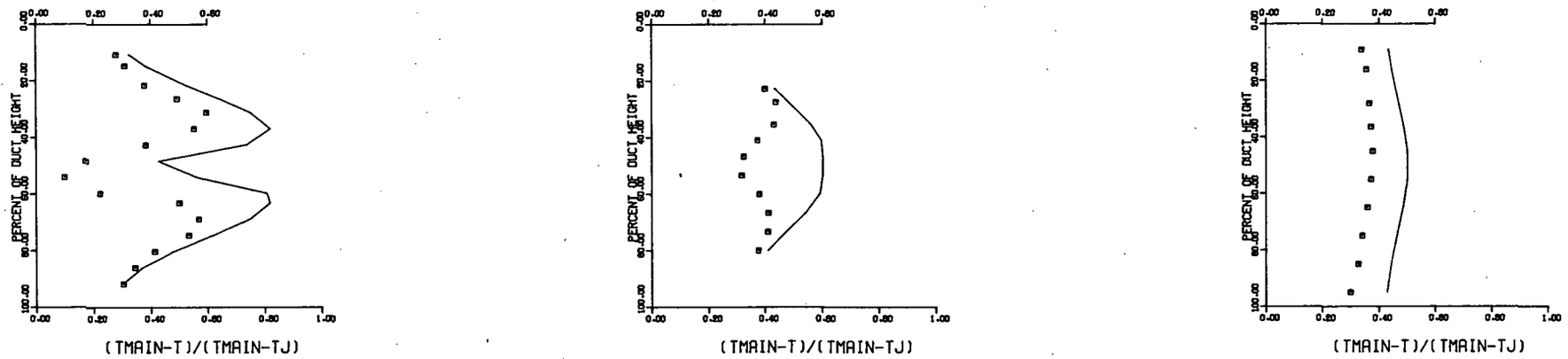

COMPARISON BETWEEN DATA AND CORRELATIONS FOR TEST NO. 25, TEST SECTION II,TM=CONST(INL), J = 6.69 , S/D =2.00 , H/D =4.00

Figure 66. Predicted Theta Distributions for Test No. 25.

S = 0.0508 METERS S/DJ = 2.520 HO/DJ = 5.039 VMAIN = 16.4 M/SEC VJET = 56.4 M/SEC TMAIN = 644.7 K TJET = 300.8 K THEB = 0.4810 BLORAT= 7.456 DENRATIO= 2.174 TRATIO=0.467

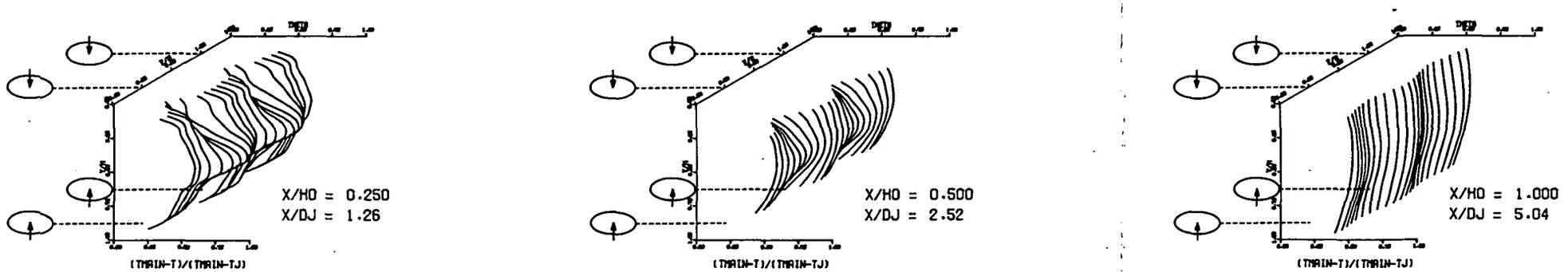

MEASURED THETA PROFILES FOR TEST NO.26, TEST SECTION II, TM=CONST(INL), J = 25.68 , S/D = 2.00 , H/D = 4.00

CONTOUR	1	2	3	4	5	6	7	8	9	10	11
VALUE	0.0500	0.1000	0.1500	0.2000	0.2500	0.3000	0.3500	0.4000	0.4810	0.6000	0.7000

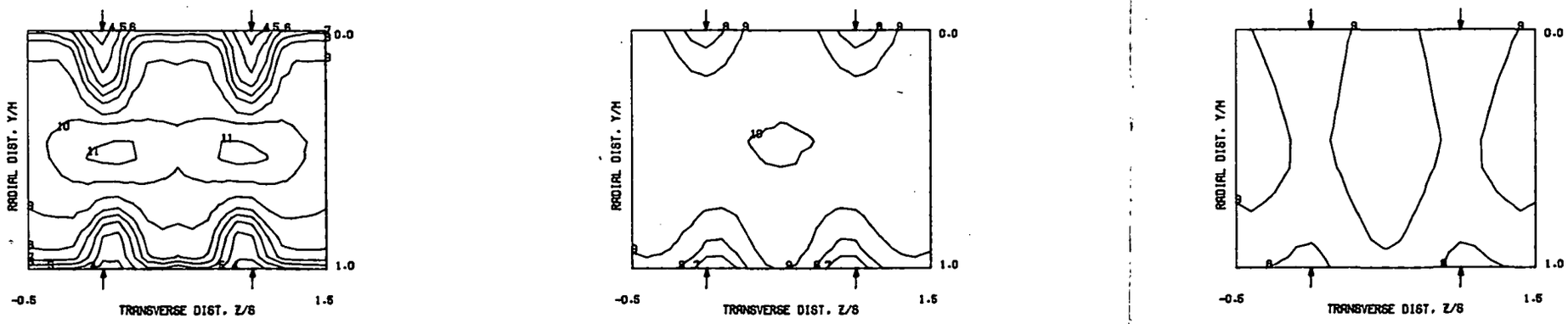

MEASURED THETA CONTOURS FOR TEST NO.26,TM=CONST (INL.), J=25.7, S/D=2.0, H/D=4.0

Figure 67. Measured Theta Distributions for Test No. 26.

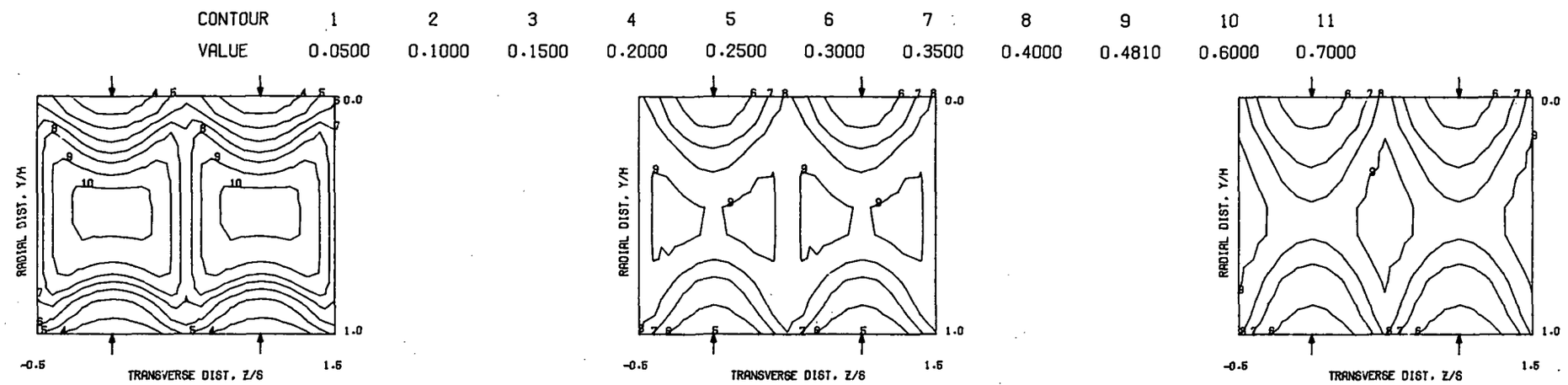

PREDICTED THETA CONTOURS FOR TEST NO 26, T.S.II, J=25.68, S/D=2.0(INL), H/D=4.0

S/DJ = 2.52 HO/DJ = 2.53 VRATIO = 3.44 TRATIO = 0.467 DENRATIO=2.174 TMAIN = 644.7 K TJET = 300.8 K **THEB = 0.4810**

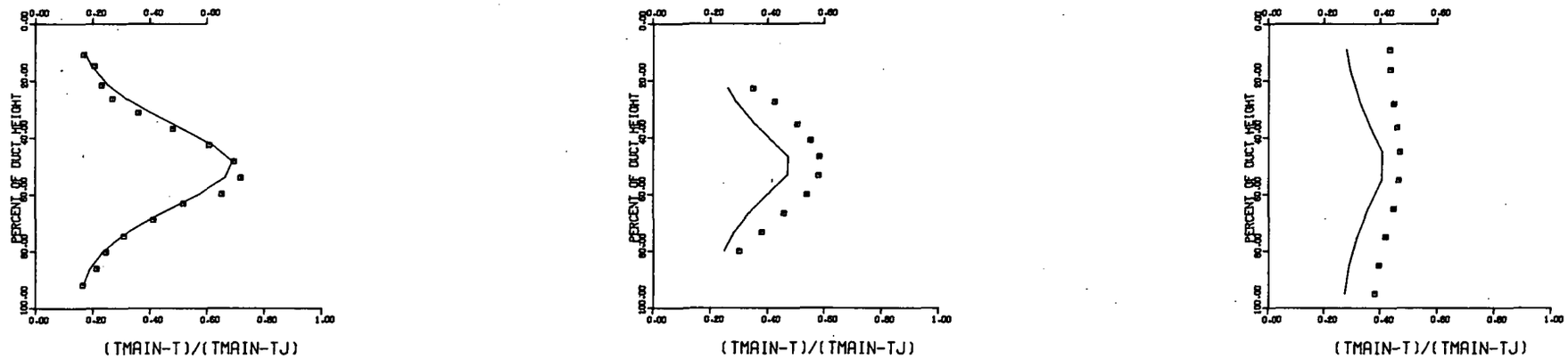

COMPARISON BETWEEN DATA AND CORRELATIONS FOR TEST NO. 26, TEST SECTION II,TM=CONST(INL), J = 25.68 , S/D =2.00 , H/D =4.00

Figure 68. Predicted Theta Distributions for Test No. 26.

S = 0.1016 METERS S/DJ = 4.905 HO/DJ = 4.905 VMAIN = 16.6 M/SEC VJET = 30.1 M/SEC TMAIN = 646.3 K TJET = 313.4 K THEB = 0.1993 BLORAT= 3.734 DENRATIO= 2.067 TRATIO= 0.485

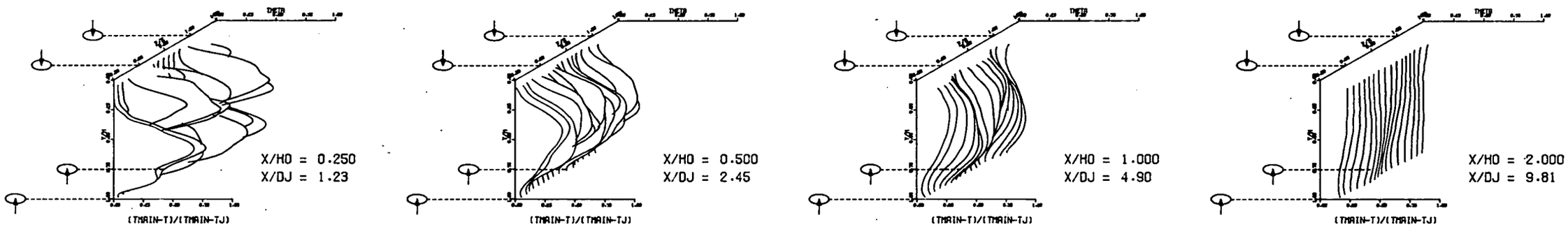

MEASURED THETA PROFILES FOR TEST NO.27, TEST SECTION I, TM=CONST (STG), J = 6.76 , S/D = 4.00 , H/D = 4.00

CONTOUR	1	2	3	4	5	6	7	8	9	10	11
VALUE	0.0500	0.1000	0.1500	0.1993	0.2500	0.3000	0.3500	0.4000	0.5000	0.6000	0.7000

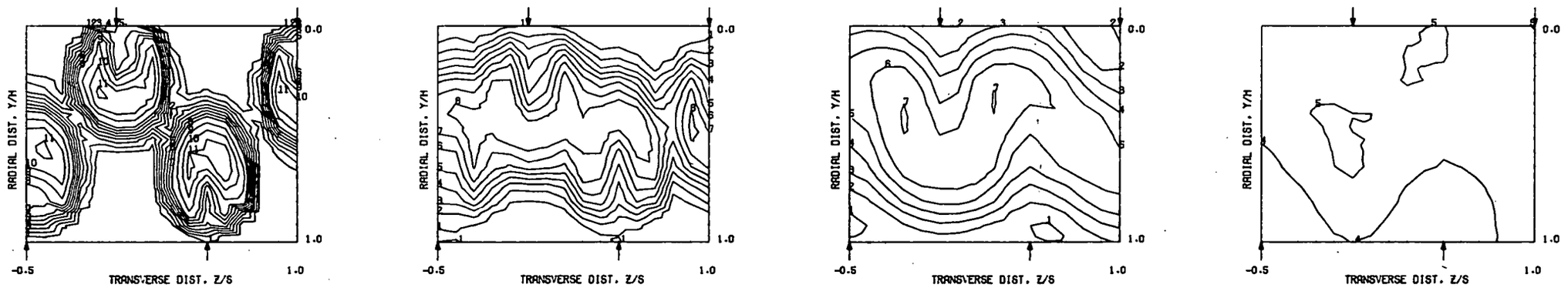

MEASURED THETA CONTOURS FOR TEST NO.27, TM=CONST (STG), J=6.76, S/D=4.0, H/D=4.

Figure 69. Measured Theta Distributions for Test No. 27.

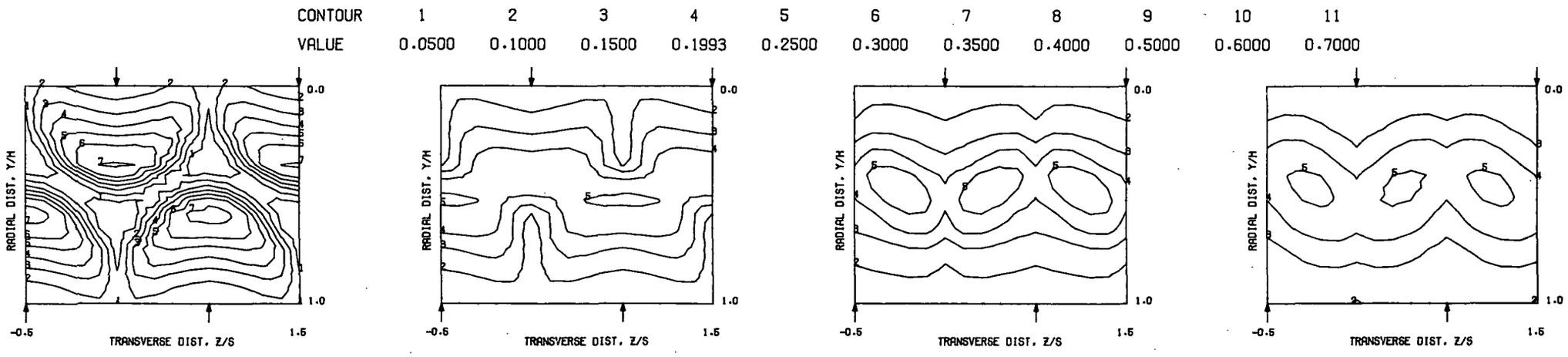

PREDICTED THETA CONTOURS FOR TEST NO 27, T.S. I, J=6.76, S/D=4.0(STG), H/D=4.0

S/DJ = 4.85 HO/DJ = 4.85 VRATIO = 1.81 TRATIO = 0.485 DENRATIO= 2.067 TMAIN = 646.3 K TJET = 313.4 K THEB = 0.205

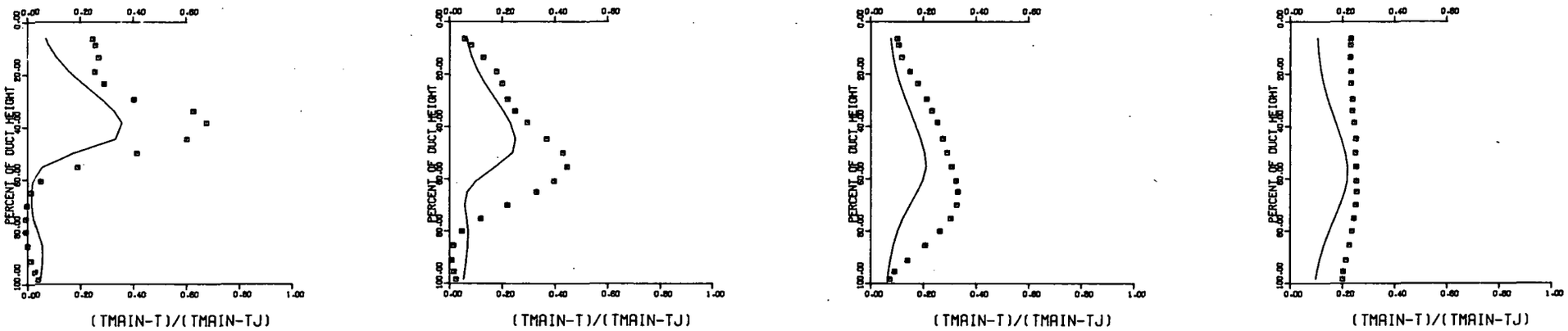

COMPARISON BETWEEN DATA AND CORRELATIONS FOR TEST NO. 27, TEST SECTION I,TM=CONST(STG), J = 6.76 , S/D =4.00 , H/D =4.00

Figure 70. Predicted Theta Distributions for Test No. 27.

S = 0.1016 METERS S/DJ = 4.974 HO/DJ = 4.974 VMAIN = 16.9 M/SEC VJET = 59.4 M/SEC TMAIN = 644.7 K TJET = 307.4 K THEB = 0.3271 BLORAT= 7.490 DENRATIO= 2.125 TRATIO= 0.477

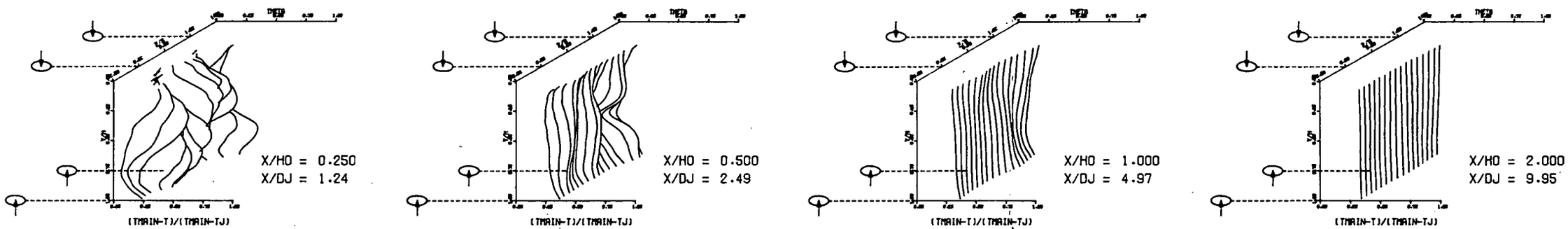

MEASURED THETA PROFILES FOR TEST NO.28, TEST SECTION I, TM=CONST (STG), J = 26.42 , S/D = 4.00 , H/D = 4.00

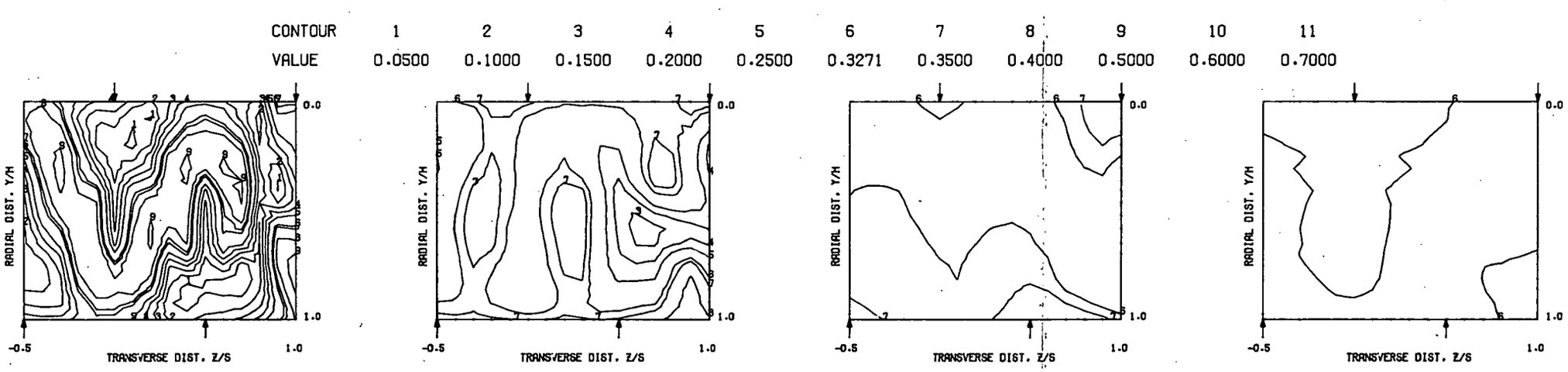

MEASURED THETA CONTOURS FOR TEST NO.28, TM=CONST (STG), J=26.42, S/D=4.0, H/D=4.

Figure 71. Measured Theta Distributions for Test No. 28.

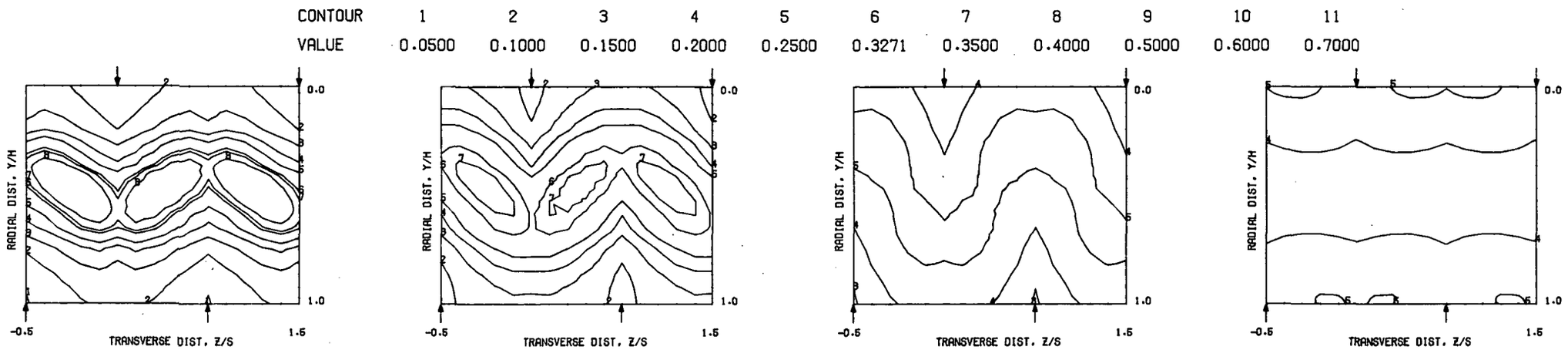

PREDICTED THETA CONTOURS FOR TEST NO 28, T.S. I, J=26.426, S/D=4.0(STG), H/D=4.0

S/DJ = 4.88 HO/DJ = 4.88 VRATIO = 3.53 TRATIO = 0.477 DENRATIO= 2.125 TMAIN = 644.7 K TJET = 307.4 K THEB = 0.334

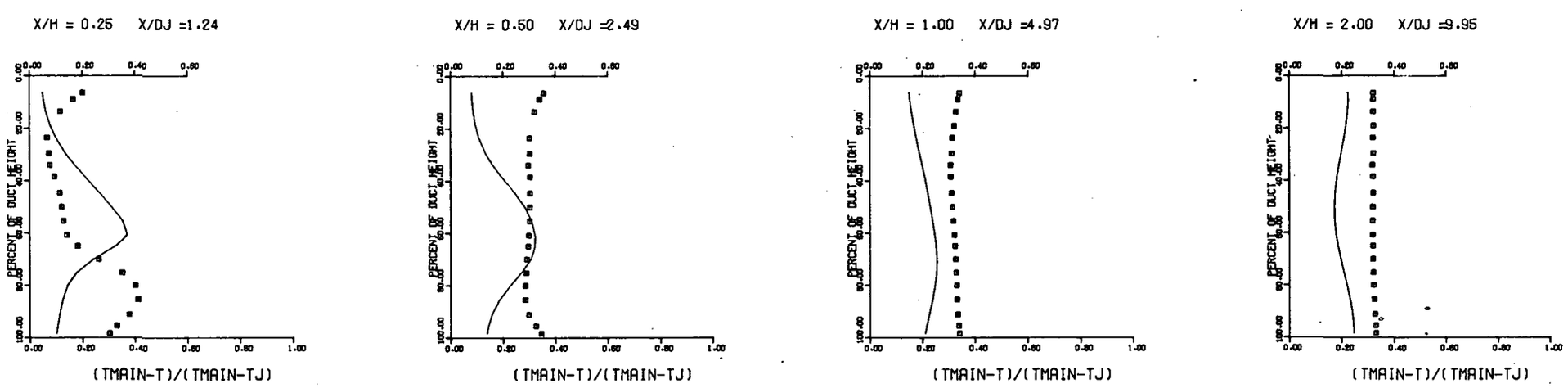

COMPARISON BETWEEN DATA AND CORRELATIONS FOR TEST NO. 28, TEST SECTION I,TM=CONST(STG), J = 26.42 , S/D =4.00 , H/D =4.00

Figure 72. Predicted Theta Distributions for Test No. 28.

S = 0.1016 METERS S/DJ = 4.980 HO/DJ = 4.980 VMAIN = 16.5 M/SEC VJET = 58.6 M/SEC TMAIN = 645.4 K TJET = 307.5 K THEB = 0.3253 BLORAT= 7.548 DENRATIO= 2.122 TRATIO= 0.476

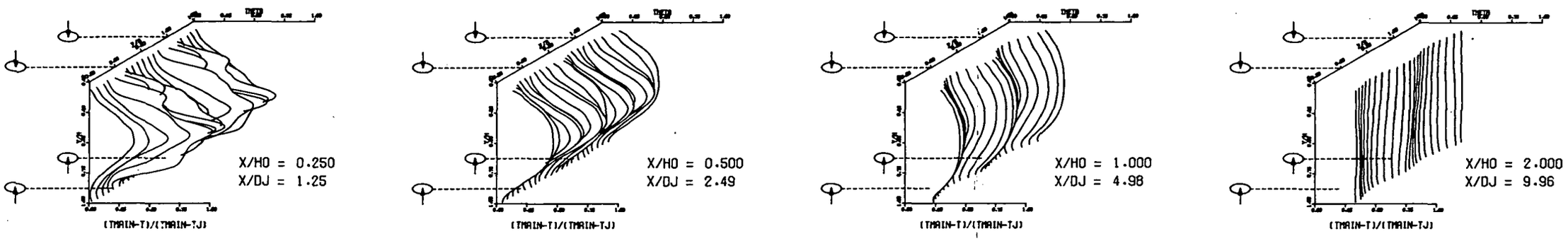

MEASURED THETA PROFILES FOR TEST NO.29, TEST SECTION I, TM=CONST (INL), J = 26.86 , S/D = 4.00 , H/D = 4.00

CONTOUR	1	2	3	4	5	6	7	8	9	10	11
VALUE	0.0500	0.1000	0.1500	0.2000	0.2500	0.3253	0.3500	0.4000	0.5000	0.6000	0.7000

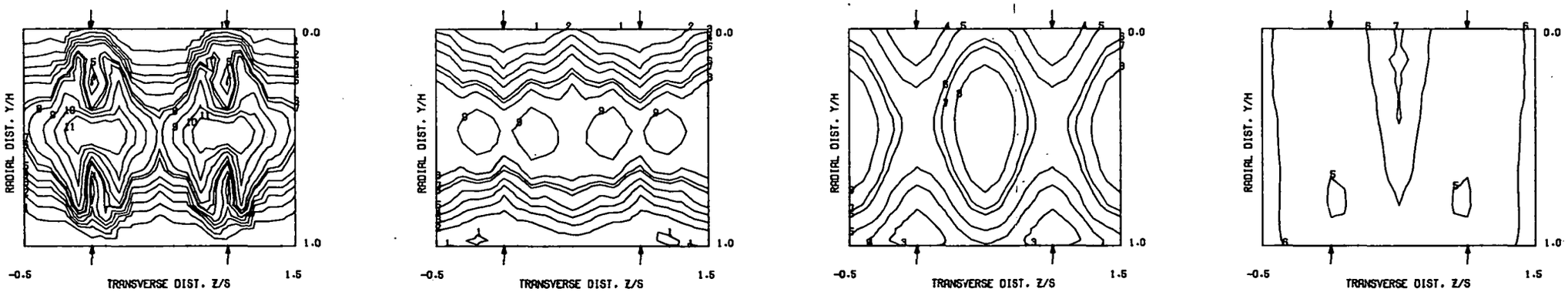

MEASURED THETA CONTOURS FOR TEST NO.29, TM=CONST (INL), J=26.9, S/D=4.0, H/D=4.0

Figure 73. Measured Theta Distributions for Test No. 29.

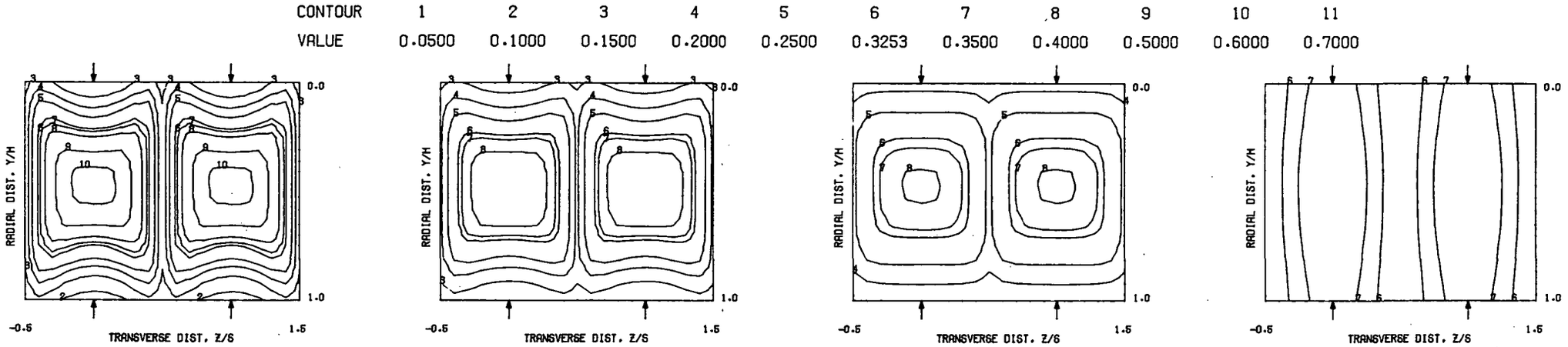

PREDICTED THETA CONTOURS FOR TEST NO 29, T.S. I, J=26.86, S/D=4.0(INL), H/D=4.0

S/DJ = 4.98 HO/DJ = 2.48 VRATIO = 3.56 TRATIO = 0.476 DENRATIO=2.122 TMAIN = 645.4 K TJET = 307.5 K THEB = 0.325

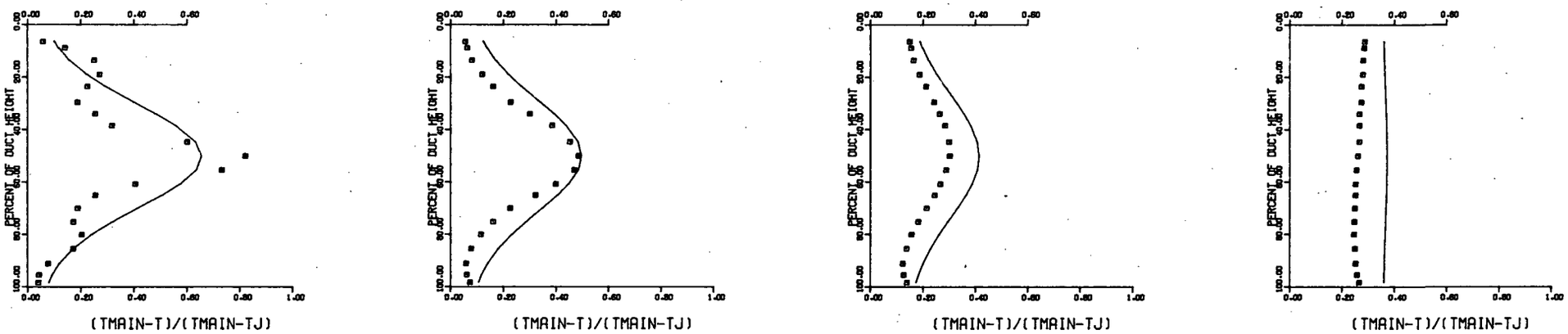

COMPARISON BETWEEN DATA AND CORRELATIONS FOR TEST NO. 29, TEST SECTION I,TM=CONST(INL), J = 26.86 , S/D =4.00 , H/D =4.00

Figure 74. Predicted Theta Distributions for Test No. 29.

S = 0.1016 METERS S/DJ = 5.000 HO/DJ = 5.000 VMAIN = 16.6 M/SEC VJET = 114.9 M/SEC TMAIN = 645.4 K TJET = 306.9 K THEB = 0.4936 BLORAT= 15.403 DENRATIO= 2.220 TRATIO= 0.475

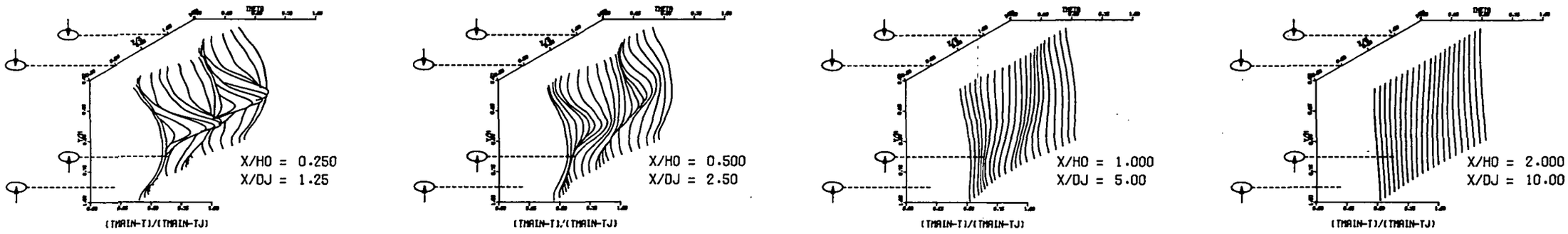

MEASURED THETA PROFILES FOR TEST NO.30, TEST SECTION I, TM=CONST (INL) , J = 106.94 , S/D = 4.00 , H/D = 4.00

CONTOUR	1	2	3	4	5	6	7	8	9	10	11
VALUE	0.0500	0.1000	0.1500	0.2000	0.2500	0.3000	0.3500	0.4000	0.4936	0.6000	0.7000

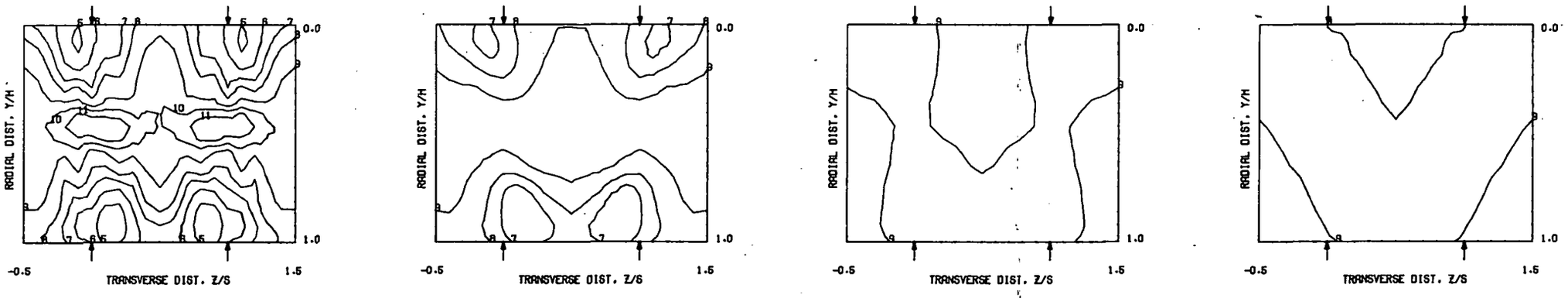

MEASURED THETA CONTOURS FOR TEST NO.30, TM=CONST (INL), J=106.9, S/D=4.0, H/D=4.

Figure 75. Measured Theta Distributions for Test No. 30.

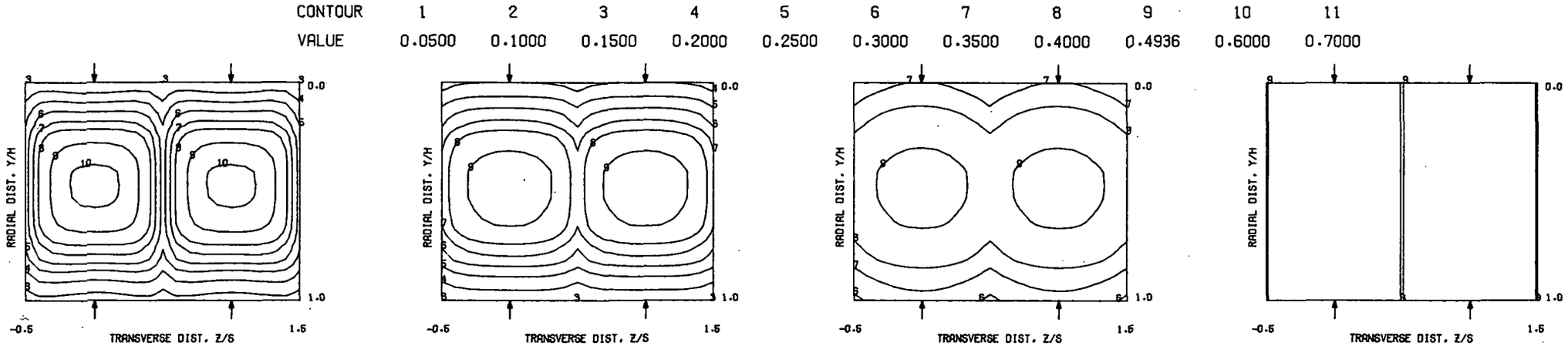

PREDICTED THETA CONTOURS FOR TEST NO 30, T.S. I, J=106.9, S/D=4.0(INL), H/D=4.0

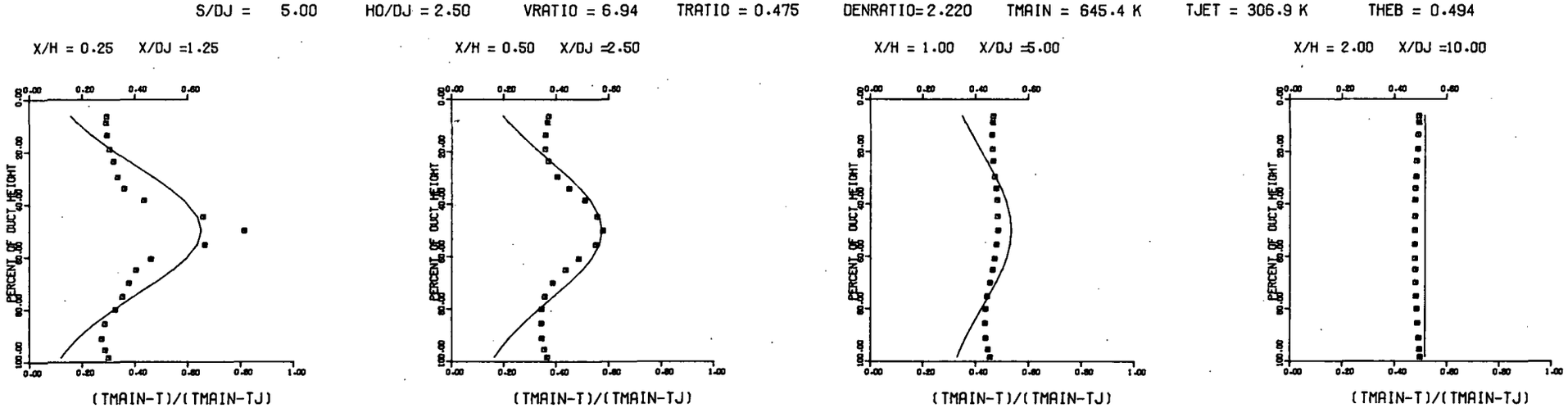

COMPARISON BETWEEN DATA AND CORRELATIONS FOR TEST NO. 30, TEST SECTION I,TM=CONST(INL), J = 106.94 , S/D =4.00 , H/D =4.00

Figure 76. Predicted Theta Distributions for Test No. 30.

S = 0.0051 METERS S/DJ = 1.152 HO/DJ = 22.763 VMAIN = 16.8 M/SEC VJET = 29.9 M/SEC TMAIN = 646.1 K TJET = 310.5 K THEB = 0.1213 BLORAT= 3.719 DENRATIO= 2.088 TRATIO= 0.481

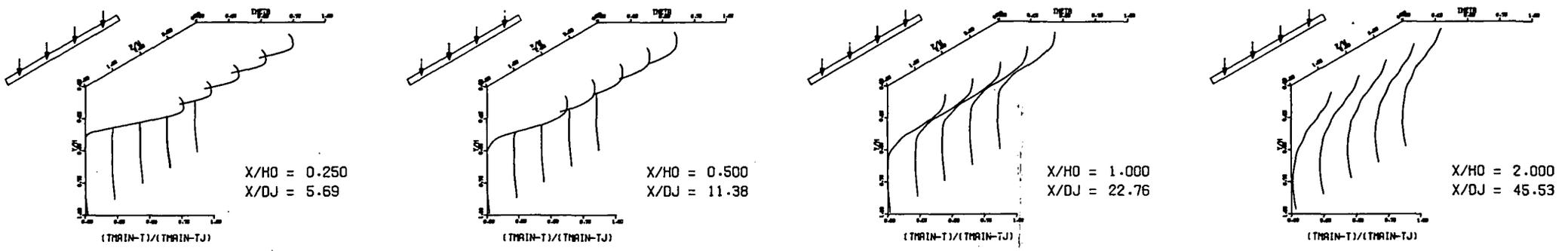

MEASURED THETA PROFILES FOR TEST NO.31, TEST SECTION I, 2-D SLOT , J = 6.63 , S/D = 1.00 , H/W=19.75

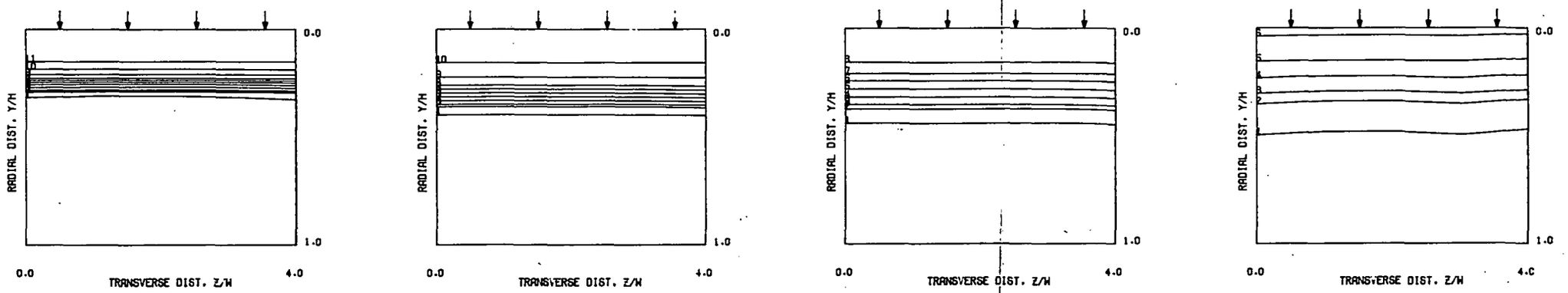

MEASURED THETA CONTOURS FOR TEST NO.31, TM=CONST (SLOT), J=6.63, H/W=19.75

Figure 77. Measured Theta Distributions for Test No. 31.

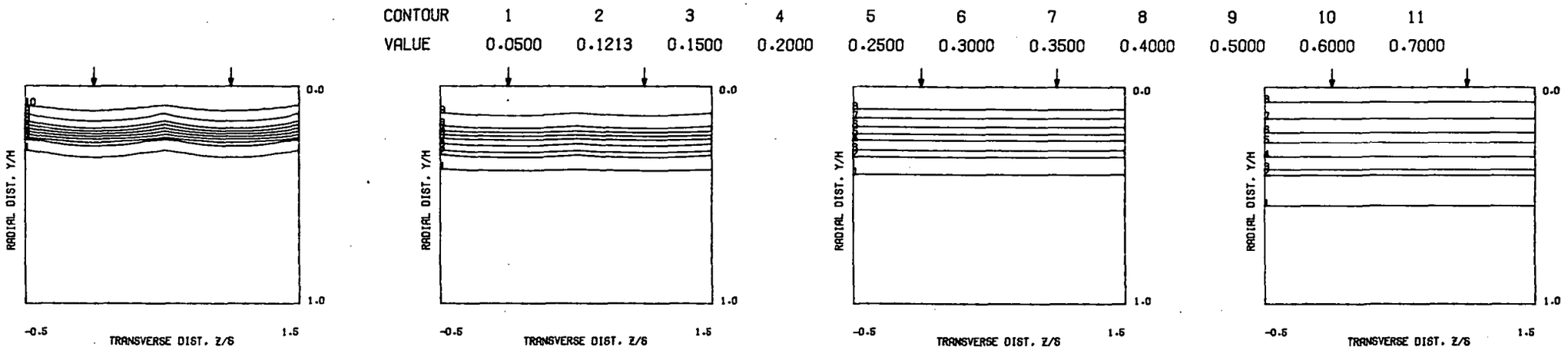

PREDICTED THETA CONTOURS FOR TEST NO. 31A, TM=CONST (SLOT), J=6.63, H/W=19.75

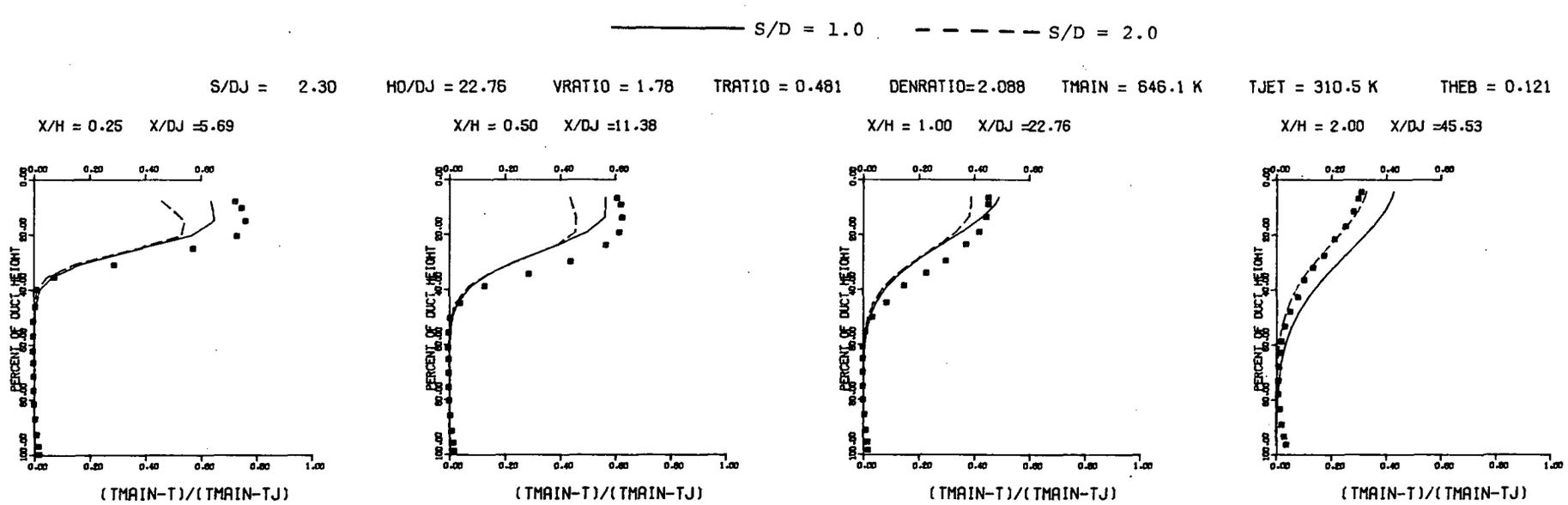

COMPARISON BETWEEN DATA AND CORRELATIONS FOR TEST NO.31A, TEST SECTION I, TM=CONST (SLOT), J = 6.63 , S/D =2.00 , H/D =19.75

Figure 78. Predicted Theta Distributions for Test No. 31A.

S = 0.0051 METERS S/DJ = 1.167 HO/DJ = 23.043 VMAIN = 16.7 M/SEC VJET = 58.4 M/SEC TMAIN = 646.8 K TJET = 308.6 K THEB = 0.2129 BLORAT= 7.464 DENRATIO= 2.134 TRATIO=0.477

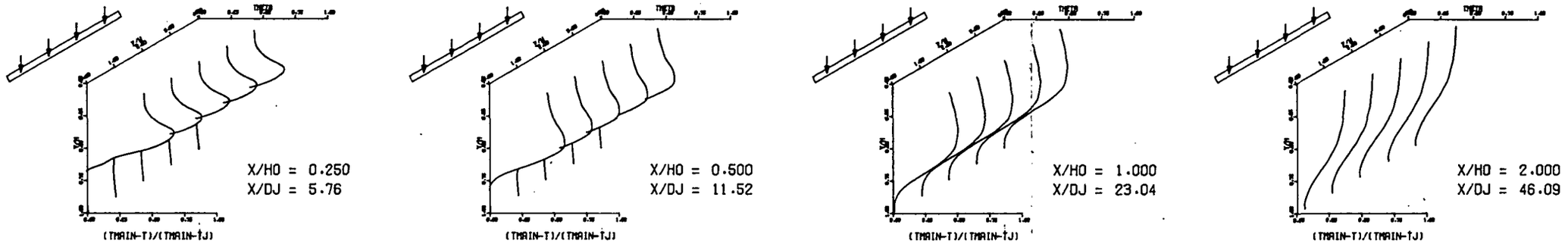

MEASURED THETA PROFILES FOR TEST NO.31, TEST SECTION I, 2-D SLOT , J = 26.13 , S/D = 1.00 , H/W = 19.75

CONTOUR	1	2	3	4	5	6	7	8	9	10	11
VALUE	0.0500	0.1000	0.1500	0.2129	0.2500	0.3000	0.3500	0.4000	0.5000	0.6000	0.7000

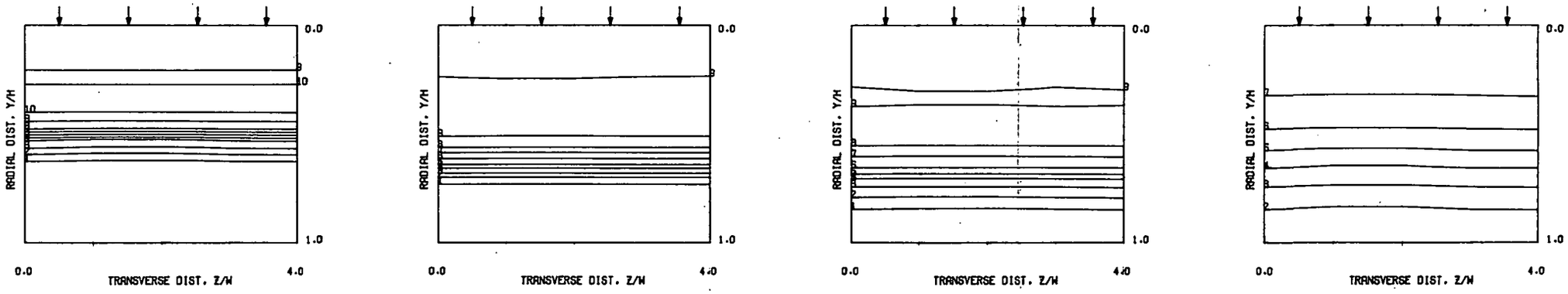

MEASURED THETA CONTOURS FOR TEST NO.31, TM=CONST (SLOT), J=26.13, H/W=19.75

Figure 79. Measured Theta Distributions for Test No. 31.

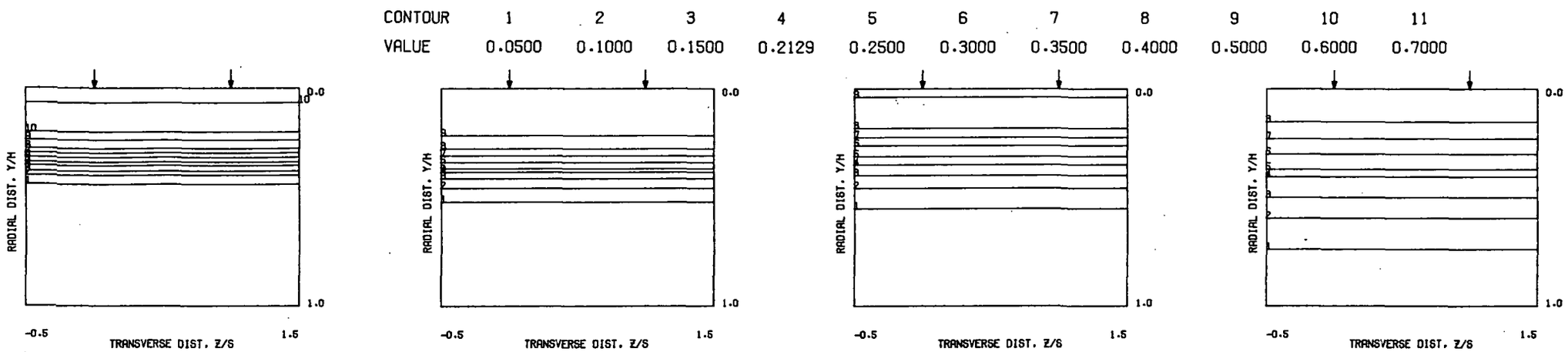

PREDICTED THETA CONTOURS FOR TEST NO. 31B, TM=CONST (SLOT), J=26.13,H/W=19.75

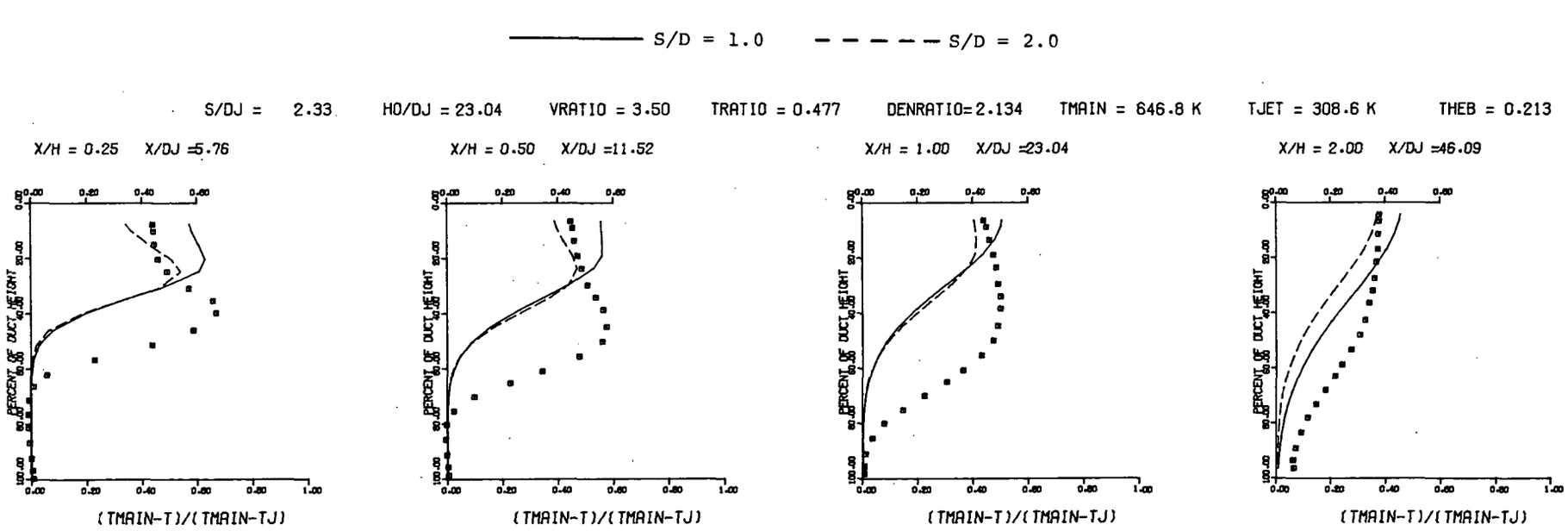

COMPARISON BETWEEN DATA AND CORRELATIONS FOR TEST NO.31B, TEST SECTION I, TM=CONST (SLOT),J = 26.13 , S/D =2.00 , H/D =19.75

Figure 80. Predicted Theta Distributions for Test No. 31.

S = 0.0051 METERS S/DJ = 1.183 HO/DJ = 23.360 VMAIN = 16.8 M/SEC VJET = 113.8 M/SEC TMAIN = 646.3 K TJET = 305.1 K THEB = 0.3520 BLORAT= 15.406 DENRATIO= 2.273 TRATIO= 0.472

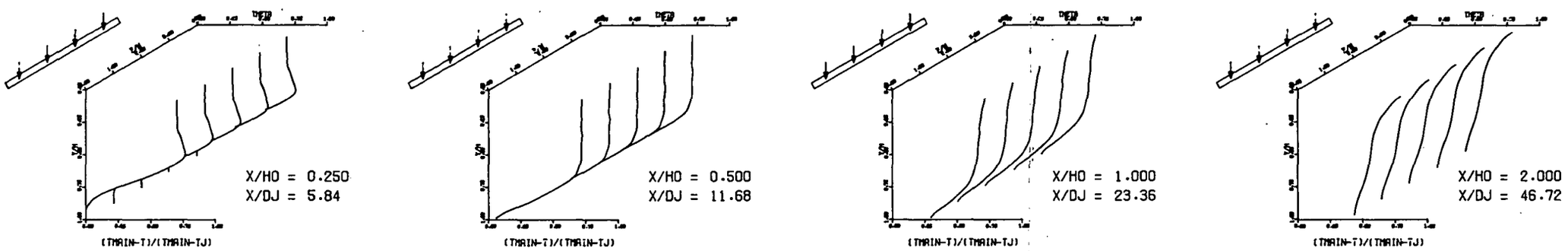

MEASURED THETA PROFILES FOR TEST NO.31, TEST SECTION I, 2-D SLOT , J = 104.49 , S/D = 1.00 , H/W = 19.75

CONTOUR	1	2	3	4	5	6	7	8	9	10	11
VALUE	0.0500	0.1000	0.1500	0.2000	0.2500	0.3000	0.3520	0.4000	0.5000	0.6000	0.7000

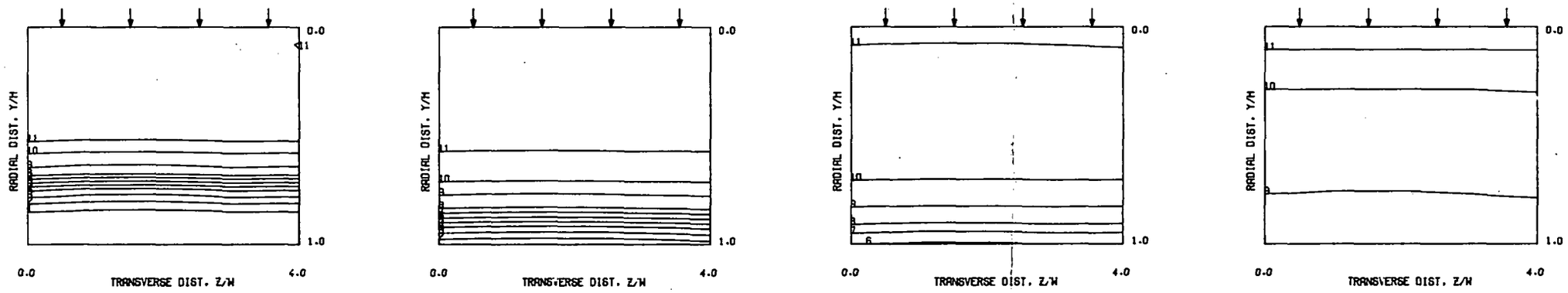

MEASURED THETA CONTOURS FOR TEST NO.31, TM=CONST (SLOT), J=104.5, H/W=19.75

Figure 81. Measured Theta Distributions for Test No. 31.

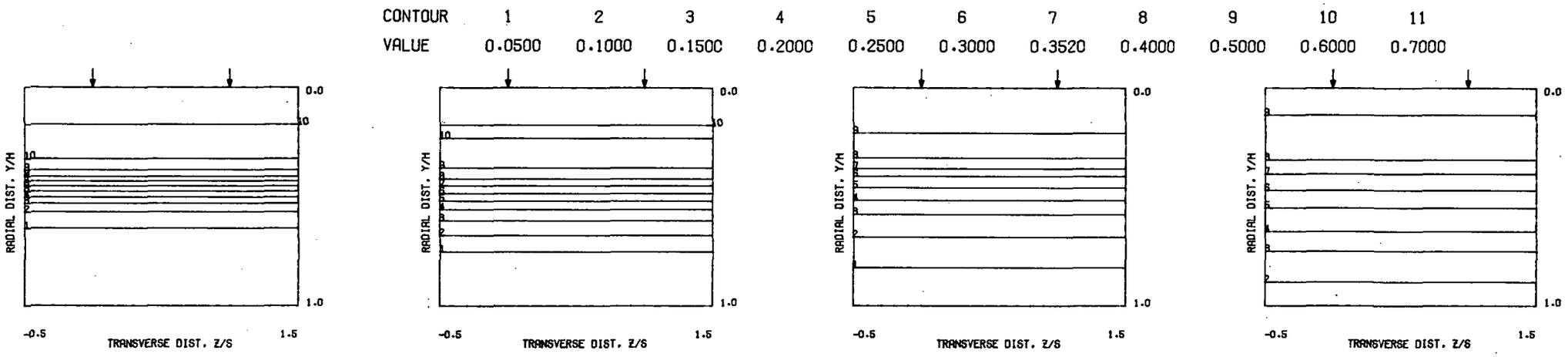

PREDICTED THETA CONTOURS FOR TEST NO. 31C, TM=CONST (SLOT), J=104.5, H/W=19.75

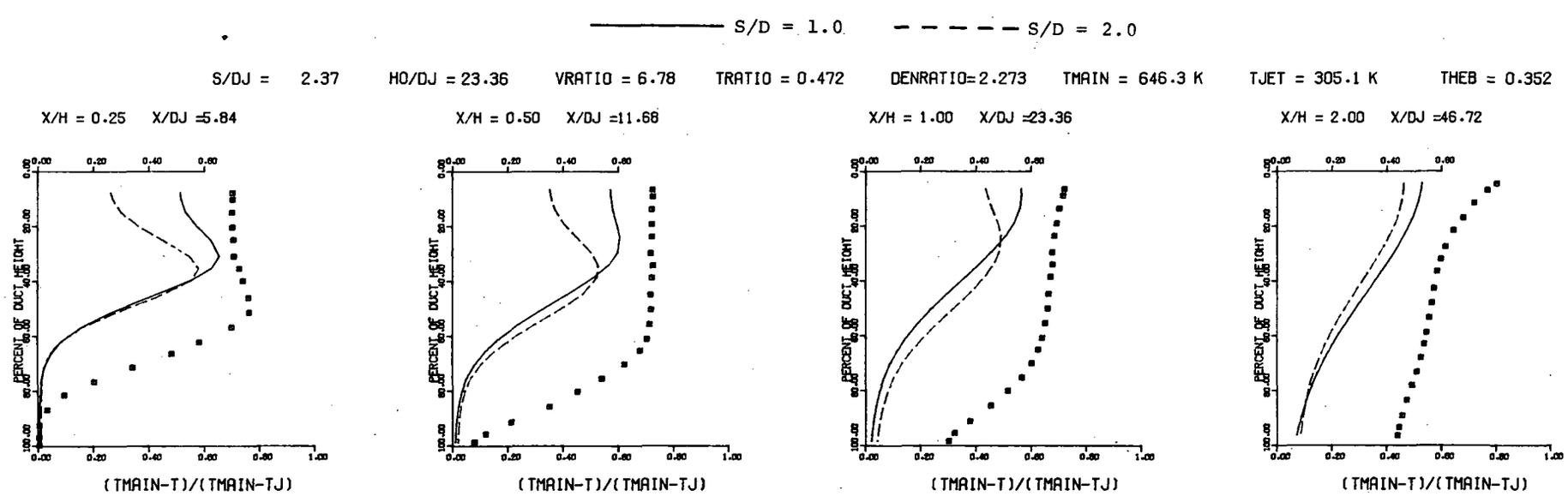

COMPARISON BETWEEN DATA AND CORRELATIONS FOR TEST NO.31C, TEST SECTION I, TM=CONST (SLOT),J = 104.49 , S/D =2.00 , H/D =19.75

Figure 82. Predicted Theta Distributions for Test No. 31.

S = 0.1016 METERS . S/DJ = 5.618 HO/DJ = 5.618 VMAIN = 16.8 M/SEC VJET = 59.1 M/SEC TMAIN = 646.5 K TJET = 311.0 K THEB = 0.1902 BLORAT= 7.409 DENRATIO= 2.105 TRATIO=0.481

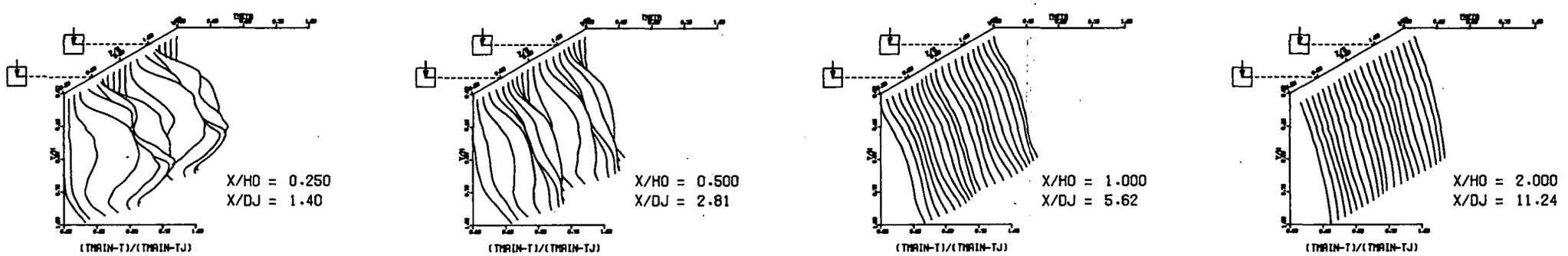

MEASURED THETA PROFILES FOR TEST NO.32, TEST SECTION I, SQUARE HOLES , J = 26.10 , S/D = 4.00 , H/D = 4.00

CONTOUR	1	2	3	4	5	6	7	8	9	10	11
VALUE	0.0500	0.1000	0.1500	0.1902	0.2500	0.3000	0.3500	0.4000	0.5000	0.6000	0.7000

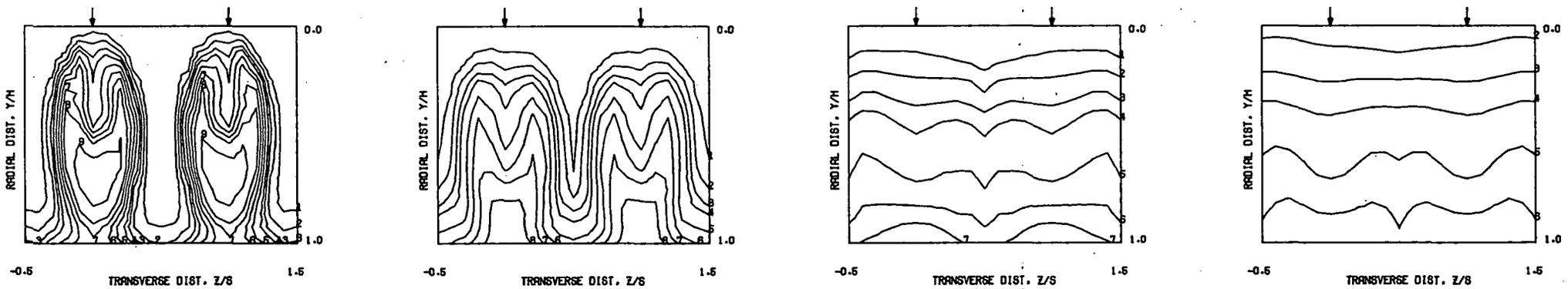

MEASURED THETA CONTOURS FOR TEST NO.32, TM=CONST , J=26.10, S/D=4.0, H/D=4.0

Figure 83. Measured Theta Distributions for Test No. 32.

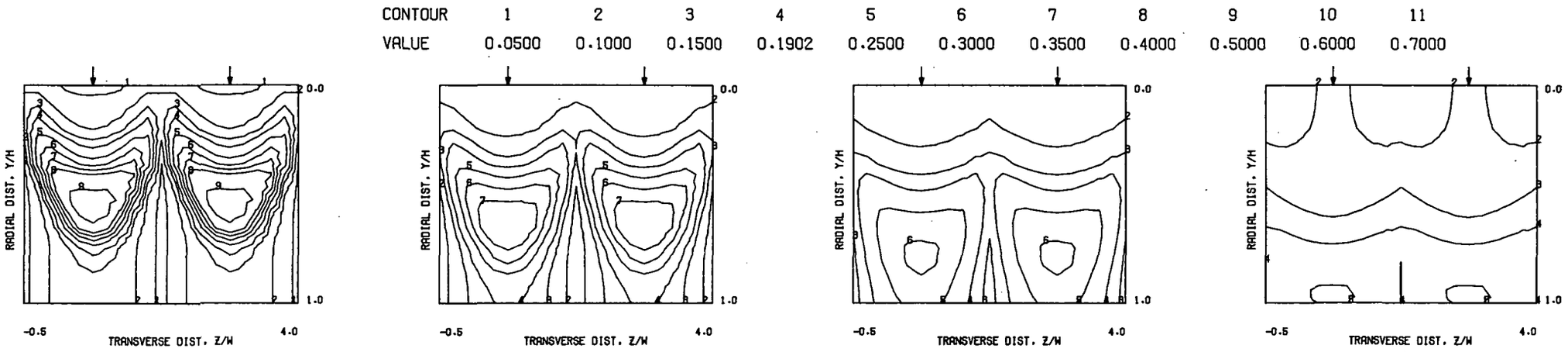

PREDICTED THETA CONTOURS FOR TEST NO. 32, SQUARE , J=26.1, S/D=4.0, H/D=4.0

S/DJ = 4.89 HO/DJ = 4.89 VRATIO = 3.52 TRATIO = 0.481 DENRATIO=2.105 TMAIN = 646.5 K TJET = 311.0 K THEB = 0.190

X/H = 0.25 X/DJ =1.22 X/H = 0.50 X/DJ =2.44 X/H = 1.00 X/DJ =4.89 X/H = 2.00 X/DJ =9.77

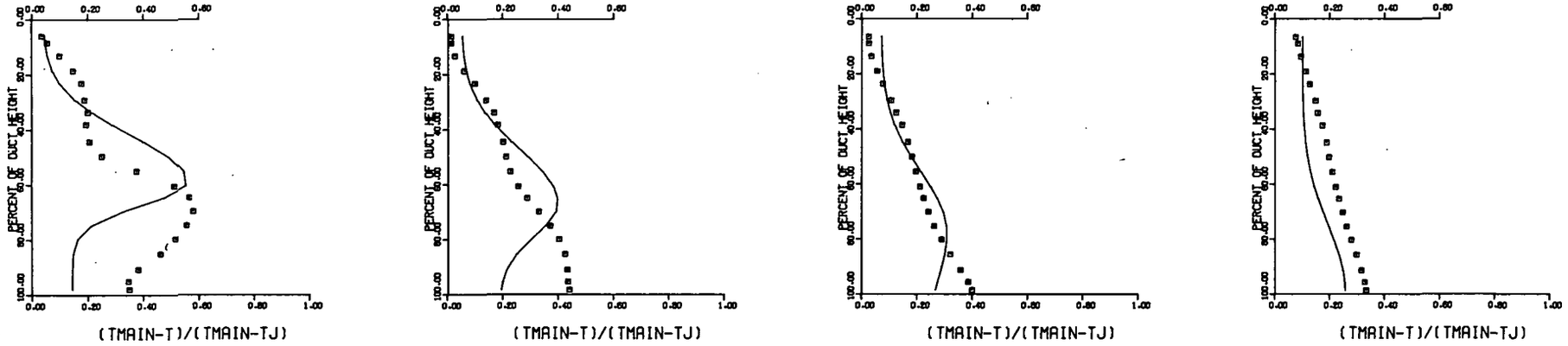

COMPARISON BETWEEN DATA AND CORRELATIONS FOR TEST NO. 32, TEST SECTION I, SQUARE HOLES, J = 26.10 , S/D =4.00 , H/D =4.00

Figure 84. Predicted Theta Distributions for Test No. 32.

S = 0.0254 METERS S/DJ = 2.520 HO/DJ = 10.080 VMAIN = 16.6 M/SEC VJET = 72.3 M/SEC TMAIN = 645.1 K TJET = 303.7 K THEB = 0.3201 BLORAT= 9.388 DENRATIO= 2.157 TRATIO= 0.471

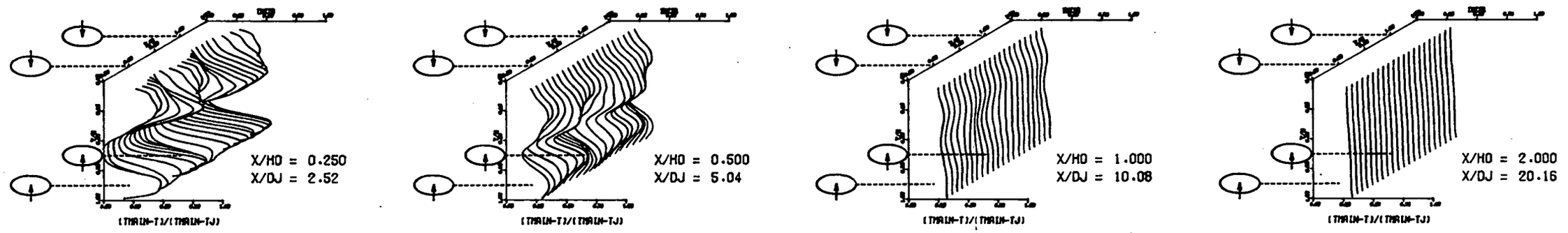

MEASURED THETA PROFILES FOR TEST NO.33, TEST SECTION I, TM=CONST (INL), JTOP=40.9, JBOT=14.7, S/D=2.0, H/D=8.0

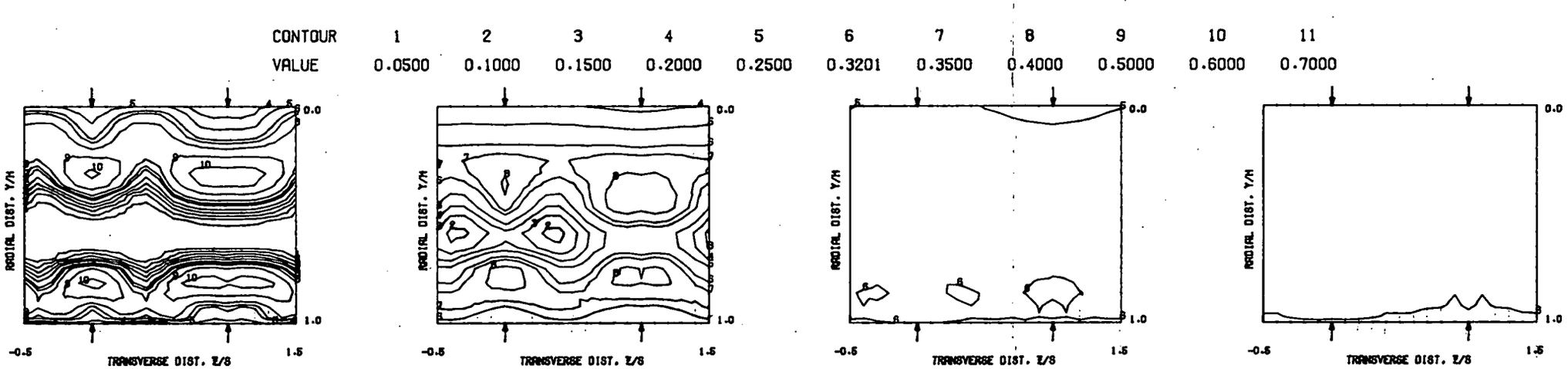

MEASURED THETA CONTOURS FOR TEST NO 33, JT=40.9, JB=14.7, S/D=2.0(INL), H/D=4.0

Figure 85. Measured Theta Distributions for Test No. 33.

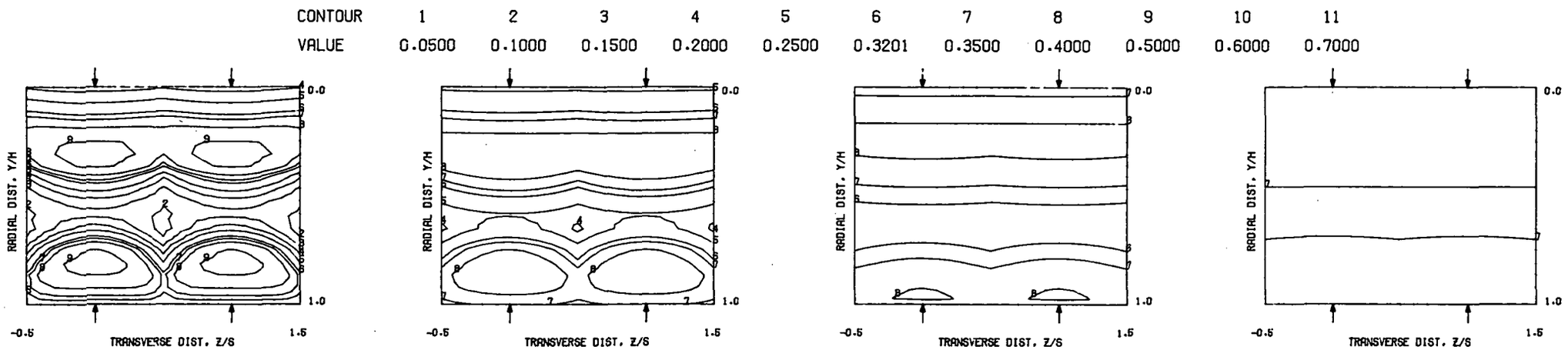

PREDICTED THETA CONTOURS FOR TEST NO 33, JT=40.9, JB=14.7, S/D=2.0(INL), H/D=8.0

S/DJ = 2.50 HO/DJ = 3.79 VRATIO = 4.35 TRATIO = 0.471 DENRATIO=2.157 TMAIN = 645.1 K TJET = 303.7 K THEB = 0.320

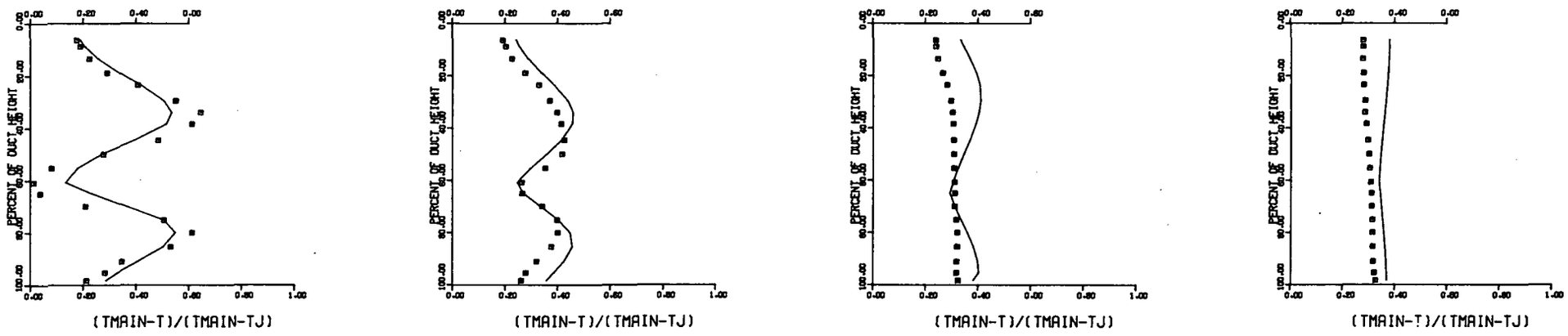

COMPARISON BETWEEN DATA AND CORRELATIONS FOR TEST NO. 33, TEST SECTION I,TM=CONST(INL), JTOP=40.9, JBOT=14.7, S/D=2.0, H/D=8.0

Figure 86. Predicted Theta Distributions for Test No. 33.

S = 0.0254 METERS S/DJ = 2.520 HO/DJ = 10.080 VMAIN = 16.6 M/SEC VJET = 85.7 M/SEC TMAIN = 645.3 K TJET = 303.2 K THEB = 0.3201 BLORAT= 11.291 DENRATIO= 2.185 TRATIO= 0.470

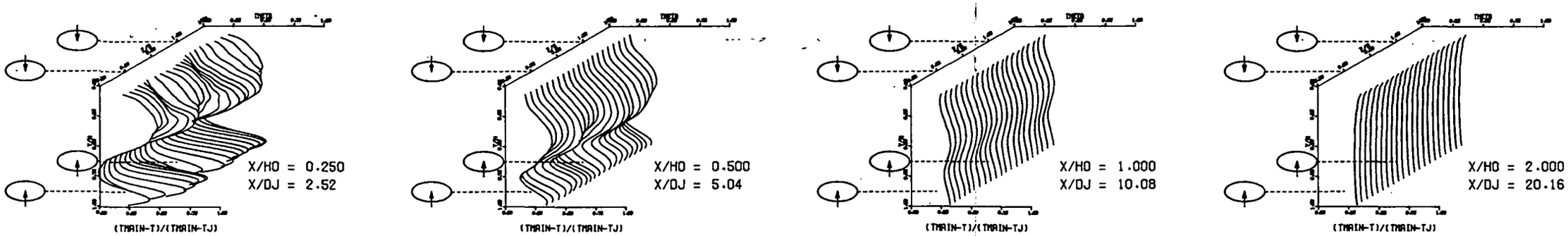

MEASURED THETA PROFILES FOR TEST NO.34, TEST SECTION I, TM=CONST (INL), JTOP=58.4, JBOT=6.47, S/D=2.0, H/D=8.0

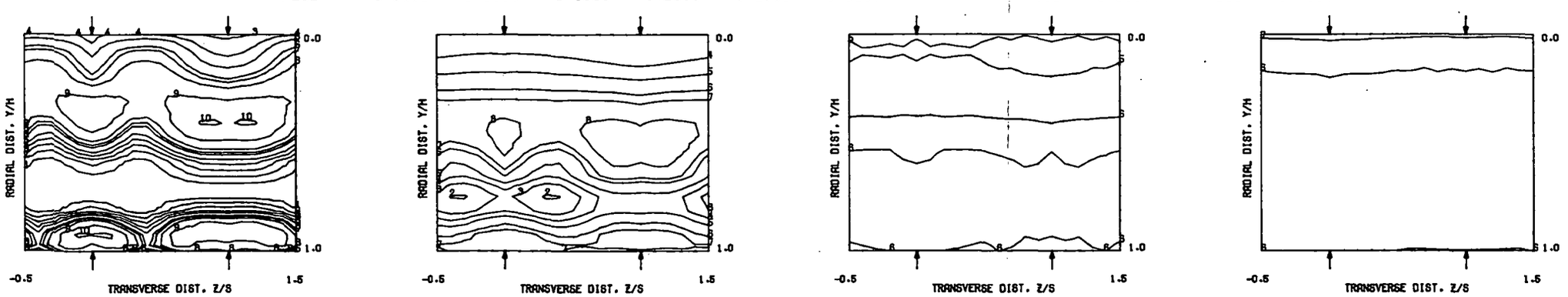

MEASURED THETA CONTOURS FOR TEST NO 34, JT=58.4, JB=6.47 , S/D=2.0(INL), H/D=4.0

Figure 87. Measured Theta Distributions for Test No. 34.

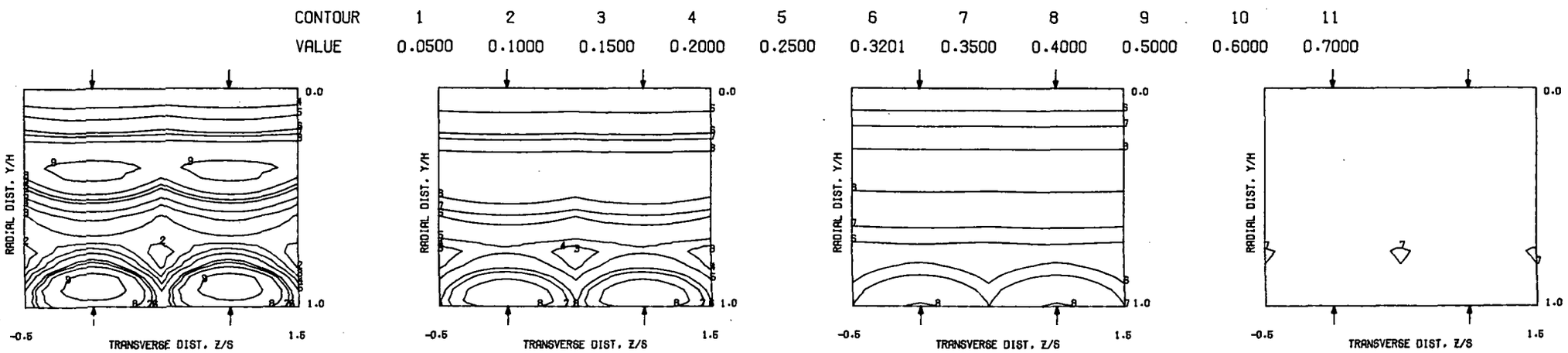

PREDICTED THETA CONTOURS FOR TEST NO 34, JT=58.4, JB=6.47, S/D=2.0(INL), H/D=8.0

S/DJ = 2.48 HO/DJ = 2.54 VRATIO = 5.17 TRATIO = 0.470 DENRATIO=2.185 TMAIN = 645.3 K TJET = 303.2 K THEB = 0.319

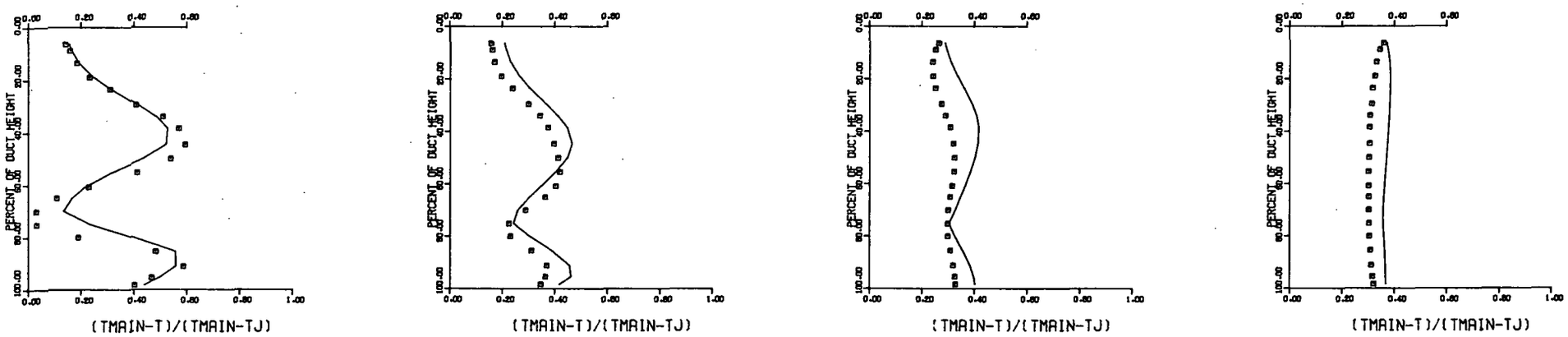

COMPARISON BETWEEN DATA AND CORRELATIONS FOR TEST NO. 34, TEST SECTION I,TM=CONST(INL), JTOP=58.4, JBOT=6.47, S/D=2.0, H/D=8.0

Figure 88. Predicted Theta Distributions for Test No. 34.

S = 0.0254 METERS S/DJ = 2.514 HO/DJ = 10.057 VMAIN = 16.4 M/SEC VJET = 57.2 M/SEC TMAIN = 645.0 K TJET = 303.4 K THEB = 0.3185 BLORAT= 7.512 DENRATIO= 2.155 TRATIO=0.470

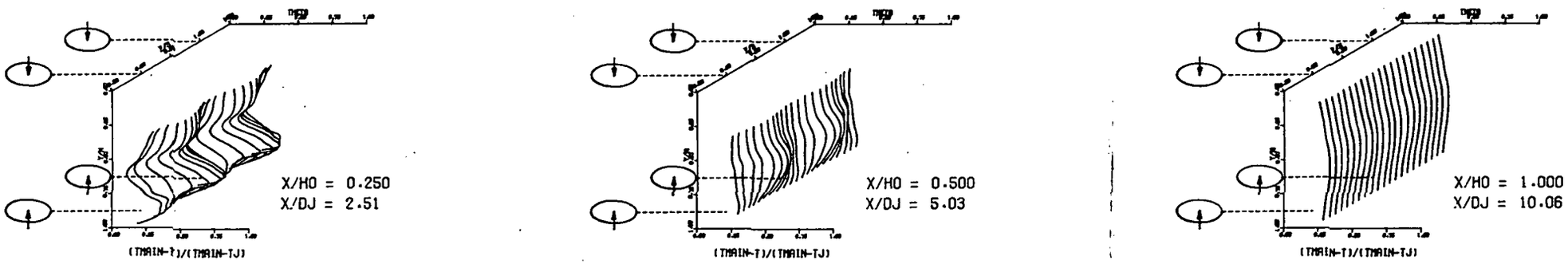

MEASURED THETA PROFILES FOR TEST NO.35, TEST SECTION III, TM=CONST(INL), J = 26.24 , S/D = 2.00 , H/D = 8.00

CONTOUR	1	2	3	4	5	6	7	8	9	10	11
VALUE	0.0500	0.1000	0.1500	0.2000	0.2500	0.3185	0.3500	0.4000	0.5000	0.6000	0.7000

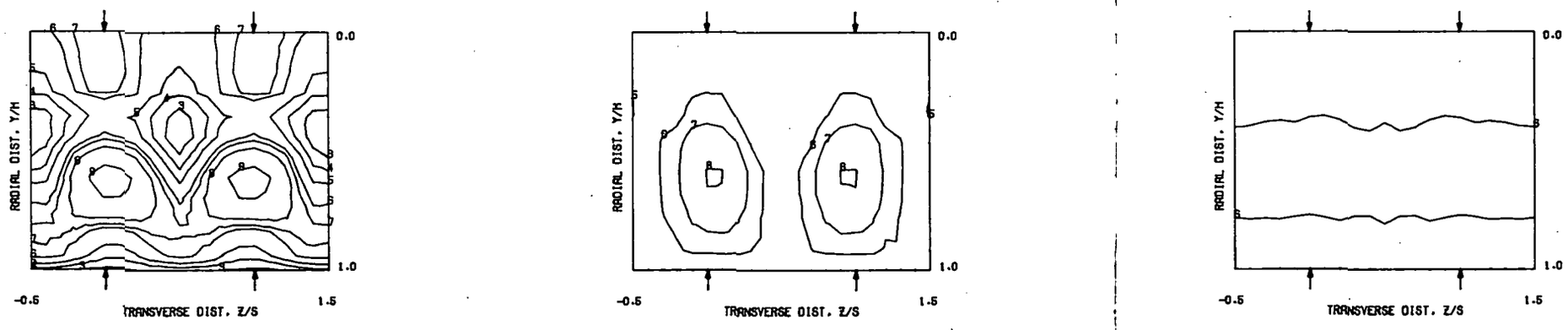

MEASURED THETA CONTOURS FOR TEST NO.35, TM=CONST (INL), J=26.2, S/D=2.0, H/D=8.0

Figure 89. Measured Theta Distributions for Test No. 35.

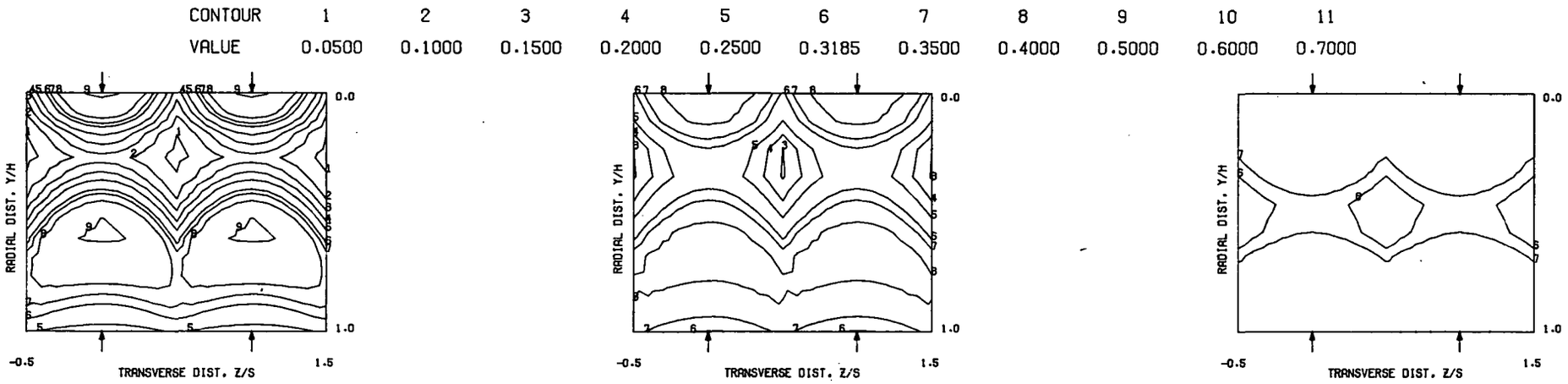

PREDICTED THETA CONTOURS FOR TEST NO 35,T.S.III, J=26.24, S/D=2.0(INL), H/D=8.0

S/DJ = 2.51 HO/DJ = 5.30 VRATIO = 3.49 TRATIO = 0.470 DENRATIO=2.155 TMAIN = 645.0 K TJET = 303.4 K **THEB = 0.3185**

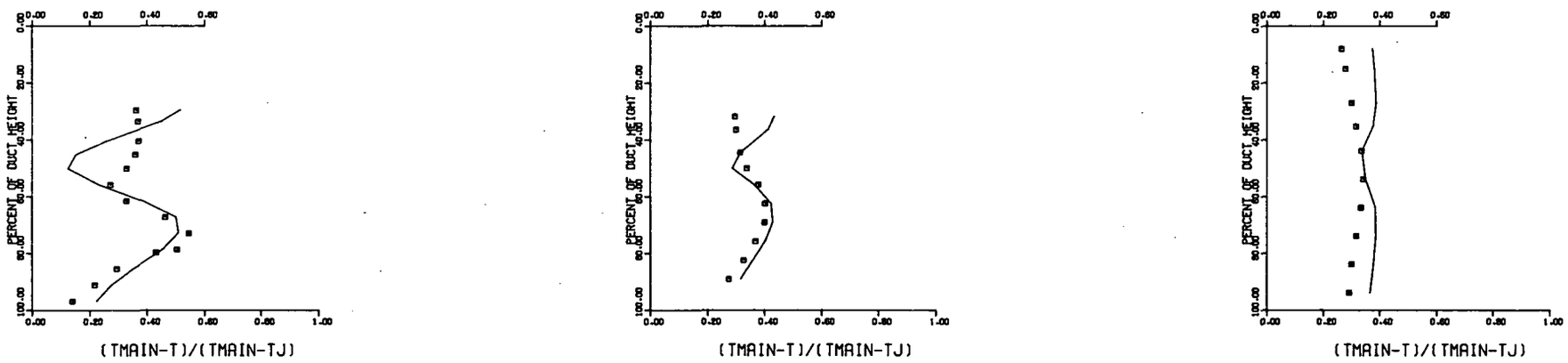

COMPARISON BETWEEN DATA AND CORRELATIONS FOR TEST NO. 35, TEST SECTION III,TM=CONST(INL), J = 26.24 , S/D =2.00 , H/D =8.00

Figure 90. Predicted Theta Distributions for Test No. 35.

S = 0.0254 METERS S/DJ = 2.520 HO/DJ = 10.080 VMAIN = 16.4 M/SEC VJET = 112.8 M/SEC TMAIN = 644.5 K TJET = 301.1 K THEB = 0.4902 BLORAT= 15.590 DENRATIO= 2.275 TRATIO=0.467

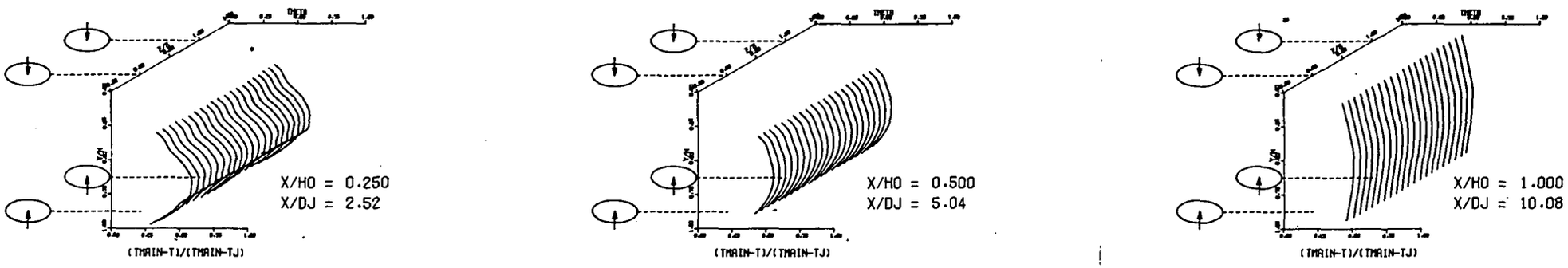

MEASURED THETA PROFILES FOR TEST NO.36, TEST SECTION III, TM=CONST(INL), J = 107.44 , S/D = 2.00 , H/D = 8.00

CONTOUR	1	2	3	4	5	6	7	8	9	10	11
VALUE	0.0500	0.1000	0.1500	0.2000	0.2500	0.3000	0.3500	0.4000	0.4902	0.6000	0.7000

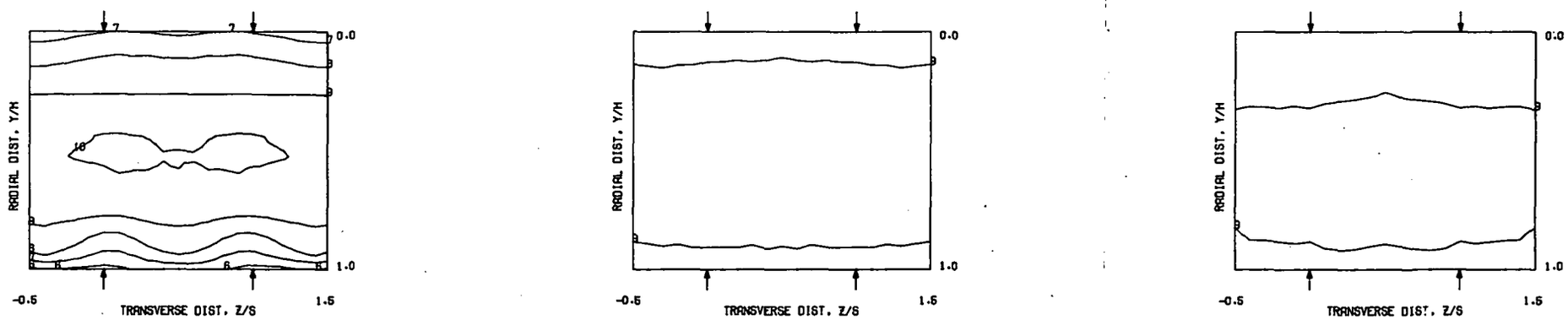

MEASURED THETA CONTOURS FOR TEST NO.36, TM=CONST (INL), J=107., S/D=2.0, H/D=8.0

Figure 91. Measured Theta Distributions for Test No. 36.

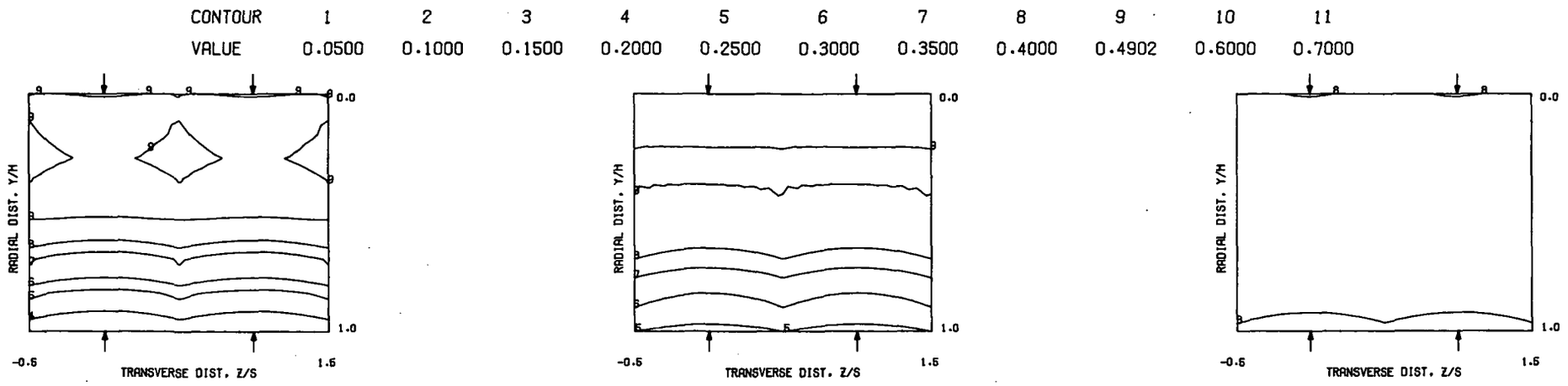

PREDICTED THETA CONTOURS FOR TEST NO 36,T.S.III, J=107.4, S/D=2.0(INL), H/D=8.0

S/DJ = 2.52 HO/DJ = 5.32 VRATIO = 6.87 TRATIO = 0.467 DENRATIO=2.275 TMAIN = 644.5 K TJET = 301.1 K THEB = 0.4902

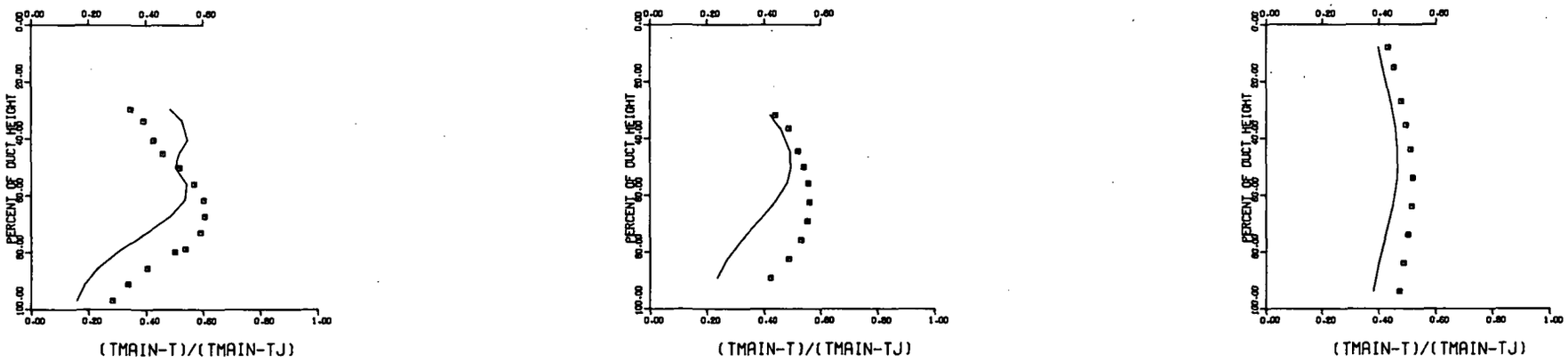

COMPARISON BETWEEN DATA AND CORRELATIONS FOR TEST NO. 36, TEST SECTION III,TM=CONST(INL), J = 107.44 , S/D =2.00 , H/D =8.00

Figure 92. Predicted Theta Distributions for Test No. 36.

S = 0.0508 METERS S/DJ = 4.993 HO/DJ = 9.987 VMAIN = 16.4 M/SEC VJET = 57.5 M/SEC TMAIN = 645.6 K TJET = 310.7 K THEB = 0.1882 BLORAT= 7.343 DENRATIO= 2.100 TRATIO= 0.481

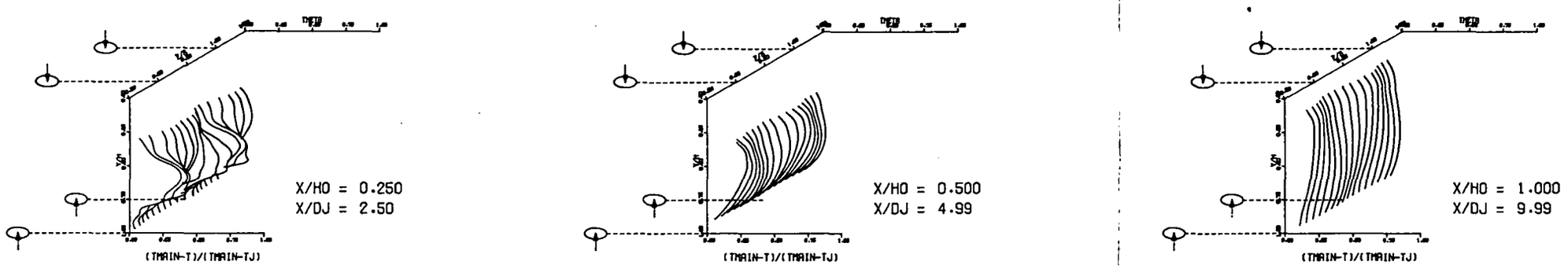

MEASURED THETA PROFILES FOR TEST NO.37, TEST SECTION III,TM=CONST(STG) , J = 25.70 , S/D = 4.00 , H/D = 8.00

CONTOUR	1	2	3	4	5	6	7	8	9	10	11
VALUE	0.0500	0.1000	0.1500	0.1882	0.2500	0.3000	0.3500	0.4000	0.5000	0.6000	0.7000

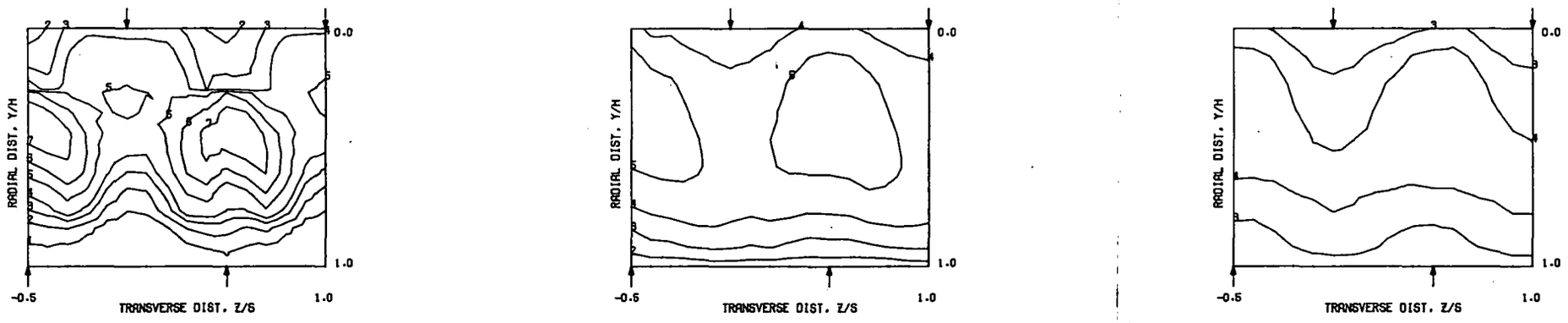

MEASURED THETA CONTOURS FOR TEST NO.37,TM=CONST (STG), J=25.70, S/D=4.0, H/D=8.0

Figure 93. Measured Theta Distributions for Test No. 37.

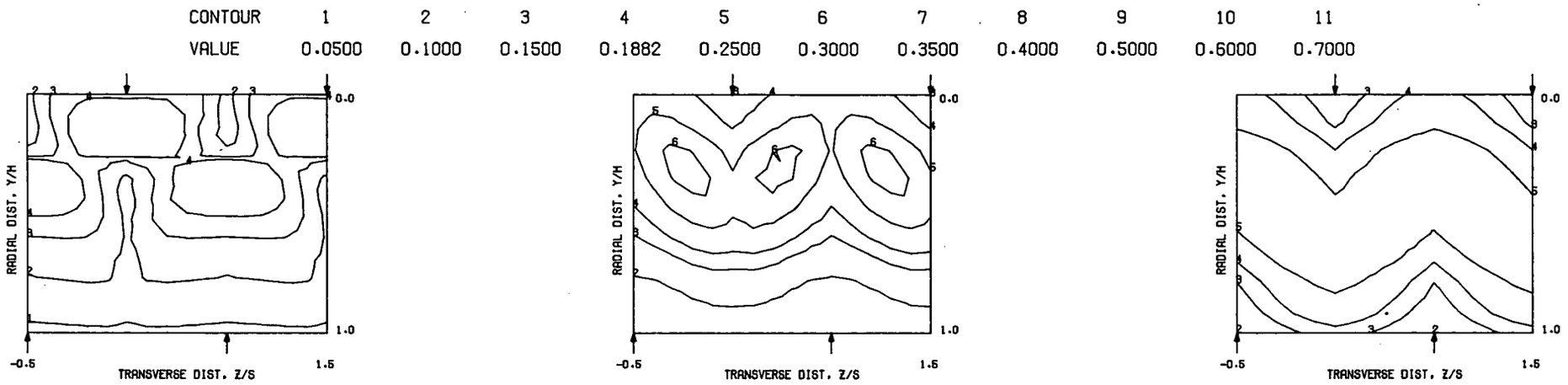

PREDICTED THETA CONTOURS FOR TEST NO 37,T.S.III, J=25.70, S/D=4.0(STG), H/D=8.0

S/DJ = 4.99 HO/DJ = 9.99 VRATIO = 3.50 TRATIO = 0.481 DENRATIO=2.100 TMAIN = 645.6 K TJET = 310.7 K THEB = 0.1882

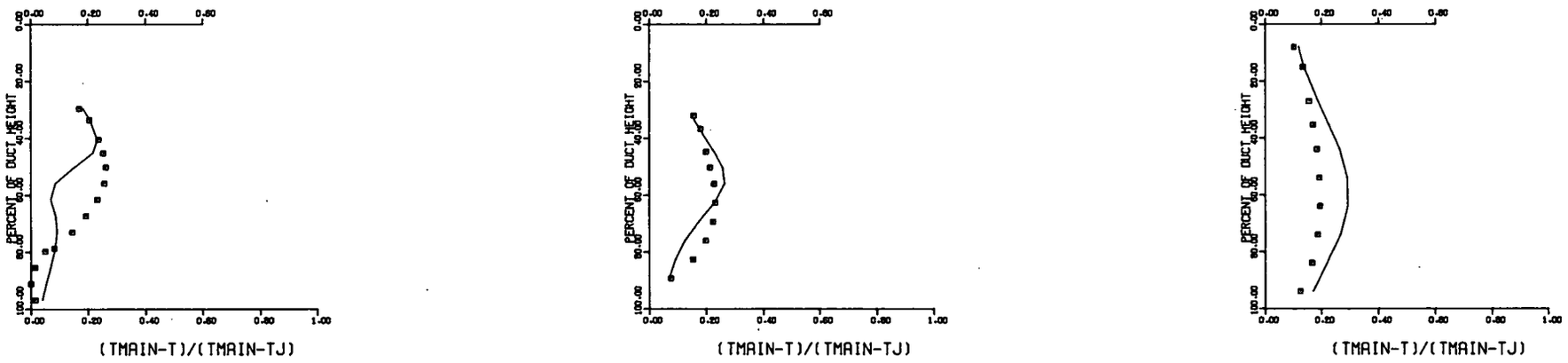

COMPARISON BETWEEN DATA AND CORRELATIONS FOR TEST NO. 37, TEST SECTION III,TM=CONST(STG), J = 25.70 , S/D =4.00 , H/D =8.00

Figure 94. Predicted Theta Distributions for Test No. 37.

S = 0.0508 METERS S/DJ = 5.040 HO/DJ = 10.080 VMAIN = 16.4 M/SEC VJET = 113.8 M/SEC TMAIN = 645.6 K TJET = 303.3 K THEB = 0.3245 BLORAT= 15.678 DENRATIO= 2.260 TRATIO=0.470

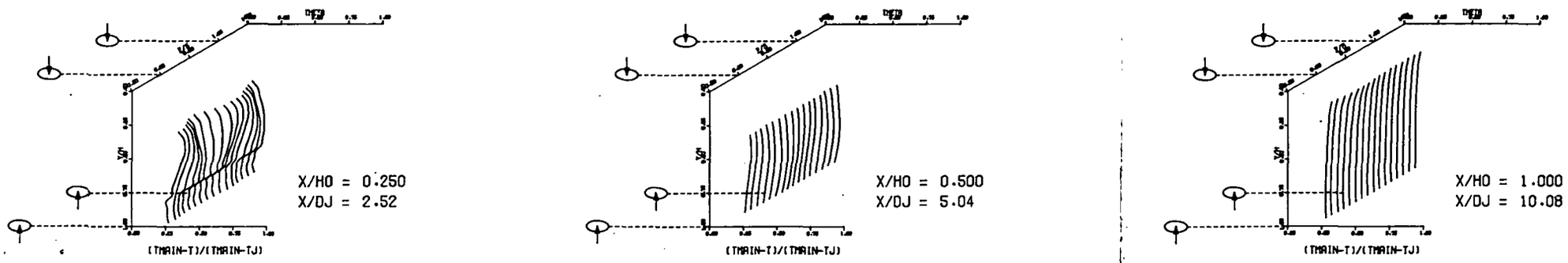

MEASURED THETA PROFILES FOR TEST NO.38, TEST SECTION III,TM=CONST(STG) , J = 109.22 , S/D = 4.00 , H/D = 8.00

CONTOUR	1	2	3	4	5	6	7	8	9	10	11
VALUE	0.0500	0.1000	0.1500	0.2000	0.2500	0.3245	0.3500	0.4000	0.5000	0.6000	0.7000

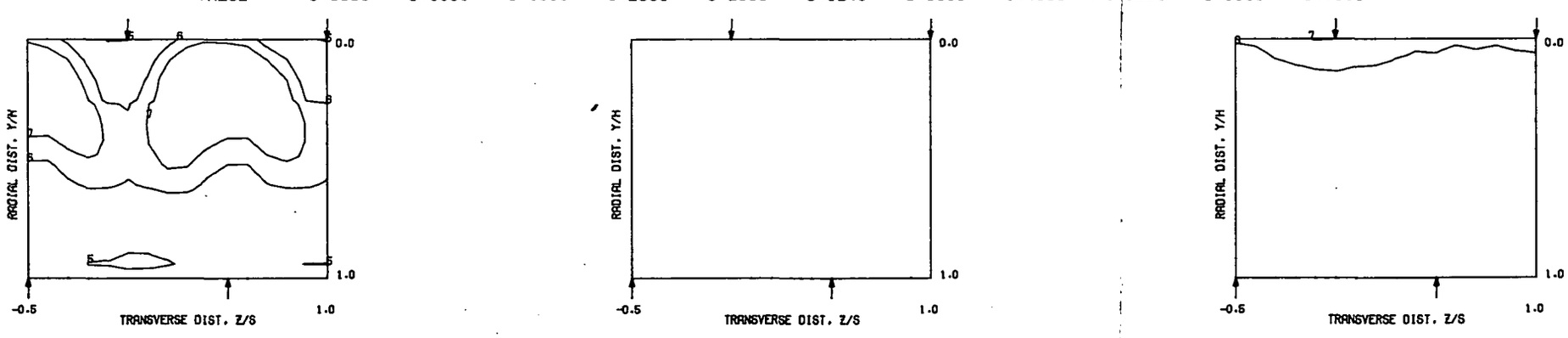

MEASURED THETA CONTOURS FOR TEST NO.38,TM=CONST (STG), J=109.2, S/D=4.0, H/D=8.0

Figure 95. Measured Theta Distributions for Test No. 38.

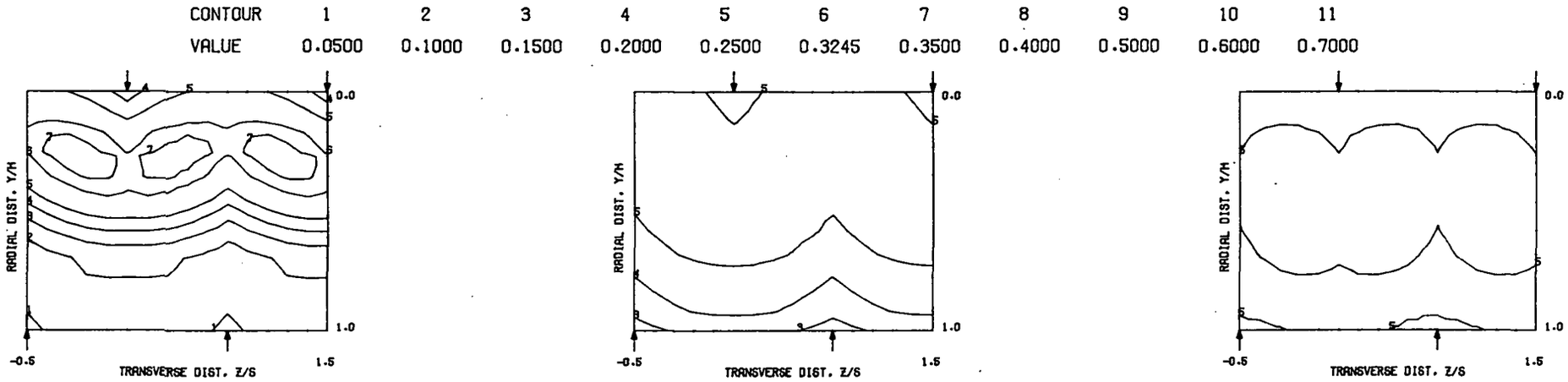

PREDICTED THETA CONTOURS FOR TEST NO 38,T.S.III, J=109.2, S/D=4.0(STG), H/D=8.0

S/DJ = 5.04 HO/DJ = 10.08 VRATIO = 6.95 TRATIO = 0.470 DENRATIO=2.260 TMAIN = 645.6 K TJET = 303.3 K THEB = 0.3245

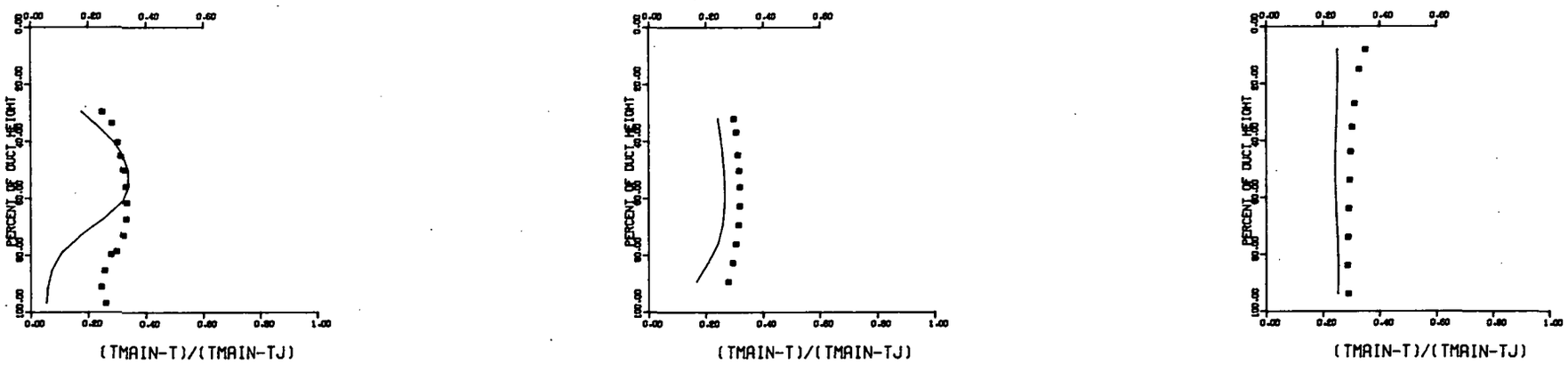

COMPARISON BETWEEN DATA AND CORRELATIONS FOR TEST NO. 38, TEST SECTION III,TM=CONST(STG), J = 109.22 , S/D =4.00 , H/D =8.00

Figure 96. Predicted Theta Distributions for Test No. 38.

S = 0.1016 METERS S/DJ = 4.862 HO/DJ = 4.862 VMAIN = 16.5 M/SEC VJET = 29.7 M/SEC TMAIN = 645.6 K TJET = 311.9 K THEB = 0.1994 BLORAT= 3.726 DENRATIO= 2.075 TRATIO= 0.483

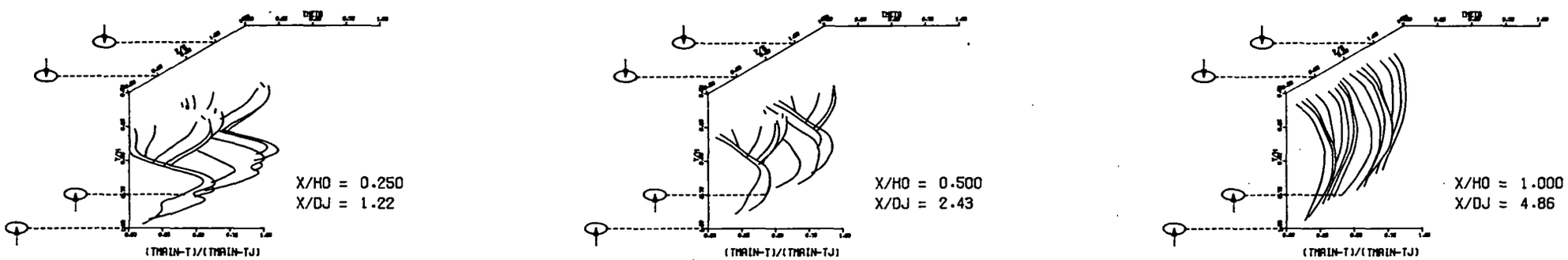

MEASURED THETA PROFILES FOR TEST NO.39, TEST SECTION III,TM=CONST(STG) , J = 6.69 , S/D = 4.00 , H/D = 4.00

CONTOUR	1	2	3	4	5	6	7	8	9	10	11
VALUE	0.0500	0.1000	0.1500	0.1994	0.2500	0.3000	0.3500	0.4000	0.5000	0.6000	0.7000

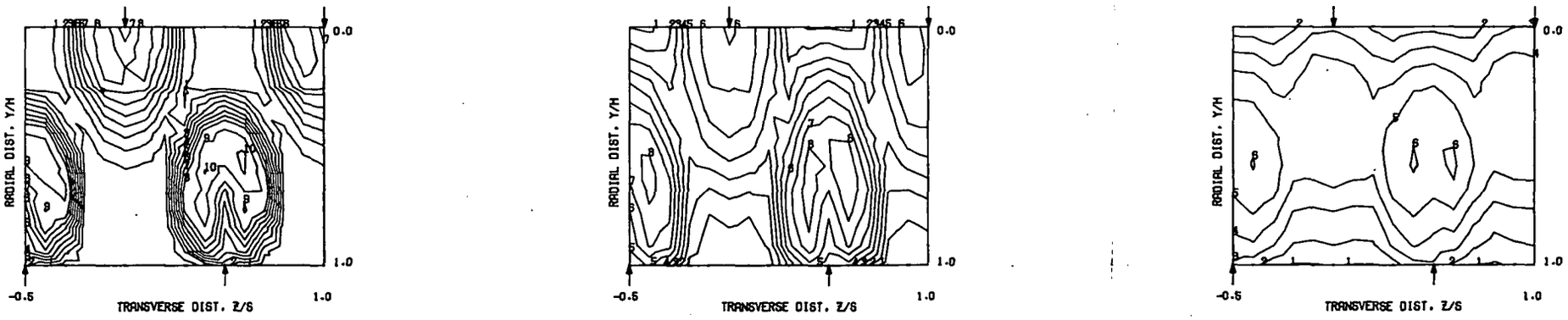

MEASURED THETA CONTOURS FOR TEST NO.39,TM=CONST (STG), J=6.694, S/D=4.0, H/D=4.0

Figure 97. Measured Theta Distributions for Test No. 39.

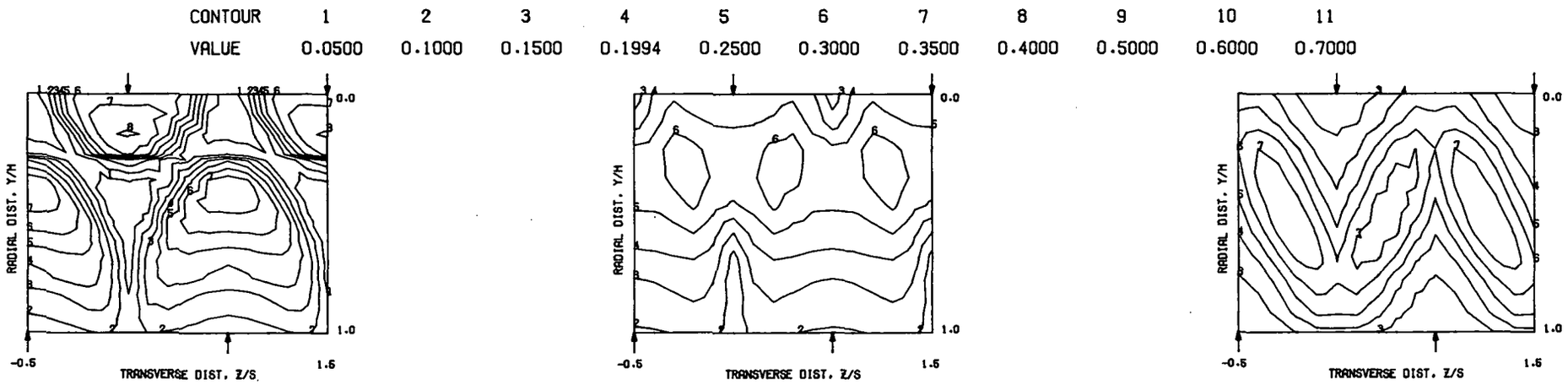

PREDICTED THETA CONTOURS FOR TEST NO 39,T.S.III, J=6.69, S/D=4.0(STG), H/D=4.0

S/DJ = 4.86 HO/DJ = 4.86 VRATIO = 1.80 TRATIO = 0.483 DENRATIO=2.075 TMAIN = 645.6 K TJET = 311.9 K THEB = 0.1994

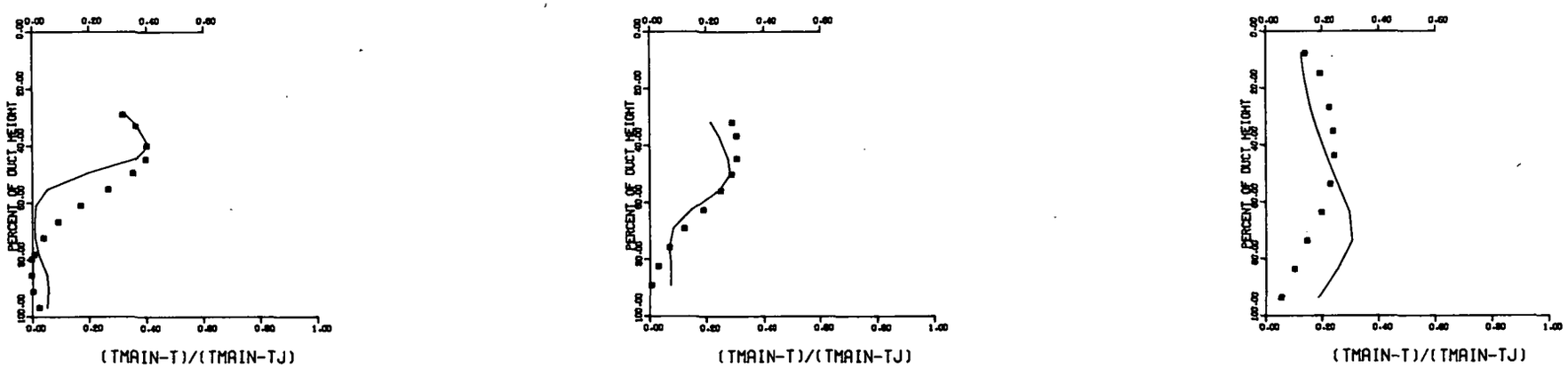

COMPARISON BETWEEN DATA AND CORRELATIONS FOR TEST NO. 39, TEST SECTION III.TM=CONST(STG), J = 6.69 , S/D =4.00 , H/D =4.00

Figure 98. Predicted Theta Distributions for Test No. 39.

S = 0.1016 METERS S/DJ = 4.977 HO/DJ = 4.977 VMAIN = 16.6 M/SEC VJET = 57.4 M/SEC TMAIN = 645.7 K TJET = 302.7 K THEB = 0.3247 BLORAT= 7.493 DENRATIO= 2.164 TRATIO= 0.469

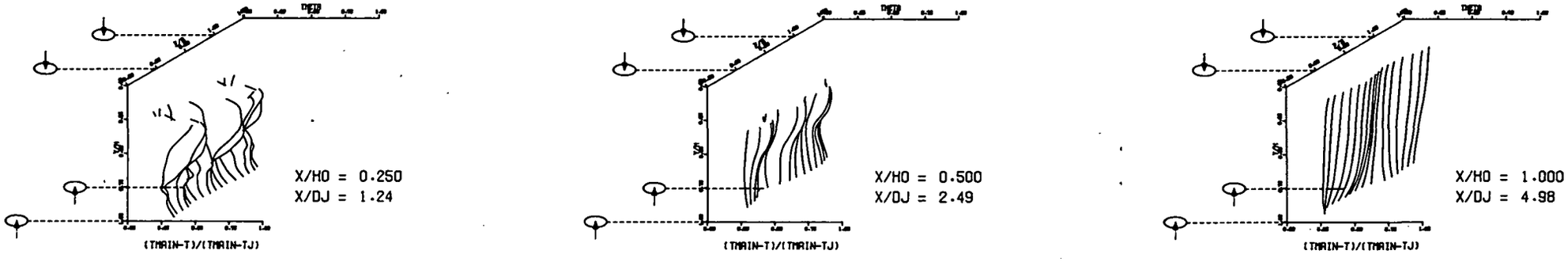

MEASURED THETA PROFILES FOR TEST NO.40, TEST SECTION III,TM=CONST(STG) , J = 25.99 , S/D = 4.00 , H/D = 4.00

CONTOUR	1	2	3	4	5	6	7	8	9	10	11
VALUE	0.0500	0.1000	0.1500	0.2000	0.2500	0.3247	0.3500	0.4000	0.5000	0.6000	0.7000

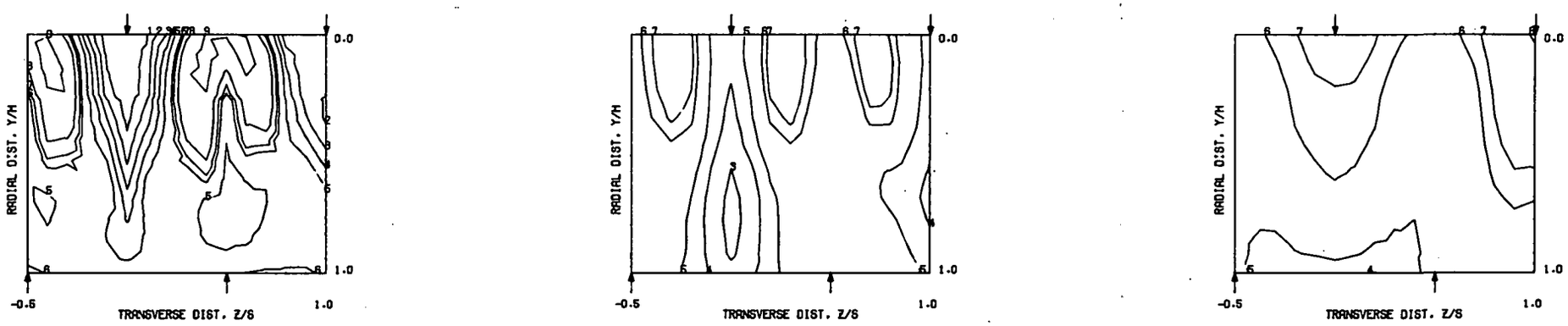

MEASURED THETA CONTOURS FOR TEST NO.40,TM=CONST (STG), J=25.99, S/D=4.0, H/D=4.0

Figure 99. Measured Theta Distributions for Test No. 40.

CONTOUR	1	2	3	4	5	6	7	8	9	10	11
VALUE	0.0500	0.1000	0.1500	0.2000	0.2500	0.3247	0.3500	0.4000	0.5000	0.6000	0.7000

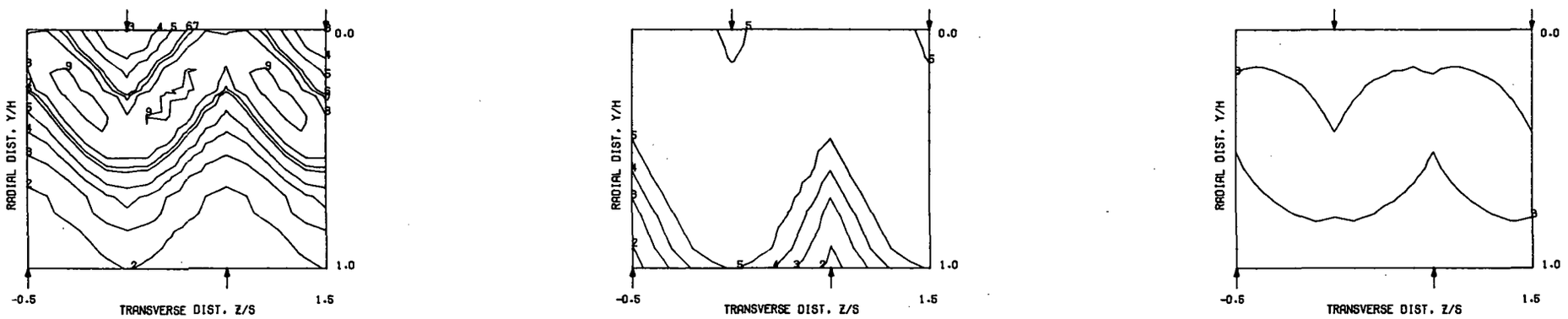

PREDICTED THETA CONTOURS FOR TEST NO 40, T.S.III(STG),J=25.99, S/D=4.0, H/D=4.0

S/DJ = 4.98 HO/DJ = 4.98 VRATIO = 3.47 TRATIO = 0.469 DENRATIO=2.164 TMAIN = 645.7 K TJET = 302.7 K **THEB = 0.3247**

X/H = 0.25 X/DJ =1.24 X/H = 0.50 X/DJ =2.49 X/H = 1.00 X/DJ =4.98

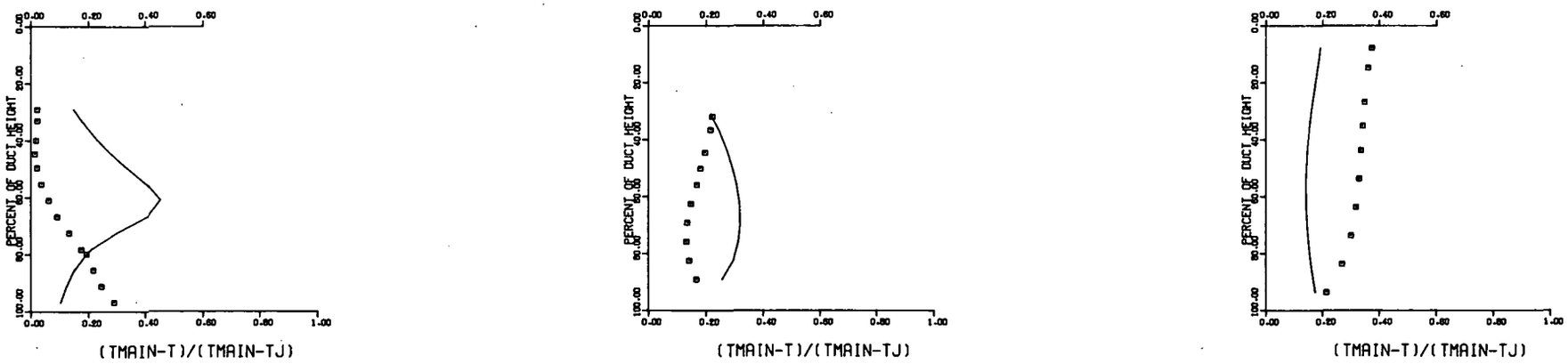

COMPARISON BETWEEN DATA AND CORRELATIONS FOR TEST NO. 40, TEST SECTION III,TM=CONST(STG), J = 25.99 , S/D =4.00 , H/D =4.00

Figure 100. Predicted Theta Distributions for Test No. 40.

S = 0.0508 METERS S/DJ = 2.462 HO/DJ = 4.924 VMAIN = 16.5 M/SEC VJET = 29.2 M/SEC TMAIN = 645.6 K TJET = 305.5 K THEB = 0.3272 BLORAT= 3.747 DENRATIO= 2.122 TRATIO=0.473

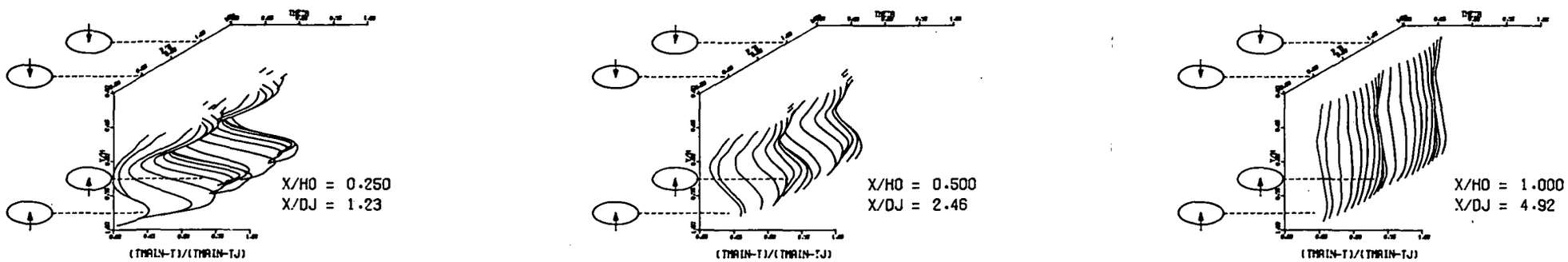

MEASURED THETA PROFILES FOR TEST NO.41, TEST SECTION III,TM=CONST(INL), J = 6.64 , S/D = 2.00 , H/D = 4.00

CONTOUR	1	2	3	4	5	6	7	8	9	10	11
VALUE	0.0500	0.1000	0.1500	0.2000	0.2500	0.3272	0.3500	0.4000	0.5000	0.6000	0.7000

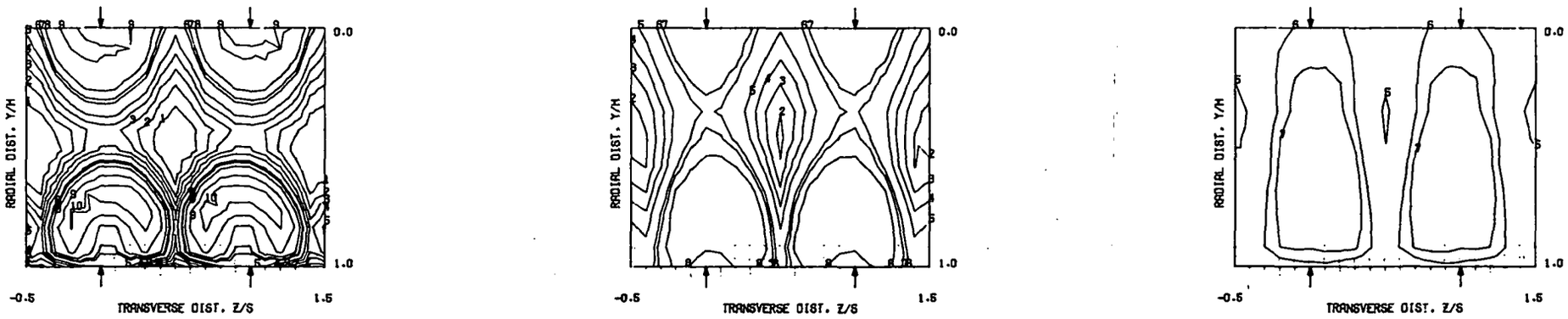

MEASURED THETA CONTOURS FOR TEST NO.41,TM=CONST (INL), J=6.636, S/D=2.0, H/D=4.0

Figure 101. Measured Theta Distributions for Test No. 41.

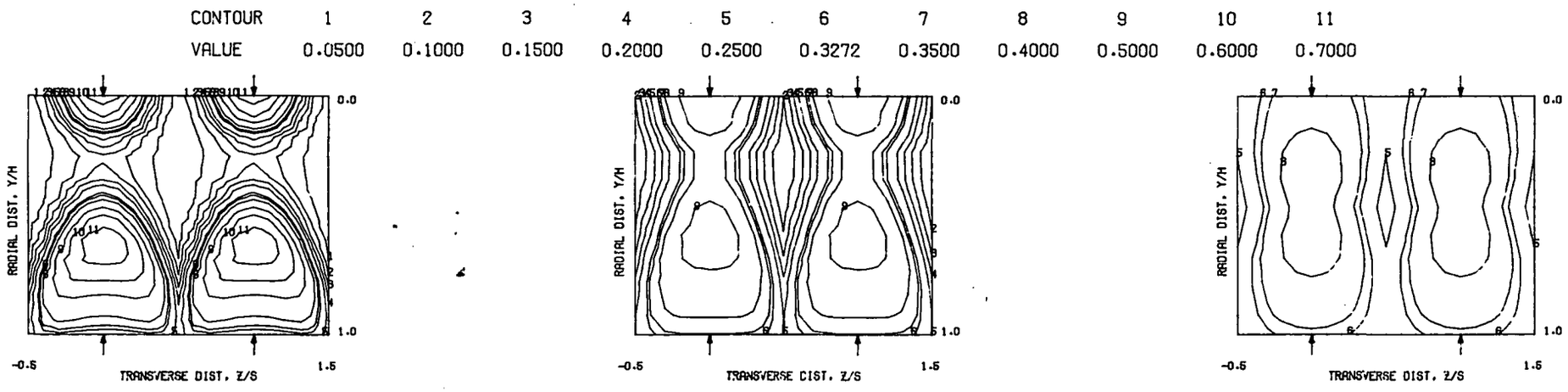

PREDICTED THETA CONTOURS FOR TEST NO 41. T.S.III(INL),J=6.64, S/D=2.0, H/D=4.0

S/DJ = 2.46 HO/DJ = 2.60 VRATIO = 1.77 TRATIO = 0.473 DENRATIO= 2.122 TMAIN = 645.6 K TJET = 305.5 K THEB = 0.3272

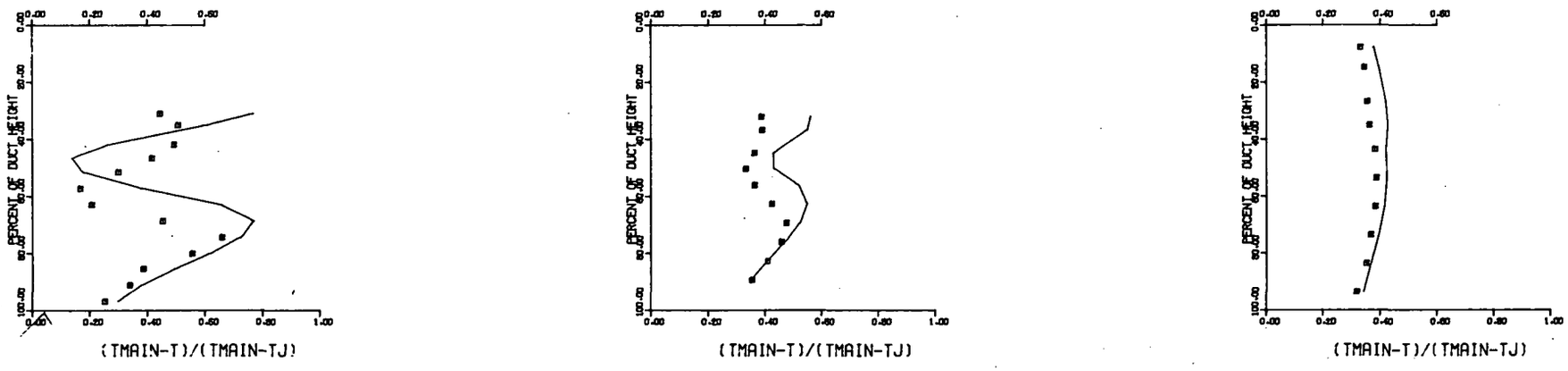

COMPARISON BETWEEN DATA AND CORRELATIONS FOR TEST NO. 41, TEST SECTION III,TM=CONST(INL), J = 6.64 , S/D =2.00 , H/D =4.00

Figure 102. Predicted Theta Distributions for Test No. 41.

S = C.0508 METERS S/DJ = 2.540 HO/DJ = 5.080 VMAIN = 16.4 M/SEC VJET = 57.2 M/SEC TMAIN = 644.8 K TJET = 302.5 K THEB = 0.4774 BLORAT= 7.518 DENRATIO= 2.164 TRATIO=0.469

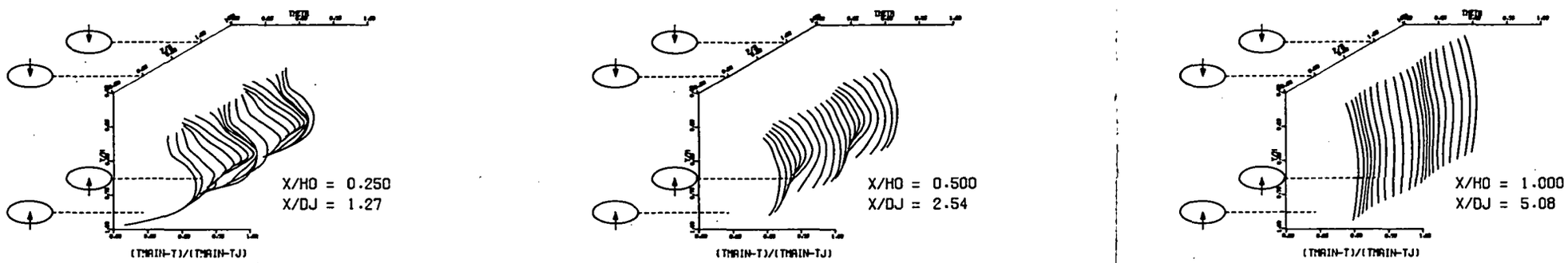

MEASURED THETA PROFILES FOR TEST NO.42, TEST SECTION III,TM=CONST(INL) , J = 26.25 , S/D = 2.00 , H/D = 4.00

CONTOUR	1	2	3	4	5	6	7	8	9	10	11
VALUE	0.0500	0.1000	0.1500	0.2000	0.2500	0.3000	0.3500	0.4000	0.4773	0.6000	0.7000

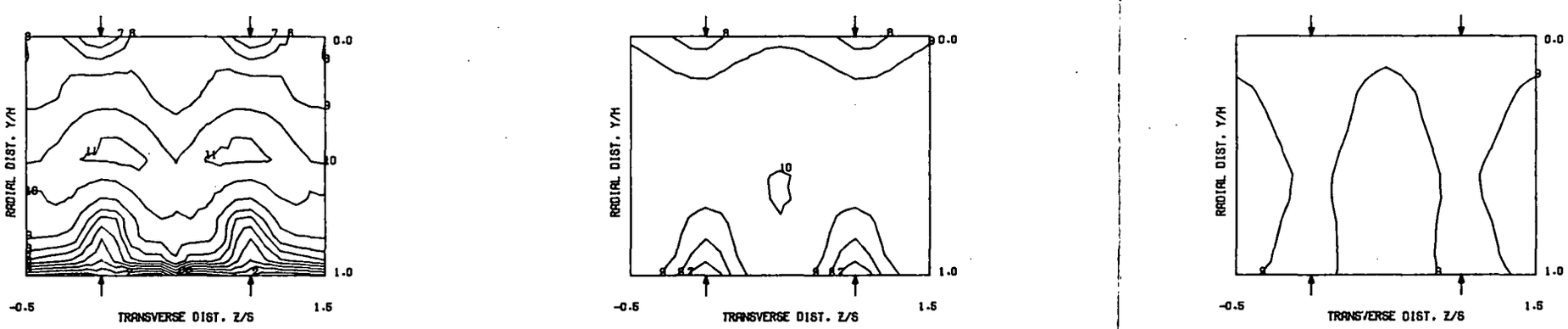

MEASURED THETA CONTOURS FOR TEST NO.42,TM=CONST (INL), J=26.25, S/D=2.0, H/D=4.0

Figure 103. Measured Theta Distributions for Test No. 42.

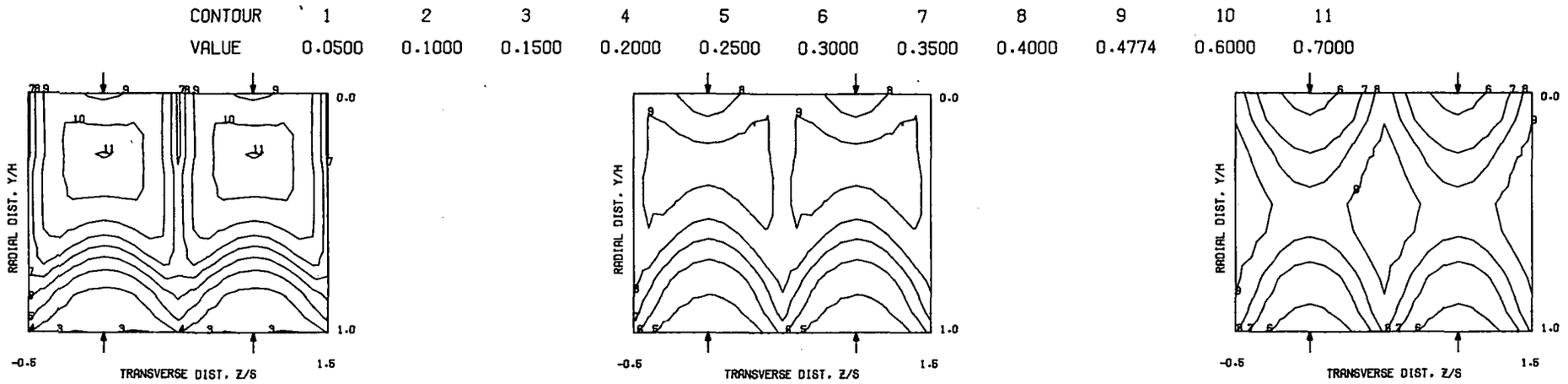

PREDICTED THETA CONTOURS FOR TEST NO 42, T.S.III, J=26.25, S/D=2.0(INL), H/D=4.0

S/DJ = 2.54 HO/DJ = 2.68 VRATIO = 3.48 TRATIO = 0.469 DENRATIO=2.164 TMAIN = 644.8 K TJET = 302.5 K THEB = 0.4774

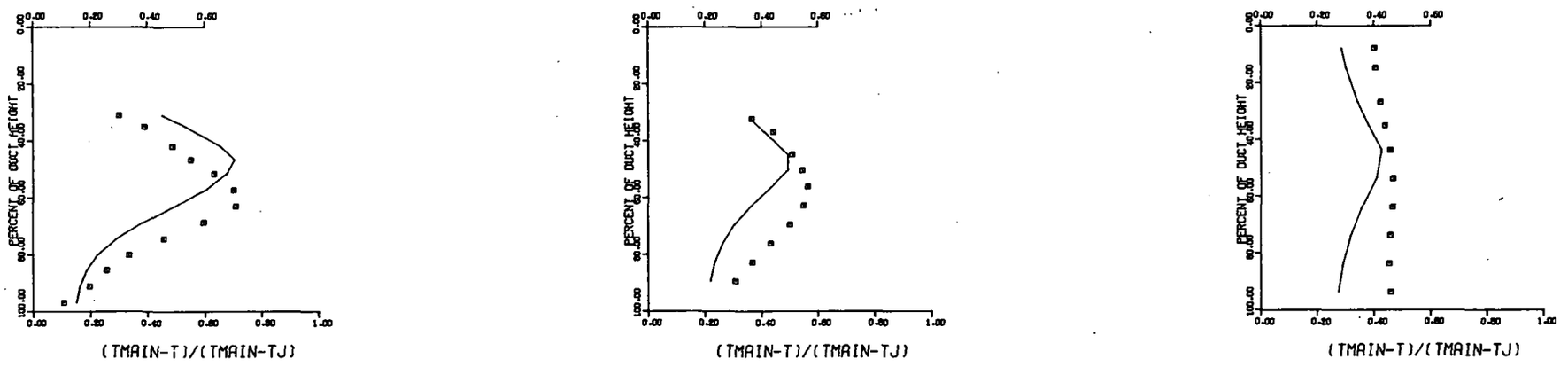

COMPARISON BETWEEN DATA AND CORRELATIONS FOR TEST NO. 42, TEST SECTION III,TM=CONST(INL), J = 26.25 , S/D =2.00 , H/D =4.00

Figure 104. Predicted Theta Distributions for Test No. 42.

S = 0.0508 METERS S/DJ = 23.546 HO/DJ = 47.091 VMAIN = 17.9 M/SEC VJET = 34.9 M/SEC TMAIN = 506.5 K TJET = 310.2 K THEB = 0.4907 BLORAT= 3.581 DENRATIO= 1.648 TRATIO=0.612

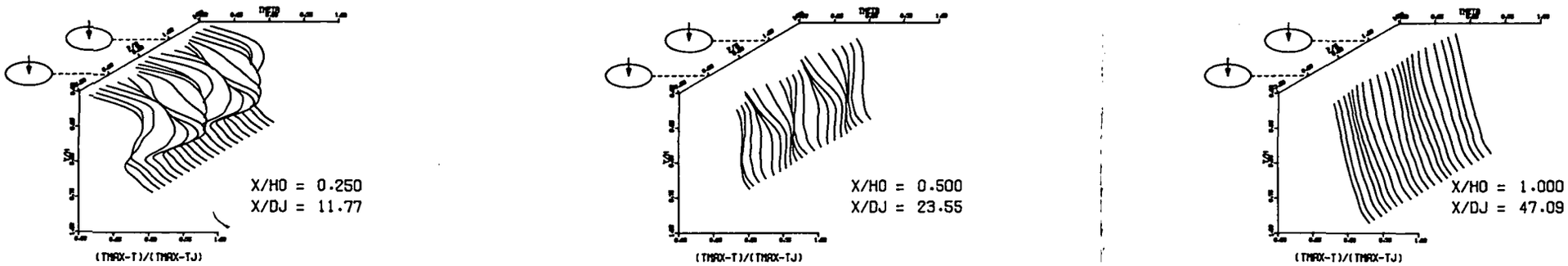

PREDICTED THETA PROFILES FOR TEST NO.43, FLAT WALL JET, TOP HOT , J = 6.26 , S/D = 2.00 , H/D = 4.00

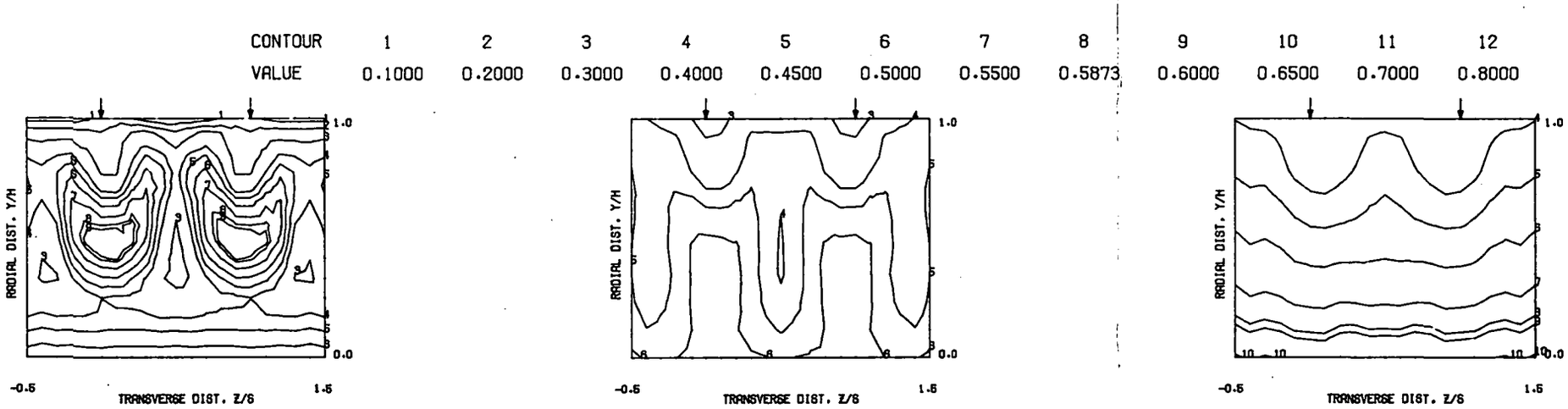

PREDICTED THETA CONTOURS FOR TEST NO 43, TOP HOT , J=6.26, S/D=2.0, H/D=4.0

Figure 105. Measured Theta Distributions for Test No. 43.

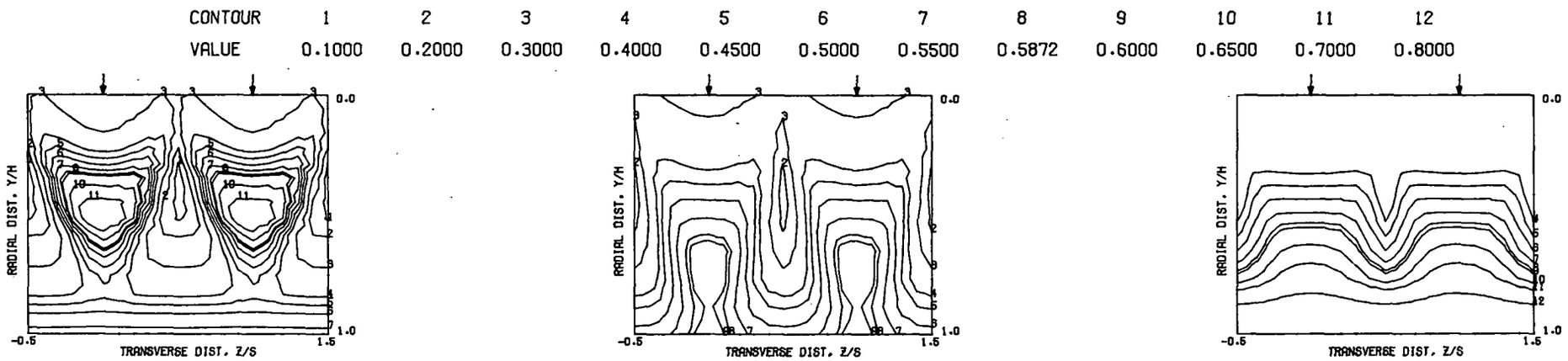

PREDICTED THETA CONTOURS FOR TEST NO.43, TOP HOT, J=6.26, S/D=2.0, H/D=4.0

S/DJ = 2.45 HO/DJ = 4.90 VRATIO = 1.95 TRATIO = 0.612 DENRATIO= 1.648 TMAIN = 506.5 K TJET = 310.2 K THEB = -0.001

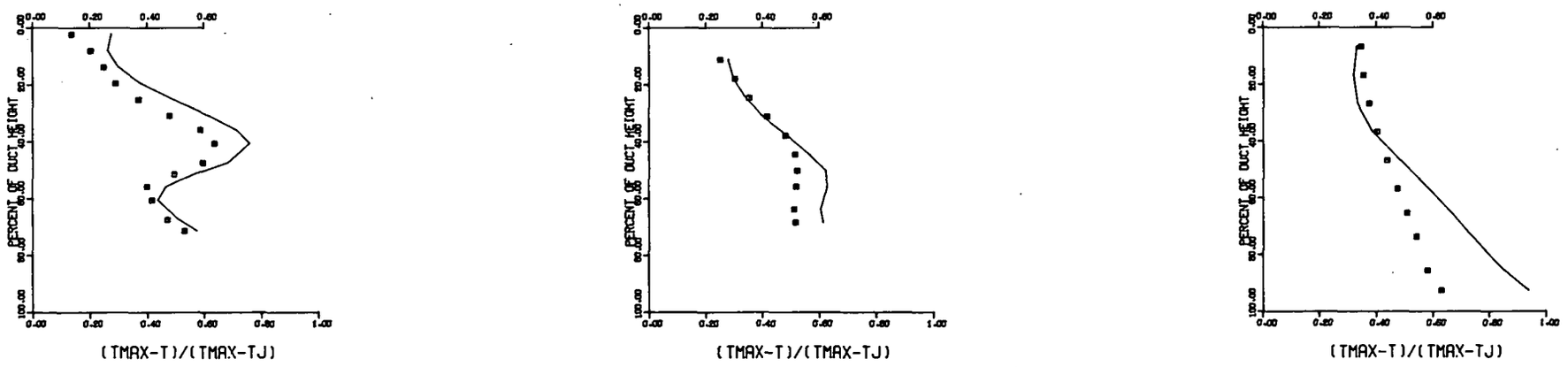

COMPARISON BETWEEN DATA AND CORRELATIONS FOR TEST NO.43, FLAT WALL INJECTION, TOP HOT, J = 6.26 , S/D =2.00 , H/D =4.00

Figure 106. Predicted Theta Distributions for Test No. 43.

S = 0.0508 METERS S/DJ = 23.546 HO/DJ = 47.091 VMAIN = 17.9 M/SEC VJET = 67.9 M/SEC TMAIN = 508.4 K TJET = 307.9 K THEB = 0.4847 BLORAT= 7.147 DENRATIO= 1.698 TRATIO= 0.606

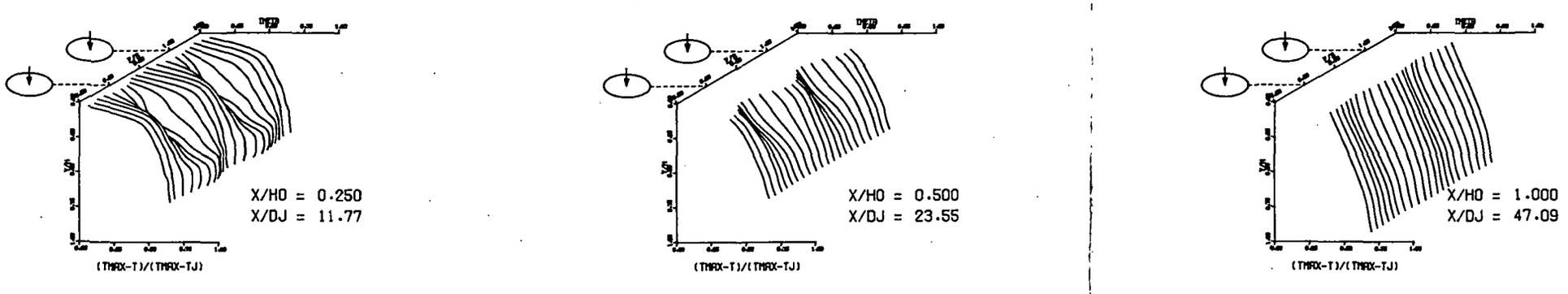

PREDICTED THETA PROFILES FOR TEST NO.44, FLAT WALL JET, TOP HOT , J = 24.31 , S/D = 2.00 , H/D = 4.00

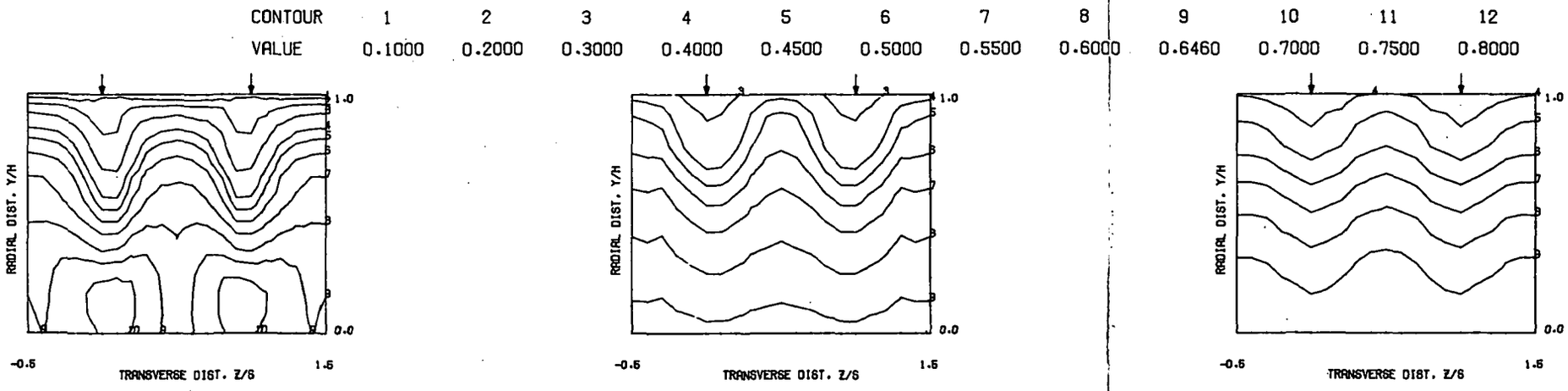

PREDICTED THETA CONTOURS FOR TEST NO 44, TOP HOT , J=24.31, S/D=2.0, H/D=4.0

Figure 107. Measured Theta Distributions for Test No. 44.

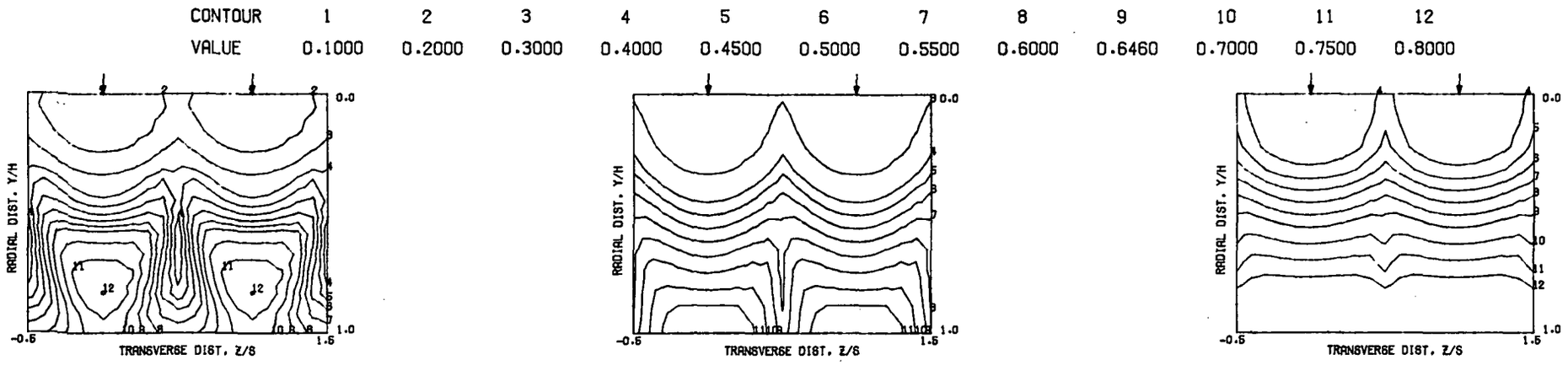

PREDICTED THETA CONTOURS FOR TEST NO.44, TOP HOT, J=24.31, S/D=2.0, H/D=4.0

S/DJ = 2.48 HO/DJ = 4.96 VRATIO = 3.78 TRATIO = 0.606 DENRATIO= 1.698 TMAIN = 508.4 K TJET = 307.9 K THEB = 0.323

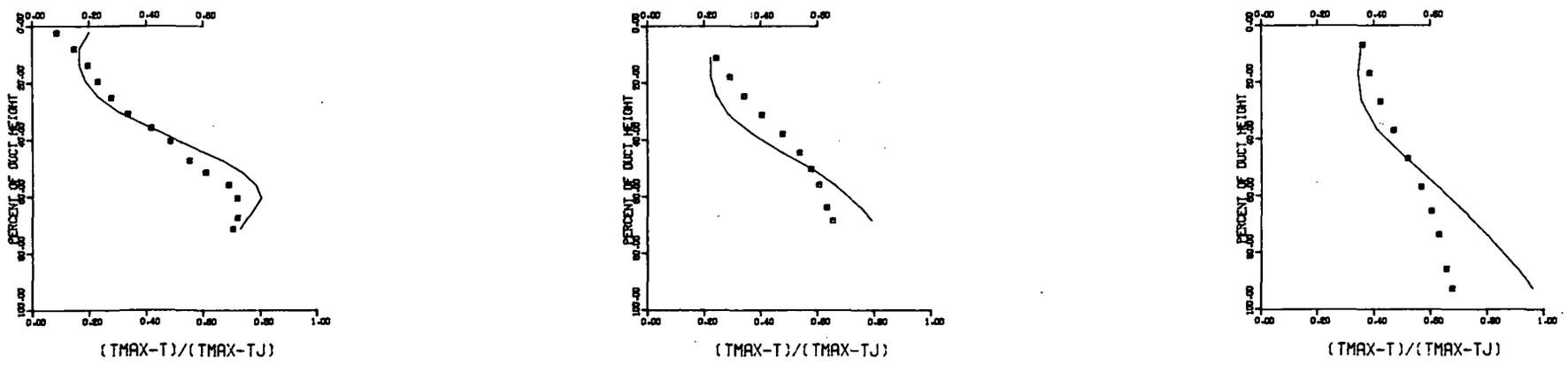

COMPARISON BETWEEN DATA AND CORRELATIONS FOR TEST NO.44, FLAT WALL INJECTION, TOP HOT, J = 24.31 , S/D =2.00 , H/D =4.00

Figure 108. Predicted Theta Distributions for Test No. 44.

S = 0.0102 METERS S/DJ = 0.189 HO/DJ = 1.876 VMAIN = 16.5 M/SEC VJET = 29.4 M/SEC TMAIN = 644.7 K TJET = 307.8 K THEB = 0.2179 BLORAT= 3.744 DENRATIO= 2.104 TRATIO=0.477

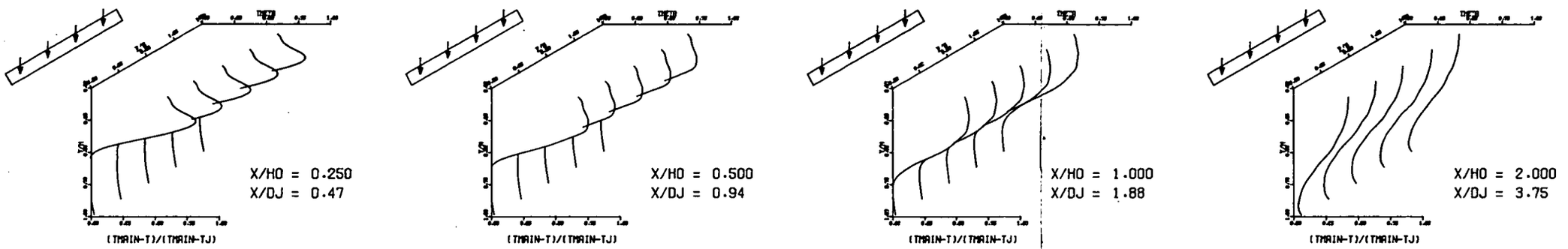

MEASURED THETA PROFILES FOR TEST NO.45A, TEST SECTION I, 1.02 CM SLOT , J = 6.66 , S/D = 1.00 , H/D = 9.92

CONTOUR	1	2	3	4	5	6	7	8	9	10	11
VALUE	0.0500	0.1000	0.1500	0.2179	0.2500	0.3000	0.3500	0.4000	0.5000	0.6000	0.7000

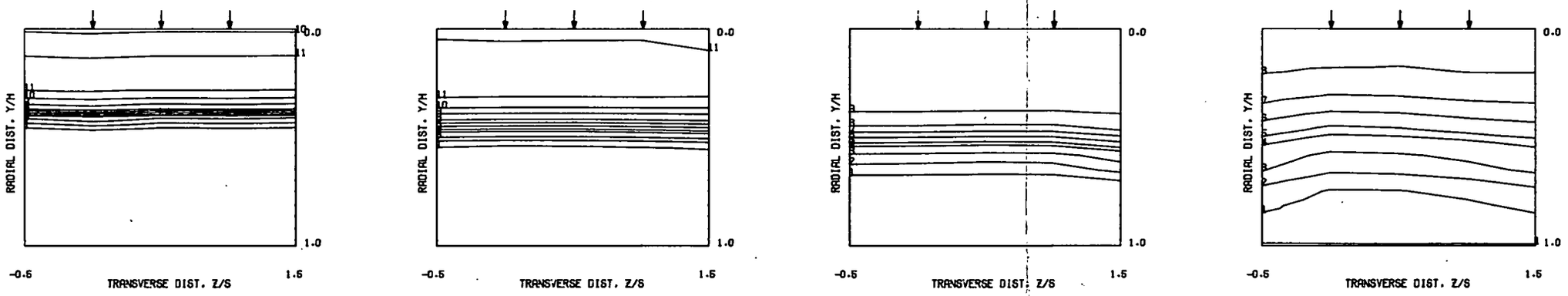

MEASURED THETA CONTOURS FOR TEST NO 45A, SLOT , J=6.66, S/W=1.0, H/W=9.92

Figure 109. Measured Theta Distributions for Test No. 45A.

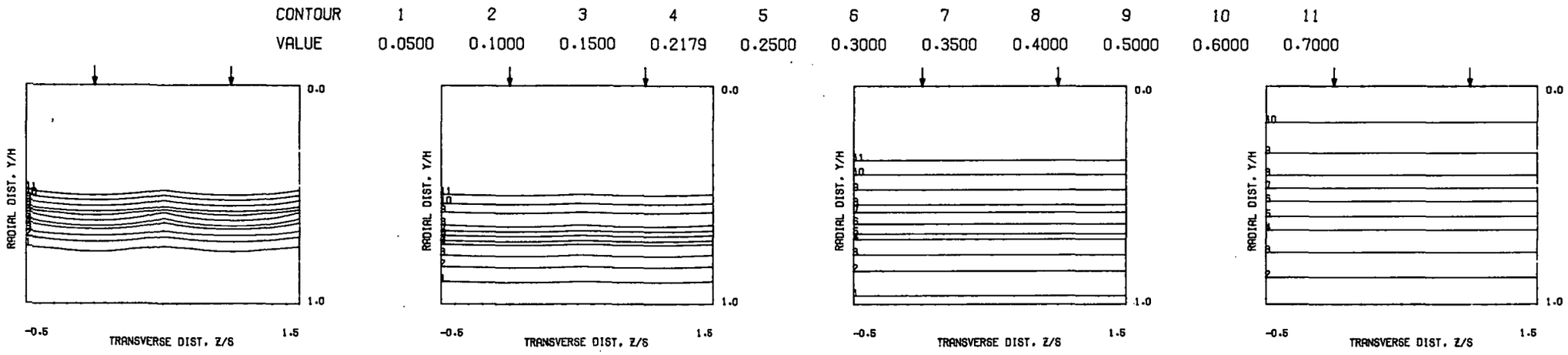

PREDICTED THETA CONTOURS FOR TEST NO. 45A, TM=CONST (SLOT), J=6.66, H/W=9.92

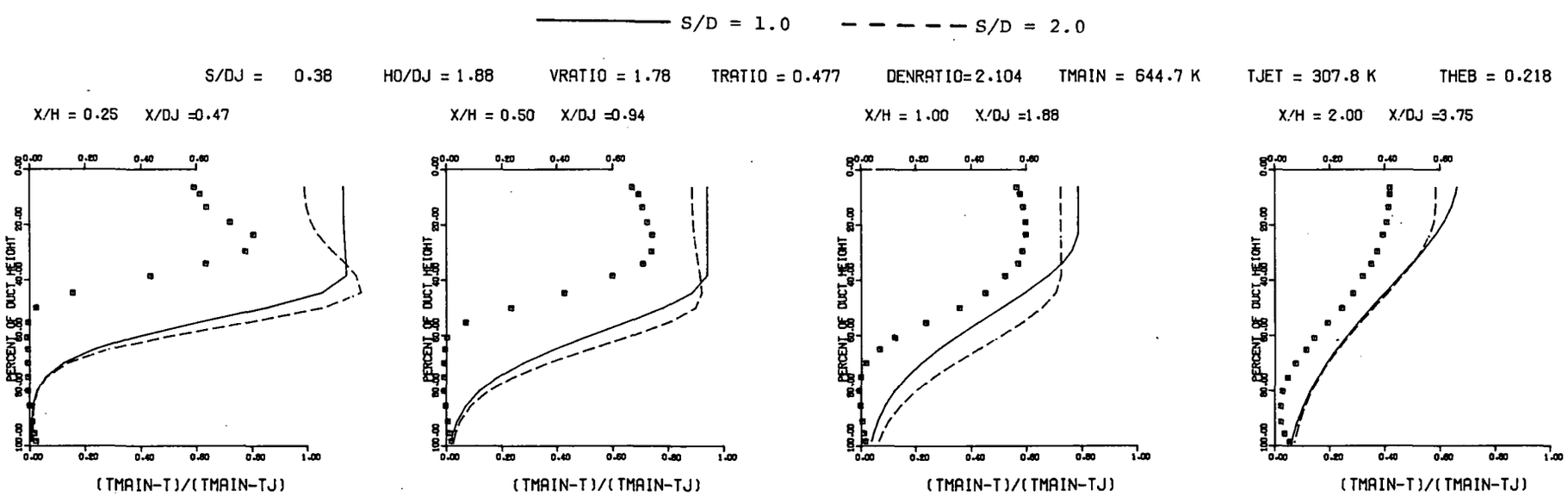

COMPARISON BETWEEN DATA AND CORRELATIONS FOR TEST NO.45A, 10.24 MM SLOT, TM=CONST, T.S. I.J = 6.66 , S/D =2.00 , H/D =9.92

Figure 110. Predicted Theta Distributions for Test No. 45A.

S = 0.0102 METERS S/DJ = 0.192 HO/DJ = 1.905 VMAIN = 16.6 M/SEC VJET = 57.3 M/SEC TMAIN = 644.4 K TJET = 308.7 K THEB = 0.3462 BLORAT= 7.335 DENRATIO= 2.125 TRATIO=0.479

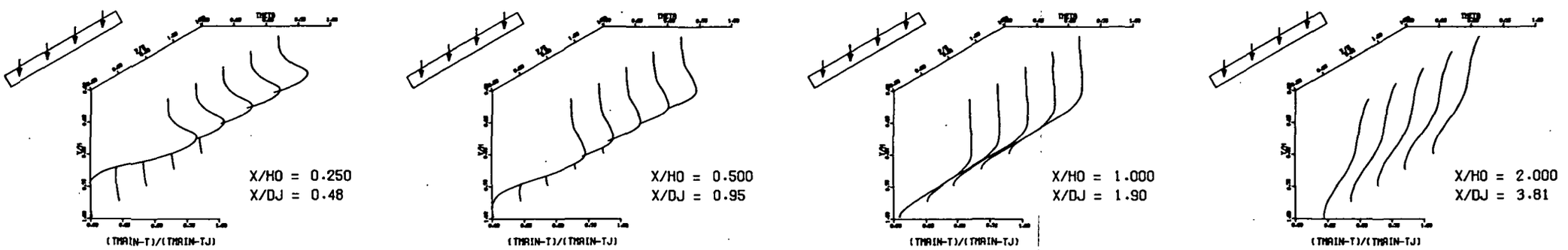

MEASURED THETA PROFILES FOR TEST NO.45B, TEST SECTION I, 1.02 CM SLOT , J = 25.34 , S/D = 1.00 , H/D = 9.92

CONTOUR	1	2	3	4	5	6	7	8	9	10	11	12
VALUE	0.1000	0.1500	0.2000	0.2500	0.3000	0.3461	0.4000	0.4500	0.5000	0.6000	0.7000	0.8000

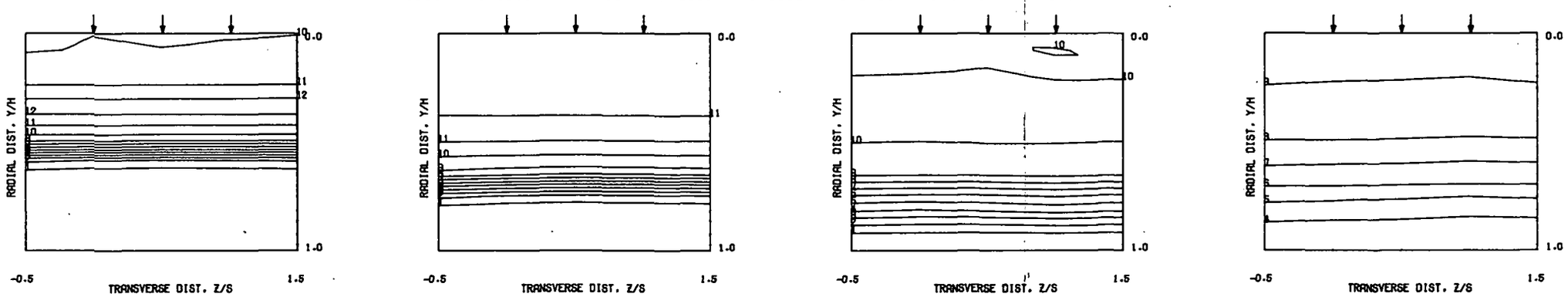

MEASURED THETA CONTOURS FOR TEST NO 45B, SLOT , J=25.34, S/W=1.0, H/W=9.92

Figure 111. Measured Theta Distributions for Test No. 45B.

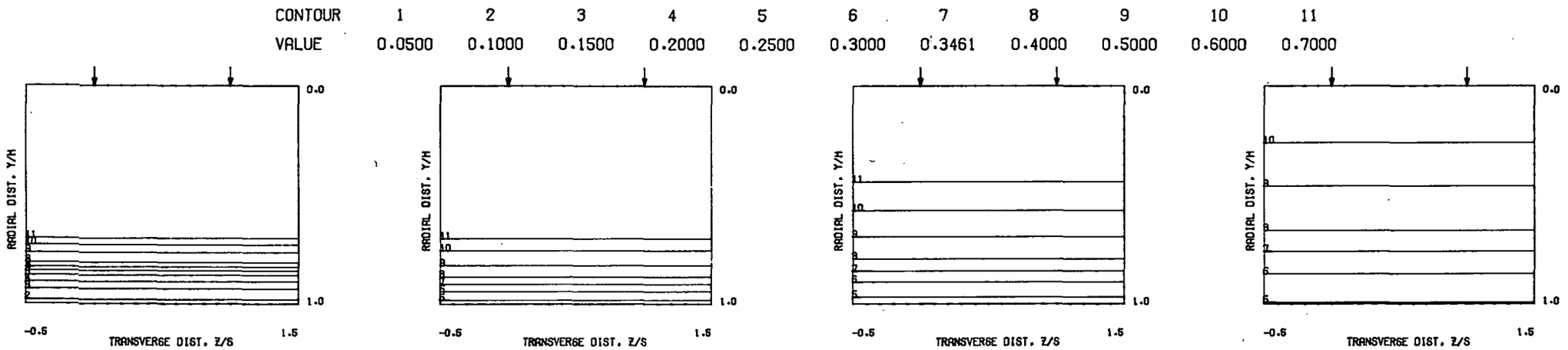

PREDICTED THETA CONTOURS FOR TEST NO. 45B, TM=CONST (SLOT), J=25.34, H/W=9.92

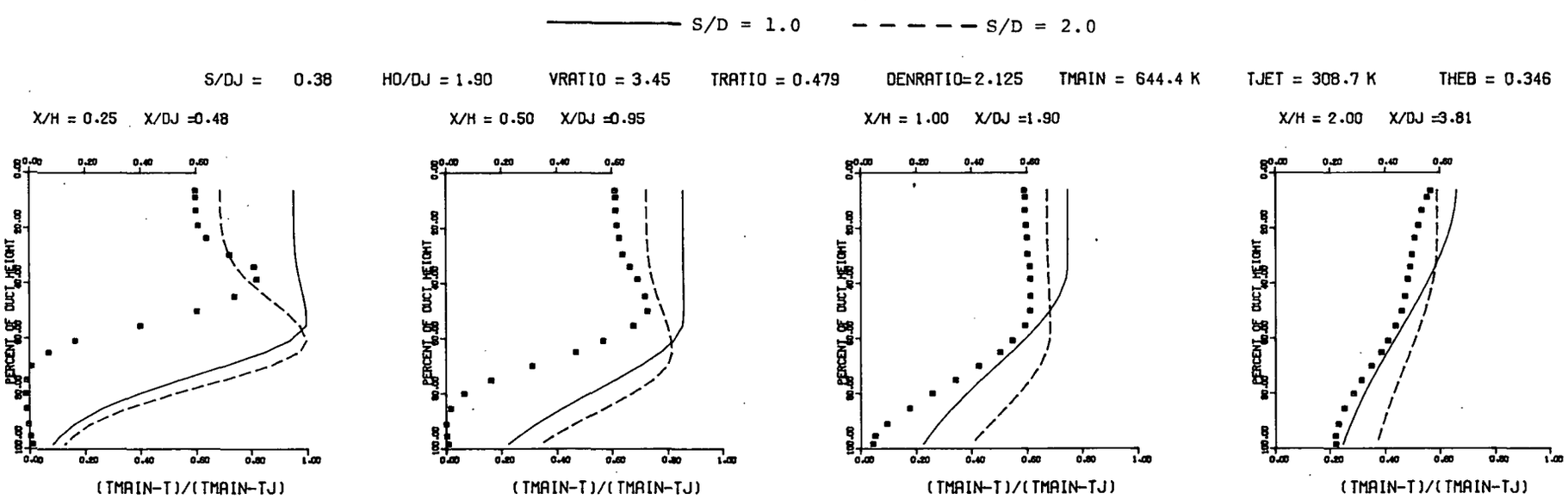

COMPARISON BETWEEN DATA AND CORRELATIONS FOR TEST NO.45B, 10.24 MM SLOT, TM=CONST, T.S. I.J = 25.34 , S/D =2.00 , H/D =9.92

Figure 112. Predicted Theta Distributions for Test No. 45B.

S = 0.0102 METERS S/DJ = 0.194 HO/DJ = 1.926 VMAIN = 16.7 M/SEC VJET = 98.9 M/SEC TMAIN = 643.9 K TJET = 307.5 K THEB = 0.4820 BLORAT= 13.185 DENRATIO= 2.223 TRATIO= 0.478

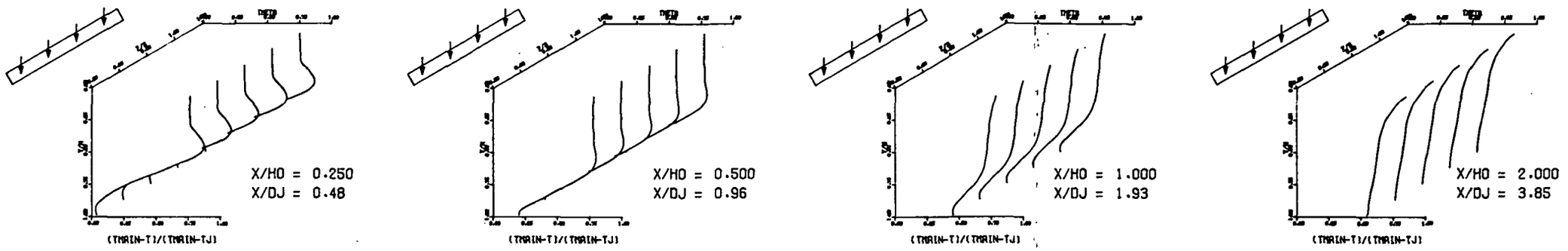

MEASURED THETA PROFILES FOR TEST NO.45C, TEST SECTION I, 1.02 CM SLOT , J = 78.33 , S/D = 1.00 , H/D = 9.92

CONTOUR	1	2	3	4	5	6	7	8	9	10	11	12
VALUE	0.1000	0.2000	0.2500	0.3000	0.3500	0.4000	0.4820	0.5000	0.5500	0.6000	0.7000	0.8000

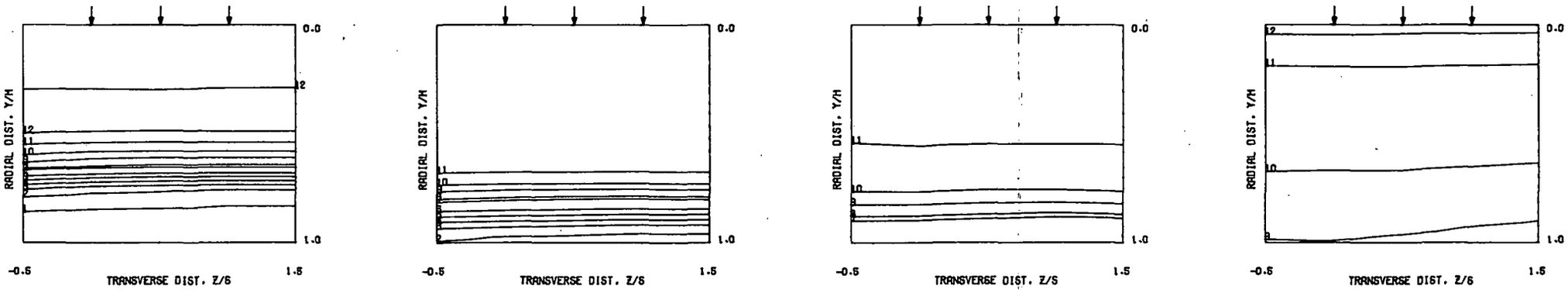

MEASURED THETA CONTOURS FOR TEST NO 45C, SLOT , J=78.33, S/W=1.0, H/W=9.92

Figure 113. Measured Theta Distributions for Test No. 45C.

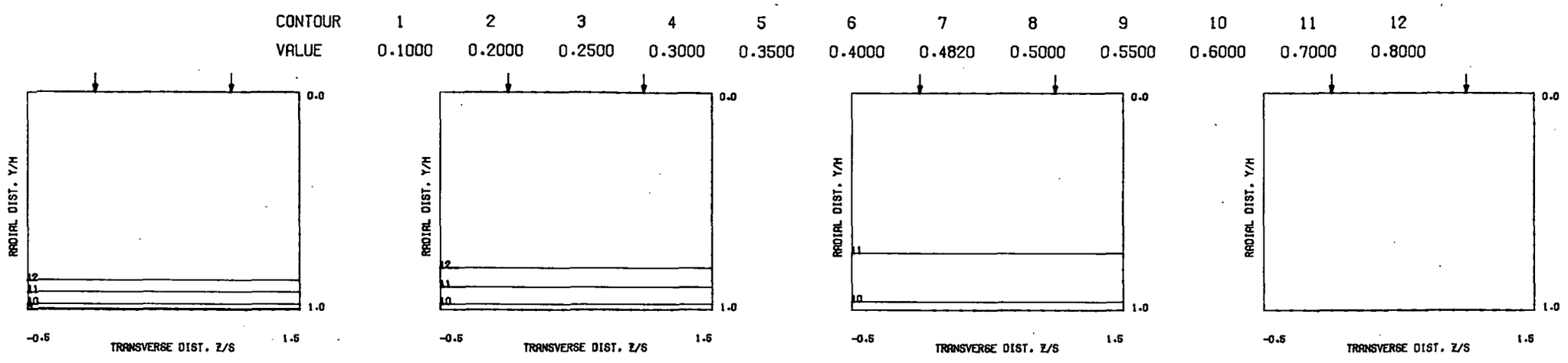

PREDICTED THETA CONTOURS FOR TEST NO. 45C, TM=CONST (SLOT), J=78.33, H/W=9.92

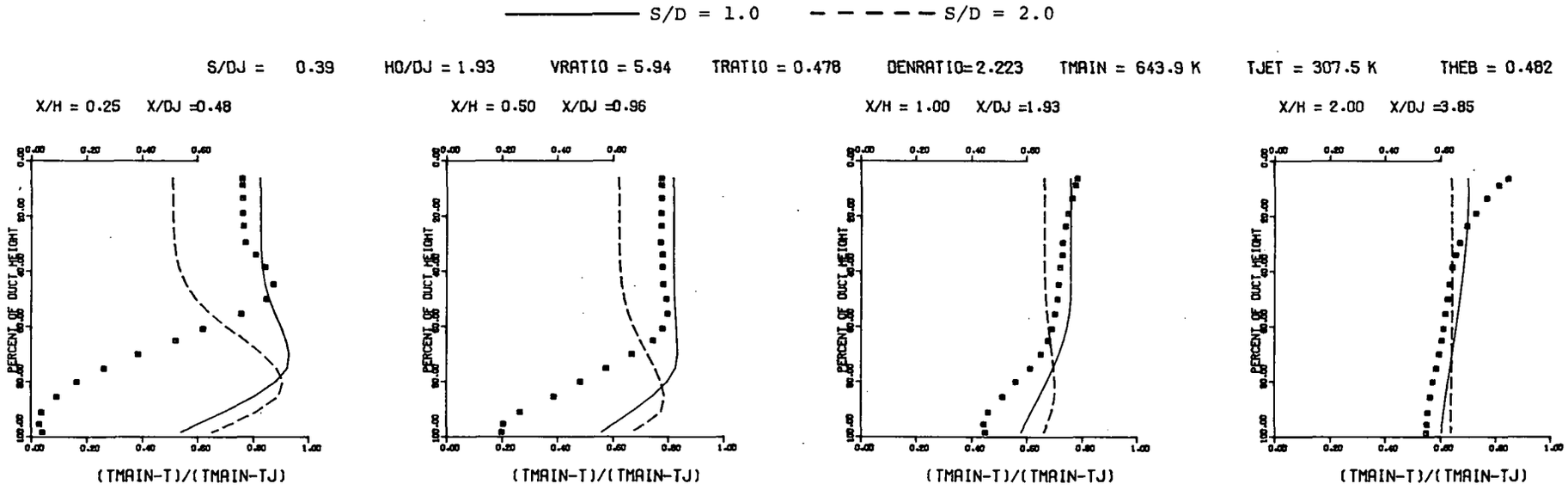

COMPARISON BETWEEN DATA AND CORRELATIONS FOR TEST NO.45C, 10.24 MM SLOT, TM=CONST, T.S. I.J = 78.33 , S/D =2.00 , H/D =9.92

Figure 114. Predicted Theta Distributions for Test No. 45C.

S = 0.0508 METERS S/DJ = 2.451 HO/DJ = 4.902 VMAIN = 16.5 M/SEC VJET = 29.4 M/SEC TMAIN = 644.3 K TJET = 304.8 K THEB = 0.3299 BLORAT= 3.767 DENRATIO= 2.119 TRATIO= 0.473

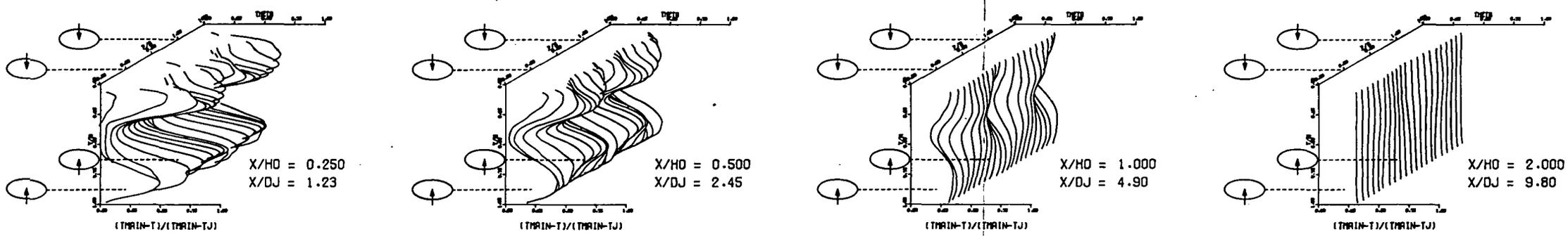

MEASURED THETA PROFILES FOR TEST NO.46, TEST SECTION I, TM=CONST(INL) , J = 6.70 , S/D = 2.00 , H/D = 4.00

CONTOUR	1	2	3	4	5	6	7	8	9	10	11
VALUE	0.0500	0.1000	0.1500	0.2000	0.2500	0.3000	0.3299	0.4000	0.5000	0.6000	0.7000

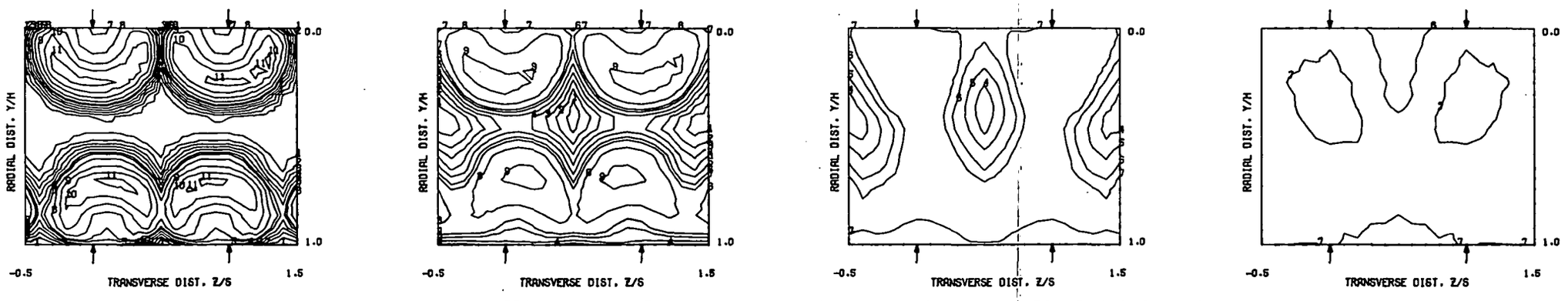

MEASURED THETA CONTOURS FOR TEST NO.46, TM=CONST (INL), J=6.70, S/D=2.0, H/D=4.0

Figure 115. Measured Theta Distributions for Test No. 46.

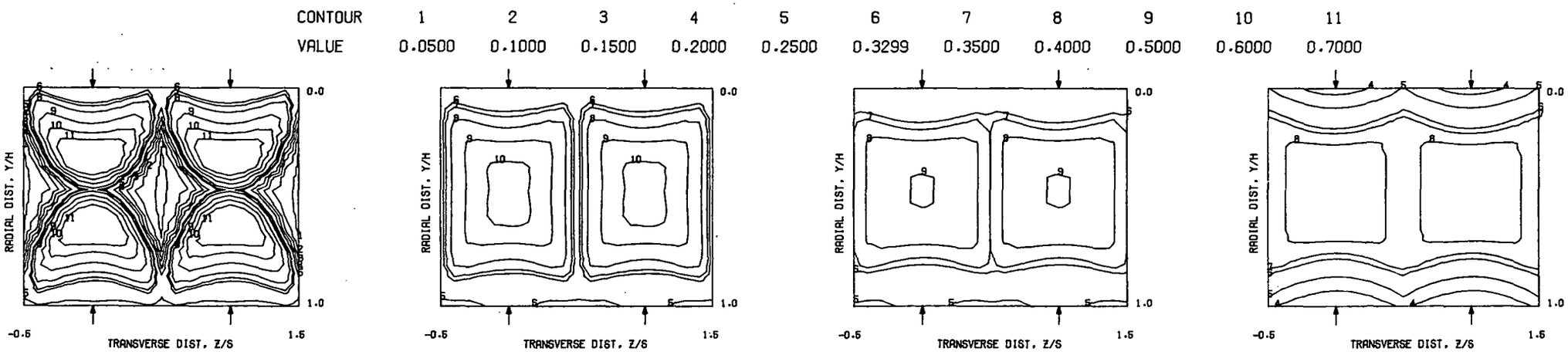

PREDICTED THETA CONTOURS FOR TEST NO 46, T.S. I, J=6.70, S/D=2.0(INL), H/D=4.0

S/DJ = 2.45 HO/DJ = 2.45 VRATIO = 1.78 TRATIO = 0.473 DENRATIO=2.119 TMAIN = 644.3 K TJET = 304.8 K THEB = 0.330

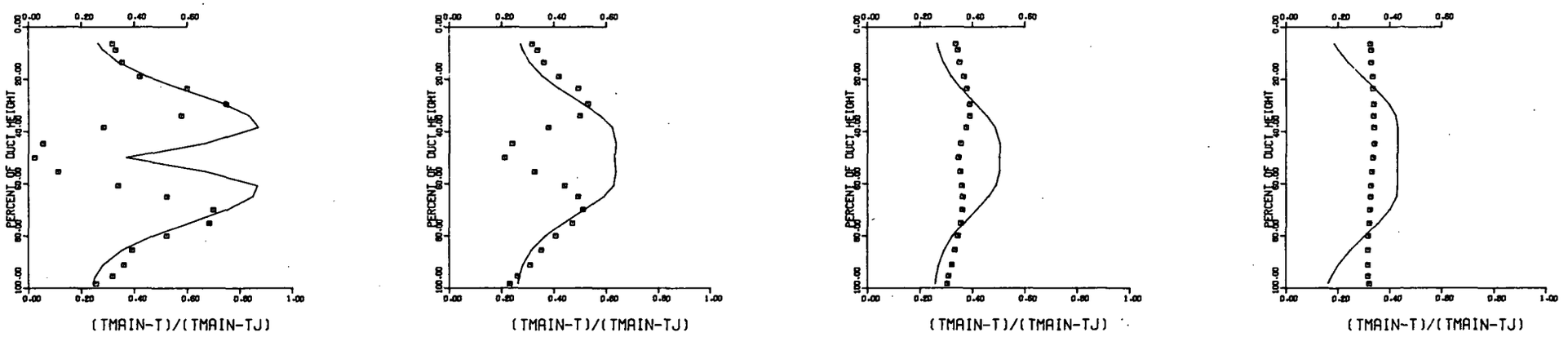

COMPARISON BETWEEN DATA AND CORRELATIONS FOR TEST NO. 46, TEST SECTION I,TM=CONST(INL), J = 6.70 , S/D =2.00 , H/D =4.00

Figure 116. Predicted Theta Distributions for Test No. 46.

S = 0.0508 METERS S/DJ = 2.488 HO/DJ = 4.977 VMAIN = 16.6 M/SEC VJET = 57.0 M/SEC TMAIN = 644.3 K TJET = 302.2 K THEB = 0.4846 BLORAT= 7.423 DENRATIO= 2.157 TRATIO= 0.469

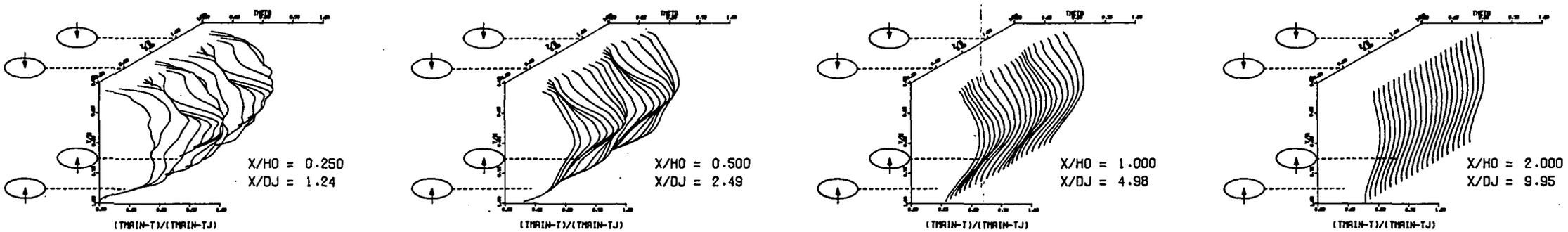

MEASURED THETA PROFILES FOR TEST NO.47, TEST SECTION I, TM=CONST(INL) , J = 25.56 , S/D = 2.00 , H/D = 4.00

CONTOUR	1	2	3	4	5	6	7	8	9	10	11
VALUE	0.0500	0.1000	0.1500	0.2000	0.2500	0.3000	0.3500	0.4000	0.4846	0.6000	0.7000

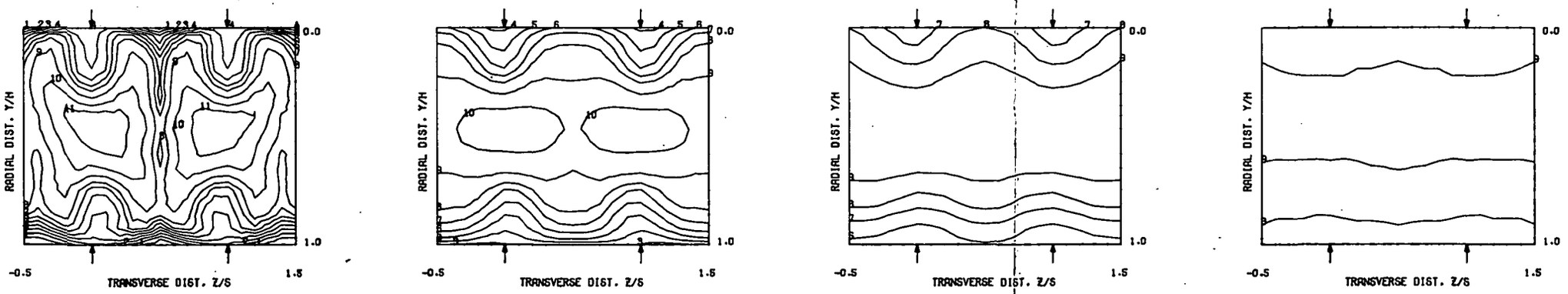

MEASURED THETA CONTOURS FOR TEST NO.47, TM=CONST (INL), J=25.56, S/D=2.0, H/D=4.

Figure 117. Measured Theta Distributions for Test No. 47.

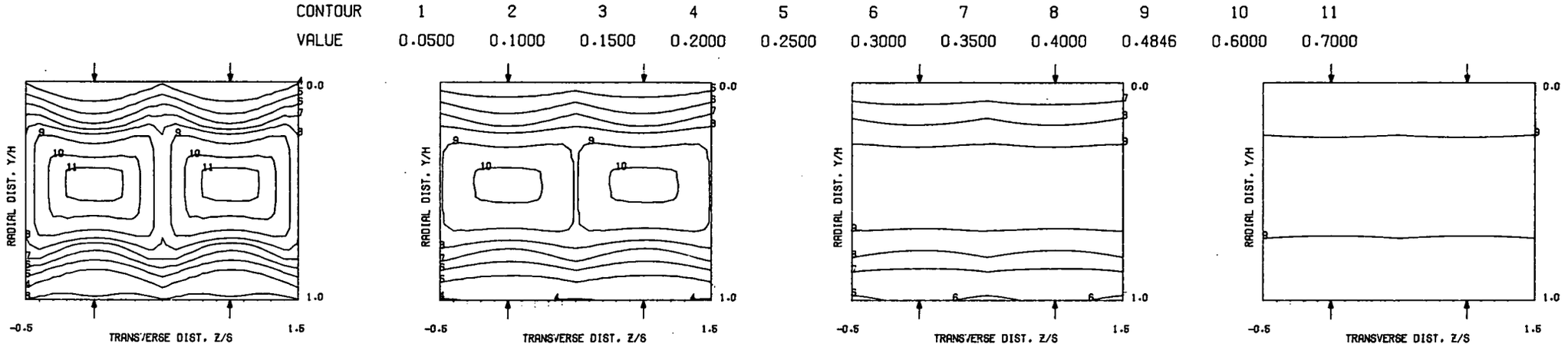

PREDICTED THETA CONTOURS FOR TEST NO 47, T.S. I, J=25.56, S/D=2.0(INL), H/D=4.0

S/DJ = 2.49 HO/DJ = 2.49 VRATIO = 3.44 TRATIO = 0.469 DENRATIO=2.157 TMAIN = 644.3 K TJET = 302.2 K THEB = 0.485

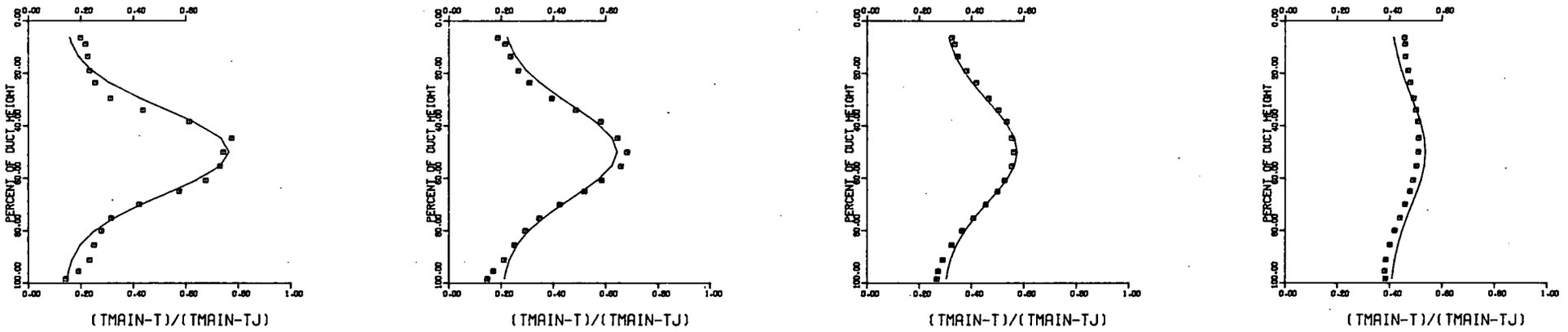

COMPARISON BETWEEN DATA AND CORRELATIONS FOR TEST NO. 47, TEST SECTION I,TM=CONST(INL), J = 25.56 , S/D =2.00 , H/D =4.00

Figure 118. Predicted Theta Distributions for Test No. 47.

S = 0.0508 METERS S/DJ = 2.500 HO/DJ = 5.000 VMAIN = 16.5 M/SEC VJET = 101.4 M/SEC TMAIN = 644.1 K TJET = 302.5 K THEB = 0.6327 BLORAT= 13.704 DENRATIO= 2.232 TRATIO= 0.470

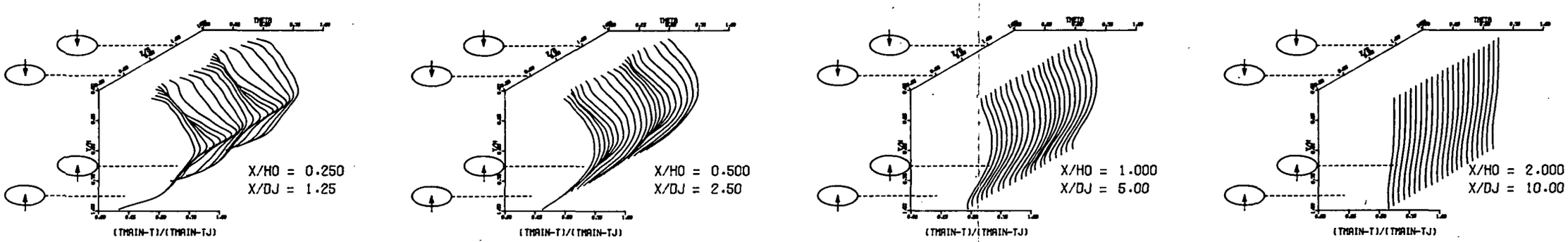

MEASURED THETA PROFILES FOR TEST NO.48, TEST SECTION I, TM=CONST(INL), J = 84.18 , S/D = 2.00 , H/D = 4.00

CONTOUR 1 2 3 4 5 6 7 8 9 10 11

VALUE 0.1000 0.2000 0.3000 0.3500 0.4000 0.4500 0.5000 0.5500 0.6327 0.7000 0.7500

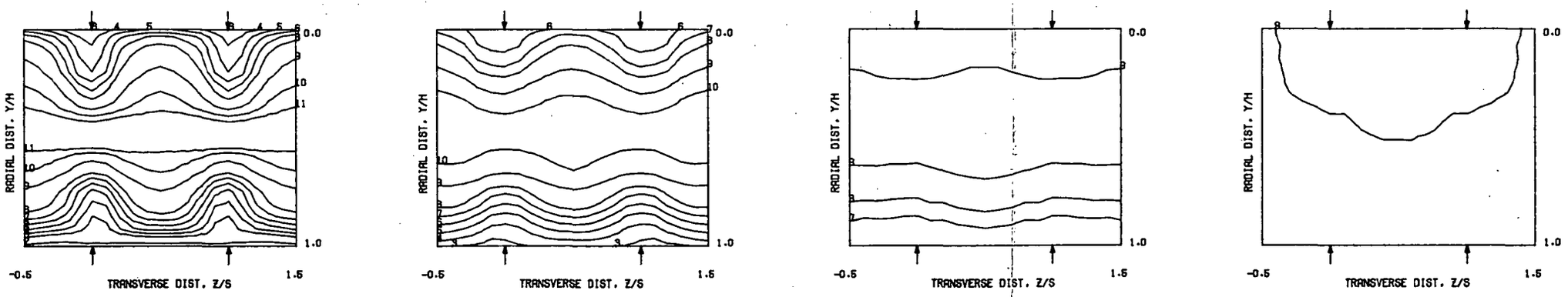

MEASURED THETA CONTOURS FOR TEST NO.48, TM=CONST(INL), J=84.17, S/D=2.0, H/D=4.0

Figure 119. Measured Theta Distributions for Test No. 48.

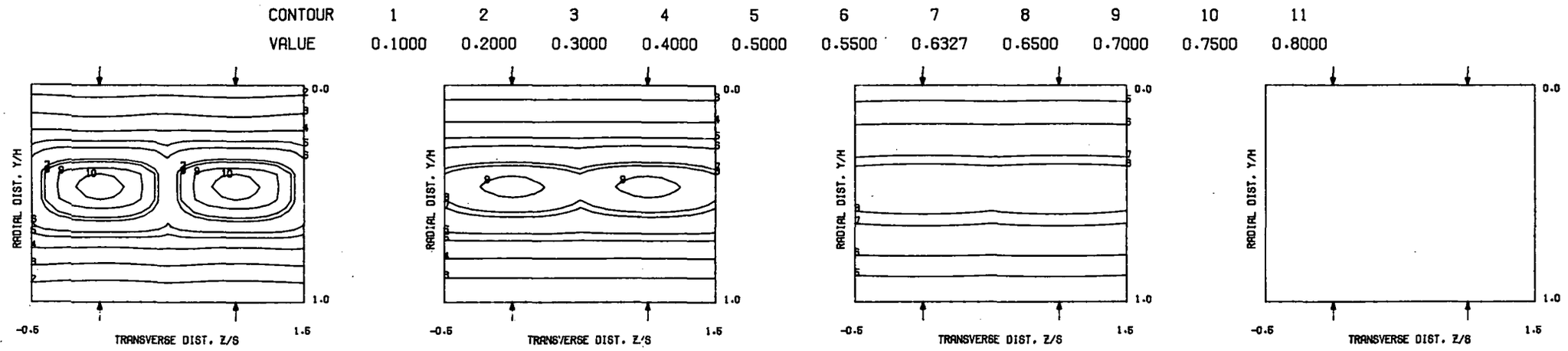

PREDICTED THETA CONTOURS FOR TEST NO 48, TM=CONST(INL),J=84.2,S/D=2.0, H/D=4.0

S/DJ = 2.50 HO/DJ = 2.50 VRATIO = 6.14 TRATIO = 0.470 DENRATIO=2.232 TMAIN = 644.1 K TJET = 302.5 K THEB = 0.633

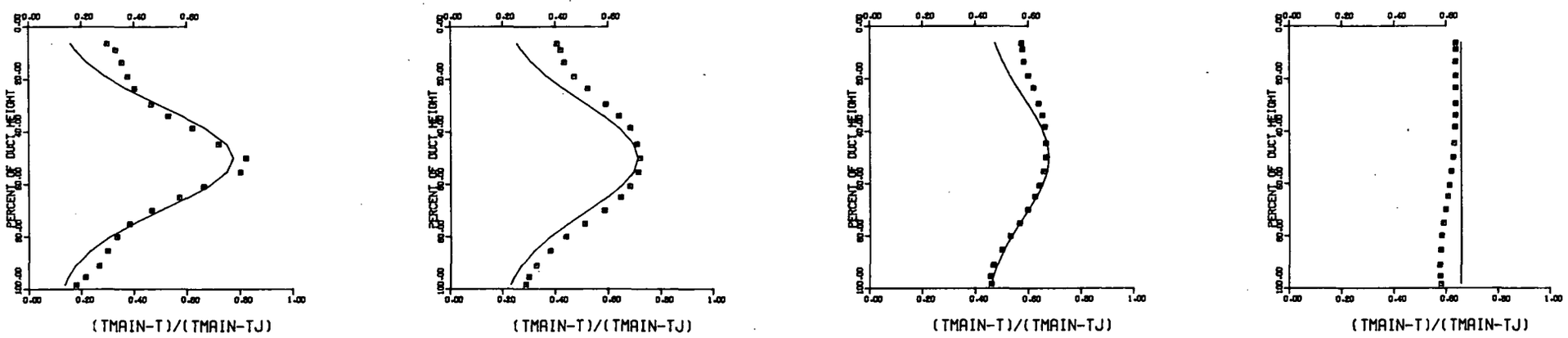

COMPARISON BETWEEN DATA AND CORRELATIONS FOR TEST NO. 48, TEST SECTION I, TM=CONST(INL), J = 84.18 , S/D =2.00 , H/D =4.00

Figure 120. Predicted Theta Distributions for Test No. 48.

S = 0.0508 METERS S/DJ = 3.322 HO/DJ = 6.644 VMAIN = 16.7 M/SEC VJET = 29.4 M/SEC TMAIN = 644.4 K TJET = 309.5 K THEB = 0.1159 BLORAT= 3.682 DENRATIO= 2.090 TRATIO=0.480

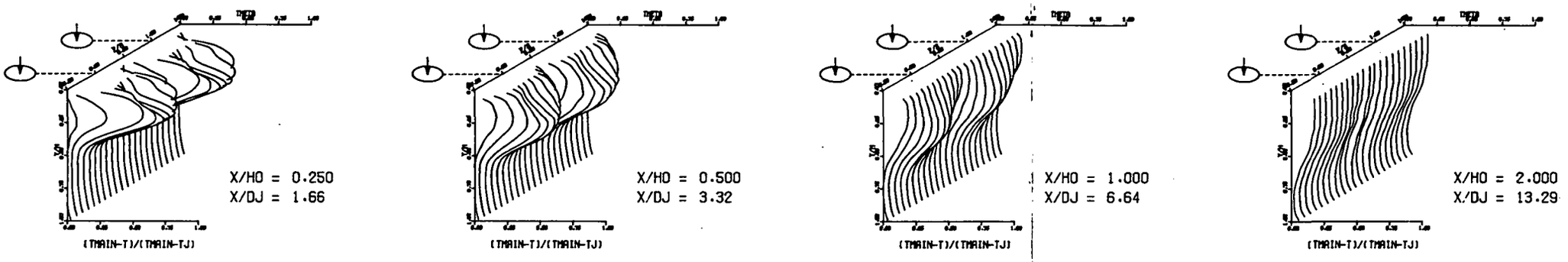

MEASURED THETA PROFILES FOR TEST NO.49, TEST SECTION I, TM=CONST , J = 6.49 , S/D = 2.83 , H/D = 5.66

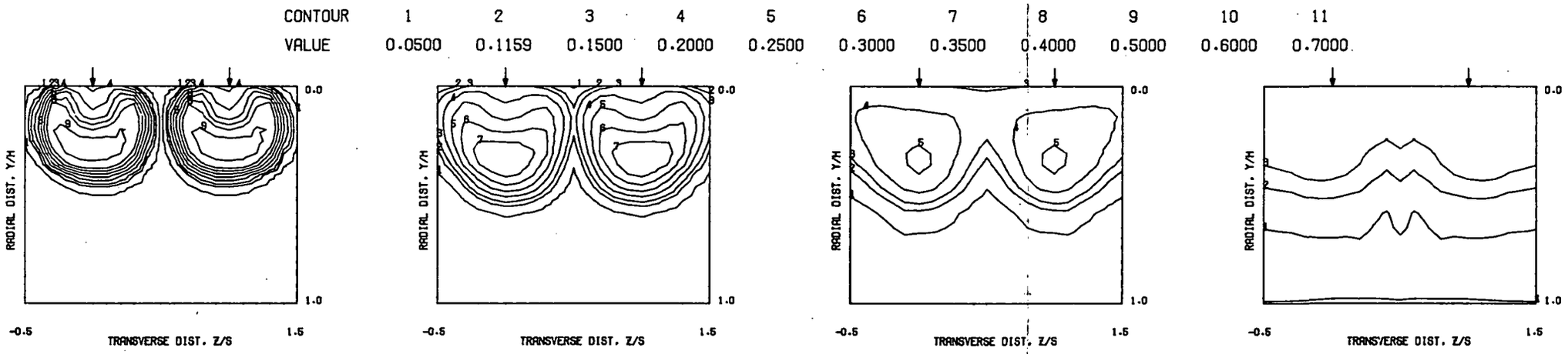

MEASURED THETA CONTOURS FOR TEST NO.49, TM=CONST , J=6.49, S/D=3.0, H/D=6.0

Figure 121. Measured Theta Distributions for Test No. 49.

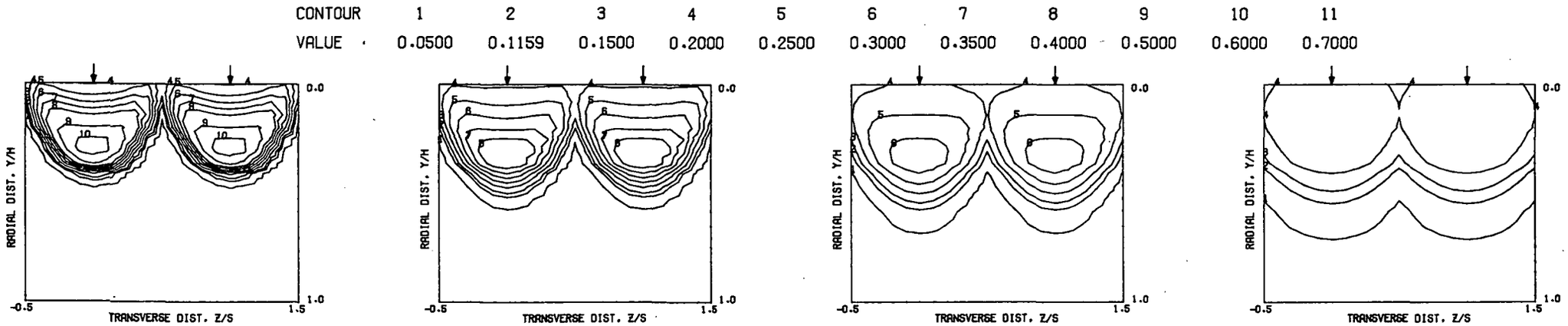

PREDICTED THETA CONTOURS FOR TEST NO.49, TM=CONST, J=6.49, S/D=2.83, H/D=5.66

S/DJ = 3.32 HO/DJ = 6.64 VRATIO = 1.76 TRATIO = 0.480 DENRATIO=2.090 TMAIN = 644.4 K TJET = 309.5 K THEB = 0.116

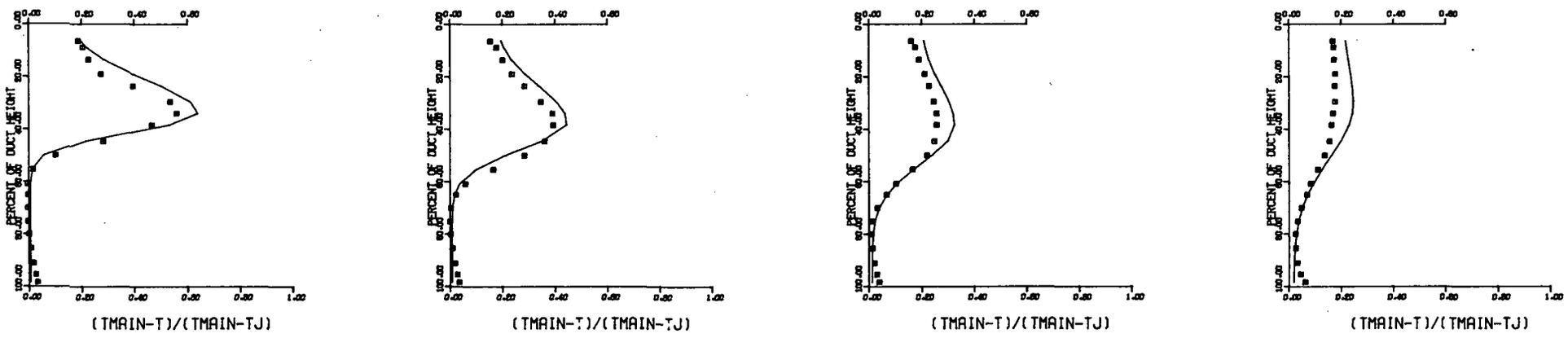

COMPARISON BETWEEN DATA AND CORRELATIONS FOR TEST NO.49, TEST SECTION I, TM=CONST, J = 6.49 , S/D =2.83 , H/D =5.66

Figure 122. Predicted Theta Distributions for Test No. 49.

S = 0.0508 METERS S/DJ = 3.369 HO/DJ = 6.737 VMAIN = 16.5 M/SEC VJET = 56.3 M/SEC TMAIN = 644.9 K TJET = 299.5 K THEB = 0.2054 BLORAT= 7.468 DENRATIO= 2.191 TRATIO= 0.464

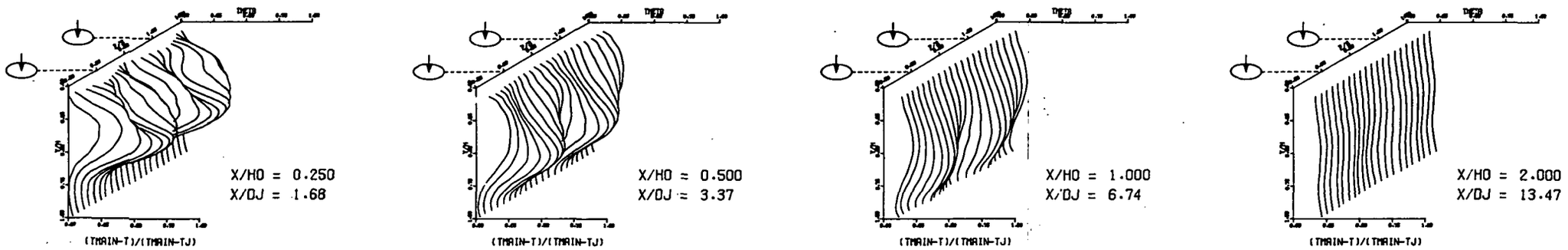

MEASURED THETA PROFILES FOR TEST NO.50, TEST SECTION I, TM=CONST , J = 25.48 , S/D = 2.83 , H/D = 5.66

CONTOUR	1	2	3	4	5	6	7	8	9	10	11
VALUE	0.0500	0.1000	0.1500	0.2054	0.2500	0.3000	0.3500	0.4000	0.5000	0.6000	0.7000

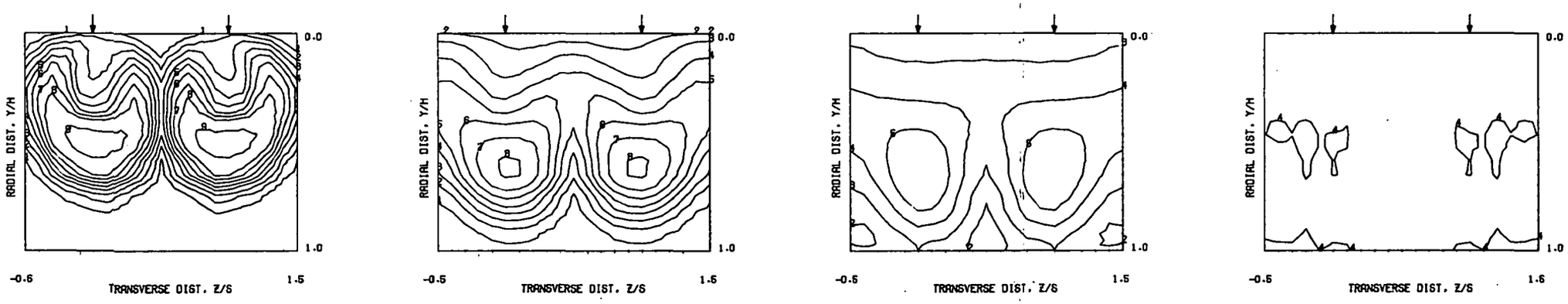

MEASURED THETA CONTOURS FOR TEST NO.50, TM=CONST , J=25.48, S/D=3.0, H/D=6.0

Figure 123. Measured Theta Distributions for Test No. 50.

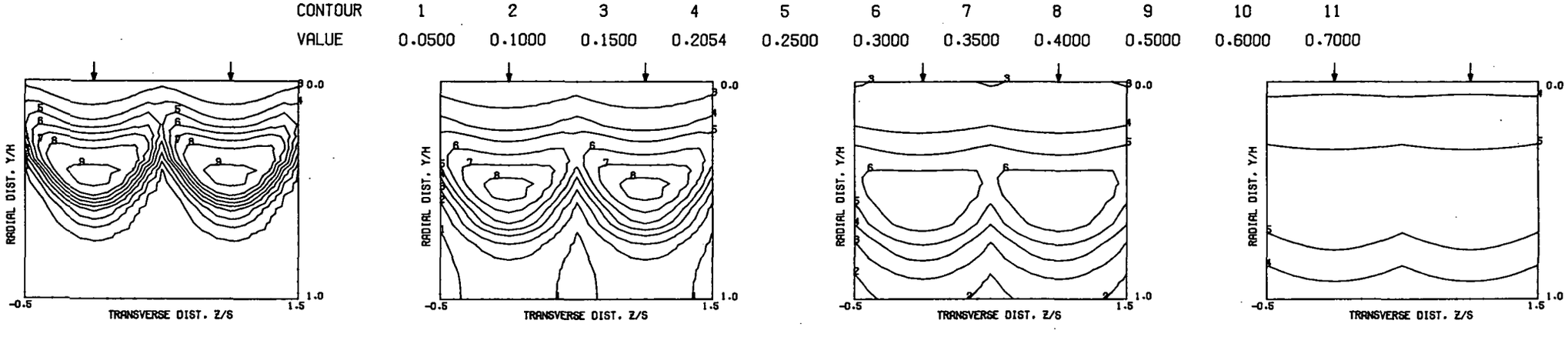

PREDICTED THETA CONTOURS FOR TEST NO.50, TM=CONST, J=25.48, S/D=2.83, H/D=5.66

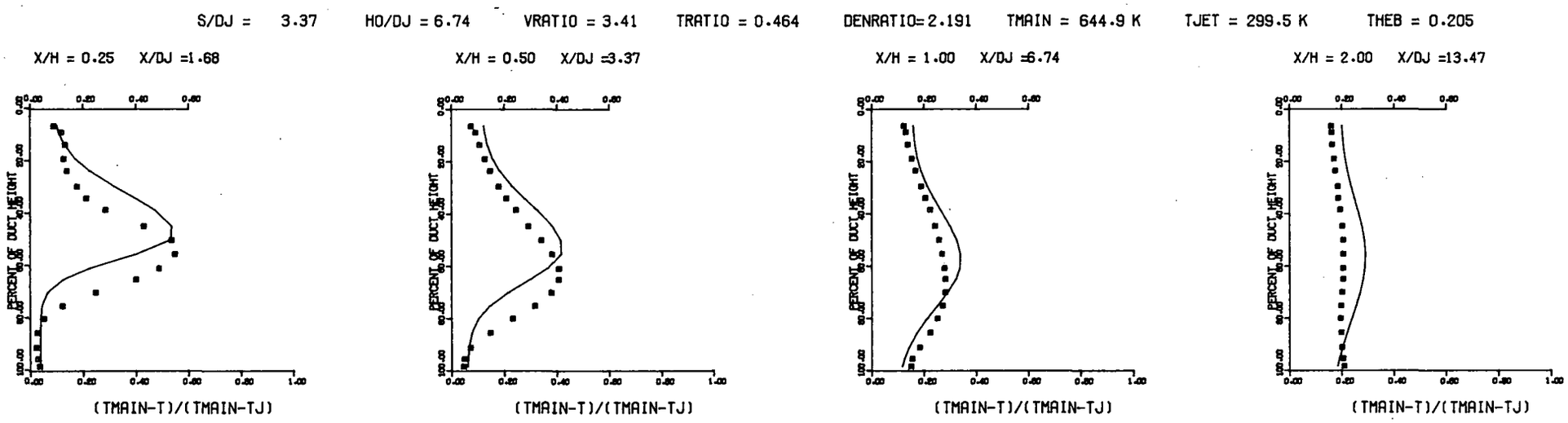

COMPARISON BETWEEN DATA AND CORRELATIONS FOR TEST NO.50, TEST SECTION I, TM=CONST, J = 25.48 , S/D =2.83 , H/D =5.66

Figure 124. Predicted Theta Distributions for Test No. 50.

S = 0.1016 METERS S/DJ = 4.869 HO/DJ = 4.869 VMAIN = 16.5 M/SEC VJET = 29.2 M/SEC TMAIN = 644.3 K TJET = 305.6 K THEB = 0.2014 BLORAT= 3.757 DENRATIO= 2.116 TRATIO= 0.474

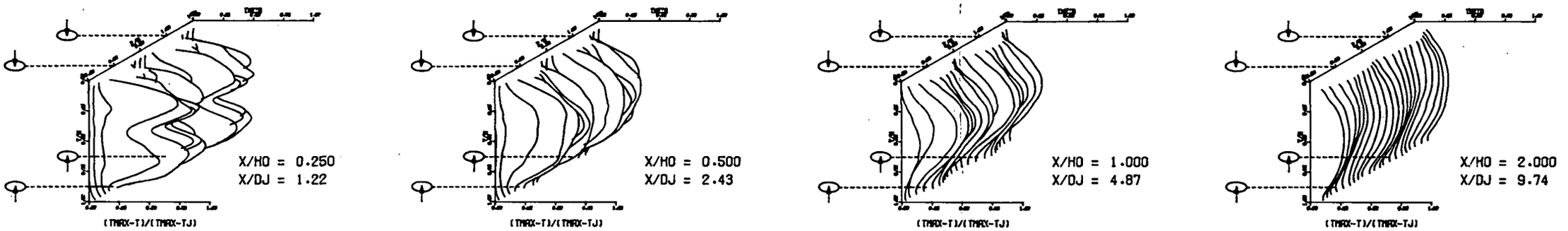

MEASURED THETA PROFILES FOR TEST NO.51, TEST SECTION I, TM=CONST(INL) , J = 6.67 , S/D = 4.00 , H/D = 4.00

CONTOUR	1	2	3	4	5	6	7	8	9	10	11
VALUE	0.0500	0.1000	0.1500	0.2014	0.2500	0.3000	0.3500	0.4000	0.5000	0.6000	0.7000

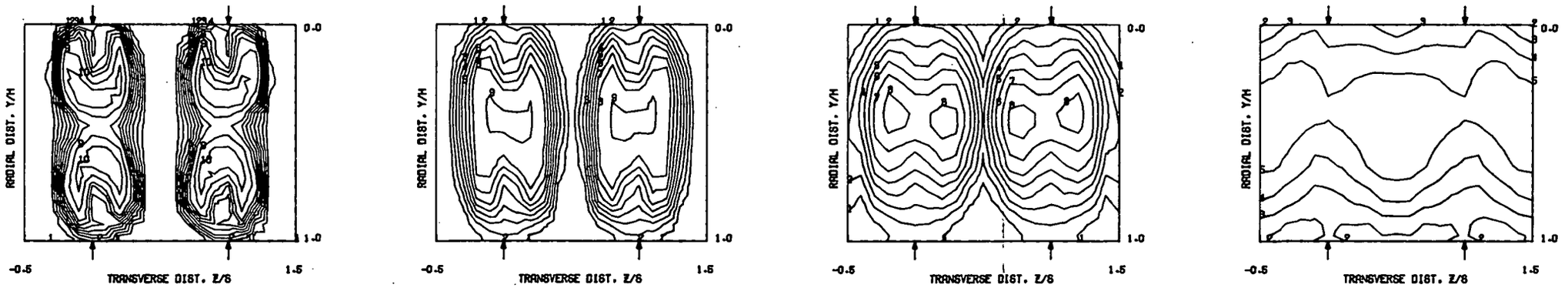

MEASURED THETA CONTOURS FOR TEST NO 51, TM=CONST(INL), J=6.67, S/D=4.0, H/D=4.0

Figure 125. Measured Theta Distributions for Test No. 51.

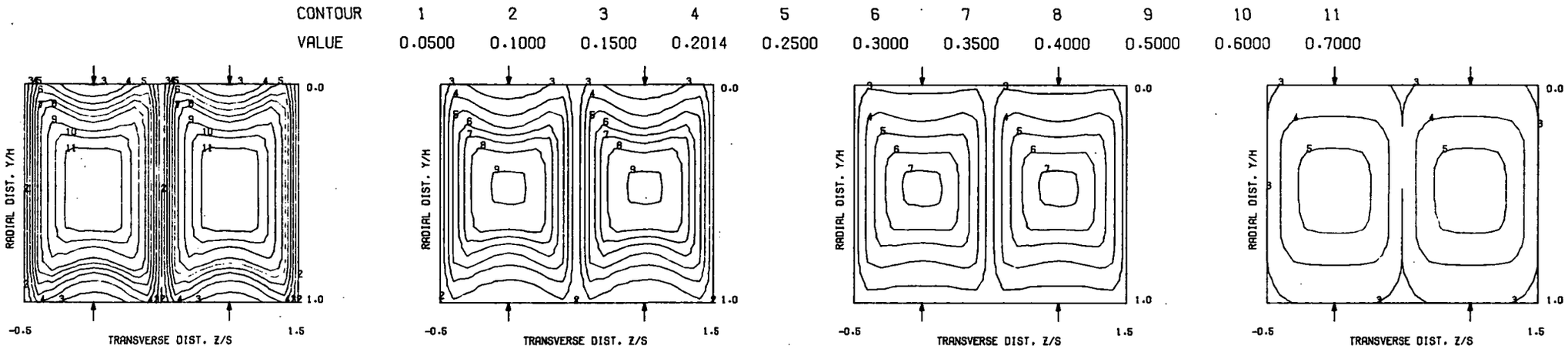

PREDICTED THETA CONTOURS FOR TEST NO 51, TM=CONST, J=6.67, S/D=4.0(INL), H/D=4.0

S/DJ = 4.87 HO/DJ = 2.43 VRATIO = 1.78 TRATIO = 0.474 DENRATIO=2.116 TMAIN = 644.3 K TJET = 305.6 K THEB = 0.201

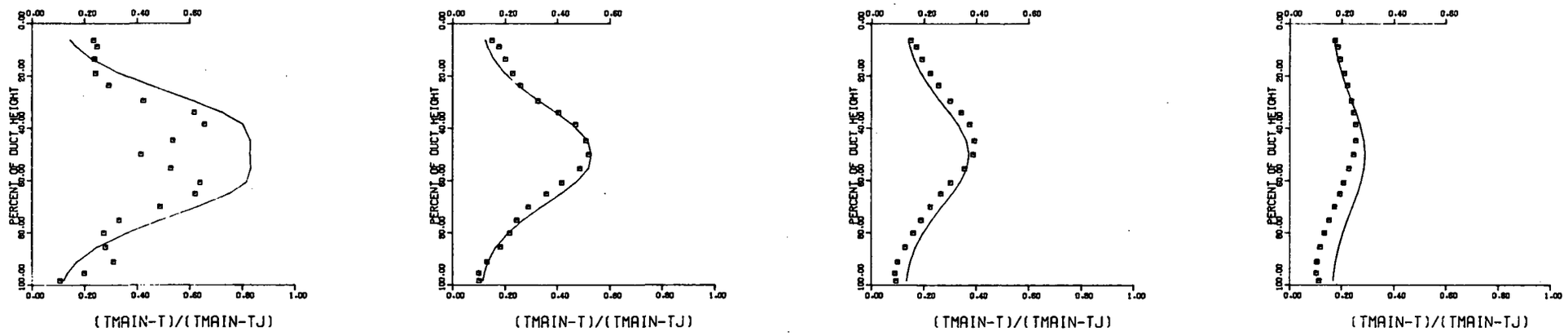

COMPARISON BETWEEN DATA AND CORRELATIONS FOR TEST NO. 51, TEST SECTION I, TM=CONST(INL), J = 6.67 , S/D =4.00 , H/D =4.00

Figure 126. Predicted Theta Distributions for Test No. 51.

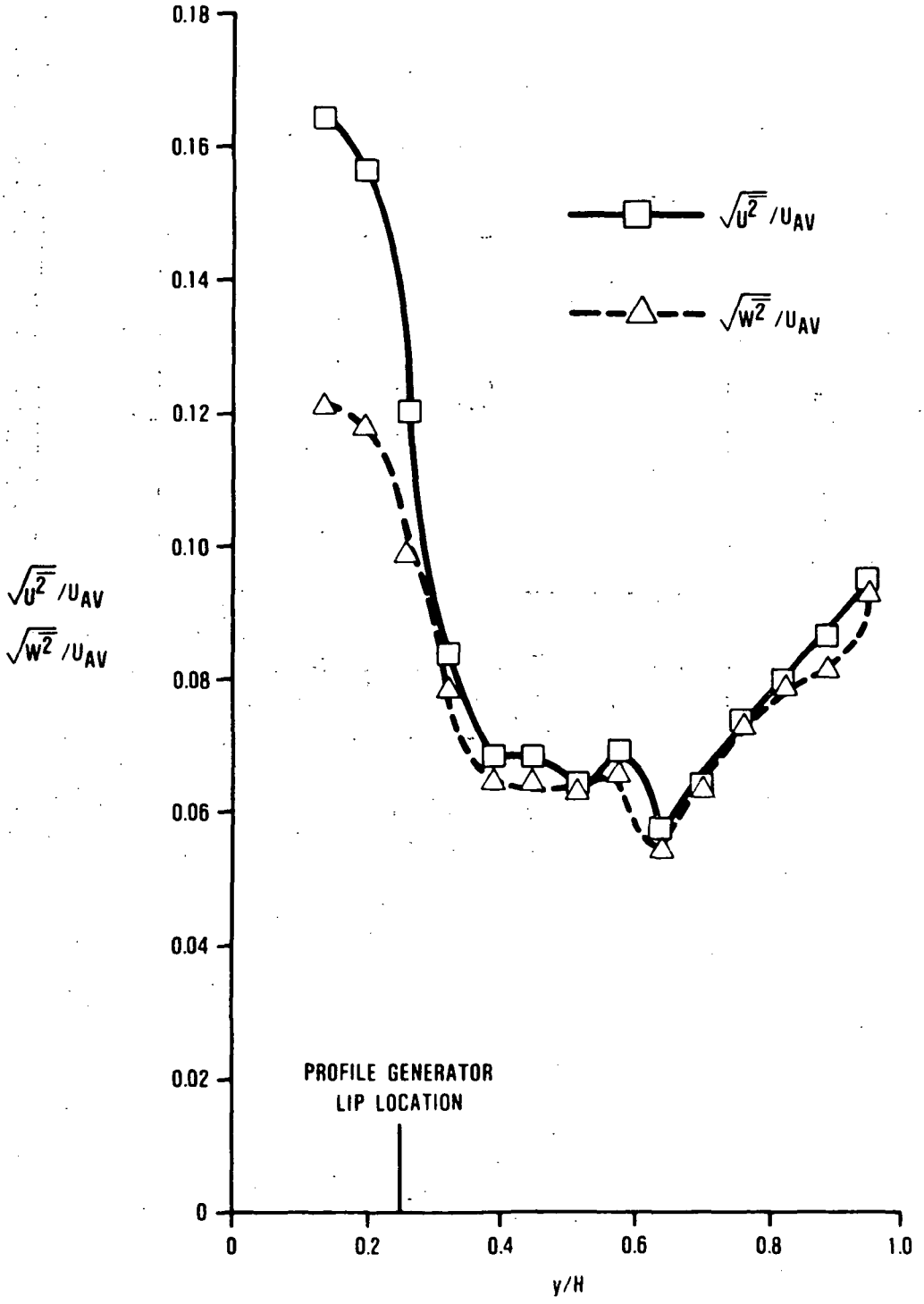

Figure 127. Hot-Wire Data on the Dilution Jet Mixing Test Rig $X/H_0 = -1.625$.

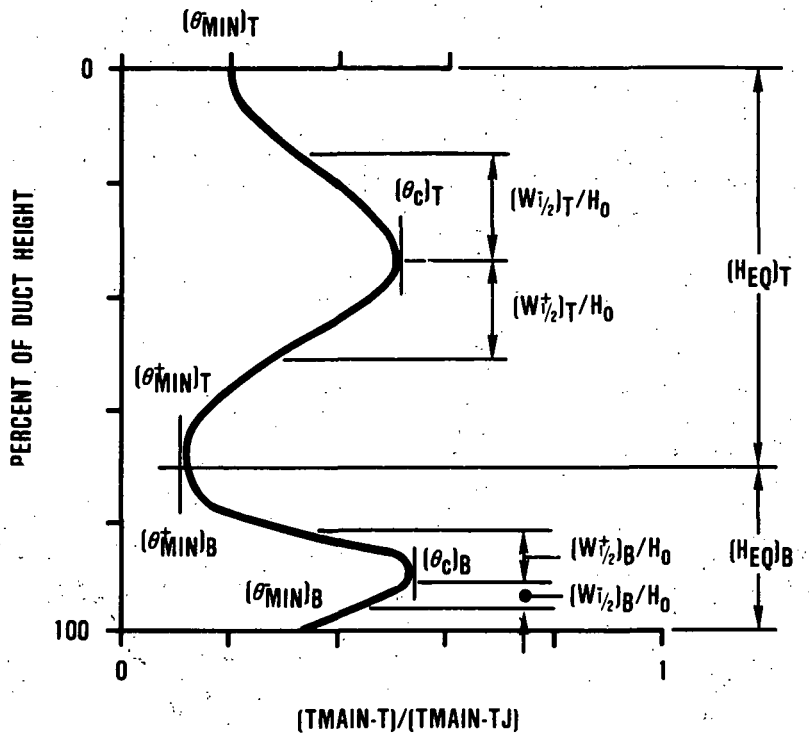

Figure 128. Schematic of Typical Radial Temperature Profile.